THE UNIVERSITY
of EDINBURGH

Metabolic remodelling driven by *MYC* overexpression regulates the p53 tumour suppressor response.

Joy Edwards-Hicks

THE UNIVERSITY
of EDINBURGH

Thesis submitted for the degree of Doctor of Philosophy
The University of Edinburgh
2017

Declaration

I declare that this thesis was written and composed solely by myself, and that it has not been submitted in any previous application for a degree. Except where stated otherwise by reference or acknowledgment, the work presented is entirely my own.

Joy Edwards-Hicks

Acknowledgements

I would like to thank my supervisor, Andrew Finch, for his support and guidance throughout my PhD studies. From the Finch lab, I would particularly like to thank Huizhong Su and Mina Pantazi, as well as Heather Barker, for their friendship and feedback throughout the project. I would also like to thank Jimi Wills for his helpful discussions and collaboration on LC-MS methodology. I would like to thank Juan-Carlos Acosta for his useful feedback on the project, as well as members of the Acosta lab: Flora Dix and Andrea Quintanilla, whose contributions to this project are clearly acknowledged throughout the thesis. Externally, I would like to thank Karl Burgess, Terry White, and Phil Whitfield for their advice during the set up of our LC-MS facility.

On a personal note, I would like to thank my boyfriend, John Sutherland, for all his love and support throughout my PhD studies. I would like to thank my family who always encouraged me to pursue a career that I enjoyed. In particular, I would like to thank my mother, Leanne Martin, for her unwavering support and shared enthusiasm for scientific learning.

Abstract

The *MYC* onocogene is frequently overexpressed in human cancer due to its capacity to promote cell growth and cell proliferation. *MYC* overexpression activates the p53 tumour suppressor pathway, which resists the pro-tumourigeneic program elicited by MYC. How *MYC* overexpression engages p53 is yet to be elucidated, and in this study I carried out a large metabolic siRNA screen to determine whether p53 responds to a specific MYC-driven metabolic pathway. Two clear lipid metabolic pathways emerged from the siRNA screen: PPARγ/arachidonate metabolism and *de novo* sphingolipid synthesis. Knockdown or inhibition of PPARγ increased p53 levels, and PPARγ ligands decreased following *MYC* overexpression. Knockdown of ceramide synthesis depleted p53 levels, and *MYC* overexpression increased *de novo* ceramide synthesis. This demonstrated that MYC-driven ceramide synthesis positively regulates p53, and highlights the role of cell metabolism in the tumour suppressor response to MYC deregulation.

Lay summary

Cell metabolism describes how a cell uses nutrients and energy. Understanding cell metabolism is an important area of cancer research because cancer cells change cell metabolism to favour their expansion and survival. The *MYC* gene is often mutated in cancer and is described as an oncogene because it promotes tumour formation. Genes that protect against tumour formation are also frequently mutated in cancer, and these genes are called tumour suppressor genes. The *TP53* tumour suppressor gene responds to cell stress and is commonly mutated in cells that have deregulated MYC. It is known the p53 is activated by MYC, and this study investigated whether p53 responds to an unidentified MYC-driven stress. From studying cell metabolism we revealed that synthesis of a set of lipids driven by MYC was required for p53 activation. Several metabolic pathways were also identified that when blocked strongly increased cell stress, specifically in cells with increased MYC. These results have important implications in the treatment of tumours with the MYC oncogene.

Table of contents

1 Chapter 1- Introduction

1.1 The Oncogene MYC

The identification of the *MYC* gene (named for 'myelocytomatosis') in the early 1960s paved the way for the discovery of retroviruses, viral oncogenes, and the exploitation of these tools to study the basis of cancer (Tansey, 2014). Among these pioneering experiments was the isolation of *V-MYC*, the viral homolog of *C-MYC*, as the transforming gene of MC29 avian leukemia virus (Sheiness *et al.* 1978; Vennstrom *et al.* 1982). Infection of fowl with MC29 caused hematopoietic neoplasia, specifically transforming myeloid cells into diffuse growths (myelocytomatosis) or solid tumours (myelocytomas) (Ivanov *et al.* 1964; Mladenov, 1967). The effort to characterise and understand the biology of MYC is ongoing, and its relevance today is highlighted by MYC appearing at an average rate of almost three publications per day in recent years (Tansey, 2014).

MYC is frequently deregulated in a wide variety of human cancers (figure 1.1), implicating MYC as an important gene to study in cancer research. MYC deregulation is predominantly driven by its constitutive overexpression; however changes in MYC mRNA and protein stability have also been described (reviewed in Kalkat *et al.* 2017). Constitutive overexpression of *MYC* is most commonly caused by gene amplification (figure 1.1), which arises through genome doubling or tandem duplications (Burrell *et al.* 2013). Overexpression of *MYC* also occurs through chromosomal translocation or increased enhancer activity. Burkitt's lymphoma is driven by chromosomal translocation of C-MYC from chromosome 8 to chromosome 14, where C-MYC is under the control of the immunoglobulin promoter (a lineage-specific enhancer) (Dalla-Favera *et al.* 1982). Acquisition of increased enhancer activity at the endogenous locus, through single nucleotide polymorphisms (Wright *et al.* 2010) or histone acetylation (Shi *et al.* 2013), upregulates MYC expression.

In the absence of MYC amplification or translocation, abberant signal transduction causes MYC deregulation. First, mutations that alter RAS/ phosphatidylinositol-4,5-bisphosphate 3-kinase (RAS/PI3K) signalling pathways increase MYC protein stability (Sears *et al.* 2000). The phosphatase and tensin homolog *(PTEN)* tumour suppressor gene, which negatively regulates PI3K, is lost in multiple tumours types (Li *et al.* 1997). Loss of *PTEN* increases serine/threonine kinase 1 (AKT)-dependent phosphorylation of glycogen synthase kinase (GSK3), which inactivates GSK3 and inhibits its ability to negatively regulate MYC protein stability. Second, mutations that cause abberant β-catenin signalling are estimated to occur in over 90% of colorectal cancers (Shi *et al.* 2017), and increase the expression of MYC (He *et al.* 1998). Loss of adenomatosis polyposis coli (APC) upstream of β-catenin is the predominant mutation in the β-catenin pathway, occurring in 85% of cases (Shi *et al.* 2017). Third, mutations in NOTCH1, which stimulates a long-range MYC enhancer

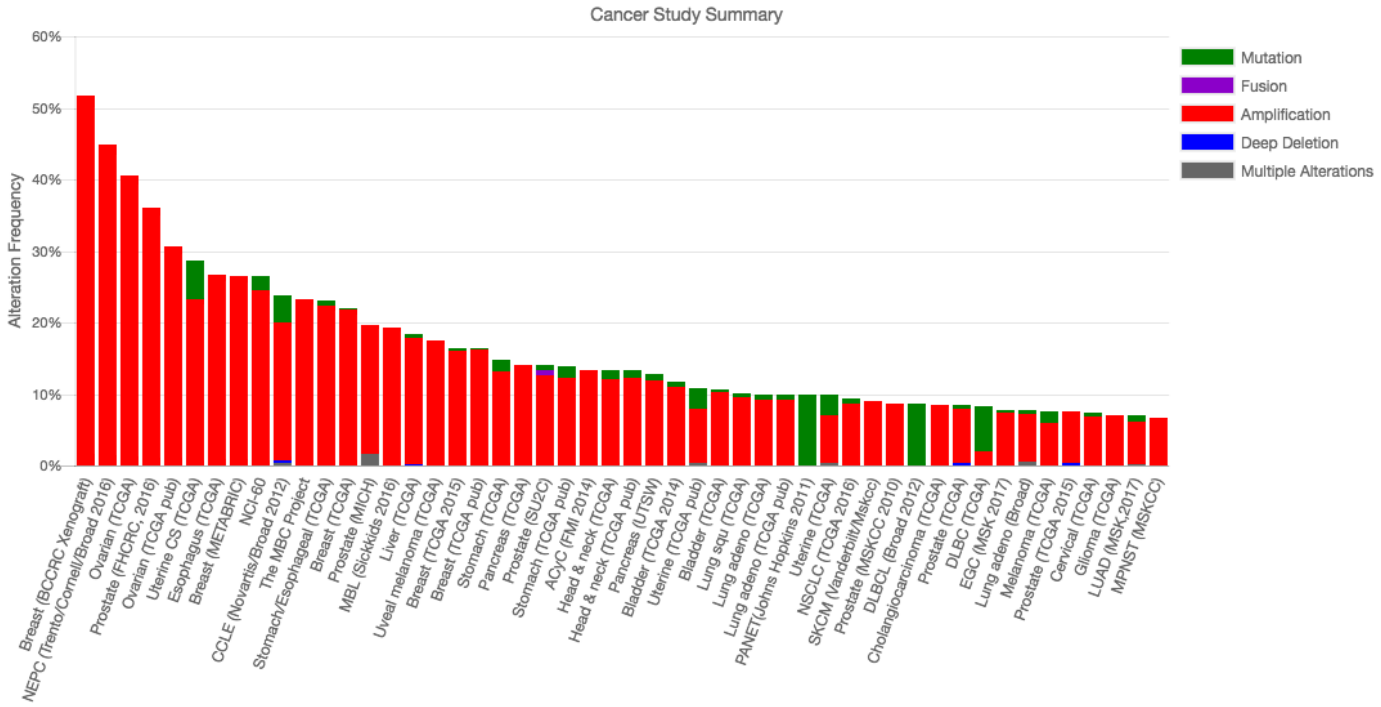

Figure 1.1. *MYC* mutation and copy number alteration frequency in human cancer (Cerami *et al.* 2012; Gao *et al.* 2013) Barplot shows the frequency of *MYC* mutation and copy number alteration based on 169 combined cancer studies. *MYC* amplification is the predominant type of MYC deregulation across the majority of cancer types. Details on individual studies used to generate this dataset may be obtained from cBioPortal for Cancer Genomics (Cerami *et al.* 2012; Gao *et al.* 2013), which was also used to create this barplot.

downstream of MYC, were present in over 65% of T-cell acute lymphoblastic leukeamias (Weng *et al.* 2004). These studies highlight the frequency, and the variety of ways in which, MYC is deregulated in human cancer.

The human MYC family comprises three members, C-MYC, N-MYC, and L-MYC, which all have described roles in human cancer (Nau *et al.* 1985, 1986, Little *et al.* 1983). All family members are basic-helix-loop-helix leucine zipper proteins (bHLH-ZIP) that regulate gene transcription (reviewed in Adhikary and Eilers, 2005). MYC proteins function only as heterodimers *in vivo*, and formation of a MYC-MAX complex is required for binding of MYC to the DNA sequence CAGGTG (E-box) (Amati *et al.* 1993). MYC-MAX hetermodimers bind E-box sequences, and recruit co-regulatory factors including TRRAP, TIP60, and GCN5 to activate transcription (Bouchard *et al.* 2001; Frank *et al.* 2003; McMahon *et al.* 2000). In the absence of MYC, heterodimerisation of MAD-MAX or MNT-MAX at E-box sequences represses gene transcription through recruitment of histone deacetylase complexes (Ayer *et al.* 1993). MYC-MAX complexes also have transrepression capacity when tethered to a core promoter element, the initiator (Inr), by the transcription factor MIZ1. When unbound, MIZ1 transcriptionally activates its target genes, however MYC-MAX binding forms a transrepressor complex that recruits DNA (cytosine-5)-methyltransferase 3α (Seone *et al.* 2001; Staller *et al.* 2001; Brenner *et al.* 2005). MAD-MAX or MNT-MAX heterodimers are predominant in resting or differentiated cells, whereas MYC-MAX complexes are often predominant in proliferating cells (Ayer and Eisenman, 1993). Independently of MAX, MYC can activate transcription of its target genes by binding to other transcription factors such as YY1 or transcription factor IIIB (TFIIIB) (Vernon and Gaston, 2000; Gomez-Roman *et al.* 2003).

1.2 MYC target genes

Mammalian MYC binds to thousands of promoters, indicating that MYC target genes cover a significant proportion of the human genome (Lin *et al.* 2012; Nie *et al.* 2012). Two recent papers have put forward an 'amplifier model' to describe the transcriptional program driven by MYC. The amplifier model suggests MYC binds and amplifies most genes that are 'on' in a given cell type (Lin *et al.* 2012; Nie *et al.* 2012). Others argue that this model is oversimplified, and fails to recognise important genes that are transrepressed or differentially regulated by MYC (Tansey, 2014; Stine *et al.* 2015). Indeed, two comprehensive studies on specific transcriptional targets of MYC have recently been published (Sabo *et al.* 2014; Walz *et al.* 2014). The current literature on how MYC alters the transcriptional program in favour of cellular expansion, through regulation of genes involved in cell proliferation, cell growth, cell metabolism, and cell differentiation, will be discussed in the subsequent sections.

1.2.1 The role of MYC in cell proliferation

The role of MYC in regulating cell proliferation, and how this becomes deregulated when *MYC* is overexpressed, has been extensively studied. Early studies of MYC documented that its mRNA and protein levels increased in response to mitogenic stimuli, and this correlated with increased cell proliferation (Kelly *et al.* 1983; Dean *et al.* 1986; Reed *et al.* 1986). The ability of MYC to respond to mitogenic stimuli was shown to be dependent on the RAS/RAF/MEK/ERK cascade; however exactly how this cascade results in *MYC* activation is yet to be elucidated (Kerkhoff *et al.* 1998). *MYC* overexpression alone was sufficient to induce cell cycle progression in quiescent cells using a conditional MYC (MYCER) model (Eilers *et al.* 1991). Concomitantly, *MYC* downregulation with antisense oligonucleotides prevented S-phase entry in human lymphoid and myeloid cells (Heikkila *et al.* 1987; Wickstrom *et al.* 1988). These studies emphasise the importance of MYC in driving cell proliferation.

In line with the capacity of MYC to drive cell proliferation, cell cycle related genes were some of the first-discovered MYC target genes, including cyclins, CDKs (cyclin-dependent kinases), and CKI (cyclin-dependent kinase inhibitor) proteins (reviewed in Meyer and Penn, 2008). *MYC* overexpression was shown to regulate 37 out of 87 genes classified as belonging to the 'cell cycle pathway' in the KEGG (Kyoto Encyclopedia of Genes and Genomes) (Yap *et al.* 2011). The need for MYC to regulate multiple cell cycle genes at multiple stages may be due in part to redundancy between most cyclins and CDKs. Only cyclins A2 and B1, and CDK1 carry no redundancy, and these are therefore considered the 'basic core elements' of the cell cycle machinery (Murphy *et al.* 1997; reviewed in Bretones *et al.* 2015). An overview of MYC stimulation of cell cycle progression is depicted in figure 1.2.

Of the 'basic core elements', MYC regulation of cyclin A (mRNA and protein) was documented in Rat1 fibroblasts with conditional or constitutive *MYC* expression (Jansen-Durr *et al.* 1993; Barret *et al.* 1995; Hoang *et al.* 1994) and MYC binding to the cyclin B1 promoter was documented in lung cancer cells and Hela cells (Seo *et al.* 2008; Menssen *et al.* 2002). Furthermore, enforced expression of *MYC* and loss of p53 were shown to be synergistic lesions that enhanced induction of cyclin B1 (mRNA and protein) in Rat1 cells and 32D myeloid cells (Yin *et al.* 2001). MYC binding to the CDK1 promoter has been described; however MYC alone was not sufficient to induce gene expression. Instead, MYC-driven cell proliferation was associated with increased CDK2, CDK4, and CDK6 activities that regulate S-phase entry (Mateyak *et al.* 1999; Hermeking *et al.* 2000).

In addition to transactivation of cell cycle genes, MYC also represses CKIs $p21^{CIP1/WAF1}$ (p21) and p27. MYC repression of p21 was shown to be via MIZ-1, which normally transcriptionally activates p21 to inhibit cell cycle progression (Staller *et al.* 2001). MYC-MIZ1 interaction has been studied by introducing a single point mutation in MYC that prevents its interaction with MIZ1. The importance of MYC-MIZ1 interaction is highlighted by loss of this interaction attenuating MYC-driven tumourigenesis *in vivo* (Van Riggelen *et al.* 2010b). MYC repression of p27 requires multiple parallel mechanisms, including transcriptional repression (Yang *et al.* 2001), mRNA silencing by microRNAs (Kim *et al.* 2010), induction of cyclins

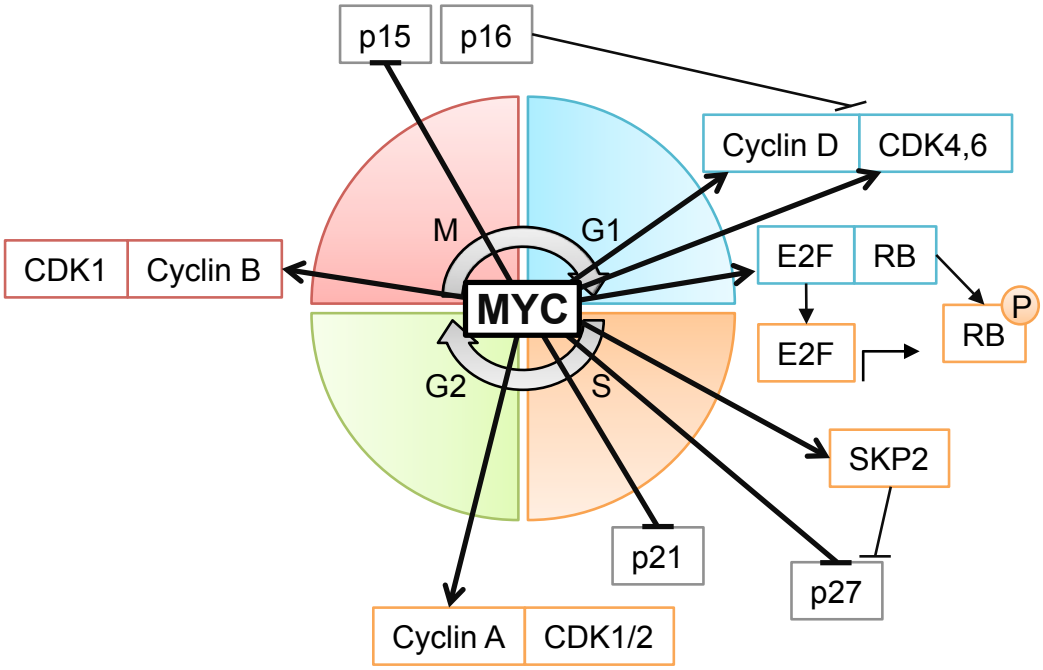

Figure 1.2. MYC regulation of the cell cycle (adapted from Bretones *et al.* 2015)

The figure shows MYC regulation of cyclins, CDKs (cyclin-dependent kinases) and CKIs (cyclin-dependent kinase inhibitors) at multiple stages of the cell cycle. To progress through G1, MYC activates cyclin D, CDK4, and CDK6 that complex to phosphorylate RB (Retinoblastoma). Release of RB frees E2F to activate transcription of its target genes required for S-phase. MYC also negatively regulates CKIs p21 and p27 to facilitate progression into S-phase. At S-phase, MYC activates cyclin A, which complexes with CDK1 and CDK2 to promote DNA replication. Cyclin A is continously expressed throughout G2. In the final phase, MYC activates cyclin B to complex with CDK1 and drive the cell through mitosis. CKIs from the INK4 family (inhibitors of CDK4) restrict reentry into G1, and these proteins (p16 and p15) are repressed by MYC.

and CDKs that outcompete p27 levels (Pérez-Roger *et al.* 1997; Bouchard *et al.* 1999) and induction of SCF^{SKP2} ubiquitin ligase components that ubiquitinate p27 (Bretones *et al.* 2011; Montagnoli *et al.* 1999). Protein levels of p27 are frequently downregulated in human cancer, and low p27 levels correlate with poor prognosis (Chu *et al.* 2008). These studies implicate MYC as a key transrepressor of tumour suppressor proteins.

After successful S-phase entry, MYC transcriptionally regulates the ORC (Origin recognition complex) genes *ORC1*, *ORC2*, *ORC4*, and *ORC5*, and the MCM (minichromosome maintenance) genes *MCM3*, *MCM4*, *MCM5* and *MCM6*, which are required for DNA replication, initiation, and elongation (Zeller *et al.* 2006). MYC also regulates a plethora of metabolic pathways (discussed in detail below) required for the biosynthesis of nucleotides (that are needed for DNA replication) (Liu *et al.* 2008). MYC regulation of the cell cycle at multiple stages implicates MYC as a 'master regulator' of cell proliferation. MYC regulation of other cell processes, such as activation of human telomerase (Wang *et al.* 1998), is likely to contribute to the ability of deregulated MYC to sustain proliferation and drive tumourigenesis.

1.2.2 The role of MYC in cell growth

Prior to S phase entry, normal cells first accumulate a critical biomass through macromolecular synthesis, which involves an accompanying increase in cell size (cell growth) (Pardee, 1974). This idea was pioneered in yeast where the 'start point' was described as a cell growth-regulated checkpoint for S-phase entry (Hartwell *et al.* 1970). Ribosome biogenesis and mitochondrial biogenesis are two processes that are essential to cell growth, and both of these processes are regulated by MYC (see subsections below).

The development of models with inducible *MYC* deletion was an essential breakthrough for *in vivo* studies because germline deletion of *MYC* was found to be embryonic lethal (Charron *et al.* 1992). Deletion of *MYC* in T lymphocytes prevented cell growth and proliferation in response to T cell receptor (TCR) stimulation by staphylococcal enterotoxin B (Wang *et al.* 2011). Analysis of general signaling pathways mediated by TCR and cytokines showed them to be largely intact, indicating the deletion of *MYC* specifically impairs activation-induced T cell growth and proliferation. Similar results to the T lymphocyte study were also documented in a model of intestinal cancer. Deletion of *MYC* in *APC*-deficient adult murine intestines inhibited colonic crypt cell growth and proliferation (Sansom *et al.* 2007), indicating MYC mediates much of the pathology associated with *APC* deletion. Importantly, these models of *MYC* deletion impacted on cell growth and cell proliferation; however models that uncouple these two processes have been documented.

A conditional *MYC* overexpression allele in B-lymphocytes demonstrated that cell proliferation was dependent on both MYC and foetal calf serum (FCS), while cell growth was regulated by MYC without FCS (Schuhmacher *et al.* 2001). This

demonstrated for the first time that MYC-driven cell growth was separable from cell proliferation, which required additional FCS-derived cellular cues. A distinct role for MYC regulation of cell growth has also been described *in vivo* using adenoviral gene transfer into liver cells (Kim *et al.* 2000).

1.2.2.1 The role of MYC in ribosome biogenesis

MYC was first hypothetically linked to ribosome biogenesis during *MYC* overexpression experiments, as increased protein synthesis would be required to support observed increases in cell proliferation and cell growth (Schuhmacher *et al.* 1999; Iritani and Eisenman, 1999). Second, overexpression experiments in Drosophila Melenogaster with the MYC homolog Dm resulted in increased nuclear, nucleolar, and overall cell size (Pierce *et al.* 2004). Third, expression of *MYC* in B-lymphocytes of transgenic mice increased overall cell size and protein synthesis (Schuhmacher *et al.* 2001).

Ribosome biogenesis is a highly coordinated process involving the transcription of ribosomal RNA (rRNA), processing of rRNA, incorporation of rRNA into pre-40S and pre-60S subunits, then maturation and assembly of ribosomal subunits into mature ribosomes in the cytoplasm (figure 1.3; reviewed in Van Riggelen *et al.* 2010a). MYC directly activates all three nuclear RNA polymerases I, II, and III (RNA pol I, II and III) (Gomez-Roman *et al.* 2003; Grandori *et al.* 2005; Arabi *et al.* 2005). Activation of RNA pol I and RNA pol II is required for rRNA transcription and processing, and activation of RNA pol III is required for transcription of 5S rRNA and transfer RNAs (tRNAs). Boon *et al.* (2001) documented that expression of *MYC* enhanced approximately 80% of ribosomal protein genes, as well as key genes involved in rRNA processing and assembly, nucleolin (*NCL*) and nucleophosmin (*NPM1*). MYC also directly activated six ribosomal protein genes *in vivo* (Kim *et al.* 2000), and transcriptionally activated eukaryotic initiation factors (eIFs) eIF4E, and eIF2α, which are required for translation initiation (Rosenwald *et al.* 1993).

The requirement for MYC regulation of ribosomal genes to initiate tumourigenesis has been explored *in vivo* (Barna *et al.* 2008). Ribosomal hemizygote mice were used as a genetic tool to reverse increased protein synthesis in Eμ-*Myc* (*Myc* driven by the immunoglobulin heavy chain enhancer) transgenic mice to normal levels (Adams *et al.* 1985). Loss of one allele of *Rpl24* or *Rpl38* decreased incidence of lymphoma by 20% and delayed tumour onset by over 100 days. In this context the oncogenic potential of MYC was suppressed by loss of translational control. Haploinsufficiency of *MYC* was found to prolong mouse lifespan and was associated with decreased ribosome biogenesis (Hofmann *et al.* 2015).

In humans, increased levels of individual ribosomal proteins have been found in breast (Henry *et al.* 1993), prostate (Vaarala *et al.* 1998), uterine cervix (Cheng *et al.* 2002), oesophagus (Wang *et al.* 2001), and liver carcinomas (Kim *et al.* 2004). Combined activation of all three RNA polymerases and specific activation of many ribosomal protein genes indicates that this is a major MYC-driven program promoting cell growth.

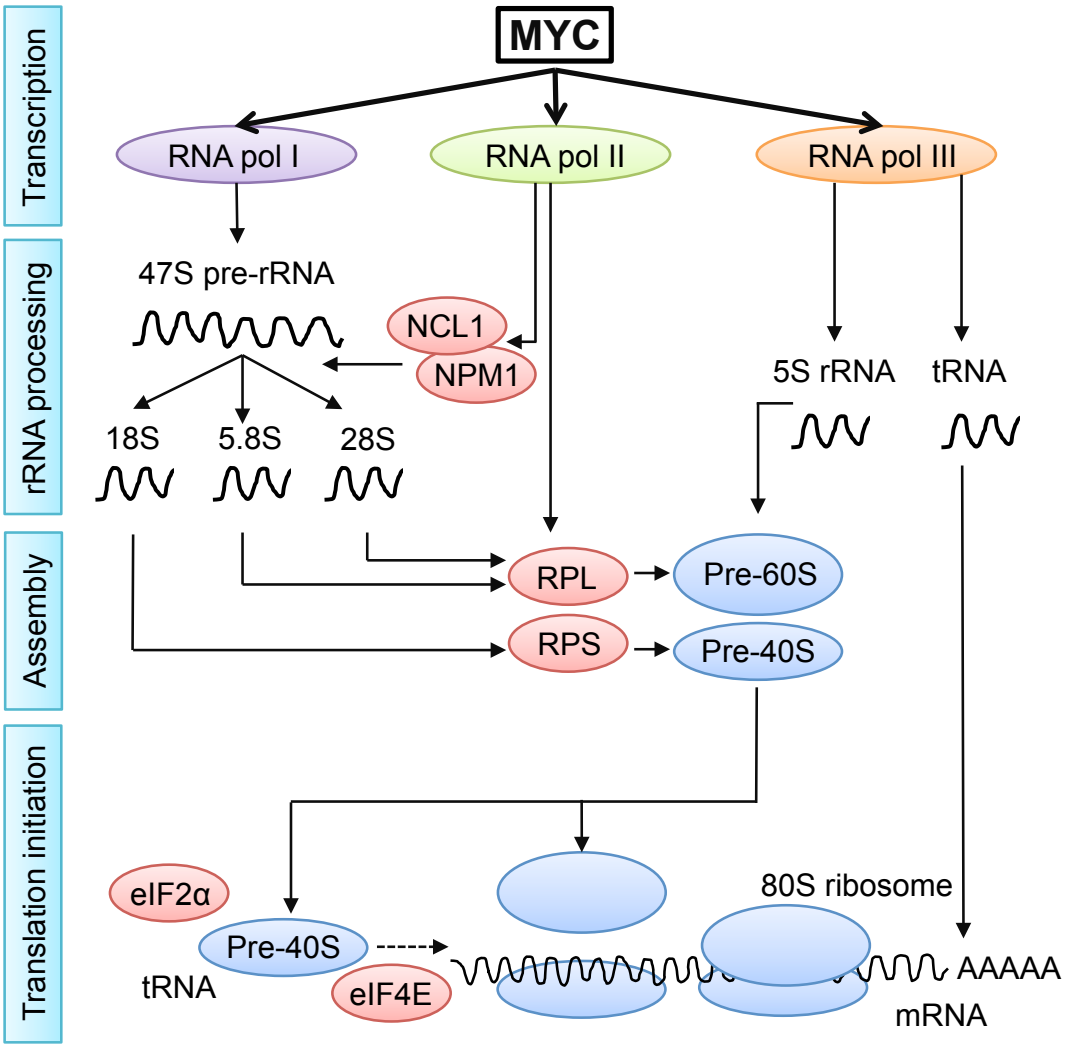

Figure 1.3. MYC regulation of ribosome biogenesis (adapted from Van Riggelen *et al.* 2010)
MYC activates all three RNA polymerases I, II, and III, which allows regulation of the four stages of ribosome biogenesis: transcription, rRNA processing, assembly, and translation initiation. Activation of RNA pol I and RNA pol II is required for rRNA processing to form the small ribosomal subunit (RPS) and large ribosomal subunit (RPL). RNA pol II synthesises nucleolin (NCL) and nucleophosmin (NPM1) that are involved in rRNA processing and export. Activation of RNA pol III is required for assembly of small and large ribosomal subunits into pre-40S and pre-60S subunits respectively. RNA pol III also encodes tRNA, which is required for translation of mRNAs by mature ribosomal subunits.

1.2.2.2 The role of MYC in mitochondrial biogenesis

Early studies on MYC identified several mitochondrial MYC target genes, including *SURF-1*, a serum-regulated complex IV assembly factor. *SURF-1* lacks an E-box site, and MYC binding at the *SURF-1* promoter is dependent on the transcription factor YY1 and its cognate binding site (Vernon and Gaston, 2000). Global analysis of the MYC transcriptome by chromatin immunoprecipitation (ChIP) analysis has highlighted MYC as a master regulator of mitochondrial biogenesis (Kim *et al.* 2008; Seitz *et al.* 2011). The genes identified as MYC targets can be broadly categorised into those involved in mitochondrial transcription, mitochondrial translation, protein import, and complex assembly (reviewed in Morrish and Hockenbury, 2014). Knockdown of several mitochondrial MYC target genes was synthetically lethal in *MYC* overexpressing cells, indicating that pharmacological inhibition of these genes may selectively kill MYC-driven tumour cells in human cancer (Sheth *et al.* 2014; Carroll *et al*. 2015).

Mitochondria are considered the 'powerhouses' of the cell, since they produce ATP by highly efficient oxidative phosphorylation and serve as a hub for multiple metabolic pathways. Mitochondrial mass also directly influences overall transcription rate in the cell (Wonsey *et al*. 2002; O'Donnell *et al.* 2006; Li *et al.* 2005). Despite clear evidence that MYC transcriptionally regulates mitochondrial biogenesis, understanding of the biological significance of this is far from understood. Studies of mitochondrial fusion and fission have implicated a role for MYC in controlling mitochondrial dynamics, in addition to structure and function (Graves *et al.* 2012). Deficiency in mitochondrial mass and morphology with loss of MYC function has been described in T cells and fibroblasts (Li *et al.* 2005).

1.2.3 The role of MYC in cell metabolism

To maintain cellular homeostasis and produce all of the precursors required for macromolecular synthesis and cell expansion, metabolic pathways must balance anabolism, ATP generation, and redox stability. This balance is sensed and maintained on two levels, transcriptionally and homeostatically. In recent years, metabolic reprogramming has been recognised as a cancer hallmark, with oncogene-driven metabolic adaptation being clonally selected for during tumourigenesis (reviewed in Ward and Thompson, 2012). MYC affects and regulates multiple metabolic pathways, including glycolysis, glutaminolysis, nucleotide biosynthesis, and lipid biosynthesis (reviewed in Stine *et al.* 2015; see subsections below).

1.2.3.1 The role of MYC in glycolysis

Increased aerobic glycolysis (increased conversion of glucose to lactate in the presence of oxygen) was one of the first described metabolic phenotypes associated with cancer (Warburg, 1956). *MYC*-transformed cells exhibit increased glucose uptake and increased expression of almost all glycolytic enzymes, including the glucose transporter *GLUT1* (Osthus *et al.* 2000). MYC activates lactate dehydrogenase-A (*LDHA*), which converts pyruvate to lactate, and *LDHA*

knockdown reduces MYC-driven cell growth (Shim *et al.* 1997). Furthermore, abrogation of lactate export, by inhibiting the activity of the MYC target MCT1 (a monocarboxylate transporter), was shown to reduce cell growth and tumourigenesis *in vivo* (Doherty *et al.* 2014; Brahimi-Horn *et al.* 2011).

Aside from lactate generation, glucose supplies carbon to key anabolic pathways, including phospholipid synthesis, the pentose phosphate pathway (PPP), amino-acid synthesis, and one-carbon metabolism (folate and methionine cycles). Following the conversion of glucose into glucose-6-phosphate (G6P) by hexokinase, G6P can be used to synthesise phosphatidic acid, from which other phospholipid species and triacylglycerol are built upon (reviewed in Vance, 2002). Alternatively, G6P can enter the PPP to generate ribose-5-phosphate for nucleotide biosynthesis, and the reducing cofactor NADPH from $NADP^+$. Finally, G6P can continue down the glycolytic pathway (see below). *MYC* deregulation in lymphocytes increased flux through glycolysis and the pentose phosphate pathway, and this was abrogated in MYC deficient cells (Wang *et al.* 2011). Expression of *MYC* increased ^{13}C labeling of ribose and purine nucleotides (Morrish *et al.* 2009).

Further down the glycolytic pathway, fructose 1,6-bisphosphate may be used to synthesise dihydroxyacetone-phosphate (DHAP) or glyceraldehyde 3-phosphate. DHAP is used to generate the glycerol head group of phospholipids (Eljamil, 2015). Glyceraldehyde 3-phosphate can be used to synthesise 3-phosphogylcerate in the glycolytic pathway. 3-phosphoglycerate can enter the serine synthesis pathway (SSP) which supports multiple pathways, including folate and methionine metabolism, nucleotide synthesis, and glutathione synthesis. These pathways have been described as essential for cancer cell proliferation (reviewed in Locasale, 2013). Serine conversion to glycine by serine hydroxymethyl transferase (SHMT) donates one-carbon to tetrahydrofolate (THF) to yield 5,10-methylene-tetrahydrofolate (me-THF). *MYC* induction increased the expression of approximately half of the genes involved in folate metabolism (Morrish *et al.* 2008), and *SHMT2* was one of few genes shown to partially rescue the slow growth phenotype of *MYC* null fibroblasts (Nikiforov *et al.* 2002). Lewis *et al.* demonstrated that SHMT2 contributed to mitochondrial NADPH and glycine pools, and that this was the predominant method of NADPH regeneration in the cells studied (Lewis *et al.* 2014).

In addition to the SSP, cells can take in exogenous serine and glycine, and Eμ-*Myc* mice showed significantly extended survival with dietary serine and glycine restriction (Maddocks *et al.* 2017). Activation of *Myc* was shown to increase SSP enzyme expression; however the reduced survival of Eμ-*Myc* mice indicates exogenous serine uptake is essential in *Myc*-driven tumours. Eμ-*Myc* tumours showed depleted GSH/GSSG ratios, and genetic modification that reduced reactive oxygen species (ROS) increased survival time. Another study in colorectal cancer cells showed that serine was utilised for *de novo* synthesis of ATP, which was required to convert methionine to S-Adenosyl methionine (SAM) for methylation reactions (Maddocks *et al.* 2016). These studies highlight the relevance of one-carbon metabolism to cancer and MYC biology, and indicate that dietary restriction of serine may be of therapeutic relevance in MYC-driven cancer.

1.2.3.2 The role of MYC in glutaminolysis

Glutaminolysis is the direction of glutamine into the TCA cycle. Glutaminolysis is a key support mechanism in cells that divert most of their glycolytic intermediates into anabolic pathways and lactate, instead of diverting pyruvate into the TCA cycle (Jin *et al.* 2016). MYC activates the glutamine transporter *SLC1A5*, and enhance mitochondrial glutaminase expression through the suppression of miR23a/b (Wise *et al.* 2008; Gao *et al.* 2009). Metabolic stable heavy-isotope tracer studies confirmed that glutaminolysis is increased by MYC (Murphy *et al.* 2013). Glutamine is also an essential amine donor for purine and pyrimidine nucleotide biosynthesis, and the dependency of *MYC* overexpressing cells on glutamine is highlighted by these cells becoming dependent upon glutamine (Yuneva *et al.* 2007).

1.2.3.3 The role of MYC in nucleotide biosynthesis

Genes involved in nucleotide biosynthesis were among the first discovered MYC-target genes, and ChIP experiments in multiple systems showed that MYC binds and activates eleven nucleotide biosynthesis enzymes. Nucleotides are required for RNA synthesis and DNA synthesis, and knockdown of *IMPDH2* (inosine-5'-monophosphate dehydrogenase 2) triggered S-phase arrest (Liu *et al.* 2008). Concomitantly, knockdown of *MYC* in several cell lines decreased expression of genes involved in nucleotide biosynthesis and triggered proliferative arrest. Ectopic expression of MYC target genes *TS* (thymidylate synthase), *IMPDH2*, or *PRPS2* (phosphoribosyl pyrophosphate synthetase 2) relieved the proliferative arrest cause by *MYC* knockdown (Mannava *et al.* 2008). PRPS2 is the rate-limiting step in purine nucleotide synthesis, and its knockdown was synthetically lethal in *MYC* overexpressing cells. Further, *PRPS2* loss prolonged the survival of transgenic mice with MYC-driven lymphoma, and induced complete tumour remission in 30% of mice (Cunningham *et al.* 2014). These studies highlight the key role of MYC in regulating nucleotide biosynthesis, and the relevance of nucleotide metabolism to MYC-driven cancer.

1.2.3.4 The role of MYC in lipid synthesis

The importance of lipid metabolism in dividing cells is a rapidly emerging area of cell metabolism. Lipids have numerous biological functions as both signalling molecules and as membrane structural components that alter membrane permeability and curvature (reviewed in Eljamil, 2015). The relevance of lipid composition to cell division was recently revealed in a study that compared synchronised Hela cells at cytokinesis to cells at S-phase (Atilla-Gokcumen *et al.* 2014). From the numerous lipid species analysed, 11 species increased at least 4-fold during S-phase, of which 8 belonged to the sphingolipid subclass. The study went on to screen a custom RNAi library targeting 244 lipid biosynthetic enzymes and individual knockdown of 23 genes (involved in sphingolipid, sterol, glycerolipid, and fatty acid metabolism) caused cytokinesis failure. Knockdown of the top 3 screen hits caused delayed

metaphase and showed unusual membrane blebbing, highlighting that lipid composition is crucial for normal cell division.

Fatty acids (FAs) are the precursors to lipids, and MYC targets include ATP citrate lyase (*ACLY*), acetyl CoA carboxylase alpha (*ACACA*), and fatty acid synthase (*FAS*). These genes are all involved in the *de novo* synthesis of saturated FAs (SFAs) up to the length of palmitate (16 carbons) in the cytosol. MYC also activates stearoyl-CoA desaturase (*SCD*), which is the rate-limiting step of monounsaturated FA (MUFA) synthesis (Zeller *et al.* 2003; Loven *et al.* 2012). Elongation and desaturation of FAs ≥16 carbons in length predominantly occurs in the endoplasmic reticulum (ER). Elongation is catalysed in a series of four enzymatic reactions: condensation, reduction, dehydration, and reduction (reviewed in Sassa and Kihara, 2014). Malonyl-CoA donates 2 carbon units with each turn of the cycle (figure 1.4). FAs from cytosolic or microsomal synthesis may be stored as neutral lipids, metabolised into sphingolipids or phospholipids, or catabolised by fatty acid oxidation (FAO, otherwise known as β-oxidation) to generate ATP. Peroxisome proliferator-activated receptors (PPARs) are a unique family of transcription factors that sense and interpret changes in FAs to modulate lipid homeostasis (reviewed in Varga *et al.* 2011).

MYC overexpression was recently shown to remodel the lipidome. Eberlin *et al.* (2014) documented distinct lipid signatures in MYC- or RAS-induced lymphoma, and predicted that this was dominated by MYC-driven lipid changes. Hall *et al.* (2016) also documented a distinct lipid shift in KRAS-driven lung adenocarcinoma with reversible activation of *Myc*. *Myc* activation increased relative levels of phosphatidylinositols and arachidonate-containing phospholipids that can serve as signalling precursors; and these changes were reversed by *Myc* inactivation. Hall *et al.* went on to show that inhibition of COX/5-LOX pathways (eicosanoid pathways downstream of arachidonic acid) reduced tumour burden *in vivo* due to reduced cell proliferation.

Several studies have also linked MYC-driven tumours to increased fatty acid oxidation (FAO). FAO intermediates were markedly increased in a MYC-driven model of triple negative breast cancer (TNBC). Pharmacologic inhibition of FAO *in vivo* and in a TNBC patient-derived xenograft reduced tumour size (Camarda *et al.* 2016). Similar results were seen with a MYC-driven Burkitt's lymphoma model by inhibiting FA import into mitochondria (Pacilli *et al.* 2013). Conversely, while MYC-driven tumours increase FAO, knockout of *Myc* in rat fibroblasts was also shown to increase FAO (Edmunds *et al.* 2014). Further studies to understand the effects of MYC on lipid metabolism in different contexts are needed.

1.2.4 The role of MYC in cell differentiation

MYC is a key regulator of cell differentiation, and its ability to induce dedifferentiation and maintain this stem-like state has been described in multiple (although not all) systems (reviewed in Soucek and Evan, 2010). *In vivo*, *Myc* activation in the intestinal epithelium induced dedifferentiation of mature goblet cells

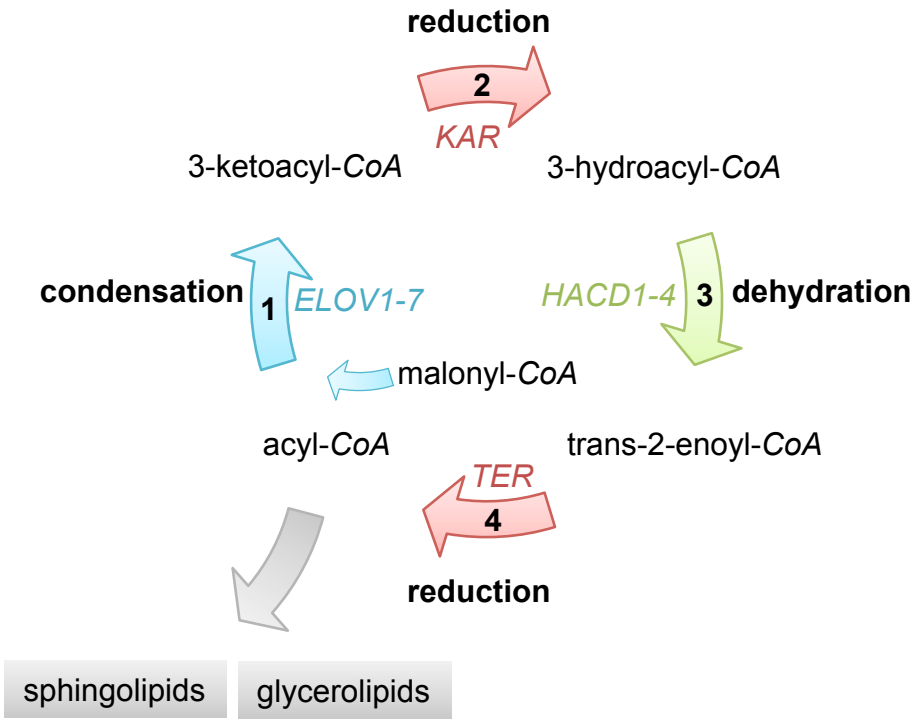

Figure 1.4. Microsomal fatty acid elongation cycle (adapted from Sassa and Kihara, 2014)

The microsomal fatty elongation cycle involves 4 enzymatic steps. The first step involves condensation of a fatty acyl CoA (≥16 carbons in length) with malonyl-CoA, which is the 2 carbon donor for the elongation reaction. ELOVL enzymes 1-7 catalyse this step with differing specificities for chain length and desaturation. The 3-ketoacyl-CoA is reduced to form a 3-hydroacyl-CoA, dehydrated to trans-2-enoyl-CoA, and reduced again to an acyl-CoA with 2 additional carbon units. The fatty acyl-CoA may be further elongated, or directed for sphingolipid or glycerolipid synthesis if it is to be used for anabolic pathways. ELOVL=fatty acid elongase, KAR=3-ketoacyl-CoA reductase, HACD=3-hydroxyacyl-CoA dehydratase, TER= trans-2-enoyl-CoA reductase.

(Finch *et al.* 2009). *Myc* activation and co-expression of *Bcl-xl* in pancreatic islet β cells induced dedifferentiation in two independent studies (Pelengaris *et al.* 2002; Finch *et al.* 2006). A recent study of regeneration in adult echinoderms found *Myc* overexpression was required for proper dedifferentiation of radial glial cells at the site of injury (Mashanov *et al.* 2015). These studies indicate the relevance of MYC induced dedifferentiation in multiple biological contexts.

MYC maintains self-renewal properties and represses differentiation by regulating miRNAs (Lin *et al.* 2009). *Myc* activation in keratinocytes disrupted differentiation and caused papillomatosis that rapidly regressed following *Myc* deactivation. Concomitantly, loss of MYC induces differentiation in multiple systems (Knoepfler *et al.* 2002; Shachaf *et al.* 2004; Sansom *et al.* 2007). Several studies have shown opposing effects of MYC on differentiation, indicating that in some contexts MYC can promote differentiation (Gandarillas and Watt, 1997; Arnold and Watt, 2001). The majority of evidence implicates MYC as a key regulator of dedifferentiation however, and this is clearly demonstrated by the discovery that MYC is one of the four factors that when combined can reprogram differentiated cells to the induced pluripotent stem (iPS) cell state (Takashi and Yamanaka, 2006).

1.3 p53 - Guarding against MYC deregulation

The cellular impact of deregulation of oncogenes such as *MYC* is restrained in the cell by activation of tumour suppressor genes, in a response often termed 'oncogene-induced tumour suppression'. Tumour suppressor genes implement tumour suppressive pathways to resist tumourigenesis. These pathways include cell cycle checkpoints, apoptosis, senescence, DNA repair, metabolism, and redox balance (reviewed in Levine and Puzio-Kuter, 2010).

For tumourigenesis to occur, a cell must acquire several mutations in oncogenes and tumour suppressor genes (reviewed in Vogelstein and Kinzler, 1993). This step-wise progression of pathogenesis is clearly demonstrated in colorectal cancer where a specific series of mutations are documented to accumulate over 20-40 years before malignant transformation occurs (figure 1.5; reviewed in Fearon and Vogelstein, 1990). Somatic mutation of the p53 tumour suppressor gene (*TP53*) is the most common lesion detected in human cancer and affects a broad range of human cancer types (figure 1.6). Germline mutations in *TP53* predispose a person to early-onset cancers, including breast carcinomas, sarcomas, brain tumors, and adrenal cortical carcinomas (Li *et al.* 1988; Olivier *et al.* 2003). The predisposition to these cancers is defined by Li-Fraumeni syndrome (Olivier *et al.* 2003).

The majority of *TP53* mutations are missense mutations in the DNA-binding domain (Petitjean *et al.* 2007). Outside this region missense mutations are less common and the majority of mutations are nonsense of frameshift. Mutations in the DNA-binding domain are are at residues that make contact with the DNA (e.g. R248) or support the structure of the DNA-binding surface (e.g. R249) (Joerger *et al.* 2007), indicating the importance of p53 transcriptional targets in resisting tumourigenesis. To

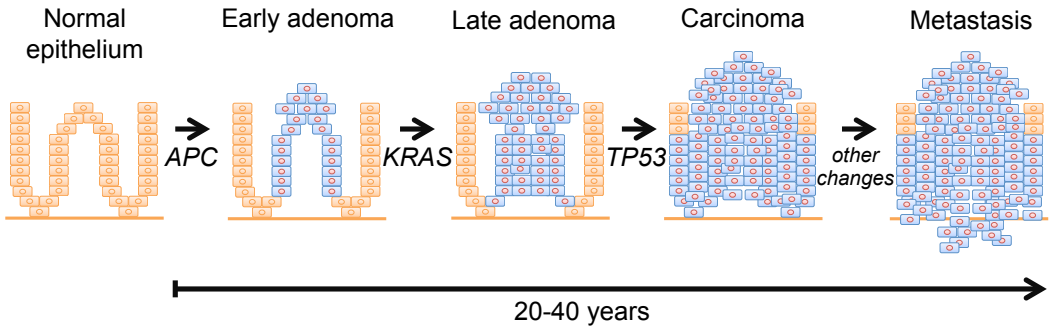

Figure 1.5. A step-wise model of colorectal tumourigenesis (adapted from Rajagopalan *et al.* 2003)

The development of colorectal cancer is documented to occur over a period of 20-40 years due to the sequential accumulation of specific mutations. Initiation of this process is predominantly caused by inactivation of the *APC* (adenomatous polyposis coli) tumour supressor gene. Mutation of oncogene *KRAS* often preceeds large polyp formation, and 10-20% of these polyps progress to cancer by aquiring an additional mutation such as loss of the p53 pathway.

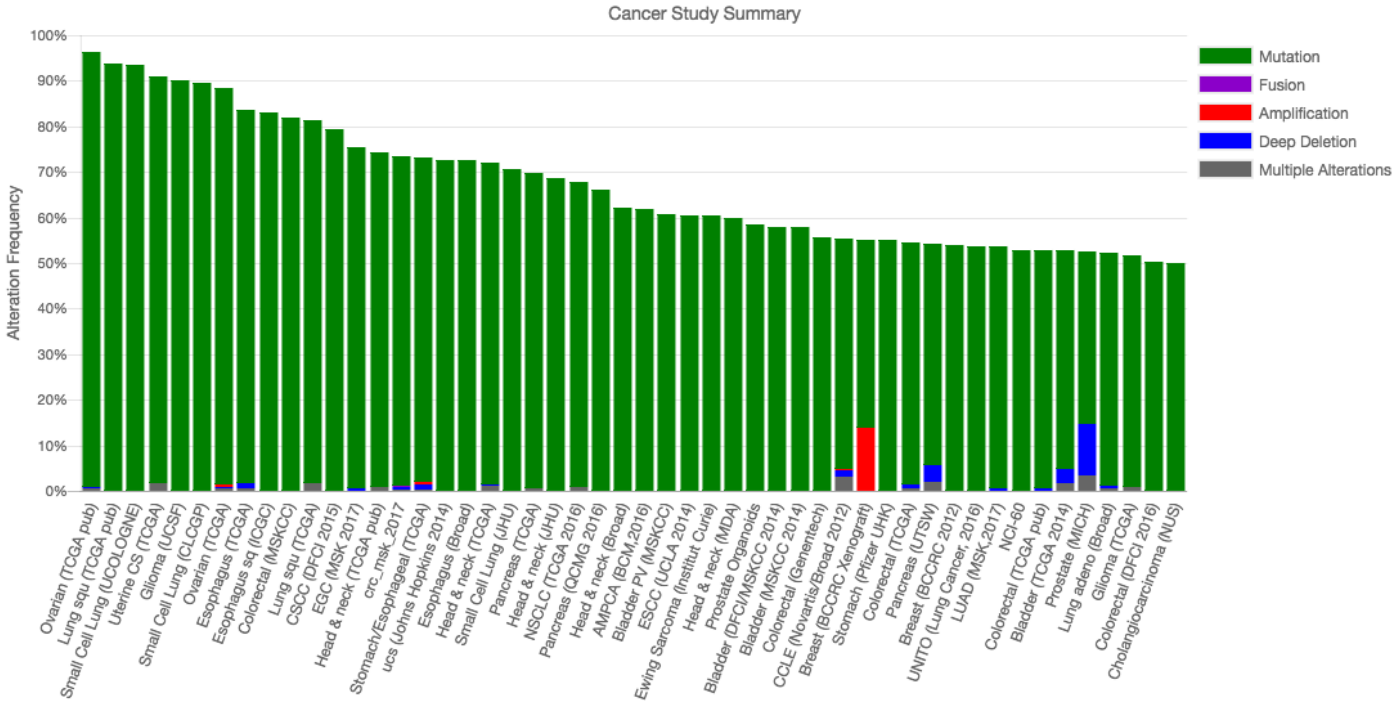

Figure 1.6. *TP53* mutation frequency in human cancer (Cerami *et al.* 2012; Gao *et al.* 2013)
Barplot shows the frequency of *TP53* mutation and copy number alteration based on 169 combined cancer studies. *TP53* mutation is the most common lesion detected in human cancer, with frequencies ranging from 95% to 50% in the cancer studies shown above. Details on individual studies used to generate this dataset may be obtained from cBioPortal for Cancer Genomics (Cerami *et al.* 2012; Gao *et al.* 2013), which was also used to create this barplot.

determine the functional effect of missense mutations (in a yeast-based functional assay), Kato *et al.* (2007) tested 2314 missense mutants for their activity at 8 different p53 response elements. All hotspot mutants showed decreased transcriptional activity at p53 response elements, fitting with a tradiotional tumour suppressor model whereby mutation of a tumor suppressor gene reults in loss of protein function. However, a small group of mutants showed partial or enhanced activity at p53 response elements, the latter of which indicates a gain of function mutation. Further studies *in vivo* using knockin of hotspot mutants *R175h* and *R273h* (Lang *et al.* 2004; Olive *et al.* 2004) showed increased metastasis compared to *Tp53* knockout mice. This confirmed that *TP53* gain of function mutants did indeed have relevance *in vivo.* Mutant p53 proteins can also exert dominant negative effects on wild-type p53 (Petitjean *et al.* 2007). This is because p53 tetramer formation is required for DNA-binding in all four DNA quarter-sites (McLure and Lee, 1998). Research is ongoing to determine the relevance of these rare mutants in human cancer (reviewed in Olivier *et al.* 2010).

MYC expression stabilises and activates p53, although *TP53* is not a direct transcriptional target of MYC (Hermeking and Eick, 1994; Lindström and Wiman, 2003). p53 is stabilised and activated by a series of post-translational modifications, including phosphorylations, acetylations, methylations, ubiquitinations, and sumoylations (figure 1.7; reviewed in Lavin and Gueven, 2006). Several modifications in the N-terminal domain stabilise p53 by releasing it from its interacting protein MDM2 (mouse double minute 2). MDM2 is a ubiquitin ligase that ubiquitinates p53 prior to its proteosomal degradation. MDM2 is also modified during stress conditions to facilitate p53 stabilisation. Several ribosomal proteins, including RPL5, RPL11, and RPL23, bind and block MDM2 activity in response ribosomal stress (reviewed in Zhang and Lu, 2009). $p14^{ARF}$ (mouse $p19^{ARF}$) is also an important negative regulator of MDM2, and *MYC* expression induces the expression of *CDKN2A* by an unknown mechanism (Zindy *et al.* 1998).

$p14^{ARF}$ is a tumour suppressor protein encoded at the *INK4A* locus. The *INK4A* locus also encodes $p16^{INK4A}$ (also a tumour suppressor protein), and the two proteins are translated by alternative reading frames (hence the acronym ARF). Deletion of *CDKN2A* from *TP53* knockout mice accelerated tumour formation (Weber *et al.* 2000), indicating a tumour suppressive function(s) of $p14^{ARF}$ that is p53-independent. Several studies have highlighted the importance of the $p14^{ARF}$-MDM2-p53 axis in resisting tumourigenesis (Pomerantz *et al.* 1998; Zhang *et al.* 1998; Kamijo *et al.* 1998; Stott *et al.* 1998).

p53 modulates several tumour suppressive pathways, and the choice of response activated by p53 may be driven by levels of stress and affinity for target gene binding (Vousden, 2000). In this model, low levels of stress (such as transient nutrient depletion) induce levels of p53 that activate high affinity growth arrest genes. In contrast, high levels of stress (such as acute DNA damage) would be sufficient to induce low affinity pro-apoptotic genes as well (Inga *et al.* 2002). This model fits with the counterintuitive observation that *TP53* is often mutated at a late

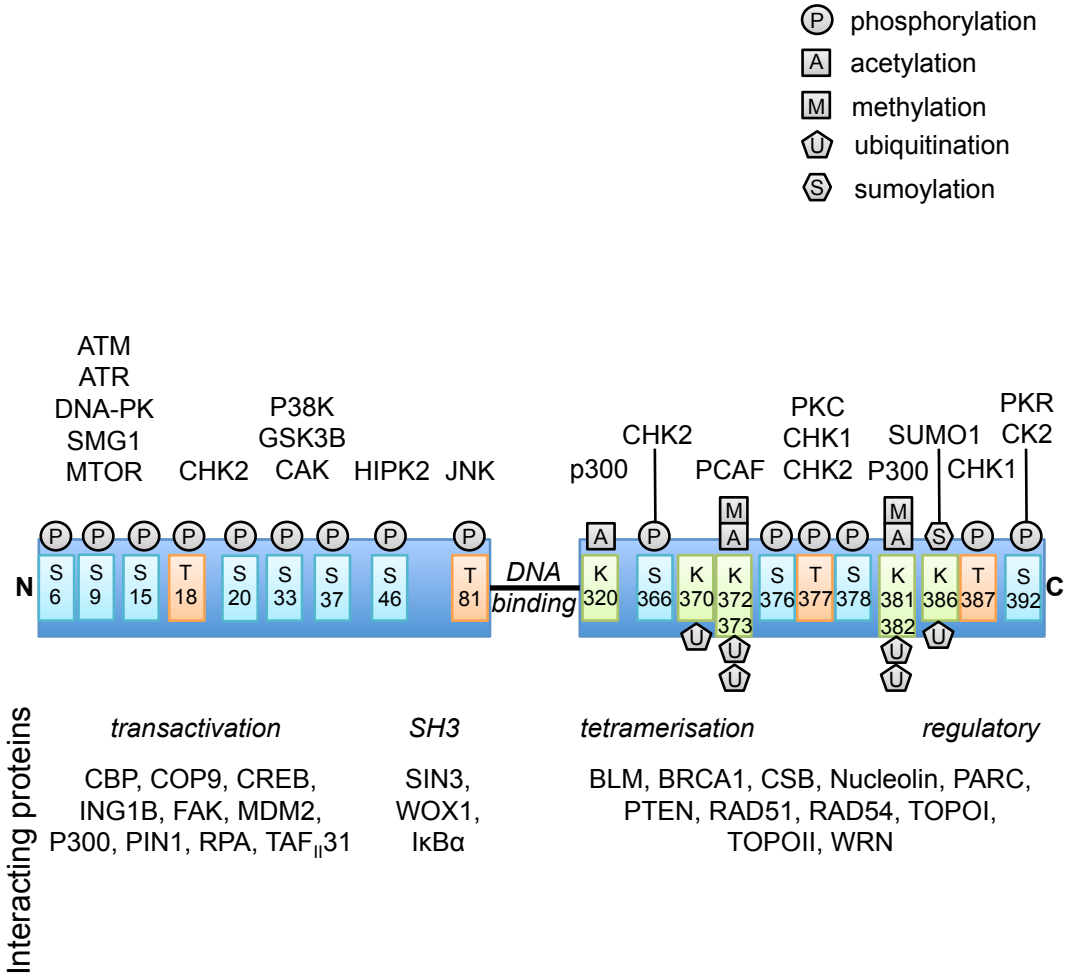

Figure 1.7. Post-translational modifications that stabilise and activate p53 (adapted from Lavin and Gueven, 2006)

Proteins that phosphorylate, acetylate, methylate or sumoylate p53 at a range of different sites across the protein are depicted in the upper portion of this schematic. Where modification occurs at the same or adjacent sites this is shown, for example, at K381, K382 methylation and acetylation. Sites of ubiquitination are represented by pentagons under the schematic. The transactivation, SH3, DNA binding, tetramerisation and regulatory domains of p53 are outlined. Proteins that interact with these domains are depicted at the bottom of the figure, for example MDM2 interacts with the N-terminal transactivtion domain. ATM=ATM serine/threonine kinase, ATR=ATR serine/threonine kinase, DNA-PK=protein kinase, DNA-activated, SMG1=SMG1, nonsense mediated mRNA decay associated PI3K related kinase, MTOR=mechanistic target of rapamycin kinase, CHK2=checkpoint kinase 2, P38K=P38 mitogen-activated protein kinases, GSK3B=glycogen synthase kinase 3 beta, CAK=cyclin-dependent kinase activating kinase, HIPK2=homeodomain-interacting protein kinase 2, JNK=c-Jun N-terminal kinase, p300=E1A binding protein p300, PCAF=p300/CBP-associated factor, PKC=protein kinase C, CHK1=checkpoint kinase 1, SUMO1=small ubiquitin-related modifier 1 precursor, PKR= protein kinase RNA-activated, CK2=casein kinase 2, CREB=cyclic-AMP response element binding protein , CBP=CREB-binding protein, COP9=COP9 signalosome, ING1B=inhibitor of growth 1B, FAK=focal adhesion kinase, MDM2=mouse double minute 2 homolog, PIN1=peptidyl-prolyl cis-trans isomerase NIMA-interacting 1, RPA=replication protein A, $TAF_{II}31$=transcription initiation factor IID, SIN3=SIN3 transcription regulator, WOX1=WUSCHEL-related homeobox 1, IκBα=nuclear factor of kappa light polypeptide gene enhancer in B-cells inhibitor, alpha, BLM=bloom syndrome recq like helicase, BRCA1=breast and ovarian cancer susceptibility protein 1, CSB=CS complementation group B protein, PARC=cullin-9, PTEN=phosphatase and tensin homolog, RAD51=RAD51 recombinase, TOPOI=DNA Topoisomerase I, TOPOII=DNA Topoisomerase II, WRN=werner syndrome recq like helicase.

stage of tumour development (such as in colorectal cancer, figure 1.5) when the high stress associated with oncogene burden would otherwise trigger apoptosis. The role of p53 and other tumour suppressor genes in guarding against MYC deregulation is discussed in the following subsections.

1.3.1 The role of p53 in cell cycle checkpoints

Cell cycle arrest in response to cellular stresses such as DNA damage is triggered by p53 at multiple checkpoints (Giono and Manfredi, 2006). Cell cycle arrest in response to exogenous *MYC* activation occured specifically at the G2 checkpoint (Felsher *et al.* 2000). Arrest at G2 was dependent on p53 and its downstream effector p21, as loss of either gene permitted proliferation when *MYC* was activated. Arrest in G2 rather than G1/S may be because MYC is capable of overriding cell cycle inhibitors at the G1/S checkpoint (Felsher and Bishop, 1999). Finch *et al.* also described an *Arf/p53*-dependent proliferative checkpoint in response to *Myc* activation *in vivo* (Finch *et al.* 2006).

1.3.2 The role of p53 in apoptosis

p53 is a master regulator of apoptosis, stimulating both death receptor signaling and mitochondrial perturbation (Vousden, 2000). In response to stress p53 transcriptionally activates multiple genes involved in apoptosis, including *BAX*, *TP53I3*, *TNFRSF10B*, *FAS*, *TP53AIP1*, *PERP*, and BH3-only proteins NOXA and PUMA (reviewed in Riley *et al.* 2008). p53 also has transcription-independent functions that promote apoptosis such as localising to the mitochondria and inducing mitochondrial outer membrane permeabilisation (Mihara *et al.* 2003; Green and Kroemer, 2009).

Constitutive expression of *MYC* leads to increased apoptosis in multiple biological systems, highlighting apoptosis as a key tumour suppressive mechanism in resisting MYC deregulation (Askew *et al.* 1991; Evan *et al.* 1992). Further, MYC deregulation was shown to sensitise cells to multiple apoptotic triggers such as serum withdrawal (Evan *et al.* 1992), glutamine withdrawal (Yuneva *et al.* 2007), and treatment with death receptor ligands such as TNF (Klefstrom *et al.* 1994) or TRAIL (Lutz *et al.* 1998). While p53 clearly activates apoptosis in response to multiple cellular stresses, the precise role of p53 in MYC-induced apoptosis is less clear. Hermeking and Eick (1994) showed that loss of *TP53 in vitro* attenuates MYC-induced apoptosis and drives cell cycle entry, indicating that p53 mediates MYC-induced apoptosis in this system. Several other studies show that loss of *TP53 in vivo* accelerates MYC-driven tumourigenesis; however this was due to enhanced proliferation not reduced apoptosis (Elson *et al.* 1995; Hsu *et al.* 1995; Finch *et al.* 2006). These *in vivo* studies indicate that p53 does not mediate MYC-induced apoptosis, and that loss of *TP53* does not engage an alternative apoptotic response despite accelerating proliferation. The synergistic importance of *MYC* overexpression and *TP53* loss is discussed further in the next section.

A homeostatic metabolic model may better describe MYC-induced apoptosis. MYC-induced apoptosis is linked to the status of pro-apoptotic and anti-apoptotic BCL-2 members, which have clear metabolic roles in the mitochondria. Anti-apoptotic BCL-2 members BCL-2 and BCL-XL protect against apoptosis associated damage such as reactive oxygen species (ROS), mitochondrial membrane potential decline, and impaired nucleotide exchange and respiratory control (Gottlieb et al. 2000, 2002, Vander Heiden et al. 1997, 1999, 2001; Hockenbery et al. 1993). Concomitantly, expression of *BCL-2* or *BCL-XL* was shown to block MYC-induced apoptosis (Fanidi *et al.* 1992). Pro-apoptotic BCL-2 family members BAX or BAK-1 are required for MYC-induced apoptosis (Brunelle *et al*. 2004; Dansen *et al.* 2006; Eischen *et al.* 2001), and the pro-apoptotic function of BAX may require the mitochondrial ATPase (Matsuyama et al., 1998). The requirement for BCL-2 family members to modulate MYC-induced apoptosis, and the function of BCL-2 family members in mitochondrial nucleotide metabolism led us to uncover a metabolic basis for MYC-induced apoptosis (unpublished data).

1.3.3 Senescence

Only recently was *MYC* overexpression shown to induce cell senescence under some circumstances. This tumour suppressive mechanism may be important in regressing MYC-driven tumours. Senescence was first observed during the propagation of human cells in culture, with the cells eventually arresting whilst retaining viability and metabolic activity (Hayflick and Moorhead, 1961). A decade later it was shown that replicative senescence was induced by telomere shortening (Olovnikov, 1970; Watson, 1972). Later it was shown that senescence was induced independently of telomere shortening by cell stresses such as oncogene activation or tumour suppressor gene loss (Serrano *et al.* 1997; Chen *et al.* 2005). In addition to growth arrest, senescent cells were shown to share several distinct biomarkers, including morphological transformation, activation of tumour suppressor networks, induction of senescence-associated β-galactosidase activity, appearance of senescence-associated heterochromatic foci, and release of a senescence-associated secretary phenotype (SASP) (Kuilman *et al.* 2010).

MYC overexpression alone does not induce senescence; however perturbation of two genes, Werner gene (*WRN*) or cyclin dependent kinase 2 (*CDK2*), induced senescence. MYC was shown to transcriptionally activate *WRN*, a conserved RecQ helicase, and loss of *WRN* led to genomic instability and induction of senescence (Grandori *et al.* 2003). This indicated that *WRN* activation by MYC may promote tumourigenesis through evasion of senescence. Further mechanistic insight into MYC-induced senescence was documented in two papers (Campagner *et al.* 2010; Hydbring *et al.* 2010). Campagner *et al.* showed that prolonged expression of *MYC* in *CDK2* knockout cells induced senescence, and this was dependent on p16, p21, p27 and retinoblastoma (RB). Overexpression of *MYC* causes evasion of senescence by oncogenic *KRAS*, and Hydbring *et al.* showed that this was dependent on CDK2-mediated phosphorylation of MYC at Serine 62. Importantly, knockdown of *CDK2* forced senescence in the presence of two oncogenes. Identification of this mechanism has significant implications for MYC-driven tumours, as

pharmacological inhibition of CDK2 could regress tumours through induction of senescence.

1.3.4 Metabolism and redox balance

The function of p53 in permanently halting pro-tumourigenic cells (through initiation of cell cycle arrest or apoptosis) has been well documented. More recently, p53 was shown to promote cell survival through regulation of metabolic pathways (reviewed in Kruiswijk *et al.* 2015). p53-driven metabolic changes include inhibition of glycolysis, gluconeogenesis, the pentose phosphate pathway (Jiang *et al.* 2011), and inhibition of the expression of NADPH-producing malic enzymes (Jiang *et al*. 2013) to block anabolism (in contrast to MYC). p53 also promotes oxidative phosphorylation (OXPHOS) (Matoba *et al.* 2006), and FAO (Assaily *et al.* 2011) to support ATP generation (figure 1.8). In support of p53 responding to cell stress, p53 directly responds to nutrient deprivation conditions (Liu *et al.* 2014a; Heoferlin *et al.* 2013; Shiraki *et al.* 2014).

Glycolysis and gluconeogenesis (the production of glucose from non-carbohydrate carbon sources) essentially generate similar intermediates, and p53 directly and indirectly inhibited multiple enzymes in both pathways. p53 transcriptionally repressed glucose transporters *GLUT1* and *GLUT4*, and indirectly inhibited GLUT3, thus preventing glucose uptake (Zhang *et al.* 2013; Kawauchi *et al.* 2008). p53-induced activity of TIGAR (TP53-inducible glycolysis and apoptosis regulator) inhibited phosphofructokinase 1 (PFK1), the rate-limiting step in glycolysis, through reduction in levels of its allosteric regulator fructose 2,6-bisphosphate. TIGAR expression reduced levels of reactive oxygen species, and TIGAR knockdown sensitised cells to p53-induced apotosis (Bensaad *et al.* 2006). Bensaad *et al.* concluded that inhibition of PFK1 diverted glycolytic carbon through the pentose phosphate pathway. As the pentose phosphate pathway generates NADPH and ribose-5-phosphate this would restore redox homeostasis and may also support the DNA repair activity of p53 (through increased nucleotide biosynthesis). In contradiction, p53 inhibited the first step of the pentose phosphate pathway G6PDH (glucose-6-phosphate dehydrogenase) (Jiang *et al.* 2011) and expression of malic enzymes (Jiang *et al.* 2013), both of which generate NADPH. More research is needed to determine cellular contexts in which p53 promotes or restricts diversion of glycolytic carbon into the pentose phosphate pathway, as demonstrated by the contradictory results of these two studies.

In opposition to the terminal conversion of pyruvate to lactate, p53 increased the activity of pyruvate dehydrogenase (PD), which converts pyruvate to acetyl-CoA in the mitochondrial matrix (Contractor and Harris, 2012; Zhang *et al.* 2011). Flux through the TCA cycle generates important reducing agents (NADH and $FADH_2$) for OXPHOS. p53 activated synthesis of cytochrome C oxidase 2 (SCO2), which positively regulates mitochondrial cytochrome C oxidase (COX) assembly, and therefore electron transport chain homeostasis (Matoba *et al.* 2006). OXPHOS is by far the most efficient way of producing ATP; however a byproduct of OXPHOS is generation of the superoxide anion radical (Cadenas and Davies, 2000). p53 may

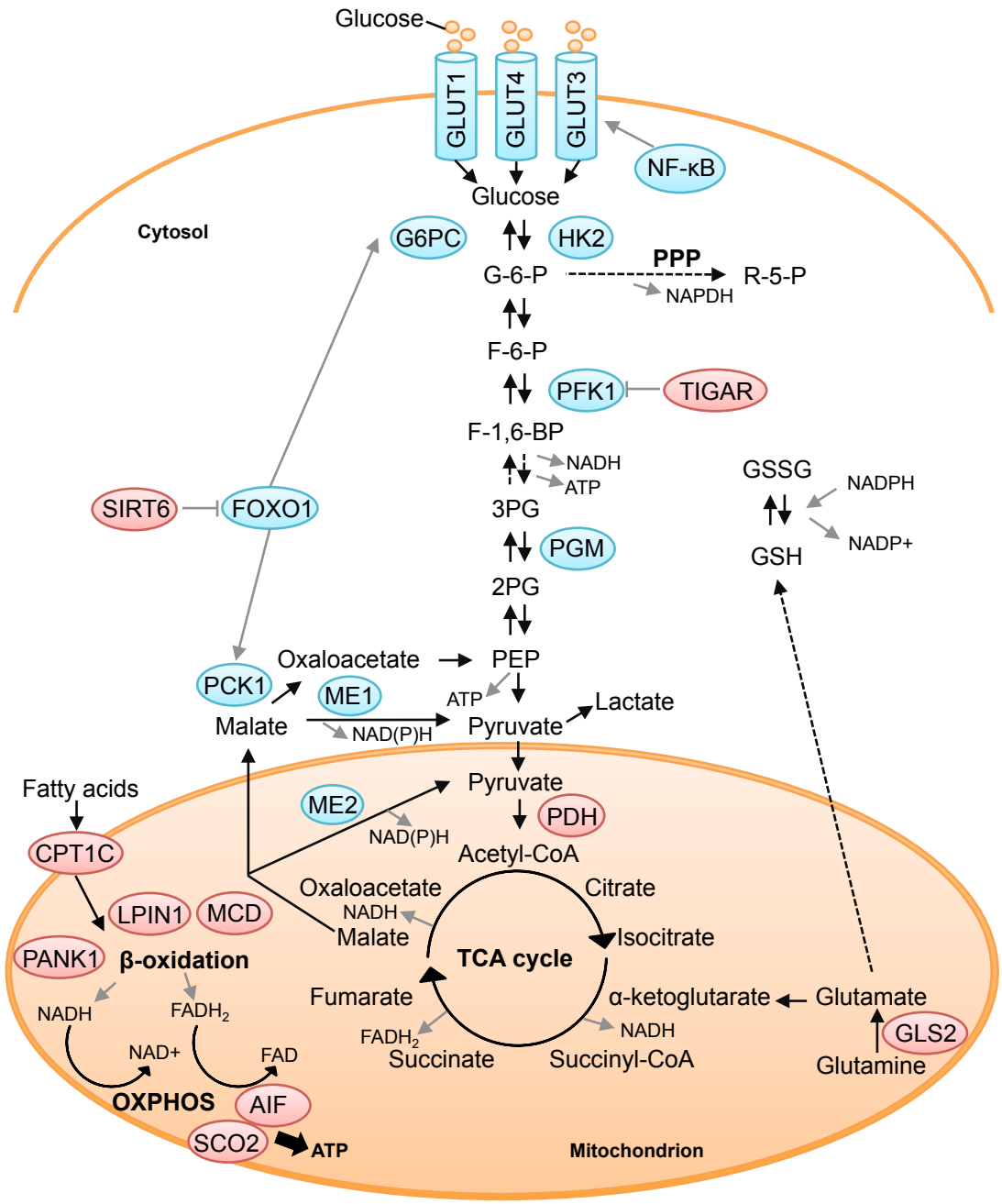

Figure 1.8. p53 regulation of metabolic pathways (adapted from Kruiswijk *et al.* 2015)

p53 limits the glycolytic rate by inhibiting glucose transporters GLUT1, GLUT3, and GLUT4, and glycolytic enzymes HK2, PFK1, and PGM. p53 inhibits gluconeogenesis through activation of SIRT1, which inhibits FOXO1 target genes *G6PC* and *PCK1*. p53 promotes OXPHOS indirectly by activating PDH and GLS2 to direct carbon into the TCA cycle, and directly by stimulating AIF and SCO2. p53 promotes FA uptake and β-oxidation by stimulating MCD, LPIN1, and PANK1. GLUT=glucose transporter type; HK2=hexokinase 2; PFK1=phosphofructokinase 1; PGM=phosphoglycerate mutase; SIRT1=sirtuin 1; FOXO1=forkhead box protein O1; G6PC=glucose-6-phosphatase; PCK1=phosphoenolpyruvate carboxykinase; OXPHOS=oxidative phosphorylation; PDH=pyruvate dehydrogenase; GLS2=glutaminase 2; AIF=apoptosis-inducing factor; SCO2=synthesis of cytochrome *c* oxidase 2; CPT1C=carnitine palmitoyltransferase 1C MCD=malonyl-coenzyme A decarboxylase; LPIN1=lipin; PANK1=pantothenate kinase 1, TIGAR=TP53-inducible glycolysis and apoptosis regulator

accommodate for this problem by activating glutaminase 2 i(GLS2). Hu *et al.* (2010) reported that p53 transcriptionally activated GLS2, increased levels of glutamate and α-ketoglutarate (via glutaminolysis), mitochondrial respiration rate and, importantly, glutathione levels. Glutamate is a key precursor of glutathione synthesis and glutathione is an important antioxidant, such that depletion in total reactive oxygen species was reported (Hu *et al.* 2010). Inability to cope with increased superoxide radical species generated by OXPHOS may be part of the reason that cancer cells activate aerobic glycolysis to promote cytosolic ATP generation.

Several p53-driven metabolic changes counter metabolic changes stimulated by MYC deregulation or cancer cells in general, including p53-mediated inhibition of glycolysis and promotion of OXPHOS. However, other metabolic changes are not as clear, such as restoration of redox homeostasis, which may favour tumourigenesis. Further, p53 has been shown to promote FAO through direct activation of carnitine palmitoyl transferase 1 (essential for FA import into the mitochondria) and pantothenate kinase 1 (essential for CoA synthesis)(see figure 1.8). As discussed earlier 1.2.3.4, MYC deregulation promotes FAO and inhibition of FAO is detrimental to MYC-driven tumours *in vivo*. More research is needed to fully explore the role of tumour suppressor genes in metabolic reprogramming, particularly in the context of oncogene activation.

1.4 Cooperation between MYC deregulation and p53 loss

Several lines of evidence have indicated that disabling p53 confers a selective advantage to MYC-driven cancer. As discussed above, MYC deregulation strongly activates the p53 pathway, which resists cell cycle progression (Hermeking and Eick, 1994; Lindström and Wiman, 2003). *In vivo*, a common 'second-hit' following MYC deregulation is loss of p53. Eμ-*Myc* transgenic mice developed B-cell lymphomas that exhibited loss of either *TP53* (28% of cases) or *CDKN2A* (24% of cases) (Eischen *et al.* 1999). *TP53* is also commonly mutated in Burkitt's lymphoma cell lines (Farrell *et al.* 1991; Wiman *et al.* 1991). The selection for *TP53* loss following MYC deregulation suggests that this lesion offers a potent tumourigeneic advantage.

Enforced expression of *MYC* and loss of *TP53* were synergistic lesions that enhanced induction of cyclin B1 (mRNA and protein) in Rat1 cells and 3D myeloid cells (Yin *et al.* 2001). *In vivo,* mice with genetically enforced expression of *Myc* and disruption of *Tp53* showed accelerated development of malignant lymphomas. Moreover accelerated malignancy was a consequence of enhanced proliferation, not reduced apoptosis (Hsu *et al.* 1995). These studies indicate that *TP53* loss relieves proliferative arrest following MYC deregulation.

Finch *et al.* offered further insight into the cooperation of genetic lesions with MYC deregulation using a switchable model of *Myc* expression in pancreatic islet β-cells (Finch *et al.* 2006; figure 1.9). *Myc* activation drove low levels of proliferation due to the proliferative restraint regulated by p53 and ARF. Apoptosis was moderately

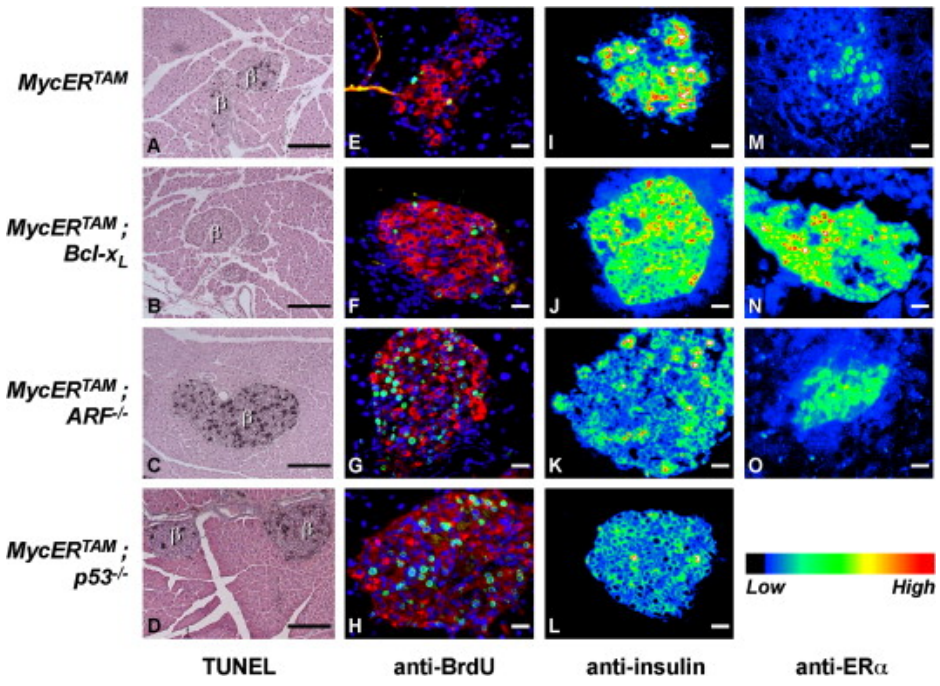

Figure 1.9. Activation of *Myc* in β cells of pancreatic islets alone or plus *Bcl-xl* overexpression, *Arf* loss, or *P53* loss (Finch *et al.* 2006)
Myc was activated in β cells of pancreatic islets (*Myc*ER^{TAM}) of mice for 3 days. *Myc*ER^{TAM} alone was compared to *Myc*ER^{TAM}; *Bcl-xl* (*Bcl-xl* overexpression), *Myc*ER^{TAM}; *Arf*$^{-/-}$ (*Arf* loss), and *Myc*ER^{TAM}; *P53*$^{-/-}$ (*P53* loss). Apoptosis was measured by TUNEL (grey with eosin counter stain; A-D). BrDU was adminitered 3.5 hr before sacrifice and S phase cells were identified with anti-BrDU (green), anti-insulin (red) and Hoescht (blue) counterstain (I-L). Staining with anti-insulin (I-L) or anti-ERα (M-O) followed by excess secondary antibody allowed quantitative imaging. Scale bars are 100 μm.

increased by *Myc* activation, and this could be rescued by overexpression of antiapoptotic protein *Bcl-xl*. Loss of *Arf* relieved cell cycle inhibition allowing increased proliferation, and also potently increased apoptotic rate. This suggests that apoptosis is homeostatically regulated because if you relieve the proliferative brake you increase apoptosis. Loss of *Tp53* increased proliferation without affecting apoptosis, indicating that p53 loss counters stresses associated with increased proliferation in some way. Due to the broad metabolic remodelling driven by MYC, and the ability of p53 to modulate and resist metabolic transformation, it is likely that loss of p53 gives *MYC* expressing cells a metabolic advantage. Further, as *TP53* is a tumour suppressor gene described to respond to metabolic changes (as discussed above) it is likely that p53 directly responds to metabolic changes driven by MYC deregulation.

Understanding the cooperation between MYC deregulation and *TP53* loss is therapeutically important because tumours with these genetic lesions are particularly aggressive. *In vivo*, *Myc*-driven *Tp53* null B-cell tumours were described as large, invasive, and irregular (Finch *et al.* 2006). In humans Hill *et al.* (2015) compared medulloblastoma biopsies at diagnosis and relapse and found combined *MYC* amplifications and p53 pathway defects commonly emerged at relapse. All patients in the group died of rapidly progressive disease post-relapse, indicating that combined *MYC* amplifications and p53 pathway defects may also drive aggressive tumourigenesis in humans.

1.5 Hypothesis

MYC expression drives an anabolic program that promotes cell growth and proliferation (section 1.2). In response to *MYC* overexpression, the p53 tumour suppressor pathway is activated via an unknown mechanism (section 1.3). Given that p53 has been documented to restrict anabolism and respond to a variety of nutrient deficiencies, I hypothesize that p53 responds to a specific MYC-driven metabolic pathway.

1.5.1 Sub-hypothesis

Tp53 mutations commonly occur following MYC deregulation *in vivo* and result in a more aggressive tumour phenotype (section 1.4). The contrasting effects of MYC (section 1.2.3) and p53 (section 1.3.4) on cell metabolism indicate that loss of *TP53* may favourably remodel the metabolism of MYC deregulated cells. I therefore hypothesize this to be the case.

1.6 Thesis questions

1. Does p53 respond to a MYC-driven metabolic pathway?
2. What metabolic changes are driven by *MYC* overexpression?
    a. Does loss of p53 function impact MYC-driven metabolic changes?
3. What lipid changes are driven by *MYC* overexpression?
4. By what mechanism do MYC-driven lipid changes regulate p53 levels?

2 Chapter 2- Materials and Methods

All solutions and compounds referred to here and in the following sections were obtained from Sigma unless otherwise stated. The composition of routinely used solutions are listed in Table 2.1.

Table 2.1 Routinely used solutions

Substance	Composition
PBS	Phosphate-buffered saline tablets
PBS-Tween (PBS-T)	PBS + 0.5 % TWEEN20
TBS-Tween (TBS-T)	10mM Tris (pH 7.5), 154mM NaCl, 0.5% Tween
PBS/BSA	In 1 litre: 10 Dulbeccos tablets, 0.1 g NaN_3, 20 g BSA
Cell lysis buffer	20mM Tris, 100mM NaCl, 5mM $MgCl_2$, 0.5%IGEPAL
10 X running buffer	25 mM Tris, 192 mM glycine, 0.1% SDS
10 X transfer buffer	25 mM Tris, 192 mM glycine

2.1 Cell culture and treatments

2.1.1 Cell culture

MRC5 human fibroblasts were obtained from the European Collection of Authenticated Cell Cultures (ECACC) via Public Health England. All cells were immortalized by transduction of retroviral hTERT, followed by either retroviral vector pM6P-blast (kind gift of F. Randow, MRC Laboratory of Molecular Biology, Cambridge UK) or pM6P-blast-MycER^{T2}. From this point onwards, MRC5 pM6P-blast cells will be referred to as 'Vec cells' and MRC5 pM6P-blast-MycER$^{T2\ cells}$ as 'Myc cells'. Myc cells were activated by 4-hydroxytamoxifen (200 ng/ml) for 48 hr (unless otherwise stated), and 4-hydroxytamoxifen was present in all Vec cell samples. HEK293ET cells were a kind gift of F. Randow, MRC Laboratory of Molecular Biology, Cambridge UK. Cells were routinely maintained in DMEM high glucose, no pyruvate +10% FBS (referred to as standard media).

2.2 Transfection of plasmid DNA

2.2.1 Polyethylenimine (PEI) transfection

To produce virus, HEK293ET cells were seeded in 75 cm^2 flasks the day before transfection. For each flask, 10 μg midi prepped plasmid DNA, pMD2G, and pGAGPol were combined with 40 μl PEI (1 mg/ml) and 450 μl standard DMEM. Medium was changed 24 hr post-transfection, and incubated for a further 24 hr for viral production. MRC5 cells were seeded in 75 cm^2 flasks the day before infection at a suitable cell density to reach confluence after 48 hr. For each MRC5 flask, 1 ml

viral media was combined with 9 mL standard DMEM and 10 µl polybrene (5 mg/ml stock). Successful infection was indicated by a GFP control, and cells were selected in an appropriate antibiotic (puromycin or blasticidin) for at least one week before harvesting.

2.3 RNA interference

2.3.1 siRNA (short interfering RNA) library design, transfection, and analysis

2.3.1.1 siRNA library design

A large metabolic siRNA library was designed in collaboration with Flora Dix and Juan-Carlos Acosta using the custom-design DHARMACON ON-TARGETplus siRNA tool. A total of 553 test siRNAs were selected to cover a broad range of metabolic pathways and transcription factors (Table 2.2). The siRNA library spanned seven 96-well plates in triplicate, with four wells on a plate targeting the same gene. Each well comprised a SMARTpool- a mixture of four siRNAs targeting the same gene provided as a single reagent. All siRNAs listed here and in the following sections were obtained from DHARMACON. Unless otherwise stated siRNAs were SMARTpools.

Table 2.2 siRNA library overview

Pathway targeted	Number of genes
Glucose metabolism	59
Nucleotide biosynthesis	22
Amino acid biosynthesis	16
Transporters	17
Transcription factors	18
Lipid biosynthesis	224
Detoxification	62
Other	115

2.3.1.2 siRNA transfection

Dharmacon SMARTpool siRNA mix (30 nM) was delivered by 'reverse transfection', meaning that the siRNA was plated first, followed by the transfection reagent, followed by the cells. DHARMAFECT1 transfection reagent (DHARMACON) was diluted 1:175 in null DMEM media, and then 17.5 µl of the solution was added per well. MRC5 cells (Vec or Myc) were seeded at 2000 cells/well in 100 ul standard DMEM. The day after transfection assays were carried out as described below.

2.3.1.3 siRNA controls

In addition to siRNA SMARTpools, two controls were included in the screen to measure the range of p53 levels. siTP53 was used as described above to demonstrate p53 antibody specificity. Actinomycin D (50 ng/ml), which was previously shown to activate p53 (Choong *et al.* 2009), was added to media 24 hr before fixation to determine maximum p53 levels.

2.3.1.4 siRNA analysis

Following immunofluorescent staining (described below), plates were acquired with the ImageXpress Micro XLS Widefield High-Content Analysis System (Molecular Devices LLC, CA). Normalisation and Z score calculations were carried out using the web cellHTS2 software package. Plates identified as having poor immunofluorescent staining were omitted from the study, and it was found necessary to carry out an additional replicate of Myc plates. A median Z score cut off of greater than 1.5 for positive hits, and less than -2 for negative hits was set as the threshold of significance. The Functional Annotation tool on The Database for Annotation, Visualization and Integrated Discovery (DAVID) was used to assign the top 5 functional annotations, as determined by lowest p-value (Huang *et al. 2009*).

2.3.2 shRNA design and production

2.3.2.1 Lentiviral shRNA design and production

shRNA constructs were designed and cDNA cloned into the lentiviral GIPZ vector (Dharmacon) by Andrea Quintanilla. Following transfection of plasmid DNA, MRC5 cells Vec and Myc were selected in puromycin (1 μg/μl) for one week before successful shRNA knockdown was verified by qRT-PCR. Details of shRNA constructs can be found in Table 2.3.

Table 2.3 Lentiviral shRNA reference numbers

Target gene	Supplier	Reference numbers
CERS4 (1-3)	Dharmacon	274306, 348840, 348844
SPTLC2 (1-3)	Dharmacon	249662, 67791, 379817
GBA (1-3)	Dharmacon	83141, 340366, 340339
SLC7A11 (1-3)	Dharmacon	196769, 251161, 392255

2.3.2.2 Retroviral shRNA design and production

shRNA constructs were designed and cDNA cloned into the pSUPER-retro vector by Andrea Quintanilla. Following viral transduction, MRC5 cells Vec and Myc were selected in puromycin (1 μg/μl) for one week before successful shRNA knockdown was verified by qRT-PCR. Details of shRNA constructs can be found in Table 2.4.

Table 2.4 Retroviral shRNA sequences

Target gene	Target sequence

SPTLC2 (1)	UCAAACAGAUACCGGUUAA
SPTLC2 (2)	AGUCUGAGGAUGUGCGCAA
CERS4 (1)	GUGCCAACCUGCUGCGCAU
DEGS2 (1)	GCAAGGAGAUACUGGCCAA
DEGS2 (2)	GGGUGAAGGUGCUCUGGGA
DEGS2 (3)	GUUCUGGGCCUACGCCUUU
DEGS2 (4)	GCAGCGACUUCGAGUGGGU

2.3.3 Retroviral overexpression constructs

Overexpression constructs were designed by Andrea Quintanilla, and cDNA of the target gene was cloned into pMSCV as a Xho1-EcoR1 fragment. Following transfection of plasmid DNA, MRC5 cells Vec and Myc were selected in puromycin (1 μg/μl) for one week before successful overexpression was verified.

2.3.4 Genetic suppressor elements

A genetic suppressor element encoding dominant negative mutant p53 peptide was transfected into Vec and Myc cells as described previously (Gallagher *et al.* 1997). Loss of p53 function was validated by inability to increase p21 levels in response to *MYC* activation.

2.4 Quantitative reverse transcription polymerase chain reaction (qRT-PCR)

2.4.1 RNA extraction

Cells were scraped in PBS, centrifuged at 6000 rpm, and pellets frozen at -80 °C. RNA was extracted using RNeasy Plus Mini Kit (QIAGEN) following manufacturer's instructions. RNA was eluted in 30-50 μl molecular biology grade RNAse-free ddH2O depending on the size of the original cell pellet. RNA concentration was quantified using a Nanodrop 2000C (Thermo Scientific).

2.4.2 Complementary DNA (cDNA) synthesis

An intermediate stock of 50 ng/μl was made up to a final volume of 25 μl for each RNA extract. For each reaction, 20 μl of the intermediate stock was combined with 8 μl 5 X QUANTA qScript RT Supermix and 12 μl H_20. cDNA synthesis was carried out on a SureCycler 8800 PCR machine (Agilent technologies). Program: 25 °C 5 min → 42 °C 30 min → 85 °C 5 min → 4 °C inf.

2.4.2.1 qRT-PCR

qRT-PCR primers were designed using the Primer3web (version 4.0.0) online tool (Table 2.5) (Untergasser *et al.* 2012; Koressaar and Remm, 2007). Primers were designed to span exon/exon boundaries to ensure only mRNA was amplified. A

primer master mix was prepared. Per sample the master mix contained: 25 µl 2X SYBR Select Master Mix (Applied Biosystems), 0.5 µl forward primer (10 µM), 0.5 µl reverse primer (10 µM), and 20 µl H_20. Primers are listed in table 2.5. Intermediate tubes representing pooled technical triplicates were prepared, each containing 47 µl of the relevant primer master mix, and 3 µl cDNA. From the intermediate tubes, 15 µl of sample was plated in triplicate onto MicroAmp Fast optical 96w reaction plates (Thermo Scientific). qRT-PCR was performed on a StepOnePlus Real-Time PCR System using the Stepone software (version 2.3). The routine program used was: hold 95 ℃ 10 min → 40 cycles (95 ℃ 15 sec → 60 ℃ 30 sec → 72 ℃ 15 sec) → melt curve 95 ℃ 15 sec, 60 ℃ 1 min, 95 ℃ 15 sec. RNAse-free ddH_2O alone was used as a control, and no contamination was detected. A threshold was established in the linear phase of the amplification plot, and the log Ct (the number of cycles to reach the threshold) for each sample was used for quantification.

Table 2.5 Primer sequences

Gene ID	Forward	Reverse
ACTIN	CATGTACGTTGCTATCCAGGC	CTCCTTAATGTCACGCACGAT
CDKN1A	CCTGTCACTGTCTTGTACCCT	GCGTTTGGAGTGGTAGAAATCT
CERS4	ATCAGACCAGGAGGCAAGTG	GGCCTCACAGAACTTCTTGGT
GBA	TTGCAGGGCTAACCTAGTGC	GGCTTGGGACATTCCTCTCT
SLC7A11	TGCTGGGCTGATTTTATCTTCG	GAAAGGGCAACCATGAAGAGG
SPTLC2	GCTCTACATGCCTGCCAAAA	AATTGGGGTGGCAGGAAATC
DEGS2	ACGACTTCCCCAGCATCC	AATCCCAGAGCACCTTCACC
TP53 (1)	GCGCACAGAGGAAGAGAATC	AGAGGAGCTGGTGTTGTTGG
TP53 (2)	TGGCTCTGACTGTACCACCA	CCAGTGTGATGATGGTGAGG
TP53 (3)	CACATGACGGAGGTTGTGAG	ACACGCAAATTTCCTTCCAC
P14ARF	CCCTCGTGCTGATGCTACTG	ACCTGGTCTTCTAGGAAGCGG
P16INK4A	CGGTCGGAGGCCGATCCAG	GCGCCGTGGAGCAGCAGCAGCT

2.5 Immunofluorescence and microscopy

2.5.1 Immunofluorescence

2.5.1.1 Antibodies and controls

Antibodies used for immunofluorescence are listed with dilutions in Table 2.6.

Table 2.6 Antibodies for immunofluorescence

Name	Supplier	Dilution	Reactivity
Primary			
p53 DO7	Leica- NCL-L-p53-DO7	1:100	Mouse

p21	Sigma- P1484	1:100	Mouse
Secondary			
Alexa-Fluor-488 Mouse IgG_1	ThermoFisherScientific	1:1000	Mouse
Alexa-Fluor-568 Mouse IgG_1	ThermoFisherScientific	1:1000	Mouse
Alexa-Fluor-488 Rabbit IgG_1	ThermoFisherScientific	1:1000	Rabbit

2.5.2 Staining protocols

At the experimental end point, cells were fixed *in situ* with 4% PFA/PBS for 30 min. Three PBS washes were carried out prior to every stage of the staining protocol (excluding addition of the primary antibody), and all staining was carried out at room temperature. Following fixation, cells were permeablised with 0.2% triton/PBS for 10 min, then incubated in blocking solution (BSA/PBS) for 30 min. Primary antibody was added for 30 min, secondary antibody for 1 hr, and DAPI for 10 min. For DAPI cell count assays, staining protocols were the same but primary and secondary antibody staining were omitted. Wells contained 100 µl PBS during data acquisition.

2.5.3 Microscopy

Plates were acquired with the ImageXpress Micro XLS Widefield High-Content Analysis System (Molecular Devices LLC, CA). For threshold-based acquisition, a 4x4 grid was set at the center of each well and the adaptive acquisition setting was used to count a total of 2000 cells/well. A threshold for secondary antibody immunofluorescent intensity was set, and the percentage of cells that scored above the threshold was calculated (using DAPI count as the total cell count for that well).

2.6 Western blotting

2.6.1 Cell lysis

Cell pellets were washed in PBS then lysed in an appropriate volume of cell lysis buffer (50-200 µl). Pellets that contained high numbers of apoptotic cells were sonicated at a moderate frequency for 30 sec. Following a 5 min incubation on ice, cells were centrifuged at 13,000 rpm for 5 min. The supernatant was removed and quantified using the Bradford Assay.

2.6.2 SDS-PAGE electrophoresis

Lysates were normalised to an equivalent protein concentration to allow 25 µg protein to be loaded per well. To each sample, 0.95 volumes of 2 x Lamelli Sample Buffer and 0.05 volumes of β-mercaptoethanol were added. Samples were heated to 95°C for 5 min, and centrifuged before loading onto 10% precast polyacrylamide gels (BIO-RAD). Gels were run in 1X running buffer (1:9; 10X running buffer:ddH_20) for 5 min at 100 V, then approximately 1 hr at 170 V.

Spectra Multicolor Broad Range Protein Ladder (Thermo Scientific) was used to estimate the molecular weight of proteins.

2.6.3 SDS-PAGE gel transfer

To prepare for the transfer, 6 sheets of chromatography paper (Whatman) were equilibrated in 1X transfer buffer (1:1:8; 10X transfer buffer:MeOH:ddH_20), and the transfer membrane (Immobilon-P, pore size 0.45 μm) was primed with methanol for 1 min. The sheets of paper were then placed either side of the gels and membrane to 'sandwich' them together. The gels were electroblotted for 1 hr in 1X transfer buffer at 100V. Ice packs were used to keep the gels cool.

2.6.4 Antibody probing

Membranes were washed 3 times in TBST, then blocked for 30 min with 2% milk in TBST. Antibodies were diluted with 2% milk in TBST, as indicated in Table 2.7. Antibodies were routinely incubated at 4 °C overnight, with the exception of β-Actin, which was incubated at room temperature for 1 hr.

Table 2.7 Antibodies for western blotting

Name	Supplier	Dilution	Reactivity
Primary			
p53 DO7	Leica- NCL-L-p53-DO7	1:1000	Mouse
Actin	ProteinTech- 60008-1-Ig	1:20,000	Mouse
c-Myc (Y-69)	Abcam- ab32072	1:5000	Rabbit
ORMDL2	Abcam- ab10762	1:1000	Rabbit
p21	Sigma- P1484	1:1000	Mouse
CAD	Cell signalling- 11933	1:500	Rabbit
PP2A C	Cell signalling- 2038	1:1000	Rabbit
PP1A	Santa Cruz- scc-6140	1:200	Goat
GRP75	Abcam- ab2799	1:500	Mouse
PPARγ	Cell signalling- C26H12	1:1000	Rabbit
Secondary			
Anti-Goat-HRP	Santa Cruz- sc2020	1:1000	Goat
Anti-Mouse-HRP	Cell signalling- 7076S	1:20,000	Mouse
Anti-Rabbit-HRP	Cell signalling	1:1000	Rabbit

2.7 Small molecule inhibitors

All drugs stocks were stored at -20 °C, and fresh dilutions in standard media were prepared immediately before treatment. A summary of the inhibitors tested can be found in Table 2.8.

Table 2.8 Small molecule inhibitors

Name	Supplier	Catalogue number
6-aminonicatinamide	Cayman Chemical	329-89-5
ATM/ATR kinase inhibitor	Calbiochem	905973-89-9
C-20 ceramide	Cayman Chemical	10724
C-24 ceramide	Cayman Chemical	62535
C-6 ceramide	Avanti Polar Lipids	860506
Conduritol B epoxide (CBE)	Cayman Chemical	15216
Ceramide from bovine spinal cord	Sigma Aldrich	22244
Ceranib 1	Tocris Bioscience	4448
CYM50260	Tocris Bioscience	4677
CYM50308	Cayman Chemical	14667
CYM5442	Cayman Chemical	16925
Fatty Acids Unsaturated Kit	Sigma Aldrich	UN10-1KT Supelco
Fuminosin B1 (FB1)	Tocris Bioscience	3103
JTE-013	Cayman Chemical	10009458
Miglustat hydrochloride (MH)	Tocris Bioscience	3117
Myriocin (MYR)	Cayman Chemical	63150
NVP-231	Calbiochem	219493
Okadaic acid	Abcam	Ab120375
PKC ζ pseudosubstrate	Tocris Bioscience	1791
Rapamycin	Enzo	BML-A275
Rosiglitazone	Cayman Chemical	71740
SEW2871	Abcam	ab120983
Sphingosine kinase inhibitor 1 (SKI-1)	Abcam	ab142209
Sphingosine-1-phosphate (S1P)	Cayman Chemical	62570
T0070907	Cayman Chemical	10026
Torin 1	Tocris Bioscience	4247
VPC 23019	Cayman Chemical	13240
W146 (trifluoroacetate salt)	Cayman Chemical	10009109

2.8 Liquid Chromatography Mass Spectrometry (LC-MS)

2.8.1 Isotope labeling

Heavy isotopes were dissolved to an appropriate concentration in DMEM, no glucose, no glutamine, no phenol red. Media was supplemented with metabolites to match their concentration in standard DMEM. Where possible 100% of the media was labeled; however in the cases of glycine, serine, and choline a 2/3 label was used due to the presence of these metabolites in the media. To label the cells, media was aspirated and replaced with the heavy-isotope labeled media for a given pulse time. Heavy-isotopes tested are listed in Table 2.9.

Table 2.9 Heavy-isotopes

Name	Supplier	Catalogue number
L-Asparagine-amide-^{15}N monohydrate	Sigma Aldrich	605166
L-Asparagine-^{13}C4	Cambridge Isotope Laboratories	CLM-8699
Choline chloride-^{15}N	Sigma Aldrich	609269
L-Cystine-^{15}N2	Cambridge Isotope Laboratories	NLM-3818
Ethanolamine-^{15}N	Cambridge Isotope Laboratories	NLM-8722-PK
D-Glucose-^{13}C6	Cambridge Isotope Laboratories	CLM-1396-5
D-Glucose-^{13}C6	Sigma Aldrich	389374
L-Glutamine-^{13}C5	Sigma Aldrich	605166
L-Glutamine-amide-^{15}N	Sigma Aldrich	490024
Glycine-2-^{13}C	Sigma Aldrich	279439
Glycine-^{15}N	Sigma Aldrich	299294
Palmitic acid-d31	Sigma Aldrich	366897
Sodium Pyruvate-^{13}C3	Sigma Aldrich	490717
D-Ribose-^{13}C5	Cambridge Isotope Laboratories	CLM-3652
L-Serine-^{13}C2	Sigma Aldrich	605174
L-Serine-^{15}N	Cambridge Isotope Laboratories	NLM-2036

2.8.2 Extraction of metabolites

Individual wells of a 6-well plate were washed with ice-cold PBS then extracted in 0.5 ml extraction buffer (50% methanol, 30% acetonitrile, 20% water at -20 ℃ or lower). Extracts were centrifuged at maximum speed and stored at -80 ℃.

2.8.3 Extraction of metabolites from RNA or DNA

To determine metabolite content specifically in RNA or DNA cells were first scraped in PBS, centrifuged at 6000 rpm, and pellets frozen at -80 °C. RNA was extracted using RNeasy Plus Mini Kit (QIAGEN) or DNA was extracted using DNeasy blood and tissue kit (QIAGEN) following the manufacturer's instructions. RNA or DNA was eluted in 30-50 µl molecular biology grade RNAse-free ddH_2O depending on the size of the original cell pellet. RNA or DNA concentration was quantified using a Nanodrop 2000C (Thermo Scientific) to ensure the extraction worked. Elulted RNA or DNA was extracted in 0.5 mL extraction buffer (50% methanol, 30% acetonitrile, 20% water at -20 ℃ or lower). Extracts were centrifuged at maximum speed and stored at -80 ℃.

2.8.4 Extraction of lipids

The lipid extraction method was adapted from Bligh and Dyer (Bligh and Dyer, 1959) as recommended by Terry K. Smith (University of St. Andrews). Individual plates (10 cm) were washed and scraped in ice-cold PBS. Cells were centrifuged at 800 g for 10 min. Pellets were suspended in 100 ul PBS and transferred to a glass test

tube. A total of 375 ul 1:2 (v/v) chloroform:methanol was added to each tube and vortexed. Suspensions were agitated vigorously for 30 min at 4 °C. Suspensions were made biphasic by adding 125 ul chloroform, vortexing, 125 ul water, vortexing, and centrifuging at 1000 rpm for 5 min. The lower phase (chloroform phase) was then transferred to a glass vial and dryed under nitrogen. Lipid extracts were stored at 4 °C, and resuspended in 2:1:1 (v/v) isopropanol:acetonitrile:water prior to analysis.

2.8.5 Metabolomic LC-MS methods

LC-MS was carried out using a Thermo Ultimate 3000 HPLC inline with a QExactive mass spectrometer. A 32 min gradient was developed over a 100 mm x 4.6 mm ZIC-pHILIC column (Merck-Millipore) from 10% buffer A (20 mM ammonium carbonate), 90% buffer B (acetonitrile) to 95% buffer A, 5% buffer B. 10 µl of metabolite extract was applied to the column equilibrated in 5% buffer A, 95% buffer B.

Samples were acquired in positive-negative switching mode and standard ESI source and spectrometer settings were applied (typical scan range 75-1050). Metabolites were identified by either standard metabolite matching to m/z and retention time, or by fragmentation fingerprint pattern.

2.8.6 Lipidomic LC-MS methods

LC-MS was routinely carried out using a Thermo Ultimate 3000 HPLC inline with a QExactive mass spectrometer or an Orbitrap Fusion Lumos Tribrid Mass Spectrometer where stated. A 10 min gradient was developed over a Phenomex C18 column from 80% buffer A (60:40 acetonitrile:water plus 10 mM ammonium formate, 20% buffer B (90:10 isopropanol:acetonitrile plus 10 mM ammonium formate) to 3% buffer A, 97% buffer B. The gradient was then held at this composition for 2 min.

All samples were acquired twice, once in positive MS2 mode, once in negative MS2 mode. The standard scan range in positive mode was 300-1000 Da, and 500-1200 Da in negative mode. The QExactive mass spectrometer was routinely used for data acquisition and identification of lipids. Metabolites were identified by either standard metabolite matching to m/z and retention time, or by high collision energy (HCD) fragmentation fingerprint. The identification of this fingerprint was partially automated with the perl script LipidSlider.pl. The Orbitrap Fusion Lumos Tribrid Mass Spectrometer was used to acquire a single dataset to test its capacity to detect lipid species. Sensitive mass analysis of HCD and CID (collision-induced dissociation) fragments allowed complete fatty acid identification of glycerophospholipids, and multistage ion activation (MS^n) allowed complete fatty acid identification of triacylglycerols.

2.8.7 Software

2.8.7.1 LipidSlider

The perl script LipidSlider.pl was designed and written in collaboration with Jimi Wills to address an unmet need for free software to identify lipid subclass by MS2 fingerprint. The software reads MS2 data in mgf format, and scans for sets of 3 ions (the subclass fingerprint) that are listed in the configuration file. The selected ions were chosen to detect glycerophospholipid and sphingolipid species. For glycerophospholipid species that have more than one fatty acid residue, the software identifies the lipid subclass and then the summed carbons and double bonds are calculated for a given lipid. As ceramide species have a sphingosine backbone that forms the subclass fingerprint, and one fatty acid residue, a generic composition solver was used to calculate the fatty acid residue, thus resolving the complete lipid composition. An estimation of the false discovery rate is printed after completion of the analysis.

2.8.7.2 LipidSearch

The ThermoScientific Software LipidSearch was tested alongside the Orbitrap Fusion Lumos Tribrid Mass Spectrometer for its ability to identify sphingolipid, glycerolipid, and glycerophospholipid species by ms2 and ms3 fingerprint. The corresponding dataset is indicated in the figure legend.

2.8.7.3 assayR

assayR was developed in collaboration with Jimi Wills and Andrew Finch to address an unmet need for free software that allows targeted analysis of heavy isotope labeled metabolites (unpublished data). The metabolites to be processed in the targeted analysis are entered in the form of a configuration file that contains metabolite name, m/z value, retention time window, peak intensity threshold, and possible isotopes. Possible isotopes of the elements hydrogen, nitrogen, and carbon are considered, and a maximum number of isotopes is assigned to each metabolite. The final output consists of a csv file, extracted ion chromatograms of all metabolites, histograms of percent isotope labeling, and histograms of absolute peak area. assayR allows for rapid processing of complex labeling experiments, and this software was used to process all LC-MS datasets following its development.

2.8.7.4 X13CMS

X13CMS software was used to analyse heavy-isotope tracer experiments in an untargeted manner (Huang *et al.* 2014). X13CMS is implemented in R, and compares unlabeled and heavy-isotope labeled samples between two biological conditions. The output from the isoDiffreport from X13CMS highlights ions that are differentially labeled between the two biological conditions. These ions were then further analysed for peak integrity using assayR, and assigned metabolite IDs by standard retention time or fragmentation pattern.

2.9 Statistical analysis

2.9.1 T-Test

Calculations of significance between pairs of means were routinely carried out with Microsoft Excel using the two-tailed Student's t-test. T-tests were carried out on a representative dataset, or where possible on biological triplicates, as indicated in the figure legends. A p-value of ≤ 0.05 was considered to be statistically significant.

2.9.2 Differential peak area analysis of lipids

2.9.2.1 Normalisation

Large lipid datasets were quantile normalised using the function 'normalize.quantiles' in the R package 'preprocessCore' (R Core Team, 2013; Bolstad *et al*, Bioinformatics, 2003).

2.9.2.2 ANOVA

Statistical analysis of large lipid datasets was carried out using the one-way analysis of variance (ANOVA) function in R (R Core Team, 2013). This method was selected due to ANOVA applying the F-test to calculate statistical significance between all means within the group.

2.9.2.3 Visualisation

Normalised peak areas were clustered using the GUI program Cluster3 (de Hoon *et al.* 2004). Cluster3 was used to log transform the data, before centering samples and peak areas on the median value. The data then underwent hierarchical clustering using the average linkage, and the output was visualized with Java TreeView (Saldanha, 2004).

2.9.2.4 Network clustering analysis

Spearman correlation values were calculated in R from normalised lipid peak areas and used to set edge weights. Mixture modeling was used to filter out edge weights with low significance (below a threshold of 0.5). The network was visualised using Cytoscape open source software (Shannon *et al.* 2003), and lipids were clustered using the Molecular Complex Detection (MCODE) plugin (Bader and Hogue, 2003). Clusters were separated by force directed layout and Fisher's exact test (Fisher, 1922) was carried out to determine whether the separation was statistically significant. Log2 values of normalised lipid peak areas were assigned to the relevant node within the network, and a thicker node border was used to indicate statistical significance from the one-way ANOVA described above.

3 Chapter 3- Metabolic mediators of p53 accumulation

The aim of this study was to investigate fundamental mechanisms of MYC-driven tumour suppression that are selected against in cancer cell lines. MRC5 human fibroblast cells were used as the experimental system for this project due to their intact genetic background and normal ploidy. This means that tumour suppressor pathways have not already been selected against and can therefore be assessed. To investigate the role of metabolic pathways in regulating MYC-driven p53 accumulation, a large metabolic loss of function siRNA screen was carried out using high-content microscopy. Functional annotation of screen hits was then carried out to identify metabolic pathways that regulate MYC-driven p53 accumulation. This chapter outlines the results and initial validation of the metabolic loss of function screen.

3.1 Primary siRNA screen

MRC5 cells were transduced with pM6P-blast (Vec) or pM6P-blast-MYCER^{T2} (Myc). Activation of *MYC* with 4OHT increased p53 levels over a 48 hr timecourse (figure 3.1A) as described previously (Hermeking and Eick, 1994; Lindström and Wiman, 2003). Accumulation of p53 also led to increased levels of its downstream target p21, indicating that the accumulation of p53 was sufficient to increase its activity (figure 3.1B). These results show that MRC5 cells transduced with conditional MYC are a suitable system to investigate how MYC activates the p53 tumour suppressor pathway.

To determine whether MYC activates p53 via a metabolic mechanism, a large metabolic loss of function siRNA screen was carried out to identify metabolic enzymes, transporters, or transcription factors that altered MYC-driven p53 accumulation. The siRNA library consisted of over 550 siRNA targets that covered a broad range of metabolic pathways, including glucose metabolism, nucleotide biosynthesis, amino acid biosynthesis, and lipid biosynthesis; as well as transporters and transcription factors (table 3.1). Screen conditions were optimised in 96-well plates using a p53 immunofluorescent readout to calculate percent p53 positive cells per well (figure 3.2). Cells transfected with non-target siRNA (siNT) were treated with vehicle or 4-hydroxytamoxifen (4OHT) to activate *MYC*. *MYC* deregulated cells (Myc +4OHT) increased percent p53 positive cells to ~40% compared to *MYC* control cells (Myc -4OHT) which had ~4% p53 positive cells. This indicated that *MYC* deregulation increased p53 accumulation, as described previously (Hermeking and Eick, 1997). Vec control cells had <1% p53 positive cells regardless of treatment with 4OHT. Two controls for the screen were used that strongly decreased or increased percent p53 positive cells compared to 40% p53 positive cells in *MYC* deregulated cells. Cells transfected with siTP53 had <1% p53 positive cells across all cell types and treatments, validating p53 antibody specificity. Actinomycin D was previouslydescribed to inhibit RNA synthesis (Perry *et al.* 1970) and activate p53 (Choong *et al.* 2009). Vec and Myc cells treated with actinomycin D (24 hr) had >70% p53 positive cells. The setup of these controls was important because they

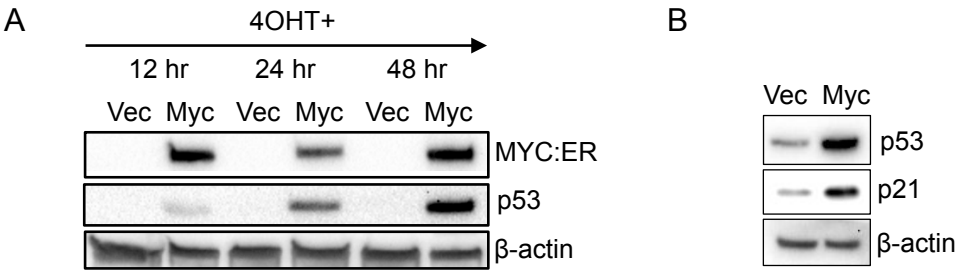

Figure 3.1. *Validation of experimental system*
(A) Western blot validates that levels of p53 protein increase over a 48 hr time course of *MYC* activation with 4OHT (n=1). (B) Western blot shows that 48 hr *MYC* activation with 4OHT increases p53 activity, as measured by increased p21 levels (a downstream target of p53) (n=3). This indicates that increased levels of p53 are sufficient to increase p53 activity.

Table 3.1. *siRNA library overview*
The table shows an overview of siRNA targets within the siRNA library. The siRNA library was designed in collaboration with Flora Dix and Juan-Carlos Acosta.

Pathway targeted	Number of genes
Glucose metabolism	59
Nucleotide biosynthesis	22
Amino acid biosynthesis	16
Transporters	17
Transcription factors	18
Lipid biosynthesis	224
Detoxification	62
Other	115

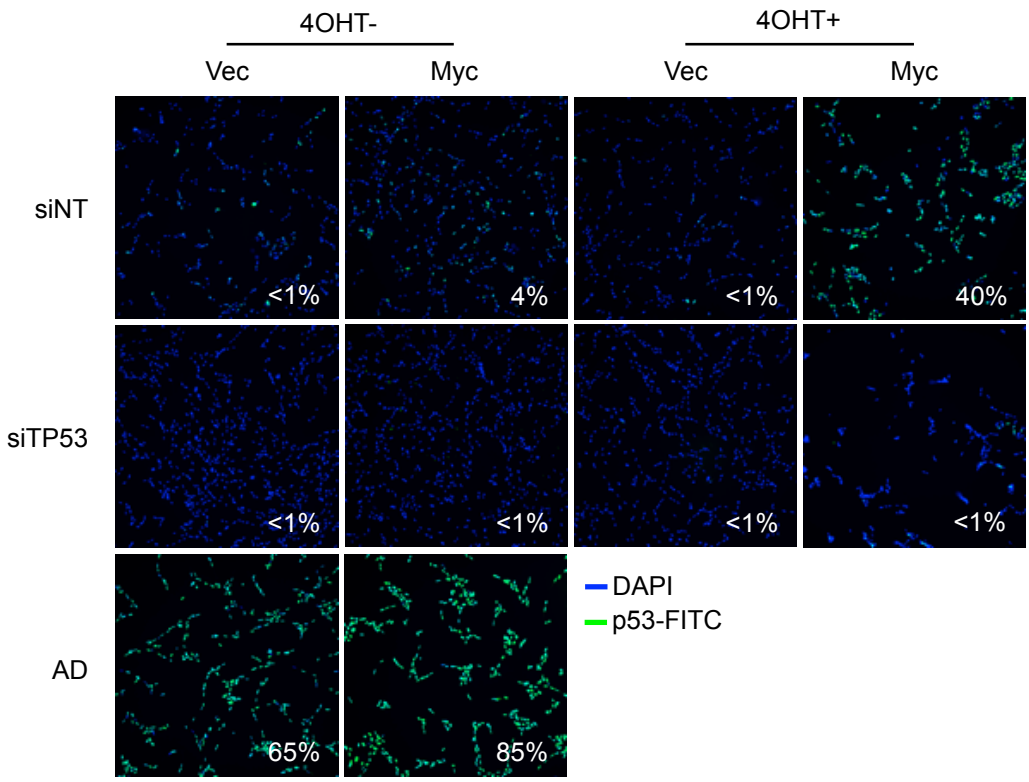

Figure 3.2. *Immunofluorescent setup of the primary siRNA screen* Immunofluorescent images show the setup conditions for a large metabolic siRNA screen to follow. Immunofluroescence shows DAPI (blue) and p53-FITC (green). Setup conditions are siNT (non-target siRNA), siTP53 as the positive control, and AD (actinomycin D, 24 hr treatment at 50 ng/ml) as the negative control. The siRNA conditions were tested +/- 4OHT treatment.

indicated that the siRNA screen could identify metabolic pathways that positively or negatively regulated p53 levels in response to *MYC* deregulation.

Following acquisition, percent p53 positive cells for each siRNA pool was calculated and the full dataset was analysed using the web-based platform webcellHTS2. Screen replicates (consisting of seven 96-well plates in quadruplicate) were batch normalised (figure 3.3A and B). Normalised median values were aligned at a value of zero, and these values were used to show good separation of controls in each plate and across the replicate (figure 3.2C and D). To identify screen hits, a Z score distribution was plotted (figure 3.3E). Sixteen siRNAs that decreased p53 accumulation with a Z score greater than 1.5 were considered positive screen hits (table 3.2). Twenty siRNAs that increased p53 accumulation with a Z score less than -2 were considered negative screen hits (table 3.3). A lower Z score threshold was set for positive hits because these were the metabolic pathways responsible for positively regulating p53, therefore the effect of their knockdown may be more subtle. In contrast, it was likely that knockdown of several metabolic enzymes would induce stress and strongly exacerbate p53 accumulation.

The 36 siRNA screen hits were assigned functional annotations using the functional annotation tool on The Database for Annotation, Visualization and Integrated Discovery (DAVID; Huang *et al.* 2009). Of the broad range of metabolic pathways included in the siRNA library (table 3.1), the top 5 functional annotations were lipid metabolism, metabolic pathways, lipid biosynthesis, sphingolipid biosynthetic process, and fatty acid biosynthetic process (as determined by lowest p-value; table 3.4). The large number of screen hits that clustered in fatty acid and sphingolipid synthesis indicated that these pathways were key in regulating the p53 response to *MYC* deregulation. Interestingly, a recent genome-wide siRNA screen in *Caenorhabditis elegans* (*C.elegans*) looking for targets that blocked the mitochondrial stress response revealed 6 hits in the sphingolipid biosynthesis pathway (Liu *et al.* 2014b). As the *C.elegans* screen was genome-wide it implicated the broader relevance of our metabolic siRNA screen in a cellular response to mitochondrial stress (see subsection below).

Positive siRNA screen hits (i.e that reduced MYC-driven p53 accumulation) were validated using 4 individual siRNAs per gene (figure 3.4). Ceramide synthase 4 (CERS4) was added to the validation screen as it is the enzymatic step between two other screen hits serine palmitoyltransferase long chain base subunit 2 (SPTLC2) and dihydroceramide desaturase 2 (DEGS2) in the *de novo* sphingolipid synthesis pathway. CERS was also one of six sphingolipid hits in the *C.elegans* screen (Liu *et al.* 2014b). CERS4 was validated specifically (there are 6 CERS subtypes) as it was a strong hit in a parallel tumour suppressor screen carried out on the same metabolic siRNA library (Dix *et al.* unpublished data). A gene was considered a strong hit if 2 or more of the 4 siRNAs decreased the percent p53 positive cells in siNT by 30 percent. The strongest hits were sphingolipid enzymes *SPTLC2* and *DEGS2* (*CERS4* was validated with 1 of the 4 siRNAs), TCA cycle enzyme oxoglutarate dehydrogenase (*OGDH*), cystine-glutamate antiporter *SLC7A11*, glycolytic enzyme

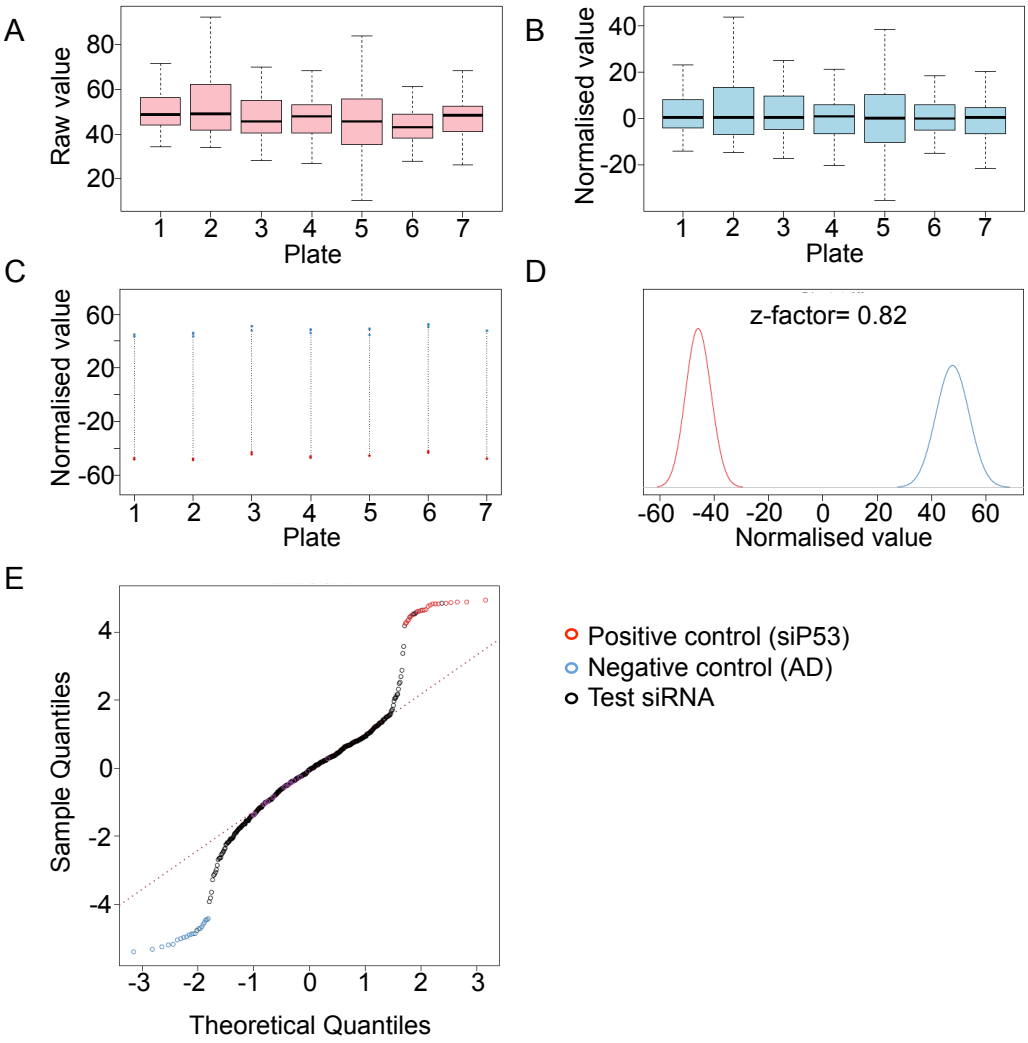

Figure 3.3. *Primary metabolic siRNA screen*
siRNA screen data was analysed using the web based program webcellHTS2. (A) Histogram shows the distribution of raw values across the 7 plates tested. (B) Histogram shows the median values of each plate normalised to zero. The median values are indicated by the black line on both histograms. (C) Figure shows the separation of normalised values for each plate. (D) Figure shows the separation of positive (siP53) and negative (AD, actinomycin D) controls. No overlap between controls and a Z score factor close to 1 is indicative of a strong screen. (E) Z score distribution shows most test siRNAs clustering on the median, with potential siRNA hits deviating from the median (dashed red line) with the positive and negative controls. A Z score threshold cut off of ≥1.5 was set for positive hits, and ≤-2 for negative hits was set, and these siRNAs were considered for further validation. Data represents a single replicate out of the four replicates included in this screen.

Table 3.2. *Metabolic siRNA positive screen hits*
The table indicates the gene ID and gene symbol for siRNA screen positive hits. The knockdown of these genes decreased p53 accumulation in response to *MYC* activation. A gene was considered a hit if the median Z score ≥1.5.

Gene ID	Gene symbol	Median Z score	Plate replicates	Hits	Hit error
4609	*MYC*	4.5	1	1	NA
441531	*PGAM4*	2.5	3	3	0.30
57521	*RPTOR*	2.5	3	2	0.43
23657	*SLC7A11*	2.2	3	3	0.18
9517	*SPTLC2*	2.2	3	2	0.17
4191	*MDH2*	2.1	1	1	NA
3991	*LIPE*	2.0	1	1	NA
8877	*SPHK1*	1.8	3	2	0.16
2629	*GBA*	1.8	2	1	NA
5105	*PCK1*	1.6	3	1	0.25
4967	*OGDH*	1.6	3	1	1.13
23761	*PISD*	1.5	3	1	0.26
123099	*DEGS2*	1.5	4	1	0.23
5297	*PI4KA*	1.5	3	1	0.45
22934	*RPIA*	1.5	3	1	0.60
150763	*GPAT2*	1.5	2	1	NA

Table 3.3. *Metabolic siRNA screen negative hits*
The table indicates the gene ID and gene symbol for siRNA screen positive hits. The knockdown of these genes increased p53 accumulation in response to *MYC* activation. A gene was considered a hit if the median Z score ≤-2.0.

Gene ID	Gene symbol	Median Z score	Plate replicates	Hits	Hit error
7372	*UMPS*	-7.7	3	3	1.40
229	*ALDOB*	-5.0	4	4	0.57
5468	*PPARG*	-4.8	3	3	0.57
29095	*ORMDL2*	-4.6	3	3	0.68
247	*ALOX15B*	-4.1	4	4	1.09
33	*ACADL*	-3.7	3	2	0.91
7528	*YY1*	-3.6	3	3	0.28
581	*BAX*	-3.4	3	3	0.41
51046	*ST8SIA3*	-3.4	3	3	0.44
55825	*PECR*	-3.4	3	3	0.17
5319	*PLA2G1B*	-3.2	3	3	0.56
79993	*ELOVL7*	-3.1	1	1	NA
8612	*PPAP2C*	-3.1	3	3	0.13
57171	*DOLPP1*	-2.9	4	3	0.90
100137049	*PLA2G4B*	-2.8	3	3	0.64
79717	*PPCS*	-2.7	2	1	NA
239	*ALOX12*	-2.7	4	4	0.33
9023	*CH25H*	-2.6	4	3	0.41
1737	*DLAT*	-2.5	4	4	0.36
64834	*ELOVL1*	-2.0	1	1	NA

Table 3.4. *Functional annotation of metabolic siRNA screen hits*
The table indicates the top 5 functional annotations, as determined by lowest p-value, assigned by the functional annotation tool on The Database for Annotation, Visualization and Integrated Discovery (Huang *et al.* 2009). The number of genes classified into each functional category, and the p-value, is indicated. The p-value is calculated using a modified Fisher Exact test to measure the gene-enrichment in annotation terms.

Functional annotation	Gene count	p-value
Lipid metabolism	15	2.6E-15
Metabolic pathways	21	4.2E-09
Lipid biosynthesis	7	1.9E-07
Sphingolipid biosynthetic process	5	2.6E-06
Fatty acid biosynthetic process	5	3.5E-06

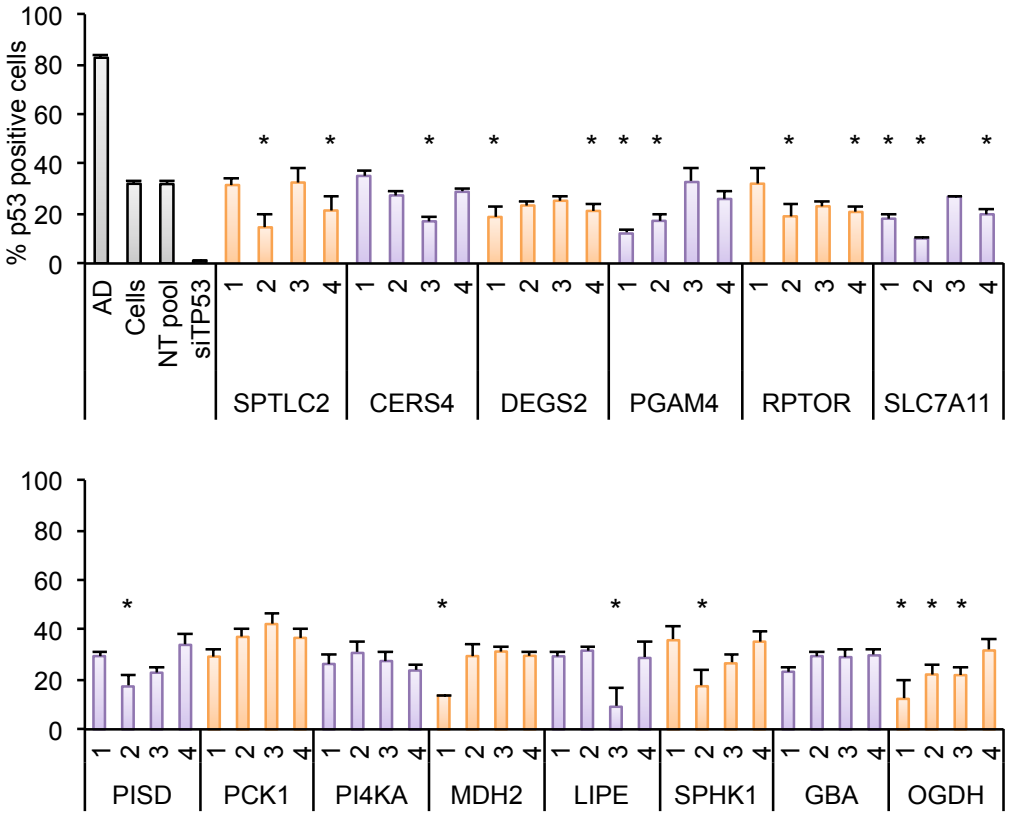

Figure 3.4. *Validation of metabolic siRNA screen positive hits*
Four individual siRNAs per gene were tested for their effect on percentage p53 positive cells. Percent p53 positive cells was calculated using an immunofluorescent p53 readout (p53-FITC), divided by total cell number (DAPI). siRNAs were considered to have a significant effect, as indicated by *, if they decreased percent p53 positive cells in the non-target (NT) pool by 30 percent. A gene was considered to be a strong hit if ≥2 of the 4 siRNAs were significantly changed.

phosphoglycerate mutase 4 (*PGAM4*), and regulatory associated protein of MTOR (*RPTOR*).

The identification of *RPTOR*, which is part of the mammalian target of rapamycin complex 1 (MTORC1), increased our confidence of the screen hits. MTOR is a master regulator of protein synthesis and collaborates with MYC to phosphorylate eukaryotic translation initiation factor 4E binding protein-1 (4EBP1) (Pourdehnad *et al.* 2013). Moreover, Pourdehnad *et al.* went on to show that MTOR-dependent phosphorylation of 4EBP1 is required for MYC-dependent tumour initiation and maintenance. Knockdown of *RPTOR* in this loss of function siRNA screen would likely inhibit MYC-driven cell growth, thereby decreasing metabolic stress, and potentially decreasing the homeostatic activation of p53. Pharmacological inhibitors of MTOR, Rapamycin and Torin 1, both significantly reduced p53 accumulation compared to the vehicle control (figure 3.5). This supported the contribution of MTOR activity to MYC-driven p53 accumulation.

Seven of the negative siRNA screen hits (i.e that increased MYC-driven p53 accumulation) were validated using 4 individual siRNAs per gene (figure 3.6). Ying-Yang 1 (*YY1*) was the strongest negative hit. As discussed above, one of the ways that MYC promotes mitochondrial biogenesis is by activating SURF-1 (a complex IV assembly factor), and this is dependent on a functional YY1 binding site (Vernon and Gaston, 2000). Knockdown of *YY1* in this screen may exacerbate metabolic stress due to dysfunctional mitochondrial homeostasis, and thus increase p53 accumulation. However, knockdown of *YY1* also significantly increased the percentage of p53 positive cells in Vec cells (figure 3.7), suggesting that increased stress caused by *YY1* knockdown is not a MYC-specific stress response. Other validated negative siRNA screen hits included the FA responsive transcription factor peroxisome proliferator-activated receptor gamma (*PPARG*), arachidonate 15-lipoxygenase, type B (*ALOX15B*), and peroxisomal trans-2-enoyl-CoA reductase (*PECR*), which is involved in FA elongation through FAO (Varga *et al.* 2011; Das *et al.* 2000). Interestingly, several of these hits are involved in arachidonate metabolism, which was previously described to be remodelled by *MYC* overexpression (Hall *et al.* 2016). Further analysis of MYC-driven changes in FA metabolism is outlined in chapter 4.

3.2 Validation of sphingolipid biosynthesis enzymes

The *de novo* sphingolipid synthesis pathway begins with the rate-limiting step, the condensation of an acyl-CoA (predominantly palmitoyl-CoA) and serine by SPT to form 3-ketosphinganine (reviewed in Eljamil *et al.* 2015). 3-ketosphinganine is then reduced in an NADPH-dependent reaction to sphinganine. Synthesis of dihydro-ceramide is catalysed by CERS, which adds an acyl-CoA that forms the FA residue of the lipid. In the last enzymatic step, DEGS desaturates dihydroceramide to ceramide in an NADPH-dependent reaction. As three consecutive *de novo* sphingolipid synthesis enzymes were validated using individual siRNAs, and these

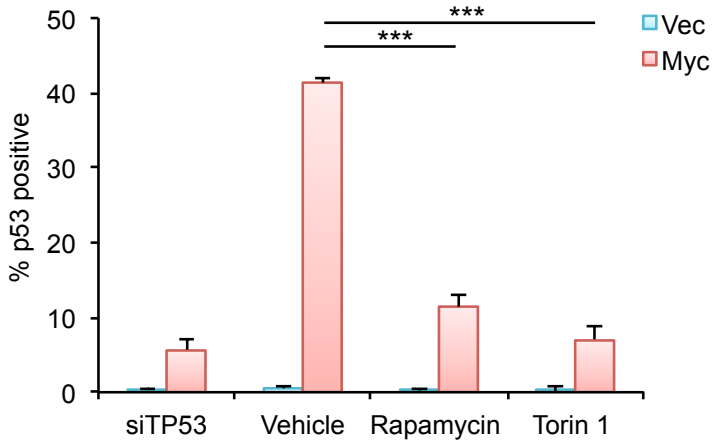

Figure 3.5. *Pharmacological inhibition of mTOR*
Cells were treated with mTOR inhibitors Rapamycin (1 nM) or Torin 1 (50 nM) at the same time as Myc activation with 4OHT for 48 hr. Error bars are the standard error (n=3). *** indicates a p-value ≤0.001 (T-test). Statistics were carried out on a single representative dataset.

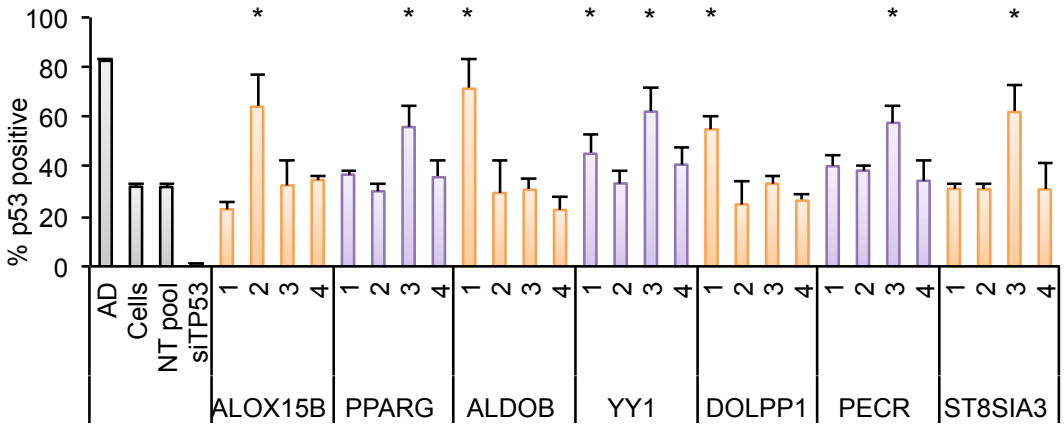

Figure 3.6. *Validation of metabolic siRNA screen negative hits*
Four individual siRNAs per gene were tested for their effect on percentage p53 positive cells. Percent p53 positive cells was calculated using an immunofluorescent p53 readout (p53-FITC), divided by total cell number (DAPI). siRNAs were considered to have a significant effect, as indicated by *, if they increased percent p53 positive cells in the non-target (NT) pool by 30 percent. A gene was considered to be a strong hit if ≥2 of the 4 siRNAs were significantly changed.

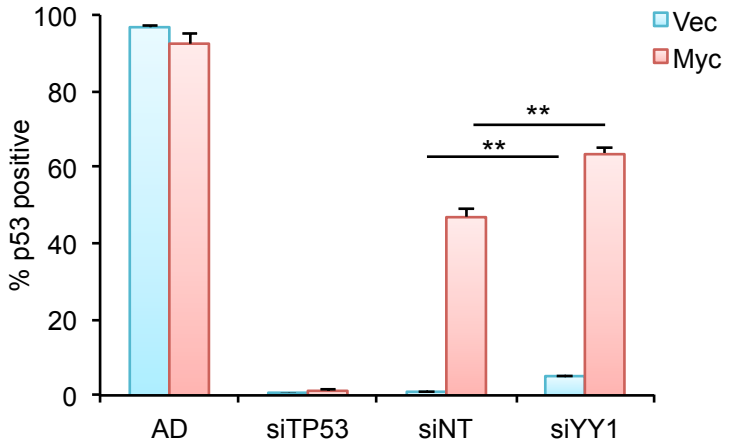

Figure 3.7. *siRNA knockdown of YY1*
Cells transfected with siNT were compared to those transfected with siYY1 for percent p53 positive cells as measured using a p53 immunofluorescent antibody. Error bars are the standard error (n=3). ** indicates a p-value <0.01 (T-test). Statistics were carried out on a single dataset.

genes were required for MYC-driven p53 accumulation, these genes were further characterised.

siRNA knockdown of *SPTLC2*, *CERS4*, and *DEGS2,* was respectively shown to significantly reduce p53 accumulation by immunofluorescent staining (figure 3.8A-C). Reduction of p53 levels was also demonstrated by western blot, whereby siRNA knockdown of *SPTLC2* or *DEGS2* reduced p53 levels to a similar extent as shown by immunofluorescent staining (figure 3.8D). Knockdown of each of the sphingolipid target genes was validated by qRT-PCR, and the decrease in mRNA expression was greater than 50 percent in all cases compared to siNT (figure 3.9A). Relative mRNA expression of *TP53* was measured to determine whether increased transcription could account for increased p53 protein levels. As described previously (Hermeking and Eick, 1997), mRNA expression increased only 3-fold (figure 3.9B), indicating that MYC-driven p53 accumulation is primarily regulated at the protein level. In keeping with this, siRNA knockdown of *SPTLC2*, *CERS4*, or *DEGS2* did not significantly change *TP53* or *CDKN2A* ($p14^{ARF}$) mRNA expression (figure 3.9C and D respectively).

Lentiviral shRNA constructs targeting *SPTLC2*, *CERS4*, *GBA*, and *SLC7A11* were each transfected into Vec or Myc cells to test their effect on p53 accumulation. Three constructs were tested for each of the genes by qRT-PCR to select the construct with the strongest knockdown of mRNA expression (figure 3.10A). The strongest construct for each gene was tested for its effect on p53 accumulation; however none of the constructs affected p53 accumulation compared to empty vector alone (figure 3.10B). This was surprising for *SPTLC2*, *CERS4*, and *SLC7A11* as all three of these genes were validated by siRNA. As *GBA* was not validated the lack of effect on p53 accumulation as a result of its knockdown was not unexpected. To determine whether there was a problem with lentiviral shRNA knockdown, retroviral shRNA constructs (regulated by different promoters) targeting *SPTLC2*, *CERS4*, and *DEGS2* were tested for their effect on MYC-driven p53 accumulation. By western blot, shSPTLC2 depleted p53 levels to a similar extent as was seen by siRNA knockdown of SPTLC2; however shDEGS2 did not affect p53 levels (figure 3.11A). By western blot, shCERS4 depleted p53 similarly to shSPTLC2 (figure 3.11B). Thus data obtained with retroviral shRNA transduction supported our initial siRNA observations.

One possibility was that *de novo* ceramide synthesis enzymes were not regulating p53 stability but were affecting *MYC* overexpression. To test this, levels of the MYC target gene carbamoyl-phosphate synthetase 2 (CAD) were measured by western blot in cells transfected with control or shSPTLC2 (Grandori and Eisenman, 1997). *MYC*-deregulated cells increased CAD protein levels to a detectable level, and this persisted in *MYC* deregulated cells with SPTLC2 knockdown, despite p53 levels decreasing (figure 3.11C). This indicated knockdown of *de novo* ceramide synthesis enzymes regulated p53 accumulation in response to *MYC* overexpression, not through inhibition of *MYC* overexpression itself.

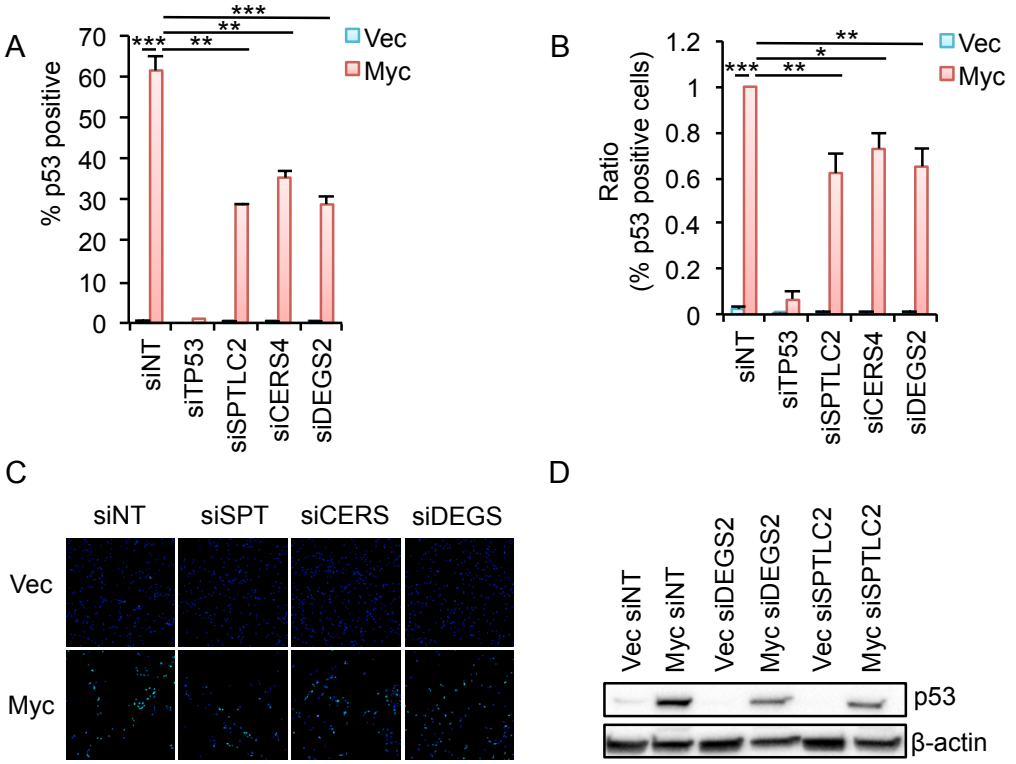

Figure 3.8. *siRNA knockdown of de novo sphingolipid synthesis- effect on protein level*

(A) Histogram compares percent p53 positive cells in the non-target pool (siNT) to siSPTLC2, siCERS4, and siDEGS2. Percent p53 positive cells was calculated using an immunofluorescent p53 readout (p53-FITC), divided by total cell number (DAPI). * indicates a p-value ≤0.05 (T-test) for a single representative dataset; however this pattern of results was obtained in triplicate. (B) As in (A), however histogram shows the ratio of percent p53 positive cells. * indicates a p-value ≤0.05 (T-test) across 3 biological replicates. (C) Immunofluorescent images show the effect of siRNA knocdown of sphingolipid synthesis enzymes *SPTLC2, CERS4,* and *DEGS2* on p53 accumulation, as quantified in (A) and (B). Immunofluroescence shows DAPI (blue) and p53-FITC (green). (D) Western blot compares p53 accumulation in siNT to siDEGS2 and siSPTLC2 (n=1).

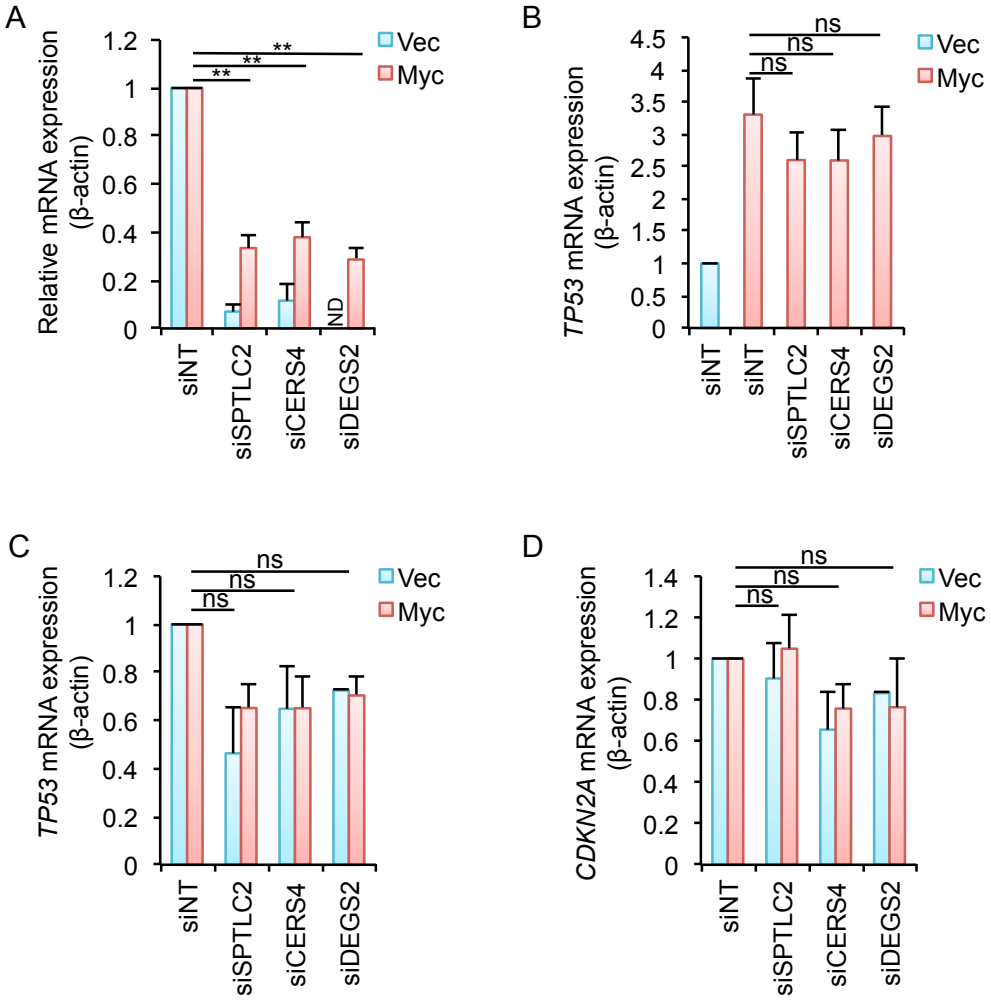

Figure 3.9. *siRNA knockdown of de novo sphingolipid synthesis- effect on mRNA expression*

(A) Histogram of qRT-PCR data indicates the knockdown efficiency of siSPTLC2, siCERS4, and siDEGS2 for their respective genes, as indicated by the relative mRNA expression (β-actin). * indicates a p-value ≤0.05 (T-test) for a single representative dataset. ND indicates that mRNA was not detected in the sample set. (B) Histogram of qRT-PCR data indicates the relative mRNA expression (β-actin) of *TP53*. ns= not significant (T-test). (C) Histogram of qRT-PCR data indicates the relative mRNA expression (β-actin) of *CDKN2A*.

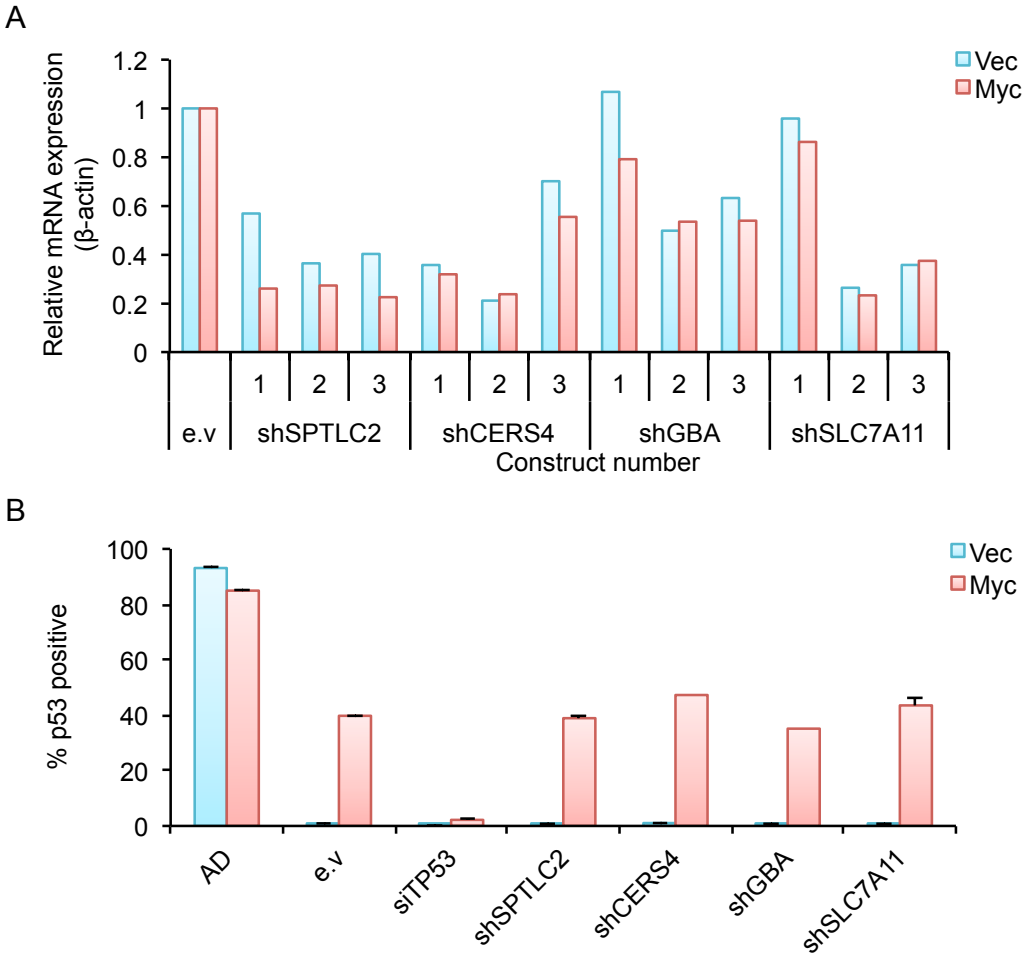

Figure 3.10. *Lentiviral shRNA knockdown of metabolic siRNA screen hits*
(A) Histogram of qRT-PCR data indicates the knockdown efficiency of 3 shRNA constructs against *SPTLC2*, *CERS4*, *GBA*, and *SLC7A11* (n=1). Values are the relative mRNA expression (β-actin). (B) Construct number 2 for each of the constructs tested in (A) was further analysed for the effect of the knockdown on p53 accumulation. Histogram compares the percent p53 positive cells in the empty vector (e.v) to shRNA knockdown of *SPTLC2*, *CERS4*, *GBA*, and *SLC7A11* (n=3). Percent p53 positive cells was calculated using an immunofluorescent p53 readout (p53-FITC), divided by total cell number (DAPI).

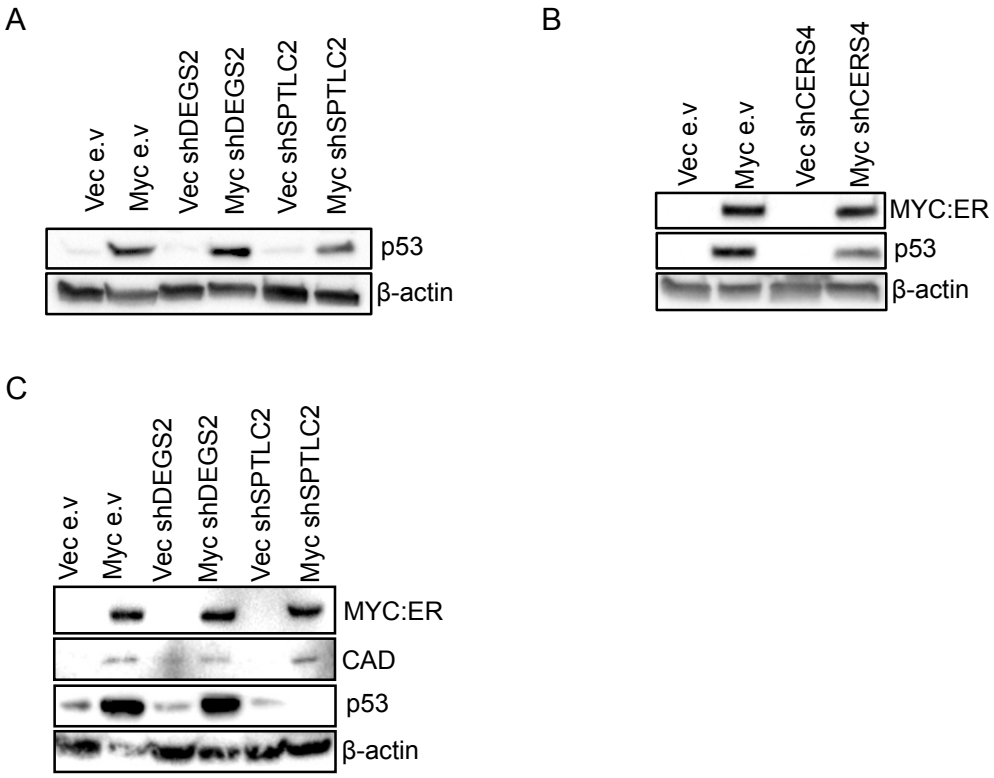

Figure 3.11. *Retroviral shRNA knockdown of of de novo sphingolipid synthesis-effect on protein level*
(A) Western blot compares p53 accumulation in the empty vector (e.v) to shDEGS2 and shSPTLC2 (n=1). (B) Western blot compares p53 accumulation in the empty vector (e.v) to shCERS4 (n=3). (C) Western blot compares CAD protein (MYC-target gene) in the empty vector (e.v) to shDEGS2 and shSPTLC2 (n=1).

Knockdown of each of the target genes was validated by qRT-PCR. Relative mRNA expression was reduced by over half using shSPTLC2 construct 2, and this was selected as the strongest construct (figure 3.12A). *DEGS2* mRNA was reduced to undetectable levels in all four shRNA constructs (figure 3.12A). *CERS4* mRNA was reduced by over 80 percent in the single construct tested (figure 3.12B). The effect of shCERS4 on *TP53* and *CDKN2A* mRNA expression was also tested and showed no significant differences (figure 3.12C and D respectively). This suggested that shRNA-mediated knockdown of *SPTLC2* and *CERS4* blocked MYC-driven p53 accumulation at the protein level, as opposed to blocking *TP53* transcription.

SPT is the first and rate-limiting enzyme in *de novo* ceramide synthesis, which synthesises the sphingosine backbone (reviewed in Eljamil *et al.* 2015). Three main SPT subunits have been identified in human tissues, of which SPTLC2 and SPTLC3 contain pyridoxal-binding motifs required for catalytic activity (Hornemann *et al.* 2006, 2007). SPTLC1 in complex with either SPTLC2 or SPTLC3 associates with a third small subunit SPTSSB. Overexpression of SPT subunits was hypothesised to potentially increase *de novo* ceramide synthesis, and thereby increase p53 accumulation; however retroviral overexpression constructs of SPTLC1, SPTLC2 or SPTSSB did not alter p53 accumulation compared to the empty vector control (figure 3.13). However, overexpression of each of the target genes was not validated by mRNA expression or by western blot.

ORMDL2 was identified as the fourth strongest hit during the loss of function siRNA screen. ORMDL proteins are negative regulators of *de novo* ceramide synthesis, and knockdown of *ORMDL2* therefore increased p53 accumulation (table 3.3). Mammalian ORMDL proteins are orthologues of the yeast Orm proteins (Orm 1/2), which negatively regulate SPT in response to changes in cellular ceramide levels (Breslow *et al.* 2010; Han *et al.* 2010; Liu *et al.* 2012). Overexpression of *ORMDL2* was hypothesised to decrease SPT activity, reduce *de novo* sphingolipid synthesis, and reduce p53 accumulation. Overexpression of *ORMDL2* was validated by western blot (figure 3.14). Surprisingly, *ORMDL2* overexpression increased p53 and p21 levels in *MYC* deregulated cells, and also increased p21 levels in Vec control cells (rather than decreased as expected). As *ORMDL2* knockdown and overexpression both increased p53 levels it is likely that ORMDL proteins have other cellular roles independent of SPT regulation.

Retroviral overexpression of *CERS4* moderately increased p53 accumulation compared to the empty vector (figure 3.15A). Interestingly, *CERS4* overexpression strongly increased *TP53* mRNA expression both in Vec control and Myc cells (>15-fold and >50-fold respectively; figure 3.15B). This indicates that overexpression of *CERS4* engages an alternative p53 response involving the transcriptional activation of p53 to that driven by *MYC* deregulation. Overexpression of *CERS4* was validated by LC-MS using a 2,3-^{13}C-serine heavy isotope label to trace *de novo* ceramide synthesis (figure 3.15C). Uptake of the M+2 label into ceramide with FA chain lengths 18:0, 20:0, and 22:0 was increased in Vec and Myc cells that overexpressed *CERS4* compared to the empty vector. Synthesis of ceramide 18:1, 20:0 was the most affected by *CERS4* overexpression; increasing percent label incorporation by over

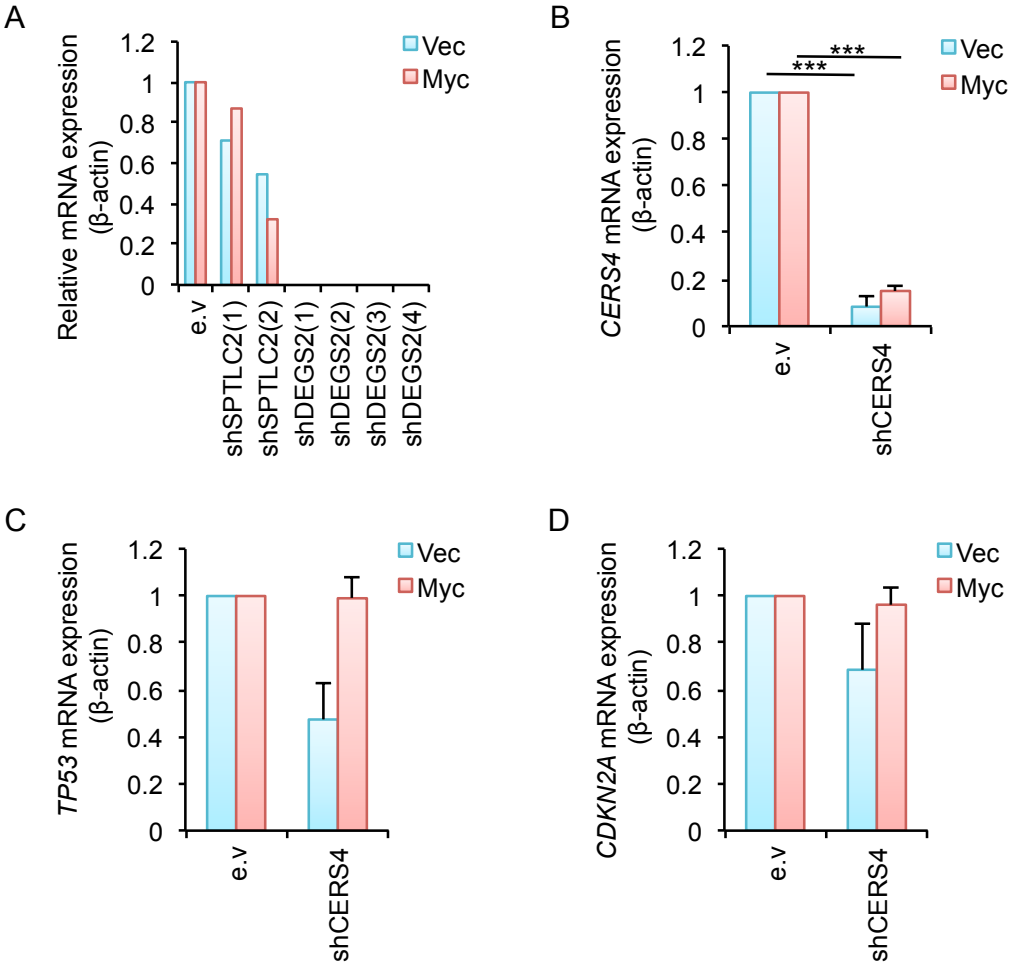

Figure 3.12. *Retroviral shRNA knockdown of of de novo sphingolipid synthesis-effect on mRNA expression*

Histograms show qRT-PCR data. Values are the relative mRNA expression (β-actin). (A) Histogram indicates the knockdown efficiency of 2 shRNA constructs against *SPTLC2*, and 4 constructs against *DEGS2*. (B) Histogram indicates the knockdown efficiency of shCERS4. Error bars are the standard error (n=3). * indicates a p-value≤0.05 comparing e.v with shCERS4. Statistics were carried out on a single dataset. (C) Histogram compares the mRNA expression of *TP53* in e.v to shCERS4. Error bars are the standard error (n=3). (D) Histogram compares the mRNA expression of *CDKN2A* in e.v to shCERS4. Error bars are the standard error (n=3).

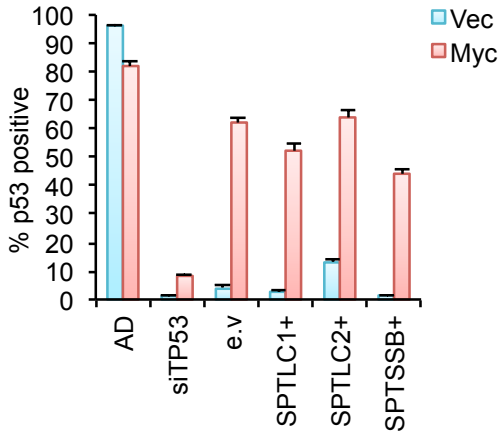

Figure 3.13. *Stable overexpression of serine palmitoyl transferase subunits*
Histogram compares the percent p53 positive cells in the empty vector (e.v) to retroviral overexpression of serine palmitoyl transferase subunits SPTLC1, SPTLC2, and SPTSSB. Percent p53 positive cells was calculated using an immunofluorescent p53 readout (p53-FITC), divided by total cell number (DAPI).

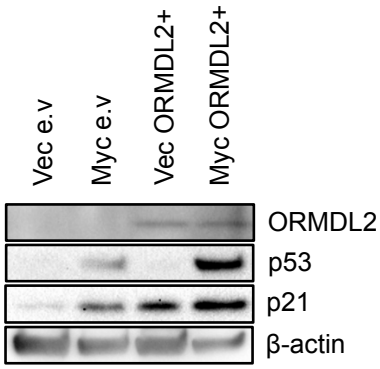

Figure 3.14. *Stable overexpression of ORMDL2*
Western blot shows overexpression of ORMDL2 (ORMDL2+), and the effect this has on accumulation of p53 and p21 following 48 hr *MYC* activation (n=1).

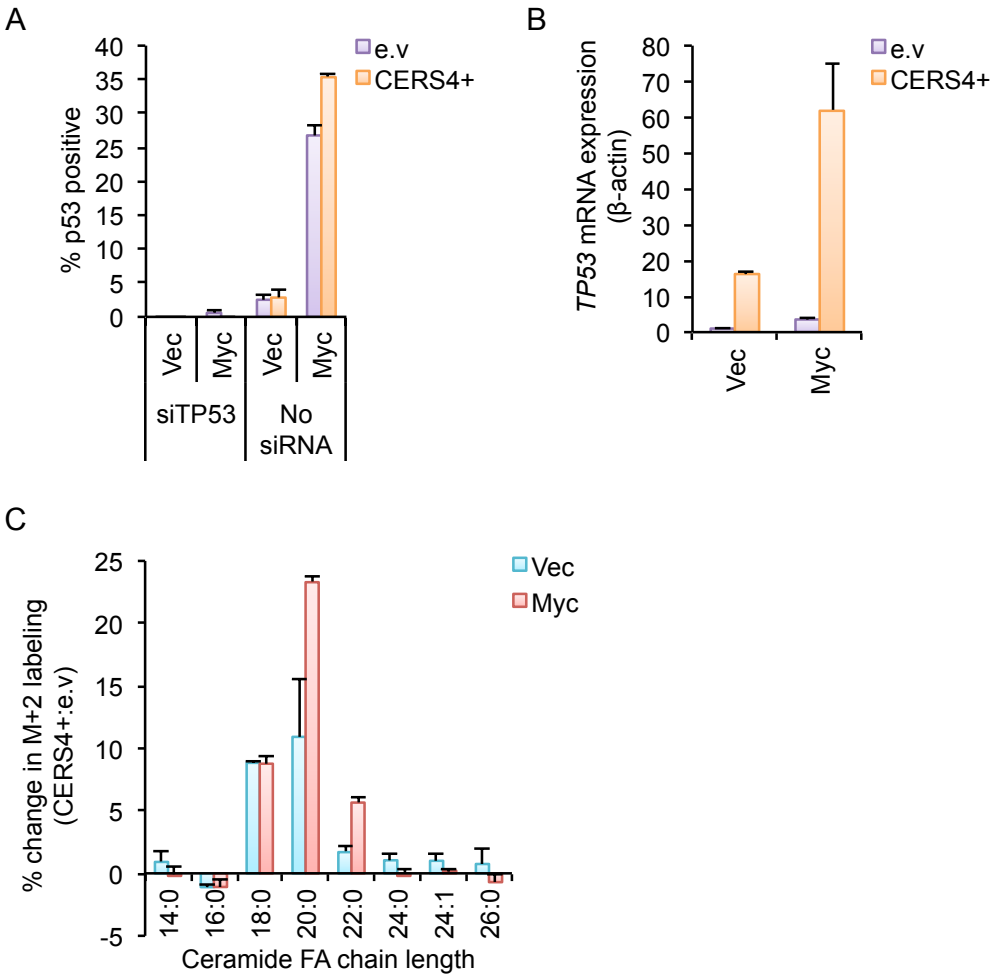

Figure 3.15. *Stable overexpression of ceramide synthase 4*
(A) Histogram compares the percent p53 positive cells in the empty vector (e.v) to retroviral overexpression of *CERS4*. Percent p53 positive cells was calculated using an immunofluorescent p53 readout (p53-FITC), divided by total cell number (DAPI). (B) Histogram of qRT-PCR data indicates the relative mRNA expression (β-actin) of *TP53*. The ratio of Vec/e.v is compared to all other conditions. (C) The histogram shows percent change in M+2 labeling (from a 48 hr 2,3-C_{13}-serine pulse) between e.v and CERS4+. The x-axis indicates the ceramide FA (fatty acid) chain length of a ceramide with a 18:1 sphingosine backbone. An increase in M+2 labeling validates *CERS4* overexpression and indicates the specificity of CERS4 for synthesis of a particular ceramide FA chain length.

10% in Vec cells and 20% in Myc cells. This validated *CERS4* overexpression, and indicated the specificity of this enzyme for C18 to C22 FA chain lengths, as previously described (Sassa and Kihara, 2014).

3.3 Mitochondrial and endoplasmic reticulum stress

As mentioned above, at the same time as the primary metabolic siRNA screen was carried out in this study, Liu *et al.* (2014b) reported a genome-wide siRNA screen with overlapping hits in sphingolipid metabolism (figure 3.16). Liu *et al.* used antimycin A treatment to disrupt mitochondrial function, and looked for siRNAs that disrupted activation of mitochondrial chaperone genes *hsp-6* and *hsp-60* in *C.elegans* (GRP75 in humans). Due to the similarity in screen hits it is highly plausible that *MYC* deregulation and sphingolipid remodelling may induce mitochondrial stress. *MYC* deregulation increased GRP75 positive cells by immunofluorescent staining (figure 3.17A and B). Induction of GRP75 following *MYC* deregulation was observed more clearly by western blot where GRP75 levels clearly increased (figure 3.17C). This may indicate the sphingolipid remodelling at the mitochondrion contributes to p53 accumulation.

As *de novo* sphingolipid synthesis occurs at the endoplasmic reticulum (ER), the effect of *MYC* deregulation on ER chaperone gene GRP78 was also tested by western blot. *MYC* deregulation had no clear effect on GRP78 levels, probably indicating that MYC-driven lipid remodelling does not cause ER stress.

3.4 Summary

Based upon a large metabolic loss of function siRNA screen, this chapter outlines the identification of two key clusters of metabolic enzymes that regulate the p53 response to *MYC* deregulation. Knockdown of enzymes involved in sphingolipid synthesis, particularly *de novo* ceramide synthesis, decreased p53 accumulation. This was with the exception of ORMDL2 whose knockdown increased p53 accumulation; however ORMDL2 is described to negatively regulate SPT and therefore validates this cluster of sphingolipid hits (Breslow *et al.* 2010). Knockdown of a second cluster of enzymes involved in FA biosynthesis, particularly arachidonic acid synthesis, increased p53 accumulation. This indicates that reduction of arachidonate metabolism may be metabolically stressful in *MYC* deregulated cells, as described previously (Hall *et al.* 2016).

Several hits in both functional clusters were validated using individual siRNAs targeting each gene, as opposed to siRNA pools. *De novo* ceramide synthesis enzymes *SPTLC2*, *CERS4*, and *DEGS2*, as well as FA synthesis enzymes *ALOX15B* and *PECR*, were validated in this manner. FA-responsive transcription factor PPARγ was also validated, indicating that PPARγ may be a key sensor of MYC-driven FA remodelling. The role of glycolytic and TCA cycle enzymes in regulating p53 was

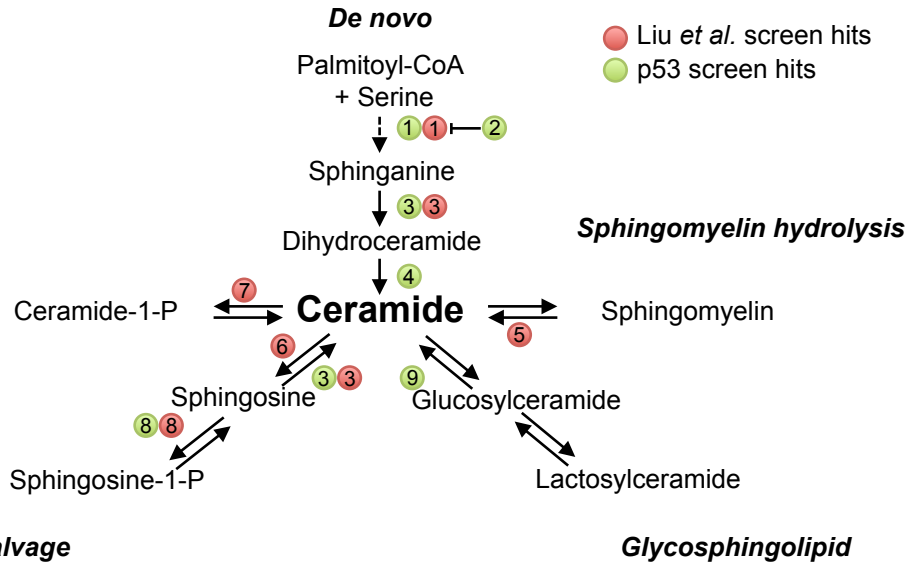

#	Gene product	Homo sapiens gene	*C.elegans* gene
1	Serine palmitoyl transferase	SPTLC2	*sptl-1, sptl-3*
2	ORMDL sphingolipid biosynthesis regulator	ORMDL2	-
3	Ceramide synthase	CERS4*	*hyl-2, hyl-1, lagr-1*
4	Dihydroceramide desaturase	DEGS2	-
5	Sphingomyelinase	-	*asm-3*
6	Ceramidase	-	
7	Ceramide kinase	-	
8	Sphingosine kinase	SPHK1	*sphk-1*
9	Glucosylceramidase	GBA	-

- gene not identified as a hit in this screen
* gene not identified in the primary siRNA screening process but later validated as a screen hit

Figure 3.16. *Diagram of sphingolipid hits and corresponding genes that overlapped between the primary siRNA screen and a genome wide siRNA screen in C.elegans*

Diagram compares sphingolipid hits from the primary siRNA screen and a genome-wide siRNA screen published by Liu *et al.* (2014b). Liu *et al.* used antimycin A treatment (a mitochondrial complex III inhibitor) to induce mitochondrial stress, and looked for hits whose knockdown blocked induction of mitochondrial chaperone genes in *C.elegans*. Sphingolipid enzymes identified as hits in either screen are indicated by a coloured dot (see key), and the number corresponds to the gene product indicated in the table below the diagram.

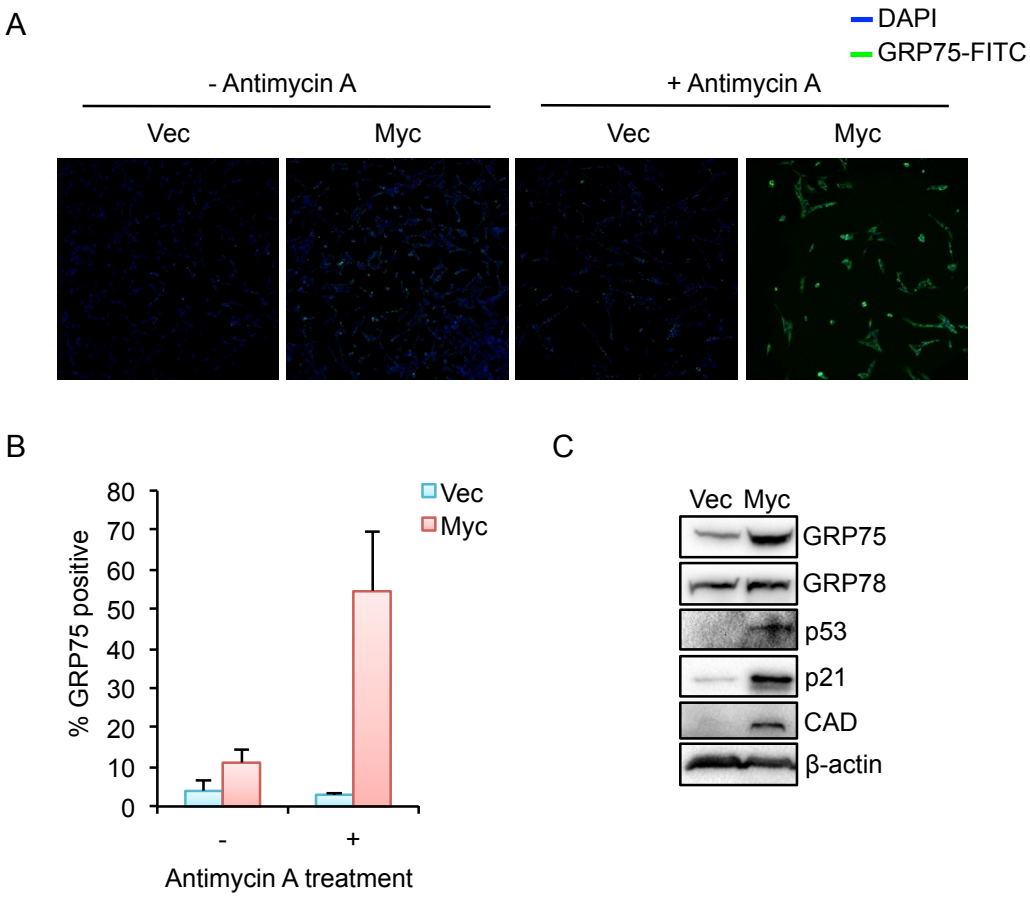

Figure 3.17. *Mitochondrial stress response*
(A) The immunofluorescent images show levels of mitochondrial chaperone protein GRP75 following *MYC* activation and/or treatment with antimycin A, which inhibits mitochondrial complex III and thereby induces mitochondrial stress. (B) The histogram quantifies levels of GRP75 protein in the images from A. Error bars are the standard error (n=3). (C) The western blot shows levels of GRP75 and endoplasmic reticulum chaperone protein GRP78 in response to *MYC* activation. MYC-target gene CAD verifies *MYC* activation.

less clear. Knockdown of PGAM4, OGDH, and malate dehydrogenase 2 (MDH2) were validated to decrease p53 accumulation, while knockdown of ALDOB increased p53 accumulation. These enzymes are likely to be important for acetyl-CoA synthesis.

Stable shRNA knockdown of *SPTLC2*, *CERS4*, and *DEGS2*, was tested to give further insight into the role of *de novo* ceramide synthesis in regulating p53. Knockdown of *SPTLC2* was initially successful (as measured by reduced mRNA expression), and reduced p53 protein levels without affecting protein levels of MYC-target gene CAD (Grandori and Eisenman, 1997). This indicated that MYC-driven ceramide synthesis was regulating p53 accumulation, as opposed to reducing *MYC* overexpression.

Following several passages, shRNA knockdown of SPTLC2 no longer reduced p53 protein levels, indicating that SPTLC2 was either compensated for or selected against. SPTLC2 and SPTLC3 have different acyl-CoA specificities for palmitoyl-CoA (C16-CoA) or mysristoyl (C14-CoA) and lauryl-CoA (C12-CoA) respectively (Hornemann *et al.* 2009). Ceramides with 18:1 backbones (derived from C16-CoA) are predominantly synthesised in mammalian cells (Hanada *et al.* 2000); however it is not clear whether SPTLC3 may compensate for SPTLC2 following its knockdown. It is possible that SPTLC3 can initially compensate for SPTLC2, but is eventually selected against. Concomitantly, Ruangsiriluk *et al.* (2012) documented no decrease in ceramides following silencing of SPTLC2 or SPTLC3, while silencing all three SPT enzymes reduced ceramide levels. This could explain why overexpression of SPTLC1, SPTLC2 or SPTSSB alone had no affect on p53 accumulation.

Retroviral shRNA knockdown of *CERS4* reduced *CERS4* mRNA expression, and *MYC* deregulated cells had reduced levels of p53 protein. CERS adds a fatty acyl-CoA to the sphinganine backbone, and six CERS enzymes confer different chain length specificities. CERS1 uses C18-CoA (Venkataraman *et al.* 2002), CERS2 uses C22-C24-CoAs (Laviad *et al.* 2008), CERS3 uses ≥C26-CoAs (Mizutani *et al.* 2006), CERS4 uses C18-C22-CoAs (Riebeling *et al.* 2003), and CERS5 and CERS6 mainly use C16-CoAs (Mizutani *et al.* 2005). In keeping with this, overexpression of CERS4 only increased the synthesis of ceramides with C18-C22 FA residues. Knockdown of *CERS4* reproducibly reduced p53 protein levels, indicating *CERS4* knockdown may be tolerable due to the small group of ceramides it catalyses, while still sufficient to affect p53 accumulation.

Stable shRNA knockdown of DEGS2 strongly reduced DEGS2 mRNA expression but had no effect on p53 protein level. Ruangsiriluk *et al.* (2012) reported that silencing DEGS1 is sufficient to reduce ceramides to a similar extent as that of silencing all three SPT enzymes. This demonstrates that DEGS1 is the predominant desaturase enzyme in mammalian cells; however it is unclear why siRNA knockdown of DEGS2 was not also compensated for by DEGS1, or why DEGS1 was not identified as a hit in the siRNA screen.

Knockdown of SPTLC2, CERS4 or DEGS2 decreased p53 protein, but did not affect *TP53* mRNA expression. This indicates that *de novo* ceramide synthesis positively regulates p53 accumulation at the protein level. The following chapters investigate whether p53 protein is stabilised in response to MYC-driven lipid and fatty acid synthesis, with a particular focus on sphingolipid synthesis and arachidonate metabolism.

4 Chapter 4- MYC-driven metabolite changes

This chapter presents data focused upon untargeted and targeted metabolite analyses to interrogate MYC-driven changes in metabolic pathways with particular focus upon MYC-driven fatty acid (FA) changes. Understanding the effect of *MYC* activation on FA synthesis was of particular importance due to the functional annotation of one of the two major screen clusters in this pathway. Further, as ceramides (components of the other major cluster) are synthesised from two fatty acyl-CoAs, FA synthesis also feeds directly into this cluster. Finally, this chapter investigates the effect of p53 loss on MYC-driven metabolite changes (using a p53 dominant negative construct), to address the hypothesis that loss of p53 gives *MYC* activated cells a metabolic advantage.

4.1 Untargeted analysis of MYC-driven metabolic flux

Stable heavy isotope labelling was used as a tool to measure flux through metabolic pathways (reviewed in Chokkathukalam *et al.* 2014). Cells were pulsed with U-^{13}C-glucose or a dual ^{15}N-amide-glutamine and $^{13}C_5$-glutamine isotope label for 6 hr before metabolite extraction. X13CMS software was used to compare Vec and Myc cells and identify significant changes ($p \leq 0.05$) in percent labelling of metabolites driven by *MYC* activation (summarised in figure 4.1). X13CMS software was used for the analysis because it compares percent labelling of ions between two biological conditions in an untargeted manner, allowing for identification of flux through pathways not typically included in targeted analyses (Huang *et al.* 2014). *MYC* activation moderately increased labelling of lactate (1.4 fold-change) from U-^{13}C-glucose, and targeted analysis of glycolysis revealed an increase in label incorporation into pyruvate (1.3 fold-change) in Myc cells (table 4.1). This indicated that MYC drives glycolysis, although perhaps not to the extent suggested previously from MYC target genes (Osthus *et al.* 2000).

Further targeted analysis following U-^{13}C-glucose labelling showed that *MYC* activation significantly increased labelling of the serine synthesis pathway (SSP), as determined by increased label incorporation into serine and glycine (4.2 and 6 fold-change respectively). Untargeted analysis of ^{15}N-amide-glutamine incorporation revealed *MYC* activation strongly increased synthesis of nucleotides, nucleosides, and nucleobases; and further targeted analysis identified nucleotide-based lipid precursors, CDP-ethanolamine, CDP-choline, and UDP-glucose, to also be significantly labelled in Myc cells (table 4.2; $p \leq 0.05$). CDP-choline and CDP-ethanolamine are used to synthesise glycerolipids, fitting with the broader classification of siRNA screen hits in lipid biosynthesis. UDP-glucose is used to synthesise glycosphingolipids and is also important for protein glycosylation. Nucleotides ATP and UTP, as well as UDP-glucose, were also identified as hits from the U-^{13}C-glucose untargeted analysis, strengthening these hits due to the overlap between two independent isotope labelling experiments.

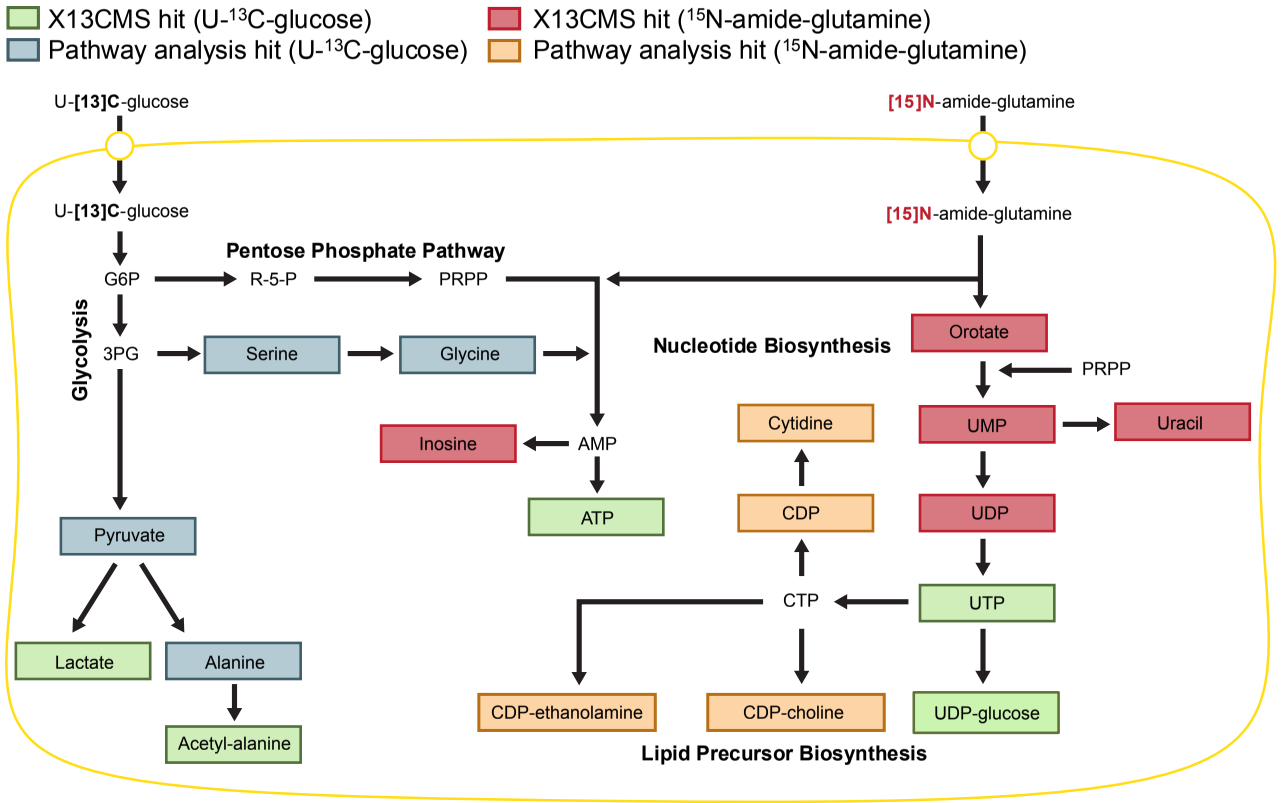

Figure 4.1. *Untargeted analysis of Myc driven isotope labeling*
U-^{13}C-glucose (25 mM) or ^{15}N-amide glutamine (4 mM) labeled media was added to Vec and Myc cells for 6 hr before metabolite extraction. An unlabeled control was also included to allow untargeted heavy isotope tracer analysis to be carried out using X13CMS software. Metabolites that were significantly labeled by U-^{13}C-glucose (green) or ^{15}N-amide-glutamine (red) in Myc compared to Vec are highlighted. Further targeted analysis of pathways containing a hit was then carried out to pull out significant metabolites that were missed using X13CMS. Pathway analysis are indicated in blue (U-^{13}C-glucose) and orange (^{15}N-amide-glutamine).

Table 4.1. *Untargeted analysis of U-^{13}C-glucose incorporation*
Table summarises isotope tracer analysis following a 6 hr U-13C-glucose pulse. X13CMS software was used to identify ions with ^{13}C incorporation, then the percent label incorporation in Vec and Myc samples was compared to identify significant changes. X13CMS hits that significantly increased or decreased in Myc are indicated in the first panel of the table. Predominant isotopologue, ratio of Vec to Myc percent label, and pvalue (T-test) are also indicated. Significant hits were taken for further processing to verify peak integrity. Peak area was then extracted and normalised to total ion count (TIC). The normalised results are indicated in the second panel of the table. The third panel 'Normalised pathway analysis hit' shows metabolites that were not pulled out by X13CMS, but were in the same pathway as a metabolite that was a hit. The panel indicates that these metabolites had a p-value ≤0.05 following normalisation.

X13CMS hits			
Increased in Myc			
Metabolites	Predominant isotopologue	Ratio	p-value
Lactic acid	M+3	1.5	0.002
Acetyl-alanine	M+5	2.0	≤0.001
Glutamic acid	M+2	1.5	0.001
Acetyl-glutamic acid	M+2	11.7	≤0.001
Acety-methionine	M+2	1.2	≤0.001
Uridine triphosphate	M+5	1.2	0.001
Adenosine triphosphate	M+6	1.2	≤0.001
Uridine disphosphate-glucose	M+11	1.1	≤0.001
Decreased in Myc			
Acetyl-aspartyl-glutamic acid	M+11	10.57	≤0.001
Normalised X13CMS hits			
Increased in Myc			
Metabolites	Predominant isotopologue	Ratio	p-value
Lactic acid	M+3	1.4	0.010
Acetyl-alanine	M+5	1.9	≤0.001
Glutamic acid	M+2	1.5	0.004
Acetyl-glutamic acid	M+2	3.0	≤0.001
Acetyl-methionine	M+2	1.2	≤0.001
Uridine triphosphate	M+5	1.1	≤0.001
Adenosine triphosphate	M+6	1.2	≤0.001
Uridine disphosphate-glucose	M+11	1.1	≤0.001
Decreased in Myc			
Acetyl-aspartyl-glutamic acid	M+11	5.62	≤0.001
Normalised pathway analysis hits			
Increased in Myc			
Metabolites	Predominant isotopologue	Ratio	p-value
Pyruvic acid	M+3	1.3	≤0.001
Alanine	M+3	1.5	≤0.001
Glycine	M+2	6.0	≤0.001
Serine	M+3	4.2	≤0.001

Table 4.2. *Untargeted analysis of ^{15}N-amide-glutamine incorporation*
Table summarises isotope tracer analysis following a 6 hr ^{15}N-amide-glutamine pulse. X13CMS software was used to identify ions with ^{15}N incorporation, then the percent label incorporation in Vec and Myc samples was compared to identify significant changes. X13CMS hits that significantly increased or decreased in Myc are indicated in the first panel of the table. Predominant isotopologue, ratio of Vec to Myc percent label, and pvalue (T-test) are also indicated. Where the ratio reads Inf, this indicates that the percent label in Vec was below the threshold of detection giving an infinite ratio. Significant hits were taken for further processing to verify peak integrity. Peak area was then extracted and normalised to total ion count (TIC). The normalised results are indicated in the second panel of the table. The third panel 'Normalised pathway analysis hit' shows metabolites that were not pulled out by X13CMS, but were in the same pathway as a metabolite that was a hit. The panel indicates that these metabolites had a p-value ≤0.05 following normalisation.

X13CMS hits			
Metabolites	Predominant isotopologue	Ratio	p-value
Uracil	M+1	Inf. (0 in control)	
Orotic acid	M+1	Inf. (0 in control)	
Cys-Gly	M+1	Inf. (0 in control)	
Inosine	M+1	Inf. (0 in control)	
Uridine monophosphate	M+1	Inf. (0 in control)	
Uridine diphosphate	M+1	Inf. (0 in control)	
Uridine diphosphate-acetyl-glucosamine	M+1	1.2	0.033
Normalised X13CMS hits			
Metabolites	Predominant isotopologue	Ratio	p-value
Uracil	M+1	29.5	≤0.001
Orotic acid	M+1	2.1	0.005
Cys-Gly	M+1	Inf. (0 in control)	
Inosine	M+1	Inf. (0 in control)	
Uridine monophosphate	M+1	Inf. (0 in control)	
Uridine diphosphate	M+1	3.3	≤0.001
Uridine diphosphate-acetyl-glucosamine	M+1	1.2	≤0.001
Normalised pathway analysis hits			
Metabolites	Predominant isotopologue	Ratio	p-value
Uridine triphosphate	M+1	1.5	≤0.001
Cytidine diphosphate	M+1	Inf. (0 in control)	
Cytidine	M+1	10.9	≤0.001
Cytidine diphosphate-choline	M+1	Inf. (0 in control)	
Uridine disphosphate-glucose	M+1	2.3	≤0.001
Cytidine diphosphate-ethanolamine	M+1	10.2	≤0.001

Incorporation of $^{13}C_5$-glutamine into the TCA cycle was observed in Vec and Myc cells (figure 4.2); however untargeted analysis of this label did not reveal any significant differences between the two cell types. This was unexpected as *MYC* activation clearly increased incorporation of glutamine-derived amide into nucleotide biosynthesis (see above), which also generates glutamate. One possibility is that increased glutamate synthesised during nitrogen donation is rapidly metabolised into downstream pathways that were not detected by X13CMS (such as glutathione metabolism).

Several studies of MYC target genes have indicated enzymes involved in nucleotide biosynthesis are required for MYC-driven cell proliferation (Liu *et al.* 2008; Mannava *et al.* 2008; Cunningham *et al.* 2014), and these isotope tracer experiments clearly demonstrate that MYC drives a demand for nucleotide biosynthesis that is met by glucose-derived carbon (through the pentose phosphate pathway) and glutamine-derived amine donation. Importantly these experiments also revealed that *MYC* activated cells increase synthesis of nucleotide-based lipid precursors, which may be indicative of increased lipid synthesis in *MYC* activated cells.

4.2 MYC-driven fatty acid changes

Several *de novo* FA biosynthesis enzymes have been identified as MYC target genes (Zeller *et al.* 2003; Loven *et al.* 2012), however as shown above no FAs were significantly labelled by a 6 hr U-^{13}C-glucose pulse (table 4.1). This was likely because a large proportion of glucose-derived carbon was used in early glycolytic pathways (such as the pentose phosphate pathway and serine synthesis pathway) rather than being converted into pyruvate (for FA synthesis) further down glycolysis. To determine the effect of *MYC* activation on *de novo* FA synthesis, Vec or Myc cells were pulsed with $^{13}C_3$-pyruvate over a timecourse of 2, 4, or 8 hr (figure 4.3). All metabolites were then normalised to a 100 percent pyruvate label at timepoint 2 hr, which allowed visualisation of percent label incorporation as a 'pulse chase' style experiment. $^{13}C_3$-pyruvate was added at a concentration of 1 mM to cells otherwise cultured in pyruvate-free medium. Labelled pyruvate was rapidly taken up into Vec or Myc cells at 2 hr and the percentage of labelled pyruvate decreased over the timecourse in both cell types, indicating rapid consumption and depletion of the labelled pyruvate. This transient labelling pattern was observed for lactate, citrate, and α-ketoglutarate, demonstrating flux of the label into downstream pathways.

MYC activated cells increased synthesis of lactate compared to control cells, in keeping with activation of the MYC target gene LDHA, and the untargeted U-^{13}C-glucose pulse described above (Shim *et al.* 1997). Synthesis of citrate was consistently increased in *MYC* activated cells across the timecourse, in contrast to synthesis of α-ketoglutarate, which was only significantly increased at 2 hr. At 2 hr there was no significant difference in palmitate (FA 16:0) or lignocerate (FA 24:0) synthesis between control and *MYC* activated cells. However, at 4 hr *MYC* activated cells significantly increased palmitate synthesis, and subsequently at 8 hr *MYC* activated cells significantly increased lignocerate synthesis ($p \leq 0.05$). This indicates

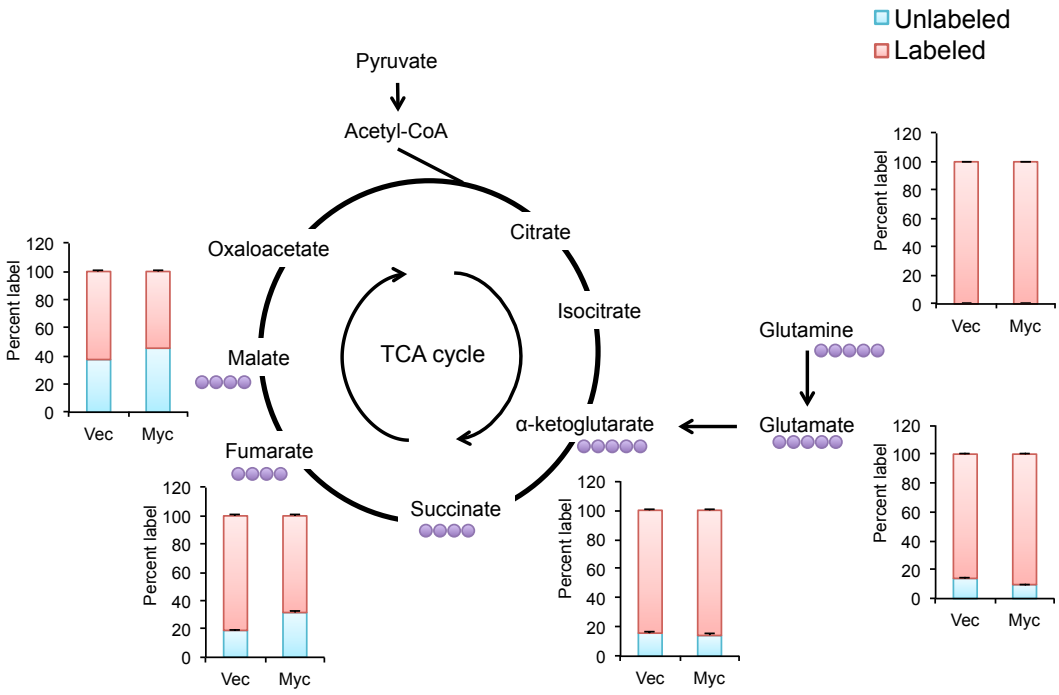

Figure 4.2. *$^{13}C_5$-glutamine labelling of the TCA cycle*
Schematic shows the percent labelling of Vec or Myc cells from a 6 hr $^{13}C_5$-glutamine pulse. Purple spots indicate the incorporation of labelled carbons (M+4 or M+5) into newly synthesised metabolites. Data is plotted relative to a 100% glutamine label. Error bars are the standard error (n=3).

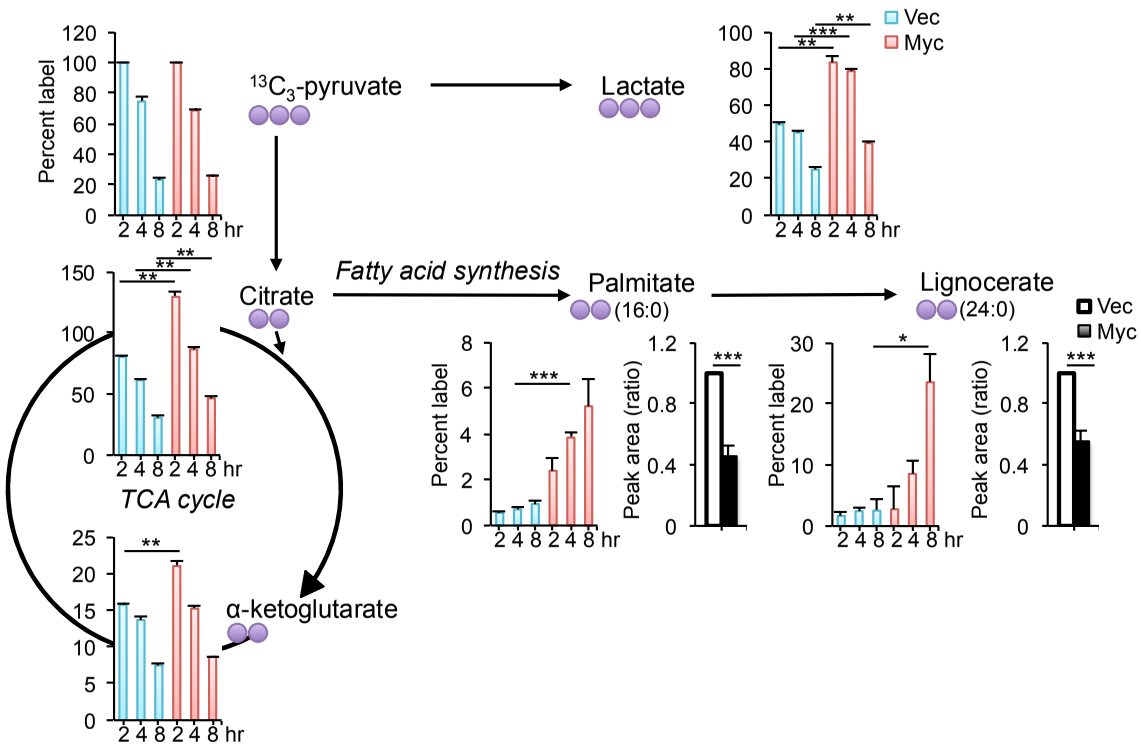

Figure 4.3. *Stable-isotope labeling timecourse of de novo fatty acid synthesis*
Schematic shows the percent labelling of Vec (blue) or Myc (red) cells from a 2, 4, or 8 hr $^{13}C_3$-pyruvate pulse. Purple spots indicate the incorporation of labelled carbons (M+2) into newly synthesised metabolites. Data is plotted relative to a 100% pyruvate label at 2 hr. Error bars are the standard error (n=3). * =p-value ≤0.05, ** =p-value ≤0.01, and *** =p-value ≤0.001 calculated using a T-test from a single dataset. Black histograms show the total peak area ratio between Vec and Myc, with Vec set to a value of 1. * indicates a significant p-value (≤0.05; T-test). Statistics were carried out on >3 biological replicates.

that MYC-drives *de novo* FA synthesis in preference to directing carbon into the TCA cycle. Further, *MYC*-activated cells particularly increased synthesis of lignocerate, which occurs from shuttling palmitate to the endoplasmic reticulum where it is elongated by elongase enzymes (ELOVLs). MYC-driven synthesis of lignocerate fits with the specificity of screen hit ELOVL1 for FA of chain lengths C22-C26 (Ohno *et al.* 2010).

Total levels of FAs were also analysed to determine the effect of *MYC* activation on FA remodelling. *MYC* activation significantly depleted levels of palmitate and lignocerate (figure 4.3), and this was true for the majority of saturated fatty acids (SFA), monounsaturated fatty acids (MUFAs), and polyunsaturated fatty acids (PUFAs) (figure 4.4A-C), such that median FA content almost halved (figure 4.5A). This indicates that MYC drives the synthesis of FAs and their remodelling into downstream pathways. In keeping with increased FA synthesis, *MYC*-activated cells also showed increased levels of 4-phospho-pantothenate, an intermediate in the CoA synthesis pathway (figure 4.5B).

FAs are used in the cell for anabolic pathways such as glycerophospholipid or sphingolipid synthesis, and for storage through triacylglycerol synthesis, fitting with the broader classification of screen hits in 'lipid metabolism'. FAs can also be catabolised by fatty acid oxidation (FAO) to generate ATP; however FAO does not typically occur at the same time as *de novo* FA synthesis (McGarry *et al.* 1978), which was shown above to be increased in *MYC* activated cells.

Over one third of siRNA screen hits whose knockdown increased MYC-driven p53 accumulation clustered in arachidonate metabolism, suggesting that arachidonate metabolites negatively regulate p53. Levels of arachidonic acid (FA 20:4) and arachidonic acid-derived FAs docosapentanoic acid (FA 22:5) and docosahexanoic acid (FA 22:6) were all significantly lowered following *MYC* activation (figure 4.4C). Docosahexanoic acid treatment was previously shown to result in its incorporation into membrane glycerophospholipids (Zerouga *et al.* 1996), indicating that *MYC* activation may drive remodeling of arachidonate metabolites into glycerophospholipid synthesis. This fits with the first results presented in this chapter that *MYC* activation drives the synthesis of phospholipid precursors CDP-choline and CDP-ethanolamine (for *de novo* phosphatidylcholine and phosphatidylethanolamine synthesis respectively). Further analysis of MYC-driven lipid synthesis is documented in chapter 5.

Whilst the majority of FAs were depleted in *MYC* activated cells, several longer chain FAs and PUFAs were increased (figure 4.4A-C). This indicates that either *MYC* activated cells are not remodeling these FAs downstream, or that the synthesis of these FAs is rapid enough to maintain levels of the FA substrate. FAs can be classified into several groups relating to their chain length: for example long-chain FAs (LCFAs) have chain lengths of C11-C20, very long-chain FAs (VLCFAs) have chain lengths >C20, and ultra long-chain FAs have chain lengths ≥C26. In particular, *MYC* activation significantly increased levels of ULC SFAs 26:0 and 28:0 (figure 4.4A), as well as ULC MUFA 28:1 (figure 4.4B)($p \leq 0.05$). ULCFAs were also

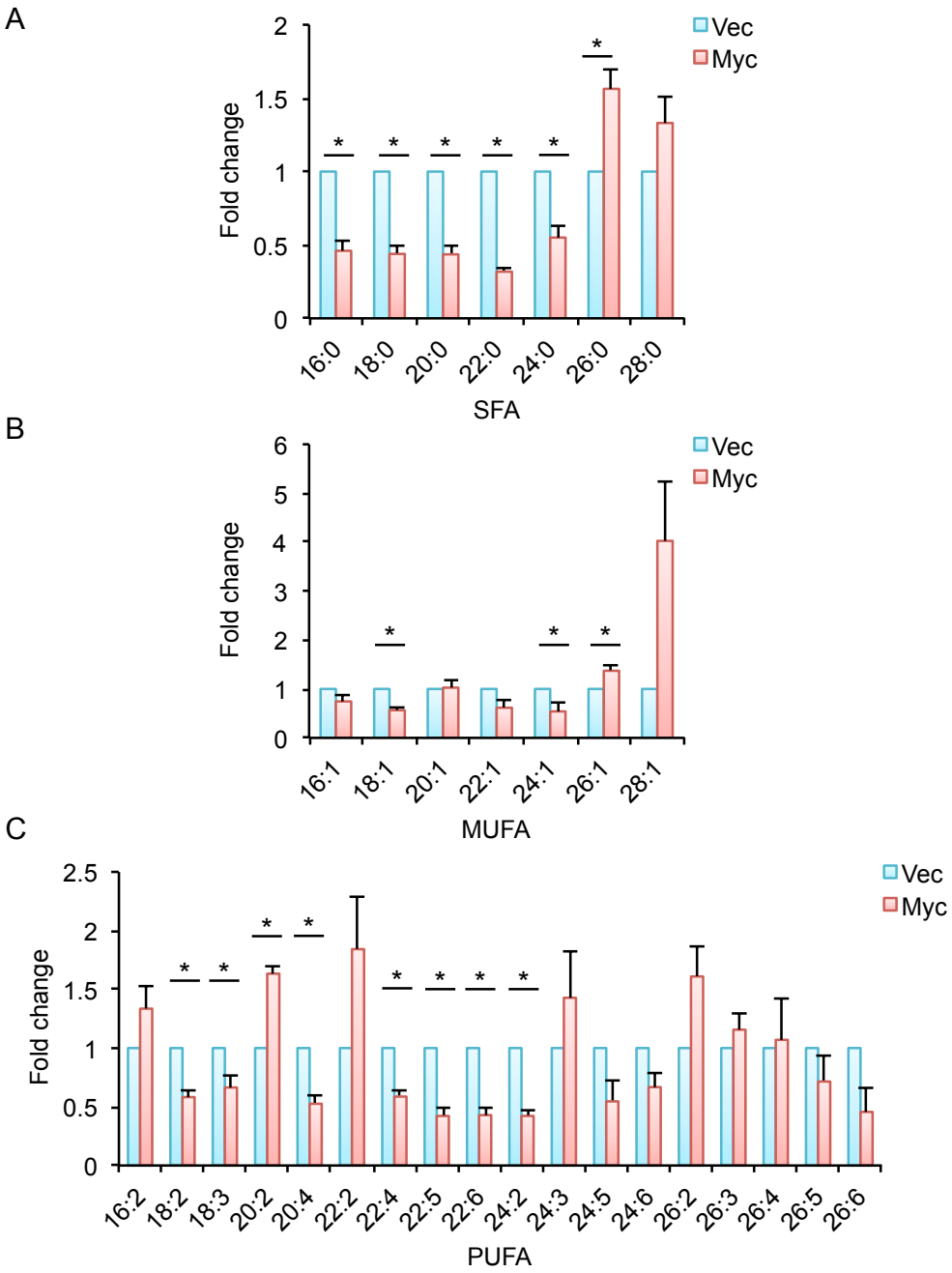

Figure 4.4. *MYC-driven changes in SFAs, MUFAs and PUFAs*
Histograms show the average fold change in SFAs (saturated fatty acids; (A)), MUFAs (monounsaturated fatty acids; (B)), and PUFAs (polyunsaturated fatty acids; (C)) between Vec and Myc. Error bars are the standard error (n>3). * indicates a p-value ≤0.05 comparing the average fold change of Vec with Myc (T-test). Statistics were carried out on 5 biological replicates.

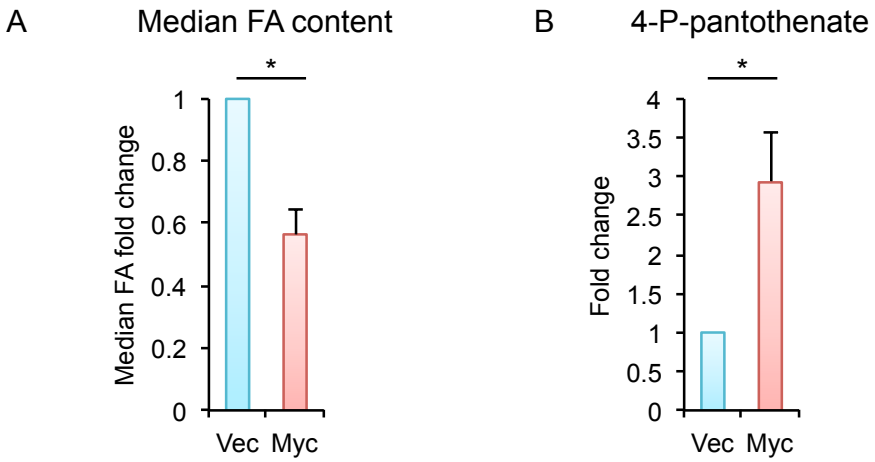

Figure 4.5. *MYC-driven changes in total FA content*
(A) Histogram shows the average median FA content of >3 biological replicates. (B) Histogram shows the average fold change between Vec and Myc of 5 biological replicates. Error bars are the standard error (n>3). * indicates a p-value ≤0.05 comparing Vec with Myc (T-test). Statistics were carried out on 5 biological replicates.

analysed over a timecourse of 72 hr *MYC* activation, and were shown to increase over the timecourse (figure 4.6). In keeping with the functional annotation of siRNA screen hits in sphingolipid synthesis, mammalian cells have been shown to predominantly utilise FAs with ≥C24 chain lengths for sphingolipid synthesis (Ohno *et al.* 2010). This may indicate that *MYC* activated cells increase synthesis of ULCFAs for sphingolipid synthesis. The relevance of MYC-driven FA changes to sphingolipid synthesis is explored in chapter 5.

4.3 The effect of p53 loss on MYC-driven metabolite changes

In a typical model of tumour suppression, loss of p53 would be expected to trigger apoptosis due to increased cell stress associated with relief of proliferative restraints. Counterintuitively, several *in vivo* studies documented that loss of p53 increases the proliferative rate of MYC-driven tumours without affecting apoptosis (Elson *et al.* 1995; Hsu *et al.* 1995; Finch *et al.* 2006). To explain these findings, we hypothesised that loss of p53 facilities remodelling of metabolic pathways in *MYC* activated cells, which supports increased proliferation. This fits with studies showing that p53 and MYC have contrasting effects on cell metabolism, favouring catabolic or anabolic pathways respectively (reviewed in Kruiswijk *et al.* 2015 and Dang *et al.* 2013). To investigate this hypothesis, Vec and Myc cells were transfected with a genetic suppressor element encoding p53 dominant negative peptide (p53DN) or control, and the four conditions were compared by targeted LC-MS analysis (Gallagher *et al.* 1997).

p53 loss did not affect median FA content alone or in *MYC* overexpressing cells (figure 4.7), and analysis of twelve common FAs detected in MRC5 cells showed similar patterns regardless of p53 status (figure 4.8A). This was with the exception of FA 24:1 (nervonic acid), which significantly increased in p53DN cells (~5-fold relative to Vec; $p \leq 0.05$, suggesting that p53 negatively regulates FA 24:1. Relative levels of FA 24:1 in Myc/p53DN cells compared to Myc cells also increased, although this was not statistically significant, indicating that MYC may drive the utilisation of FA 24:1 in downstream pathways (such as sphingolipid synthesis).

Analysis of glycolytic metabolites showed no significant difference between Myc cells and Myc/p53DN cells in the case of glucose 6-phosphate or fructose 6-phosphate (figure 4.9A and B respectively), however fructose 1,6-bisphosphate and glyceraldehyde 3-phosphate significantly increased (figure 4.9C and D respectively; $p \leq 0.05$). Levels of lactate significantly decreased in Myc/p53DN cells compared to Myc cells (figure 4.9F; $p \leq 0.05$), and there was also a small decrease in pyruvate (figure 4.9E), indicating that loss of p53 may promote diversion of upstream glycolytic intermediates into anabolic pathways.

Myc/p53DN cells significantly increased PPP metabolites ribose 5-phosphate and sedoheptulose 7-phosphate (figure 4.9H and I; $p \leq 0.05$), but not 6-phosphogluconate (figure 4.9G). This could be because the flux through 6-phosphogluconate is very rapid, as demonstrated by 6-phosphoguconate levels rapidly increasing following

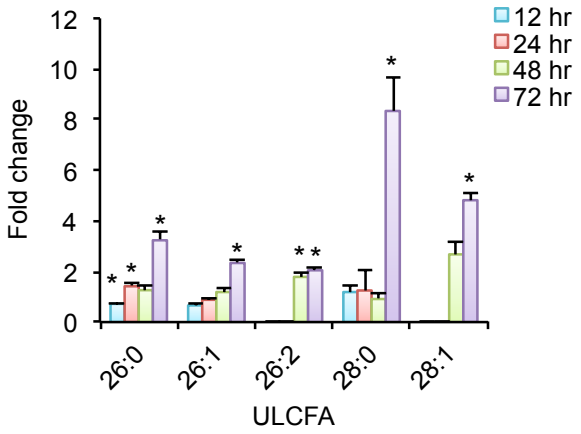

Figure 4.6. *A timecourse of MYC-driven changes in ULCFAs*
Histogram shows the average fold change in ULCFAs (ultra long chain fatty acids) across a 72 hr timecourse of *MYC* activation with 4OHT compared to Vec control. Error bars are the standard error (n=3). * indicates a p-value ≤0.05 comparing Vec with Myc samples at the specified timepoint (T-test). Statistics were carried out on a single dataset.

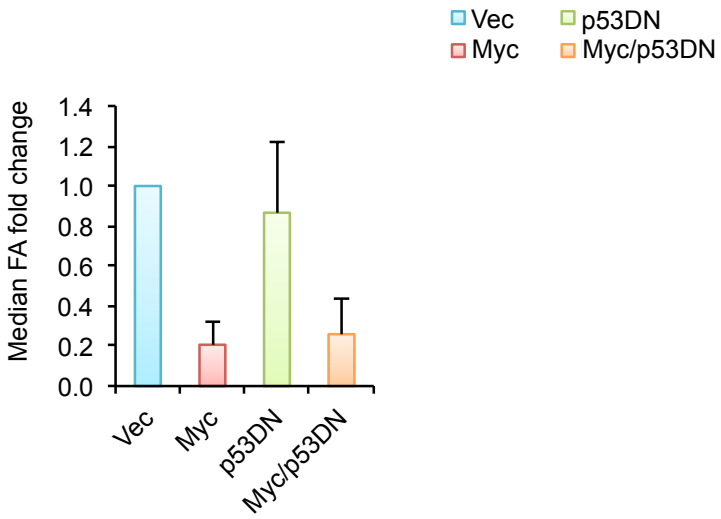

Figure 4.7. *Total changes in FA content driven by MYC overexpression and p53 loss*
Histogram shows the median fold change of 12 common fatty acids between Vec and Myc, p53DN, or Myc/p53DN. Error bars are the standard error (n=3).

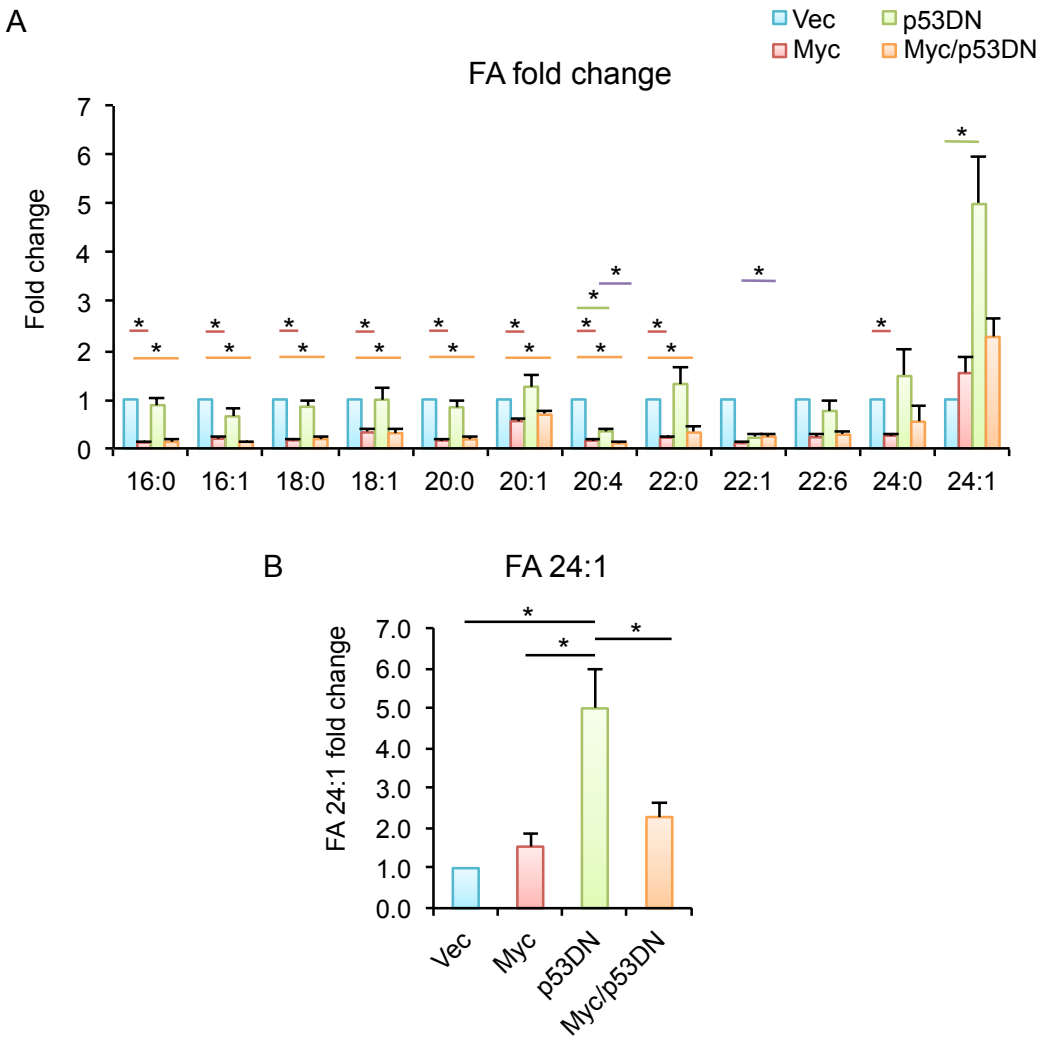

Figure 4.8. *FA changes driven by MYC overexpression and p53 loss*
(A) Histogram shows the average fold change of 12 common fatty acids between Vec and Myc, p53DN, or Myc/p53DN. Peak areas were normalised to median metabolite content prior to fold change calculations. Error bars are the standard error (n=3). * indicates a p-value ≤0.05 comparing Vec with Myc (red), Vec with p53DN (green), Vec with Myc/p53DN (orange), or Myc with Myc/p53DN (purple) (T-test). Statistics were carried out on a single representative dataset. (B) As in (A) with more detailed statistical comparisons between all conditions (T-test).

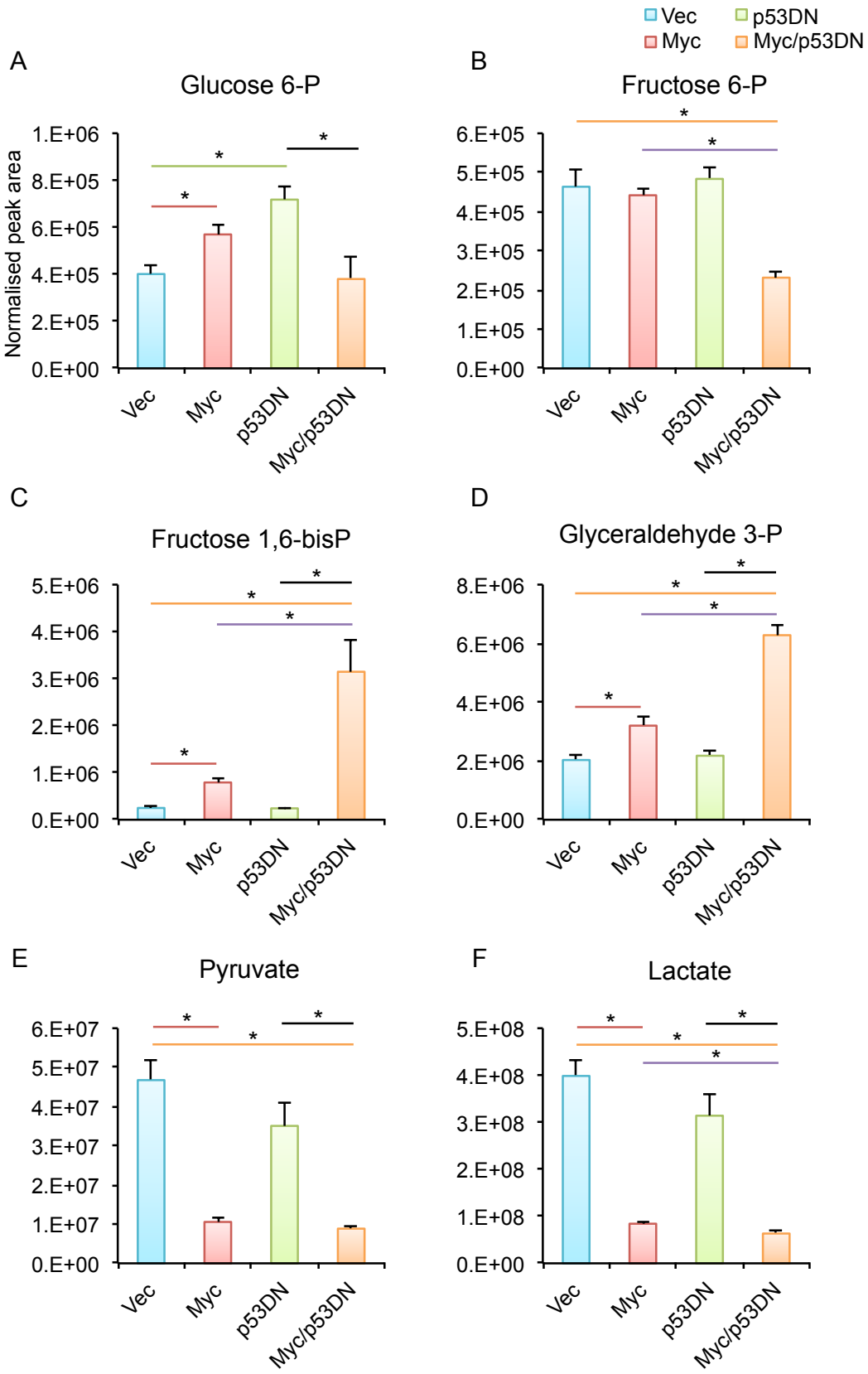
Vec
p53DN
Myc
Myc/p53DN
A
Glucose 6-P
Normalised peak area
1.E+06
8.E+05
6.E+05
4.E+05
2.E+05
0.E+00
Vec
Myc
p53DN
Myc/p53DN
B
Fructose 6-P
6.E+05
5.E+05
4.E+05
3.E+05
2.E+05
1.E+05
0.E+00
C
Fructose 1,6-bisP
5.E+06
4.E+06
3.E+06
2.E+06
1.E+06
0.E+00
D
Glyceraldehyde 3-P
8.E+06
6.E+06
4.E+06
2.E+06
0.E+00
E
Pyruvate
6.E+07
5.E+07
4.E+07
3.E+07
2.E+07
1.E+07
0.E+00
F
Lactate
5.E+08
4.E+08
3.E+08
2.E+08
1.E+08
0.E+00

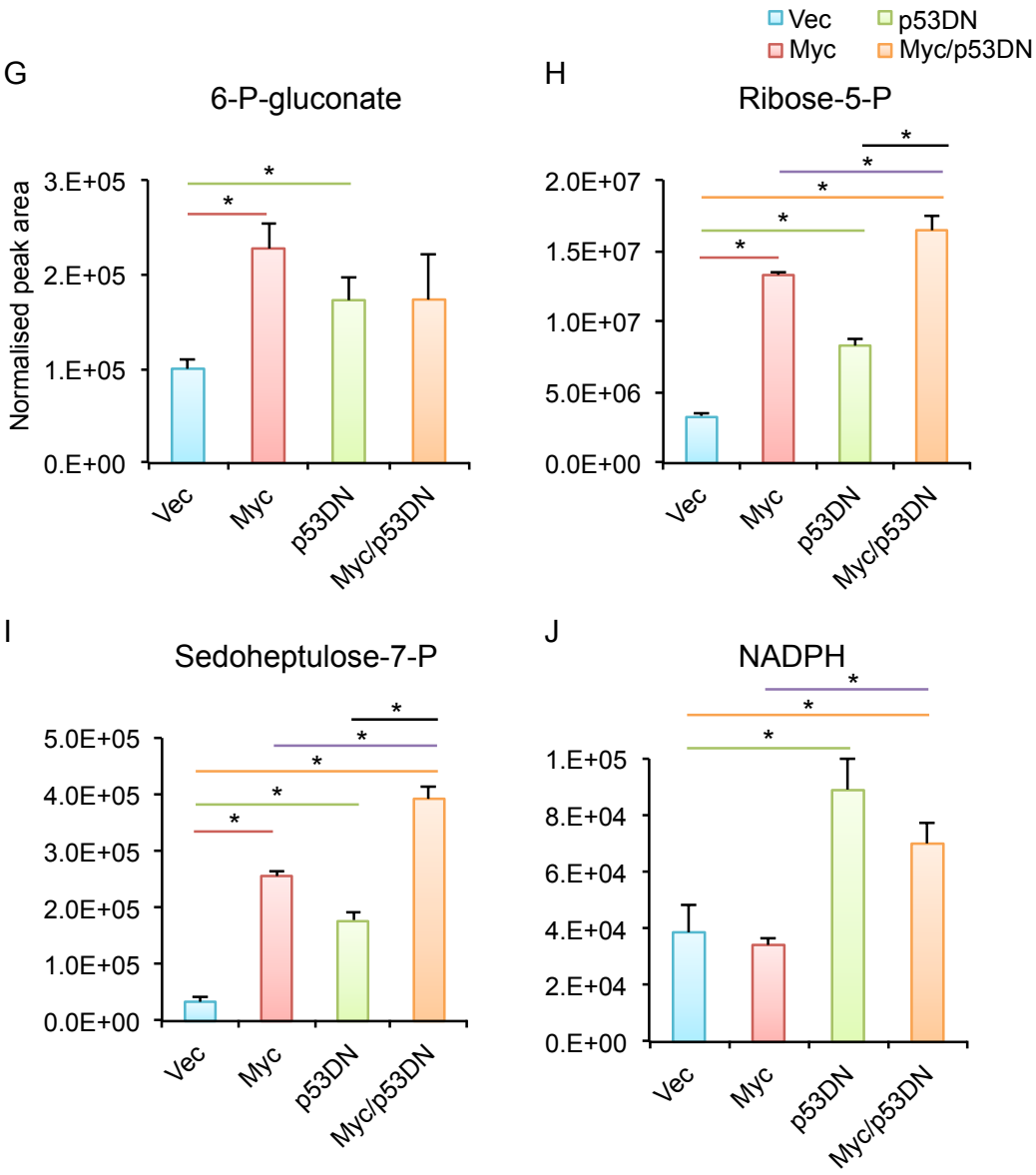

Figure 4.9. *Glycolytic and pentose phosphate pathway changes driven by MYC overexpression and p53 loss*

Histograms compare the normalised peak area of the specified metabolite between Vec, Myc, p53DN and Myc/p53DN. Peak area was normalised to median metabolite content. Error bars are the standard error (n=3). * indicates a p-value ≤0.05 comparing Vec with Myc (red), Vec with p53DN (green), Vec with Myc/p53DN (orange), Myc with Myc/p53DN (purple), or p53DN with Myc/p53DN (black) (T-test). Statistics were carried out on a single representative dataset.

pharmacological inhibition of downstream enzyme 6-phosphogluconate dehydrogenase (figure 4.10). The PPP is a key cytosolic generator of NADPH, and Myc/p53DN cells significantly increased levels of NADPH compared to Myc cells (figure 4.9J; $p \leq 0.05$), in keeping with previous studies showing that p53 inhibits NADPH synthesis (Jiang *et al.* 2011 and 2013). Myc/p53DN cells also exhibited significantly increased levels of serine and glycine compared to Myc cells (figure 4.11A and B respectively; $p \leq 0.05$). Intermediates of the pentose phosphate pathway and the serine synthesis pathway are used for nucleotide biosynthesis, and levels of all nucleotide monophosphates (NMPs) (figure 4.12A-E) and nucleotide diphosphates (NDPs) (figure 4.13A-D) significantly increased in Myc/p53DN cells compared to all other conditions ($p \leq 0.05$). Levels of nucleotide triphosphates (NTPs) (figure 4.14A-D) did not significantly change between Myc alone and Myc/p53DN cells.

To determine whether nucleotides were being utilised by Myc/p53DN for biosynthetic purposes, cells were pulsed with ^{15}N-amide-glutamine and then RNA or DNA was extracted and digested into mononucleotides prior to metabolite extraction. Heavy isotope label incorporation into RNA-derived NMPs (figure 4.15A) and DNA-derived dNMPs (figure 4.15B) was significantly increased in Myc cells compared to control cells, and significantly increased further in Myc/p53DN compared to Myc cells ($p \leq 0.01$). Label incorporation into nucleotide-based lipid precursors from whole cell metabolite extracts was also analysed and shown to follow the same pattern (figure 4.16, $p \leq 0.01$). These heavy-isotope tracer experiments demonstrated that compared to *MYC*-activated cells alone, Myc/p53DN cells increase synthesis of RNA, DNA, and lipid precursors, confirming that p53 loss increases the biosynthetic capacity of *MYC*-activated cells.

4.4 Summary

This chapter has demonstrated that *MYC* activation increases *de novo* FA synthesis, supporting the cluster of siRNA screen hits in this pathway. *MYC* activation increased palmitate synthesis, but particularly drove the synthesis of lignocerate (FA 24:0), in keeping with the substrate specificity of screen hit ELOVL1. While increasing FA synthesis, *MYC* overexpression significantly depleted median FA content, potentially indicating increased utilisation of FAs in downstream pathways. Of the screen hits involved in FA biosynthesis, several of these hits clustered in arachidonate metabolism, and *MYC* overexpression decreased all arachidonic acid. In contrast to this, *MYC* overexpression increased synthesis of several ULCFAs (and PUFAs), which may have important roles in sphingolipid synthesis (Ohno *et al.* 2010).

In addition to remodelling FA metabolism, untargeted heavy-isotope tracer analysis revealed that *MYC* overexpression drives synthesis of nucleotides, nucleobases, nucleosides, and nucleotide-based lipid precursors that may support RNA synthesis, DNA synthesis, and phospholipid synthesis. Further targeted analysis revealed *MYC* overexpression predominantly diverts glucose-derived carbon into anabolic

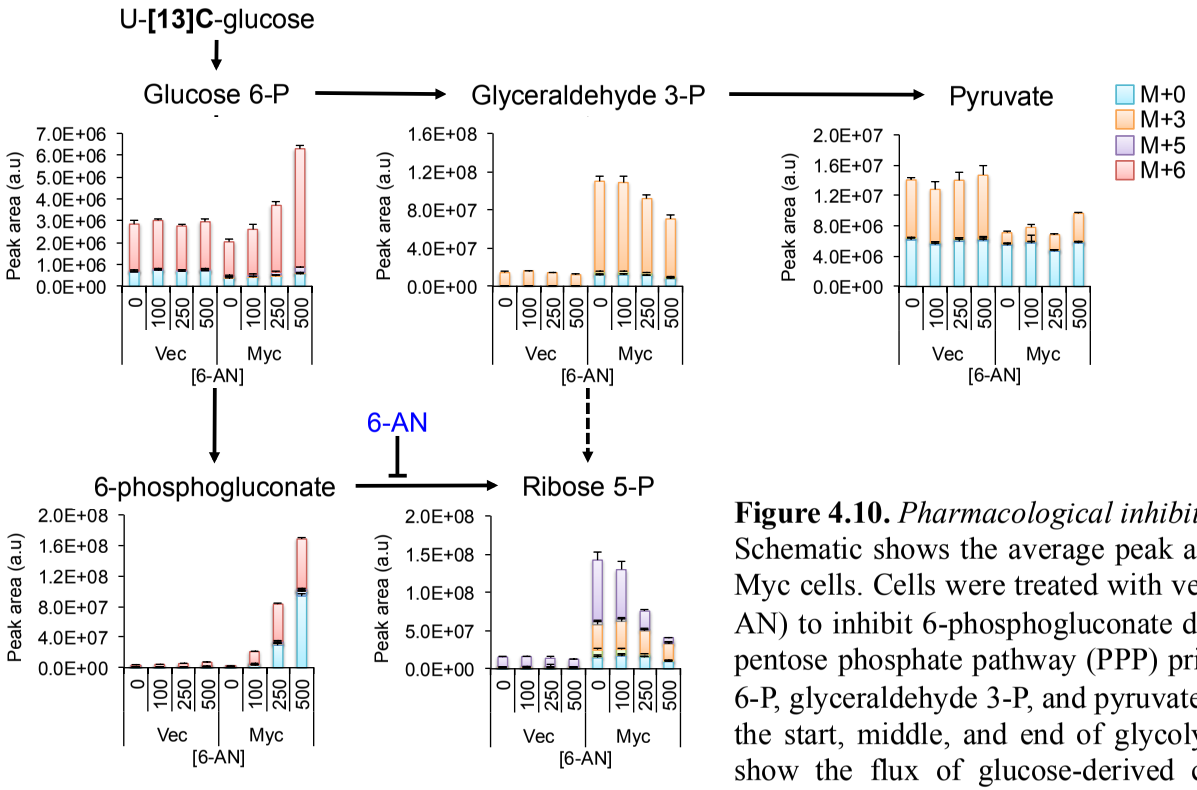

Figure 4.10. *Pharmacological inhibition of the pentose phosphate pathway* Schematic shows the average peak area of metabolites extracted from Vec or Myc cells. Cells were treated with vehicle control or 6-aminonicotinamide (6-AN) to inhibit 6-phosphogluconate dehydrogenase in the upper portion of the pentose phosphate pathway (PPP) prior to pulsing with $^{13}C_6$-glucose. Glucose 6-P, glyceraldehyde 3-P, and pyruvate are used as representative metabolites at the start, middle, and end of glycolysis. 6-phosphogluconate and ribose 5-P show the flux of glucose-derived carbon into the PPP. Colours represent different isotopolgues derived from the glucose label as indicated by the key. Isopologue label indicates whether ribose 5-P is synthesised from the upper or lower PPP. M+5 (purple) ribose 5-P label is derived from 6-phosphogluconate via the upper pentose phosphate pathway, while M+3 (orange) ribose 5-P label is derived from glyceraldehyde 3-P via the lower PPP. Inhibition of the upper PPP with 6-AN depletes M+5 label, where as M+3 label from the lower PPP is still used to synthesis ribose 5-P. Error bars are the standard error (n=3).

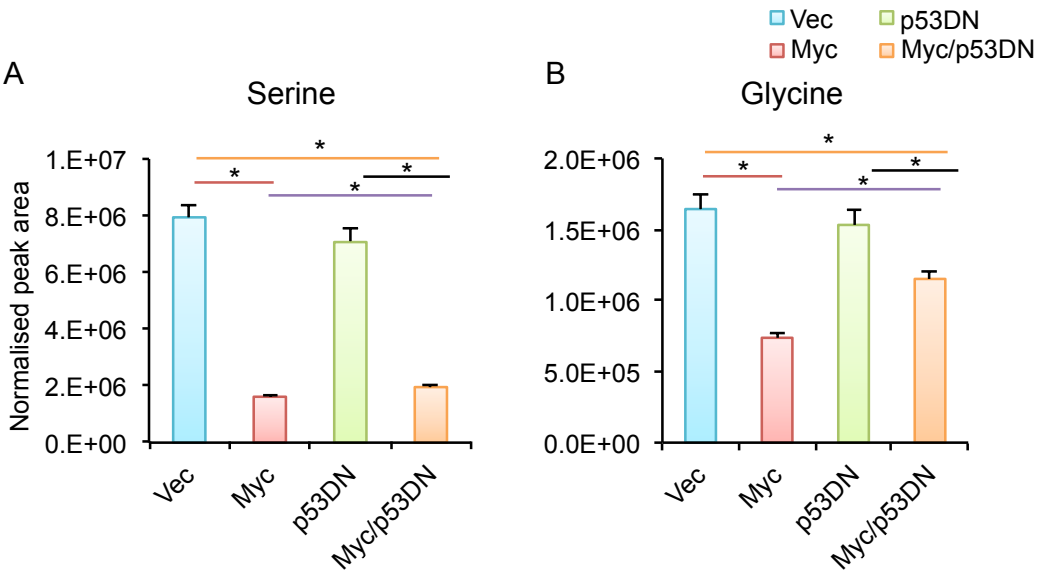

Figure 4.11. *Serine and glycine changes driven by MYC overexpression and p53 loss*

Histograms compare the normalised peak area of the specified metabolite between Vec, Myc, p53DN and Myc/p53DN. Peak area was normalised to median metabolite content. Error bars are the standard error (n=3). * indicates a p-value ≤0.05 comparing Vec with Myc (red), Vec with p53DN (green), Vec with Myc/p53DN (orange), Myc with Myc/p53DN (purple), or p53DN with Myc/p53DN (black) (T-test). Statistics were carried out on a single representative dataset.

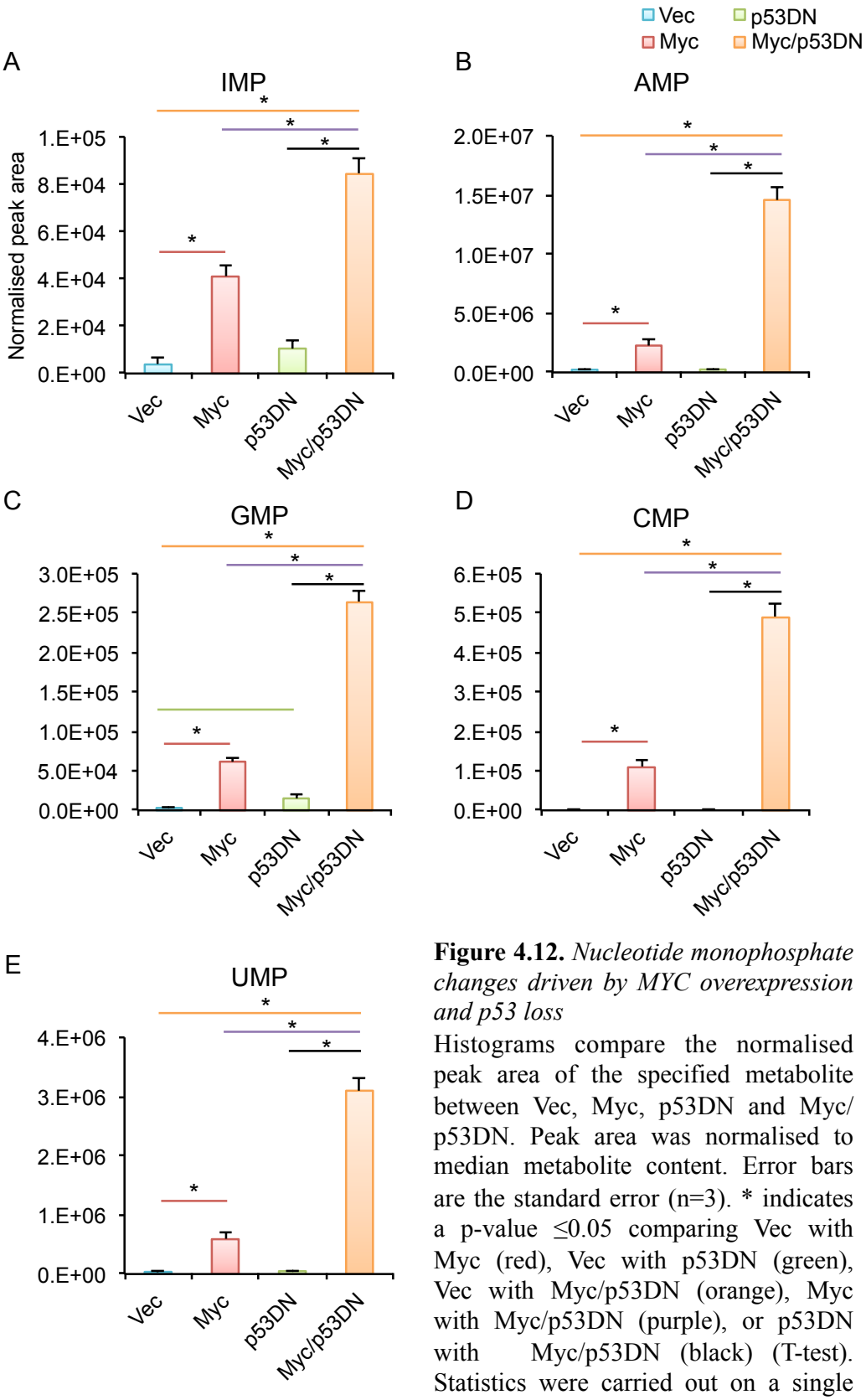

Figure 4.12. *Nucleotide monophosphate changes driven by MYC overexpression and p53 loss*

Histograms compare the normalised peak area of the specified metabolite between Vec, Myc, p53DN and Myc/p53DN. Peak area was normalised to median metabolite content. Error bars are the standard error (n=3). * indicates a p-value ≤0.05 comparing Vec with Myc (red), Vec with p53DN (green), Vec with Myc/p53DN (orange), Myc with Myc/p53DN (purple), or p53DN with Myc/p53DN (black) (T-test). Statistics were carried out on a single representative dataset.

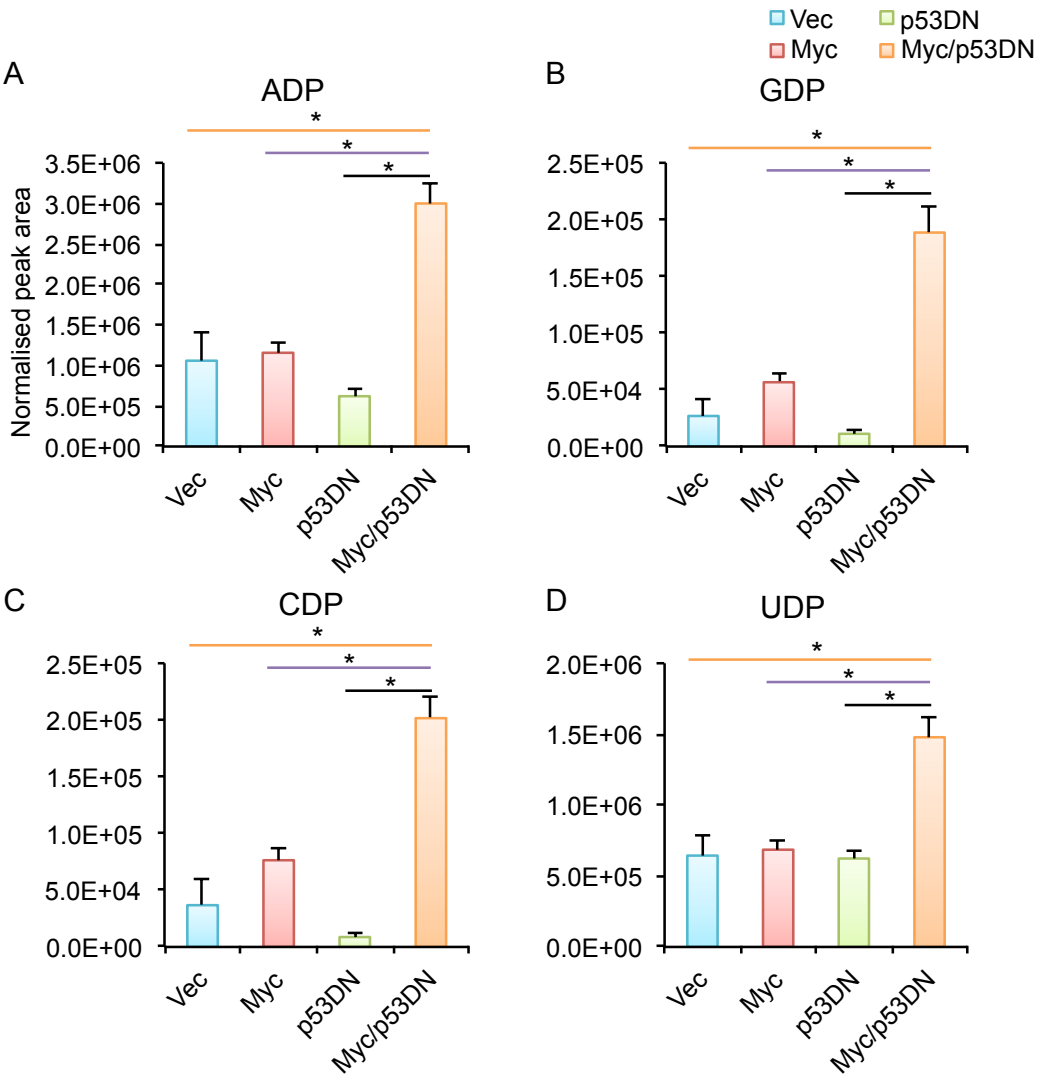

Figure 4.13. *Nucleotide diphosphate changes driven by MYC overexpression and p53 loss*

Histograms compare the normalised peak area of the specified metabolite between Vec, Myc, p53DN and Myc/p53DN. Peak area was normalised to median metabolite content. Error bars are the standard error (n=3). * indicates a p-value ≤0.05 comparing Vec with Myc (red), Vec with p53DN (green), Vec with Myc/p53DN (orange), Myc with Myc/p53DN (purple), or p53DN with Myc/p53DN (black) (T-test). Statistics were carried out on a single representative dataset.

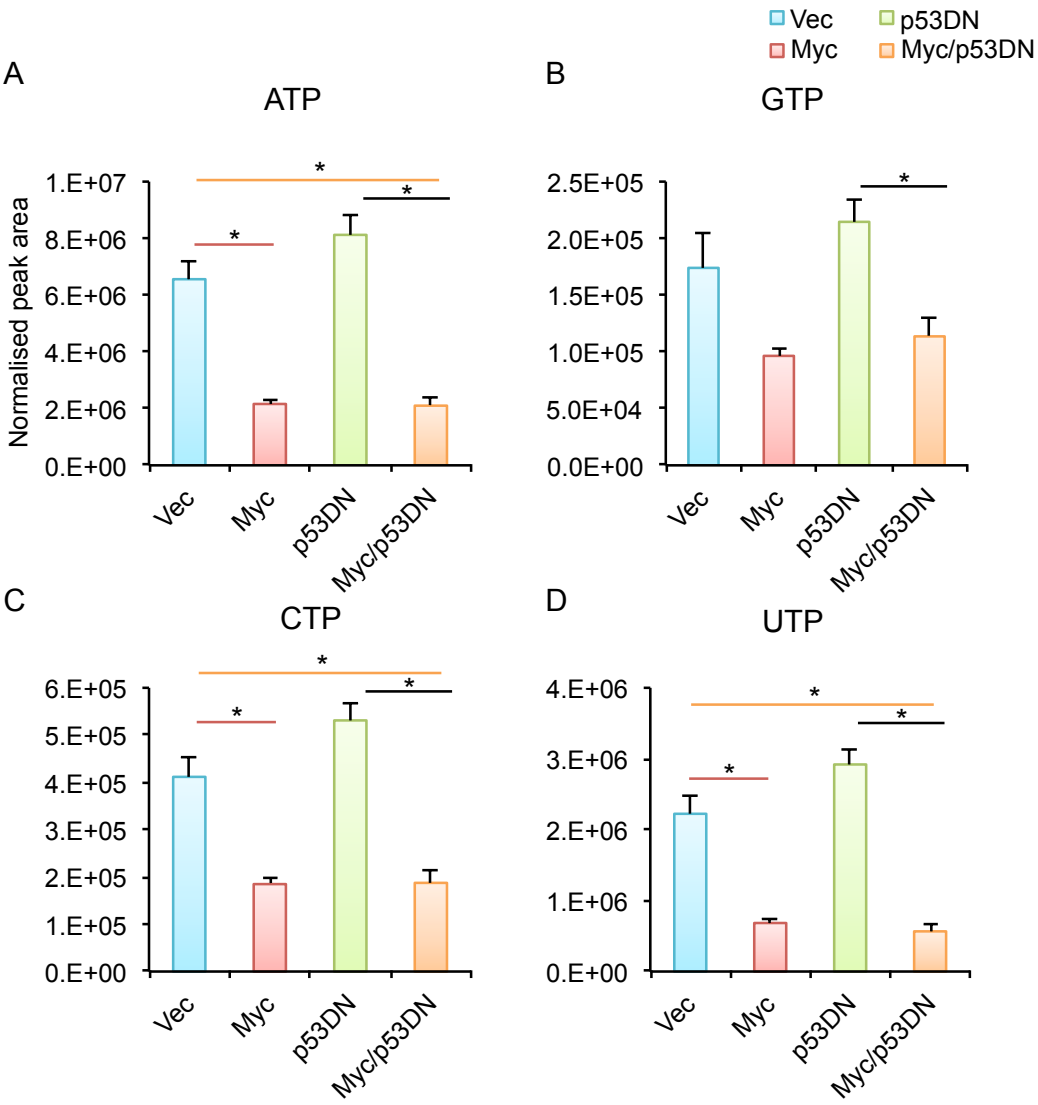

Figure 4.14. *Nucleotide triphosphate changes driven by MYC overexpression and p53 loss*

Histograms compare the normalised peak area of the specified metabolite between Vec, Myc, p53DN and Myc/p53DN. Peak area was normalised to median metabolite content. Error bars are the standard error (n=3). * indicates a p-value ≤0.05 comparing Vec with Myc (red), Vec with p53DN (green), Vec with Myc/p53DN (orange), Myc with Myc/p53DN (purple), or p53DN with Myc/p53DN (black) (T-test). Statistics were carried out on a single representative dataset.

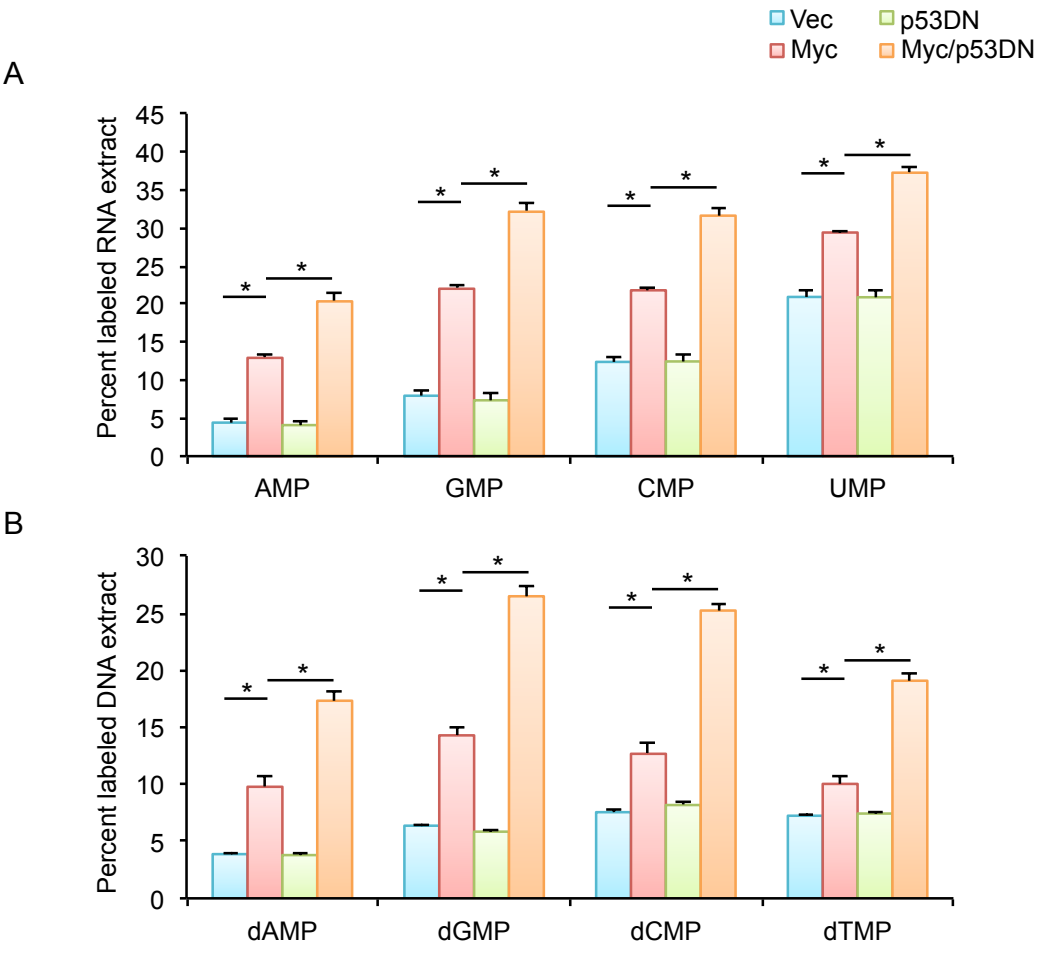

Figure 4.15. *Heavy isotope labeling of RNA and DNA synthesis*
Histograms show percent label incorporation from a 12 hr ^{15}N-amide-glutamine pulse into RNA or DNA synthesis. (A) RNA was extracted prior to metabolite extraction to show the percent label incorporation into RNA synthesis. (B) DNA was extracted prior to metabolite extraction to show the percent label incorporation into DNA synthesis. Error bars are the standard error (n=3). * indicates a p-value ≤0.01 comparing Vec cells with Myc cells or Myc cells with Myc/p53DN cells (T-test). Statistics were carried out on a single representative dataset.

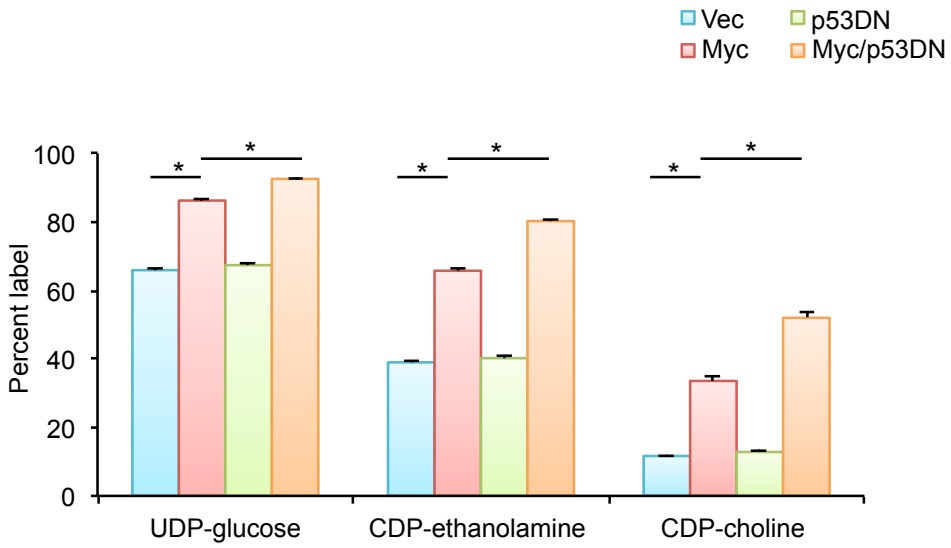

Figure 4.16. *Heavy isotope labeling of nucleotide-based lipid precursors*
Histogram shows percent label incorporation from a 12 hr ^{15}N-amide-glutamine pulse into 3 nucleotide-based lipid precursors. The predominant isotopologue (displayed) is M+1 for UDP-glucose, and M+2 for CDP-choline and CDP-ethanolamine. Error bars are the standard error (n=3). * indicates a p-value ≤0.01 comparing Vec cells with Myc cells or Myc cells with Myc/p53DN cells (T-test). Statistics were carried out on a single representative dataset.

pathways, the pentose phosphate pathway (PPP) and the serine synthesis pathway (SSP), that have previously been shown to support nucleotide biosynthesis, one-carbon metabolism, and subsequently tumourigenesis (reviewed in Locasale, 2013). *MYC* overexpression combined with p53 loss significantly accumulated intermediates in the PPP, SSP, and in nucleotide biosynthesis compared cells that overexpress *MYC* alone. Further, Myc/p53DN cells increased label incorporation into RNA synthesis, DNA synthesis, and synthesis of nucleotide-based lipid precursors. These data show that loss of p53 does indeed result in metabolic remodeling in *MYC*-overexpressing cells, which may support increased proliferation associated with p53 loss.

The following chapter will build upon these results and outline the effect of *MYC* overexpression on lipid synthesis and remodeling.

5 Chapter 5- MYC-driven lipid changes

By coupling a large metabolic loss of function siRNA screen and metabolic analysis, the previous chapters have indicated that cells expressing deregulated *MYC* may remodel sphingolipid and phospholipid metabolism. Chapter 3 outlined the functional annotation of siRNA screen hits in lipid metabolism, within which two major clusters involved in fatty acid synthesis/arachidonate metabolism and sphingolipid biosynthesis were identified. Chapter 4 presented results demonstrating that cells expressing deregulated *MYC* increase *de novo* fatty acid (FA) synthesis, particularly of longer-chain FAs, and remodel FAs (including arachidonic acid) into downstream pathways. This chapter investigates the effect of *MYC* deregulation on sphingolipid and phospholipid remodelling with the hypothesis thay *MYC* deregulation changes these pathways.

5.1 MYC-driven changes in sphingolipids

To determine the effect that *MYC* overexpression has on the cellular compartment of sphingolipid species, lipid extractions were carried out on Vec and Myc cells and analysed by LC-MS. A correlation network was created to look for distinct clusters of sphingolipids that changed following *MYC* activation. This method was selected to allow more subtle changes within the sphingolipid network to be identified due to co-clustering of similar species, which may have been missed by carrying out a one-way ANOVA alone. Of over 50 sphingolipid species analysed, including ceramides, dihydroceramides, hexosylceramides and lactosylceramides, 2 distinct clusters formed in the correlation network (figure 5.1) whose separation was statistically significant (Fisher's test; $p=1.7x10^{-6}$). The majority of sphingolipid species decreased in response to *MYC* activation but a cluster of 6 sphingolipid species with longer ≥C24 FA residues increased. The sphingolipid species in this cluster included ceramides and lactosylceramides, and several individual species were found to significantly increase in addition to the cluster as a whole (one-way ANOVA; $p \leq 0.05$).

The initial results of the correlation network were repeated three times, and representative histograms were plotted to show the total levels (figure 5.2A) and the fold change between Vec and Myc for 12 common ceramide species (figure 5.2B). Ceramides with <C24 FA residues consistently decreased in response to *MYC* activation, while ceramides with ≥C24 FA residues consistently increased. Ceramides and lactosylceramides with ≥C24 FA residues have previously been described to have important structural and signalling roles at cell membranes (Sassa *et al.* 2013; Sonnino *et al.* 2009), which may indicate that MYC-drives membrane remodelling.

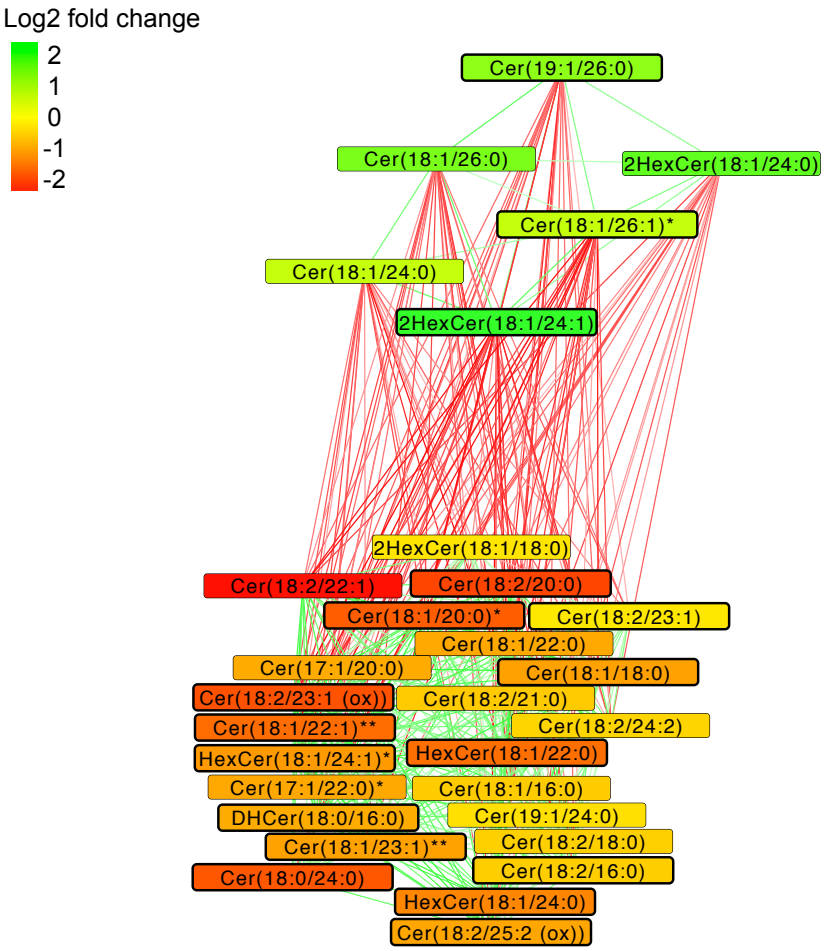

Figure 5.1. *Correlation network of MYC-driven sphingolipid changes*
The correlation network depicts clusters of sphingolipid species that change following *MYC* activation. Lipid peak areas were quantile normalised in R using peak areas of >150 lipids from sphingolipid and phospholipid subclasses. A one-way ANOVA was carried out on normalised sphingolipid peak areas comparing Vec and Myc samples, and FDR-corrected, significant ($p \leq 0.05$) sphingolipids were highlighted in the correlation network by thicker node borders. Log2 fold change between Vec and Myc was represented by node colour, as indicated by the key. An asterisk at the end of a lipid name indicates that more than one isomer of the lipid was identified across a single chromatographic peak.
Log2 fold change values were used to calculate spearman correlation values, and weak correlations were removed using mixture modeling (threshold ~0.5). Correlation values were attributed to edge weights and imported into Cytoscape where the MCODE plugin was used to identify clusters of correlation within the network. Positive correlations were colour coded as green edges, and negative correlations were colour coded as red edges. A force-directed layout was used to separate clusters for visualisation. Fisher's test was carried out to determine if clusters significantly separated ($p=1.7 \times 10^{-6}$).

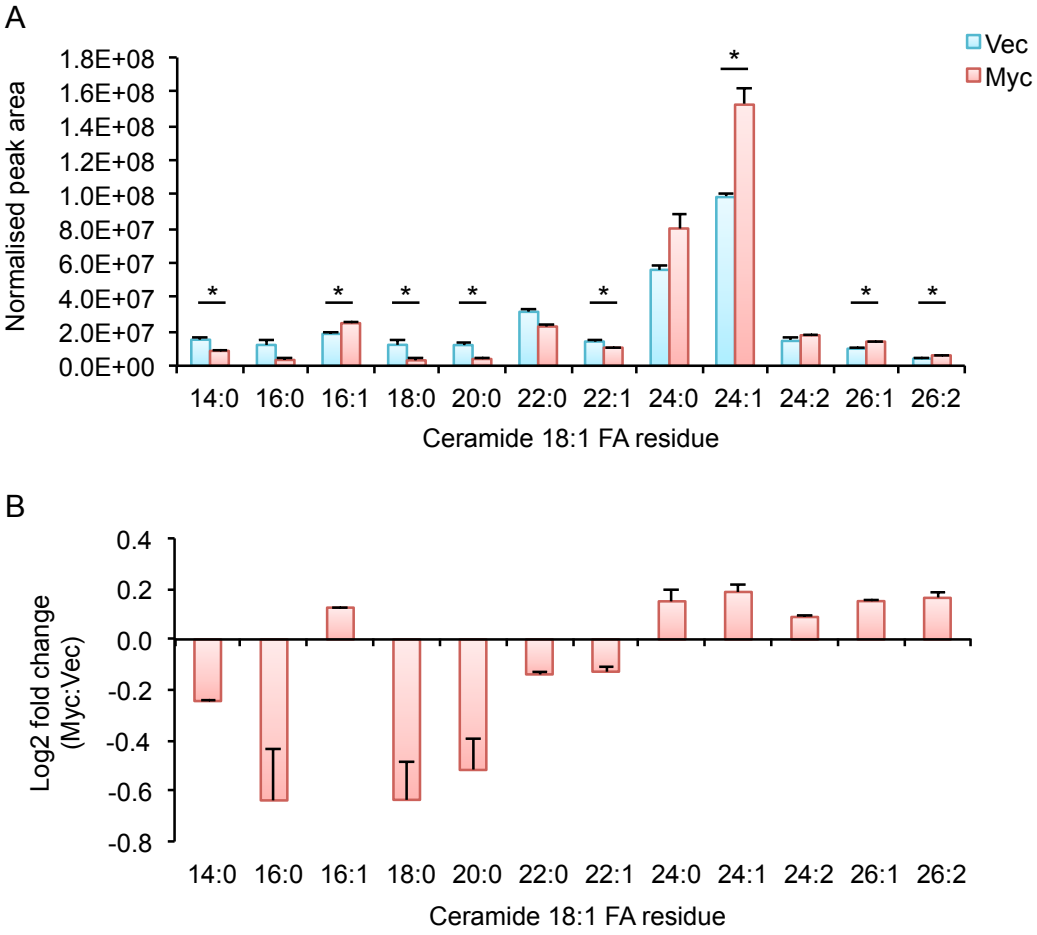

Figure 5.2. *MYC-driven changes in sphingolipids*
The histogram shows peak areas of 12 ceramide species normalised to median lipid content. Error bars are the standard error (n=3). * indicates statistical significance of a single representative dataset ($p \leq 0.05$). The same pattern of results was observed in 3 biological replicates. (B) The histogram shows the log2 fold change between Vec and Myc for each ceramide specie detected in (A) to highlight changes in lower abundance ceramide species.

5.2 MYC-driven changes in phospholipids

In addition to sphingolipid synthesis, FAs may be utilised in acylglycerols such as triacylglycerols (TGs), or for synthesis of phosphatidic acid and other glycerophospholipids including phosphatidylethanolamines (PEs) or phosphatidylcholines (PCs) (reviewed in Eljamil, 2015). Analysis of TGs showed *MYC* activation significantly increased levels of several TG species (one-way ANOVA; $p<0.05$), to the extent that Vec and Myc samples formed two distinct hierarchical clusters (figure 5.3). TGs are an important store of FAs that can be released from lipid droplets in times of need. Two enzymes involved in FA storage and release were identified as screen hits whose knockdown decreased p53 accumulation. This could indicate that TG-derived FAs are used for sphingolipid synthesis. Glycerol-3-phosphate acyl transferase 2 (GPAT2) condenses a fatty acyl-CoA with glycerol-3-phosphate to synthesise lysophosphatidic acid (LPA). Lipase E (also known as Hormone Sensitive Type) hydrolyses a FA from TG in the second of three reactions catalysed by distinct enzymes. As knockdown of both the synthesis and release of TGs decreases MYC-driven p53 accumulation, TG remodelling may have biological significance in *MYC*-deregulated cells.

PEs also clustered separately according to MYC status, and all PEs that significantly changed were increased compared to Vec (figure 5.4; one-way ANOVA; $p\leq0.05$). Of the PCs that significantly changed (one-way ANOVA; $p\leq0.05$), 2 hierarchical clusters formed based on those that increased or decreased (figure 5.5). Almost all PCs that increased in Myc samples comprised at least one docosahexanoic acid (DHA; 22:6) residue. Two PE species that significantly increased in Myc samples also comprised a DHA residue, and one of the PE species contained an arachidonic acid (AA) residue (one-way ANOVA; $p\leq0.05$). This confirmed that *MYC* activated cells deplete polyunsaturated fatty acids, due their utilisation in glycerophospholipid synthesis. DHA treatment has been documented to affect membrane structure and function by increasing membrane fluidity, permeability, vesicular fusion, elastic compressibility, and flip-flop rate (reviewed in Stillwell and Wassall, 2003). In keeping with the changes in sphingolipid synthesis, this may indicate that *MYC* activation specifically drives an accumulation of glycerophospholipid species that can alter membrane structure and function.

5.3 MYC-driven changes in lipid synthesis

The previous sub-sections outlined MYC-driven changes in total lipid levels. Moving forwards, stable heavy-isotope labelling was used to measure lipid synthesis. As serine is condensed with palmitoyl-CoA at the first step of *de novo* sphingolipid synthesis it was hypothesised that stable heavy-isotope labelled serine could be used to measure the rate of *de novo* ceramide synthesis. At the same time as *MYC* activation with 4-hydroxytamoxifen (4OHT), cells were pulsed with 2,3-^{13}C-serine for 48 hr prior to lipid extraction and analysis by LC-MS. Incorporation of serine-derived carbon was approximately doubled in Myc samples compared to Vec samples across 6 common ceramide species detected in MRC5 cells (figure 5.6).

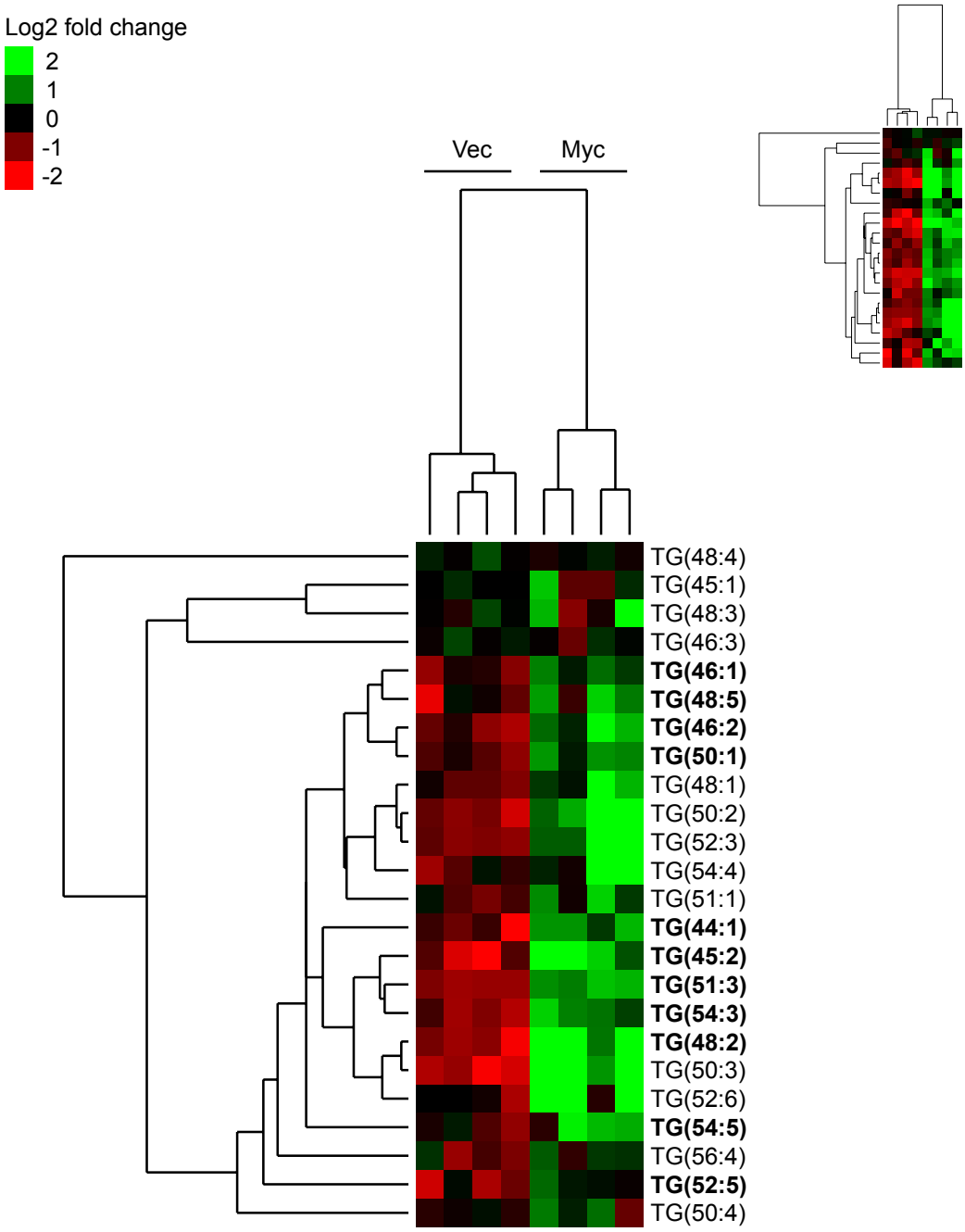

Figure 5.3. *MYC-driven changes in triacylglycerides*
The heat map shows hierarchical clustering on the y-axis, and clustering of 4 biological replicates of Vec and Myc on the x-axis. Values are the log2 fold change calculated on quantile normalised peak areas for each lipid. The heat map in the top right hand corner displays the raw peak area for each lipid. A one-way ANOVA was carried out on all lipid subclasses identified in figure 1, and lipids with a p-value≤0.05 are indicated in bold. Data was acquired using an Orbitrap Fusion Lumos Tribrid Mass Spectrometer, and lipids were identified using LipidSearch.

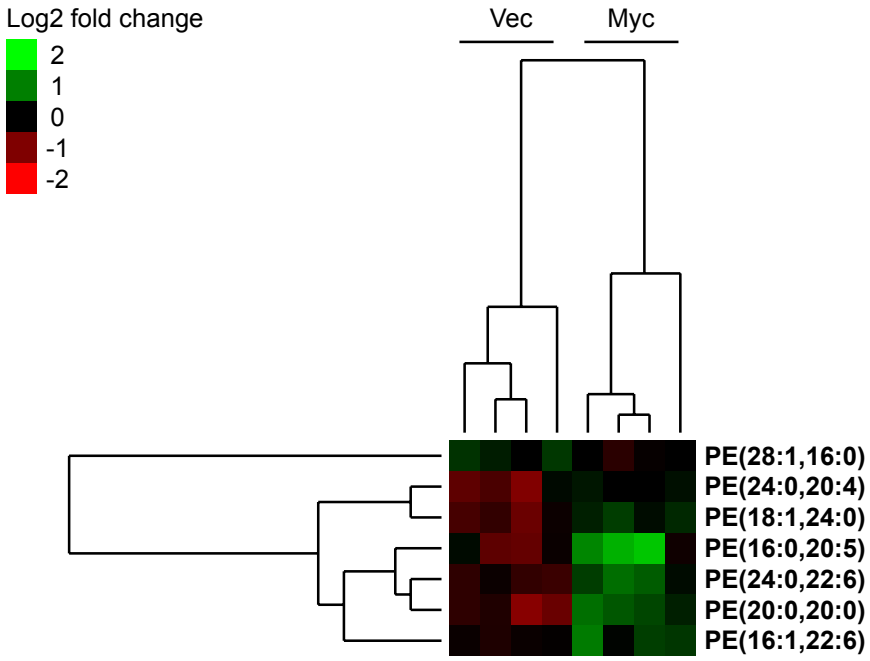

Figure 5.4. *MYC-driven changes in phosphatidylethanolamines*
The heat map shows hierarchical clustering on the y-axis, and clustering of 4 biological replicates of Vec and Myc on the x-axis. Values are the log2 fold change calculated on quantile normalised peak areas for each lipid. A one-way ANOVA was carried out on all lipid subclasses identified in figure 1, and lipids with a p-value≤0.05 are indicated in bold. Due to space constraints, only significant phosphatidylethanolamine species have been displayed in this heatmap. Data was acquired using an Orbitrap Fusion Lumos Tribrid Mass Spectrometer, and lipids were identified using LipidSearch.

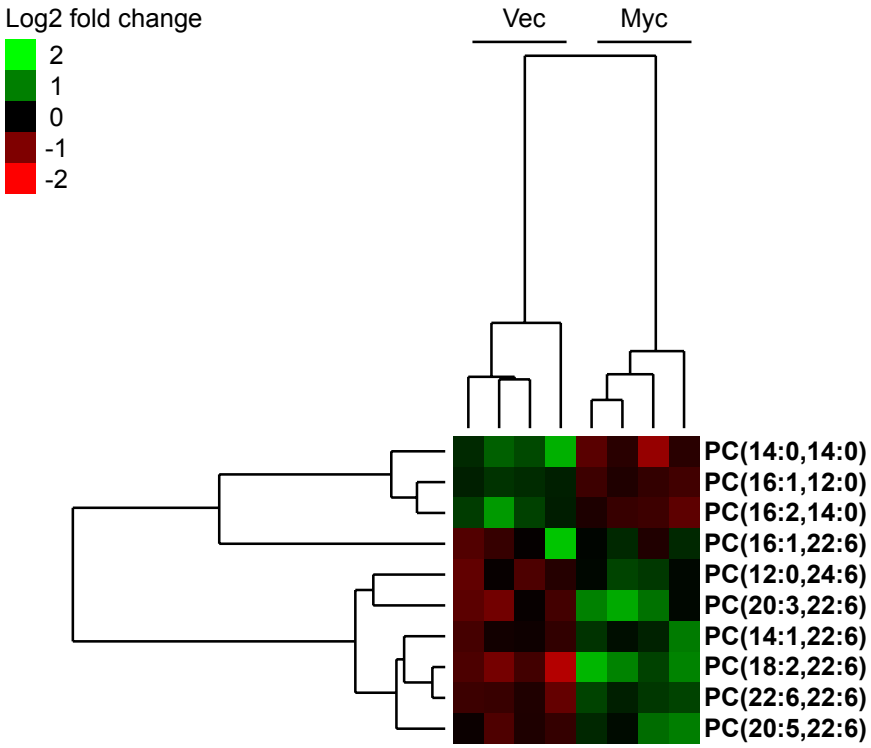

Figure 5.5. *MYC-driven changes in phosphatidylcholines*
Heat map shows hierarchical clustering on the y-axis, and clustering of 4 biological replicates of Vec and Myc on the x-axis. Values are the log2 fold change calculated on quantile normalised peak areas for each lipid. A one-way ANOVA was carried out on all lipid subclasses identified in figure 1, and lipids with a p-value≤0.05 are indicated in bold. Due to space constraints, only significant phosphatidylcholine species have been displayed in this heatmap. Data was acquired using an Orbitrap Fusion Lumos Tribrid Mass Spectrometer, and lipids were identified using LipidSearch.

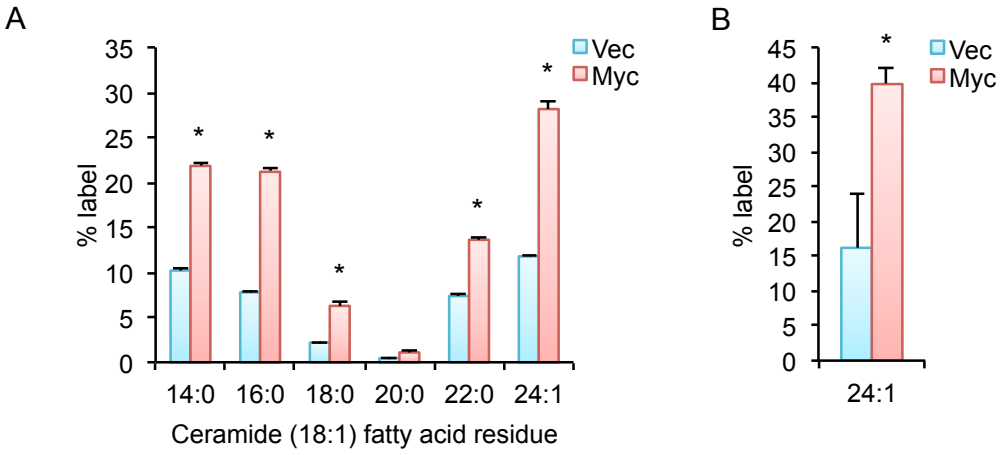

Figure 5.6. *Stable-isotope labeling of de novo ceramide synthesis*
(A) Histogram shows 2,3-^{13}C-serine labeling of the six predominant ceramide species in MRC5 cells. *indicates a pvalue≤0.05 (T-test) comparing Vec and Myc percent labeling in a single representative biological replicate. (B) Histogram shows heavy isotope serine labeling of ceramide (18:1, 24:1). *indicates a p-value≤0.05 (T-test) comparing Vec and Myc percent labeling across 3 independent biological replicates.

This indicated that MYC drives *de novo* sphingolipid synthesis at almost twice the rate of control cells, in keeping with results from chapter 3 that showed *de novo* sphingolipid enzymes were required for MYC-driven p53 accumulation.

To gain further insight into synthesis of sphingolipids and glycerophospholipids, a simultaneous ^{15}N-serine, ^{15}N-ethanolamine, and ^{15}N-choline stable heavy-isotope labelling timecourse was carried out. Following 48 hr *MYC* activation with 4OHT, cells were labelled for 2, 4, 8, or 24 hr prior to metabolite or lipid extraction. This meant that at 24 hr labelling *MYC* had been activated for 72 hr. Cellular incorporation of serine (as measured by percent labelling of serine; figure 5.7A) and ethanolamine (as measured by percent labelling of phosphoethanolamine; figure 5.7C) was very rapid, meaning Vec and Myc cells were both fully labelled at 2 hr. Incorporation of choline (as measured by percent labelling of phosphocholine; figure 5.7B) occurred gradually over 8 hr and was slightly increased in Myc cells.

MYC deregulated cells showed consistently increased label incorporation across the timecourse compared to Vec control cells (figure 5.8), and this trend was significant in sphingolipids with longer ≥C22 FA residues (one-way ANOVA; $p<0.05$). In contrast, label incorporation into PEs or PCs showed a similar trend in *MYC* deregulated and control cells (figure 5.9 and 5.10 respectively), indicating that while some phospholipid changes were significant they may not be biologically significant (one-way ANOVA; $p<0.05$). These data indicate that *MYC* deregulated cells strongly increase *de novo* ceramide synthesis, while only moderately affecting phospholipid synthesis, in keeping with the major cluster of screen hits in sphingolipid biosynthesis.

Sphingolipid and glycerophospholipid metabolism converges at the synthesis of sphingomyelins (SMs), which are important plasma membrane components (reviewed in Eljamil, 2015). The summed contribution of heavy-isotope from ceramide and either PE or PC was calculated to investigate whether MYC drives SM synthesis. Synthesis of SMs at 24 hr was similar in Vec and Myc samples, however percent labelling of several SM species did significantly change across the timecourse (figure 5.11). There was no clear hierarchical clustering of SMs based on FA chain length or desaturation. This result is possibly unexpected as *MYC* deregulation clearly increases *de novo* ceramide synthesis; however it is possible that ceramides are being remodelled into other downstream pathways (such as the salvage pathway, ceramide phosphate synthesis, or glycosphingolipid synthesis, see figure 6.2A).

5.4 Summary

In summary, this chapter has demonstrated that *MYC* deregulation remodels sphingolipid and phospholipid metabolism, which may have important biological consequences. Data presented in chapter 3 showed that *de novo* sphingolipid synthesis was required for MYC-driven p53 accumulation, indicating that p53 somehow responds to this pathway. Concomitantly, this chapter presents data

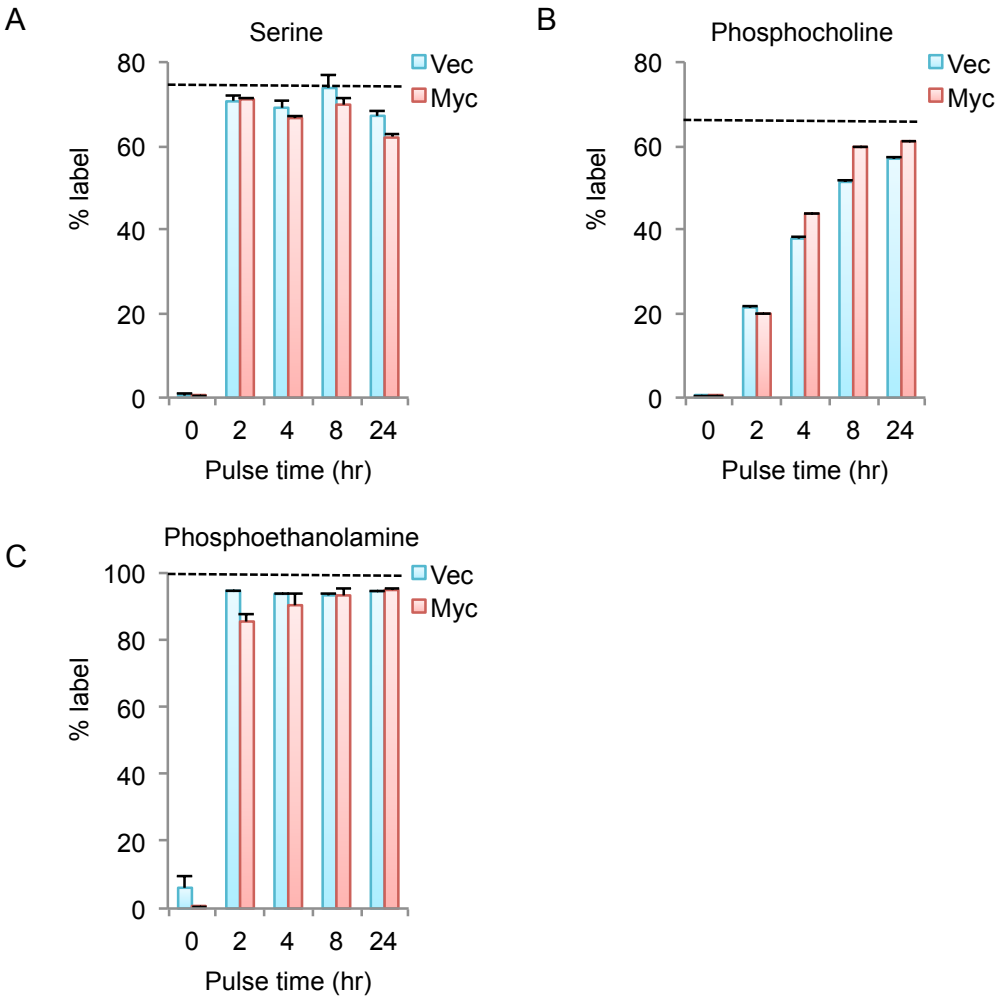

Figure 5.7. *Stable-isotope labeling timecourse of sphingolipids and glycerophospholipids*

Hisotgrams show percent label incorporation of ^{15}N-serine into serine (A), ^{15}N-choline into phosphocholine (B), and ^{15}N-ethanolamine into phosphoethanolamine (C). Media was pulsed with heavy isotope at time point 0 hr, 48 hr after Myc activation, and metabolites were extracted at 0 hr, 2 hr, 4 hr, 8 hr, and 24 hr. Due to the presence or absence of natural abundance metabolite in the media, ^{15}N-serine in the pulse media was at ¾ label, ^{15}N-choline at ⅔ label, and ^{15}N-ethanolamine at 100% label. The dashed black line on each graph indicates maximum theoretical label. Cells were labeled simultaneously with all 3 heavy isotope labels.

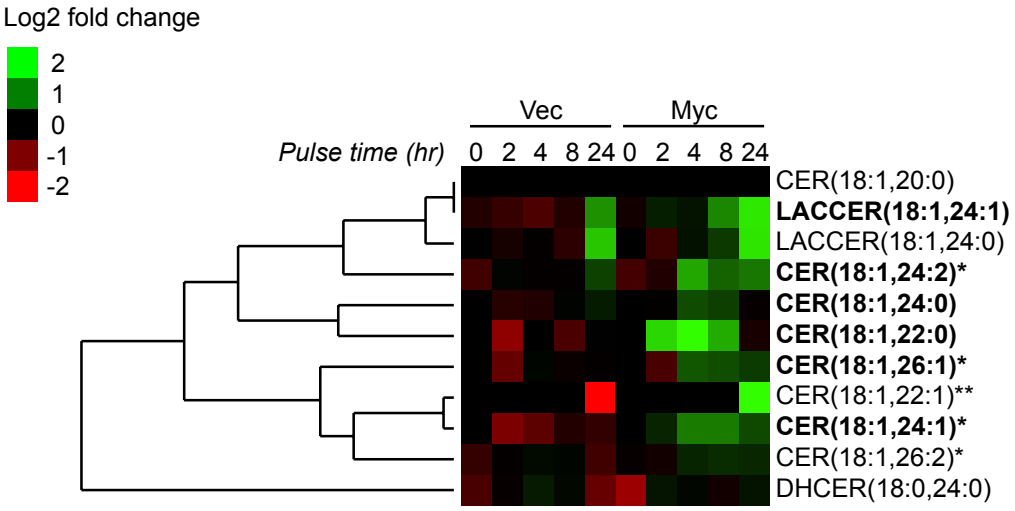

Figure 5.8. *Stable-isotope labeling timecourse of de novo ceramide synthesis*
The heatmap shows hierarchical clustering of ceramide species across a ^{15}N-serine labeling time course of 0 hr to 24 hr. Media was pulsed with heavy isotope at time point 0 hr, 48 hr after *MYC* activation, and lipids were extracted at 0 hr, 2 hr, 4 hr, 8 hr, and 24 hr. Data was acquired using an Orbitrap Fusion Lumos Tribrid Mass Spectrometer, and lipids were identified using LipidSearch. Values are fold-change in average percent label (n=3-4). A one-way ANOVA was carried out on all ceramide species, and lipids with a p-value ≤0.05 across the time course are indicated in bold. An asterisk at the end of a lipid name indicates that more than one isomer of the lipid was identified across a single chromatographic peak.

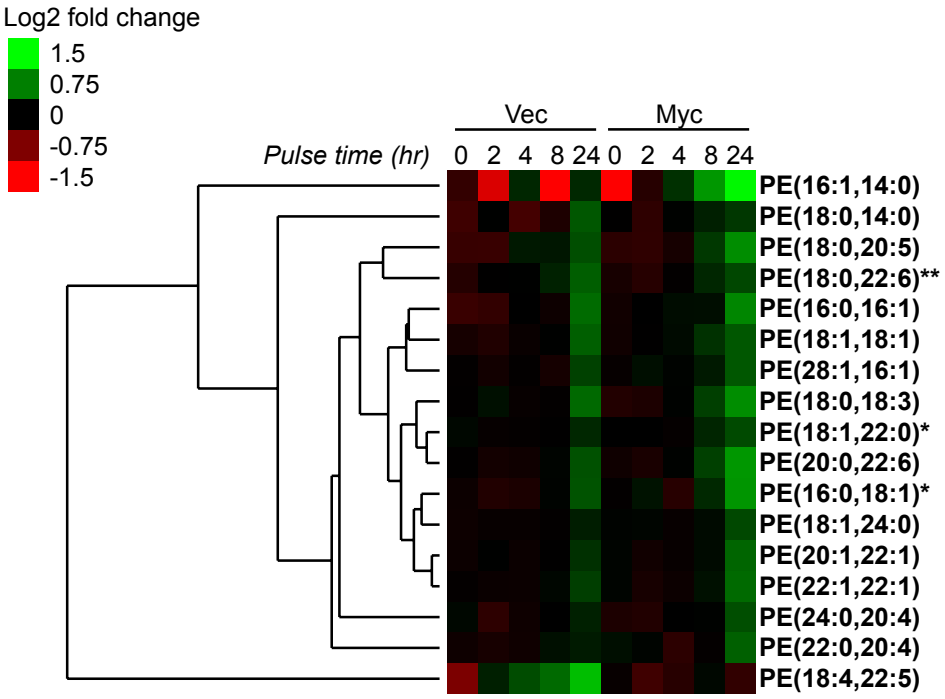

Figure 5.9. *Stable-isotope labeling timecourse of phosphatidylethanolamine synthesis*

The heatmap shows hierarchical clustering of phosphatidylethanolamine (PE) species across a ^{15}N-ethanolamine labeling time course of 0 hr to 24 hr. Media was pulsed with heavy isotope at time point 0 hr, 48 hr after *MYC* activation, and lipids were extracted at 0 hr, 2 hr, 4 hr, 8 hr, and 24 hr. Data was acquired using an Orbitrap Fusion Lumos Tribrid Mass Spectrometer, and lipids were identified using LipidSearch. Values are the average percent label for a lipid at a given time point (n=3-4). A one-way ANOVA was carried out on all PE species, and lipids with a p-value ≤0.05 across the time course are indicated in bold. An asterisk at the end of a lipid name indicates that more than one isomer of the lipid was identified across a single chromatographic peak. Due to space constraints, only significant PE species have been displayed in this heatmap.

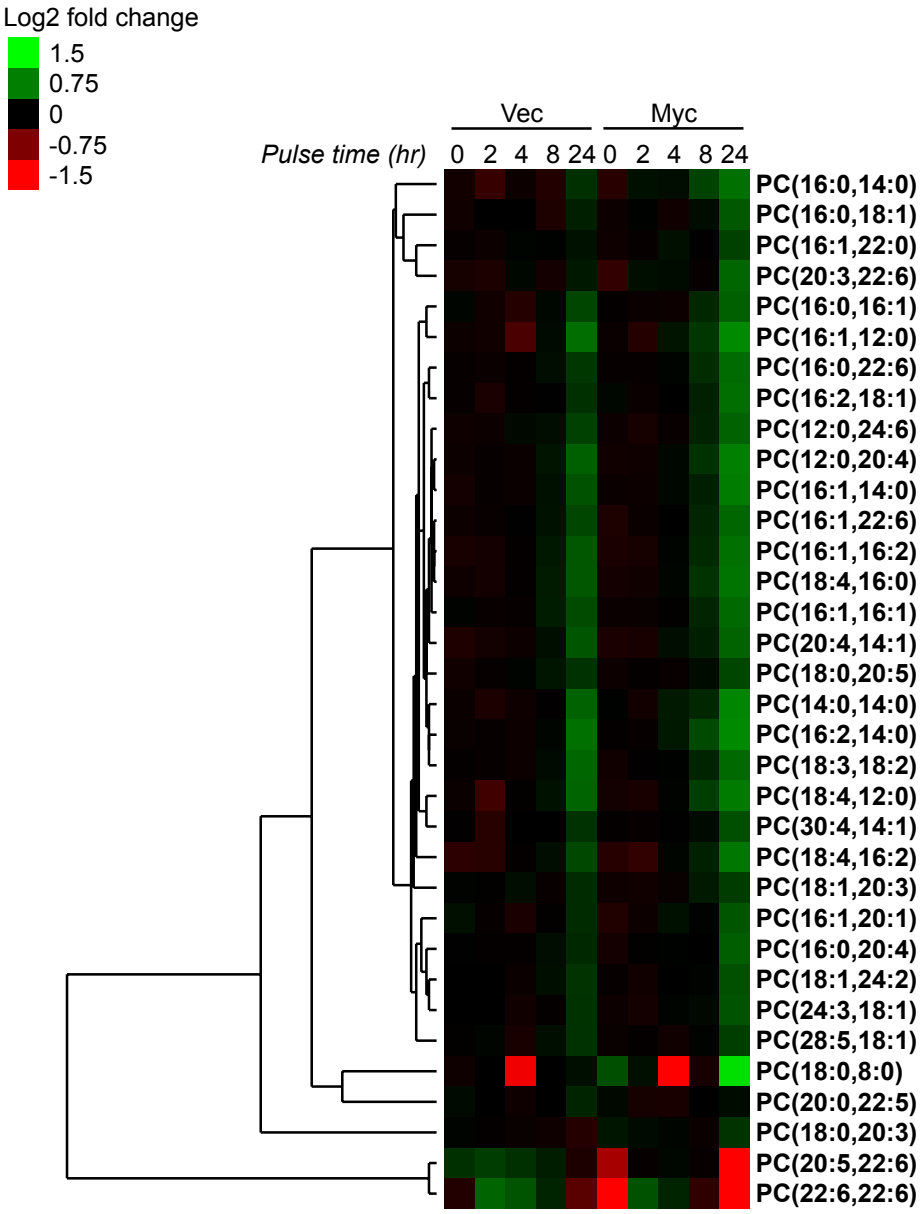

Figure 5.10. *Stable-isotope labeling timecourse of phosphatidylcholine synthesis* The heatmap shows hierarchical clustering of phosphatidylcholine (PC) species across a dual ^{15}N-choline and ^{15}N-ethanolamine labeling time course of 0 hr to 24 hr. Media was pulsed with heavy isotope at time point 0 hr, 48 hr after *MYC* activation, and lipids were extracted at 0 hr, 2 hr, 4 hr, 8 hr, and 24 hr. Data was acquired using an Orbitrap Fusion Lumos Tribrid Mass Spectrometer, and lipids were identified using LipidSearch. Values are the average percent label for a lipid at a given time point (n=3-4). A one-way ANOVA was carried out on all PC species, and lipids with a p-value ≤0.05 across the time course are indicated in bold. An asterisk at the end of a lipid name indicates that more than one isomer of the lipid was identified across a single chromatographic peak. Due to space constraints, only significant PE species have been displayed in this heatmap.

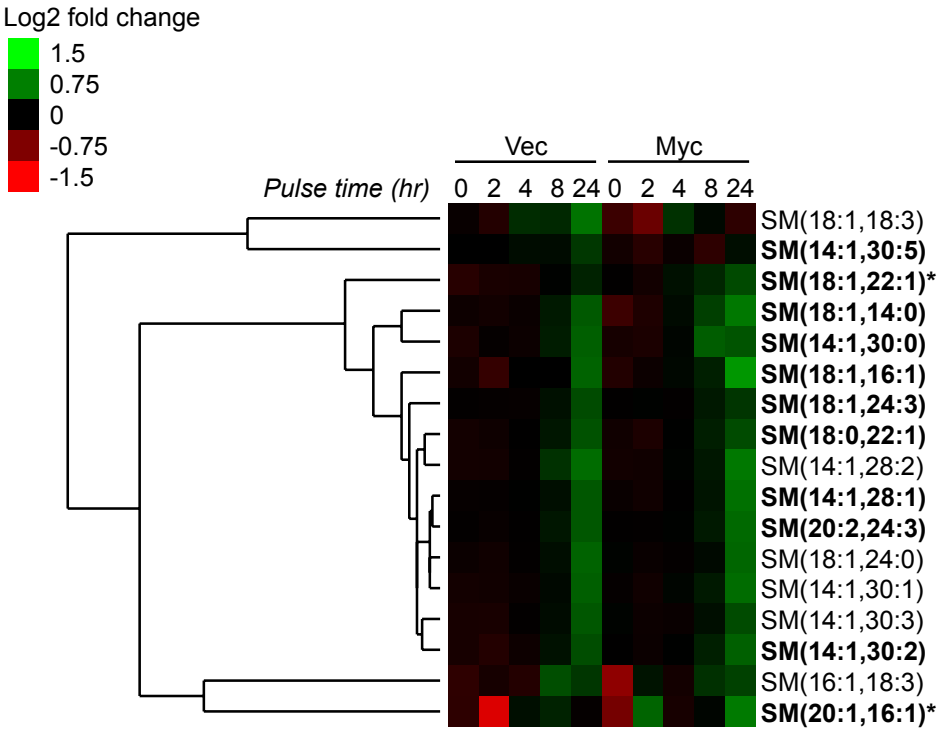

Figure 5.11. *Stable-isotope labeling timecourse of sphingomyelin synthesis*
The heatmap shows hierarchical clustering of sphingomyelin (SM) species across a dual ^{15}N-serine, ^{15}N-choline and ^{15}N-ethanolamine labeling time course of 0 hr to 24 hr. Media was pulsed with heavy isotope at time point 0 hr, 48 hr after *MYC* activation, and lipids were extracted at 0 hr, 2 hr, 4 hr, 8 hr, and 24 hr. Data was acquired using an Orbitrap Fusion Lumos Tribrid Mass Spectrometer, and lipids were identified using LipidSearch. SM species can be labeled by ^{15}N derived from ^{15}N-serine, as well as ^{15}N derived from either ^{15}N-choline or ^{15}N-ethanolamine. Values are the summed (M+1 and M+2) average percent label for a lipid at a given time point (n=3-4). A one-way ANOVA was carried out on all SM species, and lipids with a p-value $\leq$0.05 across the time course are indicated in bold. An asterisk at the end of a lipid name indicates that more than one isomer of the lipid was identified across a single chromatographic peak.

demonstrating that *MYC* deregulated cells potently drive *de novo* ceramide synthesis at almost twice the rate of control cells. This was demonstrated at 48 hr *MYC* activation (the same time-point used to measure p53 accumulation), and was also shown to persist 24 hr beyond this time-point. Whilst MYC-driven ceramide synthesis showed no FA chain length specificity, analysis of total levels of sphingolipid revealed an accumulation of ceramides with longer ≥C24 FA residues following 48hr *MYC* activation. This is in keeping with results from chapter 4 that showed MYC drives an accumulation of longer ≥C26 FAs.

In addition to sphingolipid remodelling, *MYC* deregulated cells remodelled phospholipid species. In particular, PC species that comprised at least one DHA residue (FA 22:6) increased, and these lipids clustered separately from lipids with other FA chain lengths or desaturation level. These results differ from lipid remodelling in response to *MYC* overexpression documented by Hall *et al.* (2016) who found increased incorporation of AA, not DHA, into PCs. Several studies have demonstrated that treatment with polyunsaturated FAs (such as DHA) has profound effects on mitochondrial membrane phospholipid composition and mitochondrial function due to incorporation of DHA into phospholipid species (reviewed in Stanley *et al.* 2014). Moreover, treatment with a mixture of DHA and EPA (eicosapentaenoic acid, 20:5) was shown to improve mitochondrial tolerance to Ca^{2+}-induced mitochondrial permeability transport pore (MPTP) opening (O'Shea *et al.* 2009). This may indicate that *MYC* deregulated cells promote remodelling of polyunsaturated FAs (including DHA) into phospholipids to delay MPTP opening as a result of MYC-induced mitochondrial stress.

As presented in chapter 3, the metabolic siRNA screen results presented here clearly overlapped with a genome-wide siRNA screen in *C.elegans* looking for regulators of the mitochondrial stress response (Liu *et al.* 2014b). Multiple sphingolipid biosynthesis enzymes were identified in both siRNA screens (figure 3.16). Furthermore, *MYC* deregulated cells were shown to increase levels of mitochondrial chaperone gene GRP75, the mammalian equivalent of the readout of the *C.elegans* screen. Together with the data presented in this chapter, these data indicate that p53 responds to MYC-driven lipid remodelling at the mitochondria.

Finally, *MYC* deregulation potently accumulated TGs of varying lengths and levels of desaturation, which may be hydrolysed during periods of high-energy demand to generate precursors for sphingolipid and phospholipid synthesis (reviewed in Coleman and Lee, 2004). The following chapter will give further mechanistic insight into how MYC-driven remodelling of FAs, phospholipids, and sphingolipids regulates p53.

6 Chapter 6- Perturbation of p53 accumulation

The previous chapters have demonstrated that *MYC* activation drives fatty acid and lipid remodelling that regulates MYC-driven p53 accumulation. MYC-driven synthesis of sphingolipids was required for p53 accumulation, and this chapter documents further mechanistic insight into how ceramide positively regulates p53. This includes perturbation of downstream sphingolipid pathways and known ceramide signalling targets (see subsections below).

While *de novo* ceramide synthesis positively regulated p53 (meaning knockdown of ceramide synthesis enzymes blocked full p53 accumulation), knockdown of FA synthesis enzymes or PPARγ increased p53 accumulation. The majority of FA synthesis enzymes identified as siRNA screen hits were involved in arachidonate metabolism (figure 6.1), including *ELOVL7* (fatty acid elongase 7), which shows high specificity for linolenic acid (Ohno *et al.* 2010), the substrate for *de novo* arachidonic acid synthesis; as well as *PLA2G1B* (phospholipase A2 group IB) and *PLA2G4B* (phospholipase A2 group IVB), which hydrolyses membrane glycerophospholipids to release arachidonic acid (Dennis and Norris, 2015). The fact that knockdown of *de novo* synthesis and release pathways of arachidonic acid increased MYC-driven p53 accumulation implicates the key role of arachidonate metabolism in regulating p53 (as one pathway does not compensate for the other).

Polyunsaturated Fas, including AA and DHA, were previously described to activate PPARγ (figure 6.1; Kliewer *et al.* 1997), which was one of the strongest siRNA screen hits. Analysis of FA remodeling driven by *MYC* deregulation showed that AA, DPA, and DHA all significantly decreased compared to extracts from control cells (figure 4.4C). We therefore hypothesised that PPARγ negatively regulates p53 in response to MYC-driven FA remodeling. To investigate this hypothesis this chapter documents experiments that perturb PPARγ activity and FA metabolism (see subsections below).

6.1 Perturbation of sphingolipid metabolism

In chapter 3 it was demonstrated that knockdown of *de novo* sphingolipid enzymes blocked full p53 accumulation, while overexpression of CERS4 increased p53 accumulation beyond the level driven by *MYC* deregulation. Small molecule inhibitors that perturbed sphingolipid metabolism were tested for their effect on p53 accumulation. These inhibitors were selected to cover 5 key sphingolipid pathways: *de novo* synthesis, sphingomyelin hydrolysis, glycosphingolipid, salvage, and ceramide phosphate (figure 6.2A). Four of the inhibitors tested are known to block the remodeling of ceramide into downstream pathways, and were shown to increase

MYC-driven p53 accumulation in a dose-dependent manner (except perhaps for Miglustat hydrochloride) (figure 6.2Bi-iv). The remaining three compounds are reported to inhibit ceramide synthesis, and had no clear effect on MYC-driven p53 accumulation (figure 6.2Ci-iii). Of the compounds tested, ceranib 1 and NVP-231

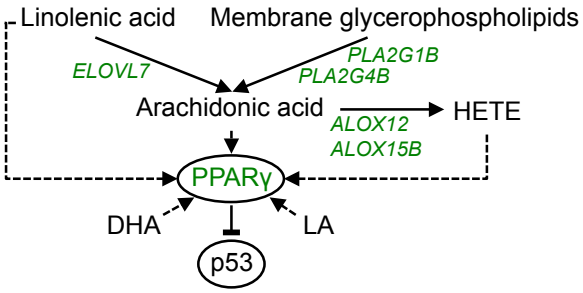

Figure 6.1. *siRNA screen hits in arachidonate metabolism and PPARγ* signalling
The diagram depicts primary siRNA screen hits involved in arachidonate metabolism (highlighted in green). *PLA2G1B* and *PLA2G4B* enocode phospholiase A2s that degrade membrane glycerophospholipids to release arachidonic acid. Arachidonic acid may be used to synthesise eicosinoid HETE (hydroeicosatetraenoic acid) for leukotriene synthesis by *ALOX12* and *ALOX15B*. Arachidonate metabolites were previously described to activate PPARγ (Kliewer *et al.* 1997), as indicated by the dashed line. As knockdown of PPARγ increased p53 accumulation it was hypothesized that PPARγ negatively regulates p53.

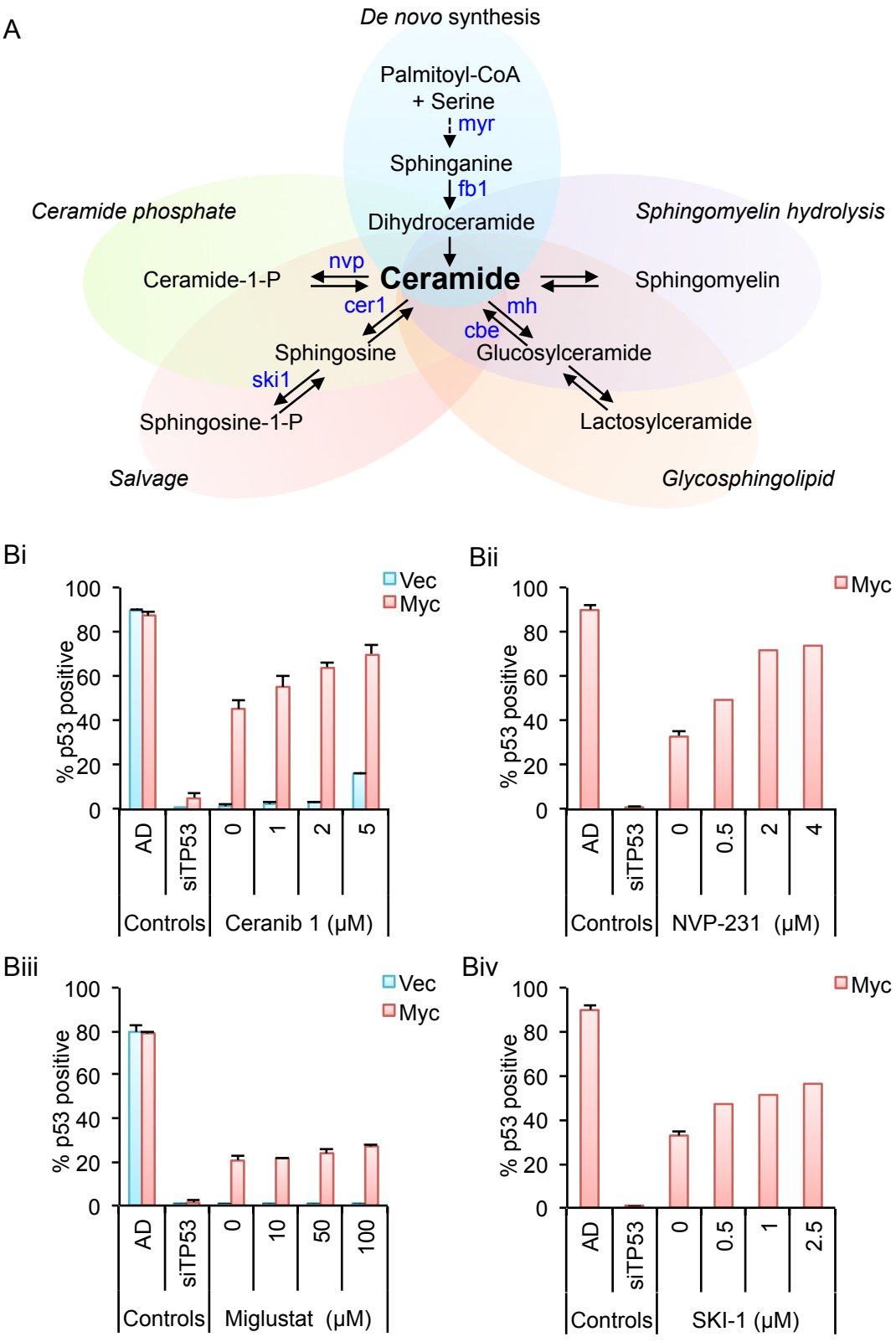
A
De novo synthesis
Palmitoyl-CoA
+ Serine
myr
Sphinganine
fb1
Dihydroceramide
Ceramide phosphate
Sphingomyelin hydrolysis
Ceramide-1-P
nvp
Ceramide
Sphingomyelin
cer1
mh
cbe
Sphingosine
Glucosylceramide
ski1
Sphingosine-1-P
Lactosylceramide
Salvage
Glycosphingolipid
Bi
Vec
Myc
% p53 positive
100
80
60
40
20
0
AD
siTP53
0
1
2
5
Controls
Ceranib 1 (μM)
Bii
Myc
% p53 positive
AD
siTP53
0
0.5
2
4
Controls
NVP-231 (μM)
Biii
Vec
Myc
% p53 positive
AD
siTP53
0
10
50
100
Controls
Miglustat (μM)
Biv
Myc
% p53 positive
AD
siTP53
0
0.5
1
2.5
Controls
SKI-1 (μM)

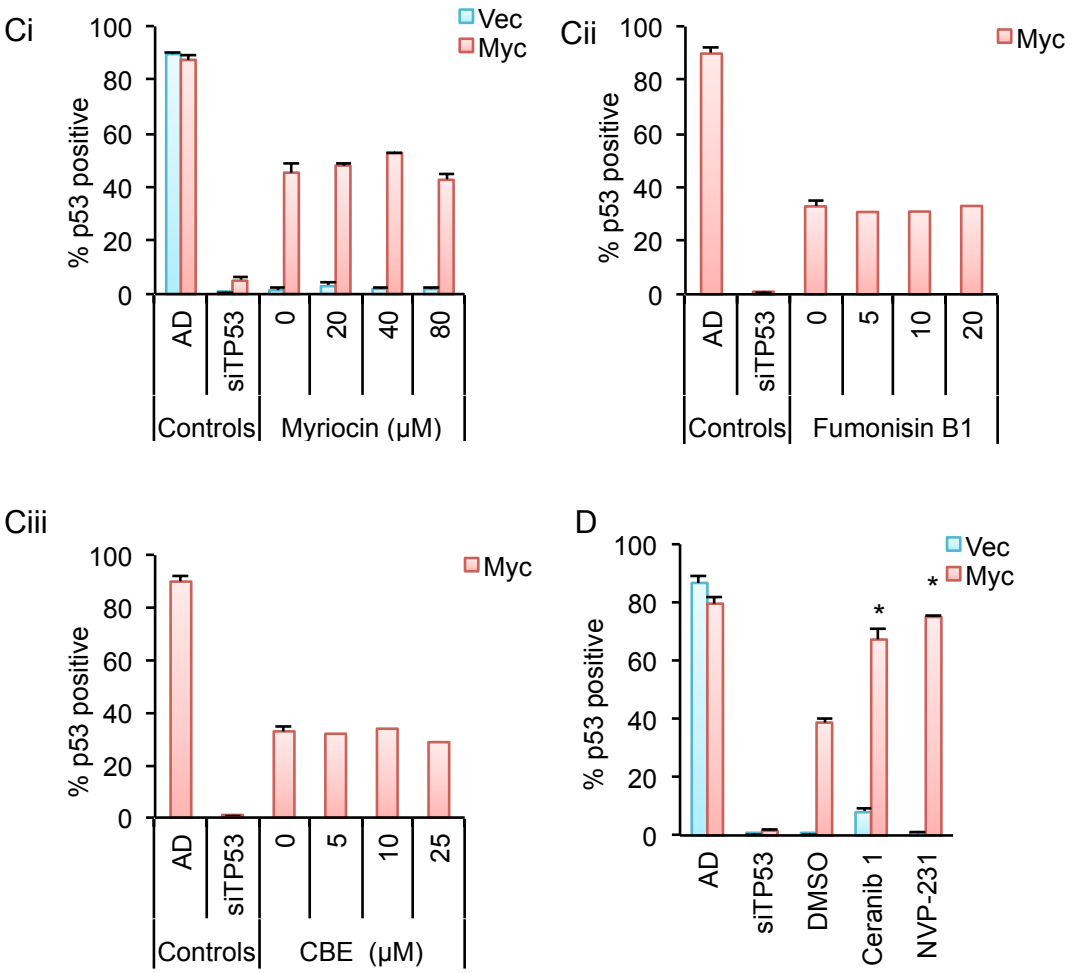

Figure 6.2. *The effect of sphingolipid pathway inhibitors on p53 accumulation*
(A) The diagram summarises five key sphingolipid pathways: *De novo*, Sphingomyelin hydrolysis, Glycosphingolipid, Salvage, and Ceramide phosphate. Dashed arrows indicate multiple enzymatic steps, and arrow head indicates the direction of the reaction. Small molecule inhibitors tested for their effect on P53 stabilisation are indicated in lower case blue (myr= Myriocin, fb1= Fumonisin B1, mh= Miglustat hydrochloride, cbe= Conduritol B Epoxide (CBE), cer1= Ceranib 1, ski1= Sphingosine Kinase Inhibitor-1 (SKI-1), nvp= NVP-231). Ceranib 1, NVP-231, Miglustat, and SKI-1 inhibit ceramide remodeling into downstream pathways; while Myriocin, Fumonisin B1, and CBE inhibit ceramide synthesis. (B) Histograms shows concentration responsive effects of the indicated drug on percent p53 positive cells. Where no error bar is shown n=1. All inhibitors in (B) inhibit ceramide remodeling into downstream pathways. (C) Histograms shows concentration responsive effects of the indicated drug on percent p53 positive cells. Where no error bar is shown n=1, otherwise n=3. All inhibitors in (C) inhibit ceramide synthesis. (D) The histogram compares percent p53 positive cells in vehicle to treatment with Ceranib 1 or NVP-231. These drugs were selected as having the greatest effect on p53 accumulation from the dose response histograms in (B). * indicates a significant p-value (≤0.05; T-test) from a single biological replicate.

had the strongest effect on p53 accumulation, and these compounds are known to function by blocking the conversion of ceramide to sphingosine or ceramide to ceramide phosphate respectively. The optimal concentration of these inhibitors (as determined from the dose-dependent effects on percent p53 positive cells) was further tested and shown to significantly increase p53 accumulation (figure 6.2D). These results indicate that it was the accumulation of ceramide in general that exacerbated MYC-driven p53 accumulation, as opposed to a particular downstream pathway. However, further analysis to validate that the compounds inhibit the pathway they are documented to is required, for example myriocin (an SPT inhibitor) does not recapitulate that results seen with siRNA or shRNA knockdown of SPT (Wadsworth *et al.* 2013).

Sphingosine-1-Phosphate (S1P), which is synthesised from sphingosine downstream of ceramide, was previously described to regulate cell growth (Zhang *et al.* 1991) and suppress programmed cell death (Cuvillier *et al.* 1996) through its interaction with G-protein-coupled-receptors (GPCRs). To test whether S1P signaling effects MYC-driven p53 accumulation a panel of S1P receptor agonists and antagonists were tested across a range of relevant concentrations. Of the 7 small molecules tested there was no clear effect on p53 accumulation, indicating that S1P signaling through the S1P receptors does not affect the p53 response to *MYC* overexpression (figure 6.3).

6.2 Ceramide signalling

Several proteins have been shown to interact with ceramide that may offer mechanistic insight into how p53 responds to deregulation of *MYC* via *de novo* ceramide synthesis. These include protein phosphatases such as protein phosphatase 1 (PP1) and protein phosphatase 2A (PP2A) (Chalfant *et al.* 1999, 2004), as well as protein kinase C zeta (PKCζ) (Müller *et al.* 1995; Bourbon *et al.* 2002). The effect of *MYC* deregulation on PP1A and PP2AC was investigated by western blot (figure 6.4). *MYC* deregulation did not clearly affect PP1A levels, but increased levels of PP2AC (PP2A catalytic subunit). The effect of protein phosphatase and PKCζ knockdown on p53 was analysed by immunofluorescent staining (figure 6.5), and knockdown of PP1A subunits *PPP1CA* or *PPP1CC* had no effect on p53 accumulation, while knockdown of PP2A catalytic subunit *PPP2AC* moderately decreased p53 accumulation ($p \leq 0.05$). Knockdown of PRKC2 had no effect on p53 accumulation. These results indicate that PP2A may be involved in regulating p53 in response to MYC-driven *de novo* ceramide synthesis.

Small molecule inhibitors of protein phosphatases and PKCζ were also tested. Okadaic acid was previously shown to inhibit PP1 (IC_{50} = 3 - 15 nM) and PP2A (IC_{50} = 0.1-1 nM) (Mailhes *et al.* 2003), and was hypothesised to decrease p53 accumulation similarly to siPPP2AC at lower doses. Okadaic acid significantly reduced MYC-driven p53 accumulation at a concentration known to inhibit PP2A (1 nM; figure 6.6A), and showed a trend towards increasing p53 higher concentrations known to inhibit PP1 (15 nM). The reduction in p53 accumulation with low dose

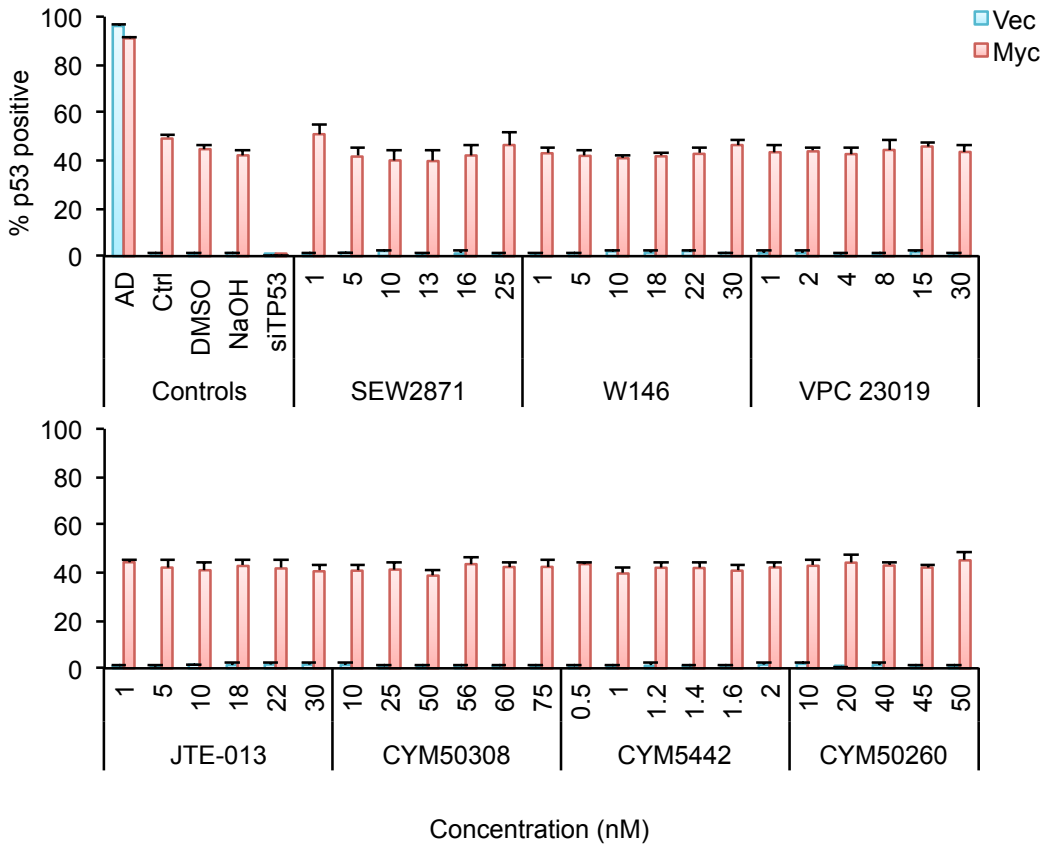

Figure 6.3. *The effect of sphingosine-1-phosphate signaling perturbation on p53 accumulation*

Histogram shows the effect of a panel of sphingosine-1-phosphate receptor agonists and antagonists on p53 accumulation across an appropriate concentration range. Two vehicle controls were included due to the different drug solubilities; however no significant difference on percent p53 positive cells was detected. This experiment is a single biological replicate. Error bars are the standard error (n=3).

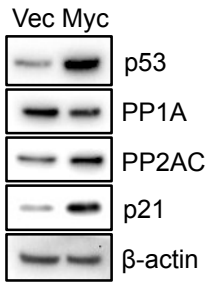

Figure 6.4. *The effect of Myc activation on Protein Phosphatases*
Western blot shows the effect of *MYC* activation on PP1A and PP2AC following 48 hr *MYC* activation with 4OHT (n=2).

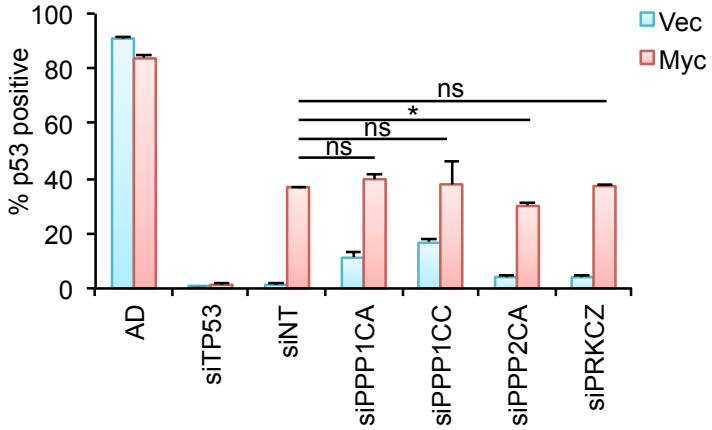

Figure 6.5. *Knockdown of protein phosphatases and protein kinase C zeta*
Histogram compares percent p53 positive cells in the non-target pool (siNT) to siRNA knockdown of *PP1CA*, *PPP1CC*, *PPP2CA*, and *PRKCZ*. Error bars are the standard error (n=3). * indicates a significant p-value (≤0.05; T-test). Statistics were carried out on a single biological replicate.

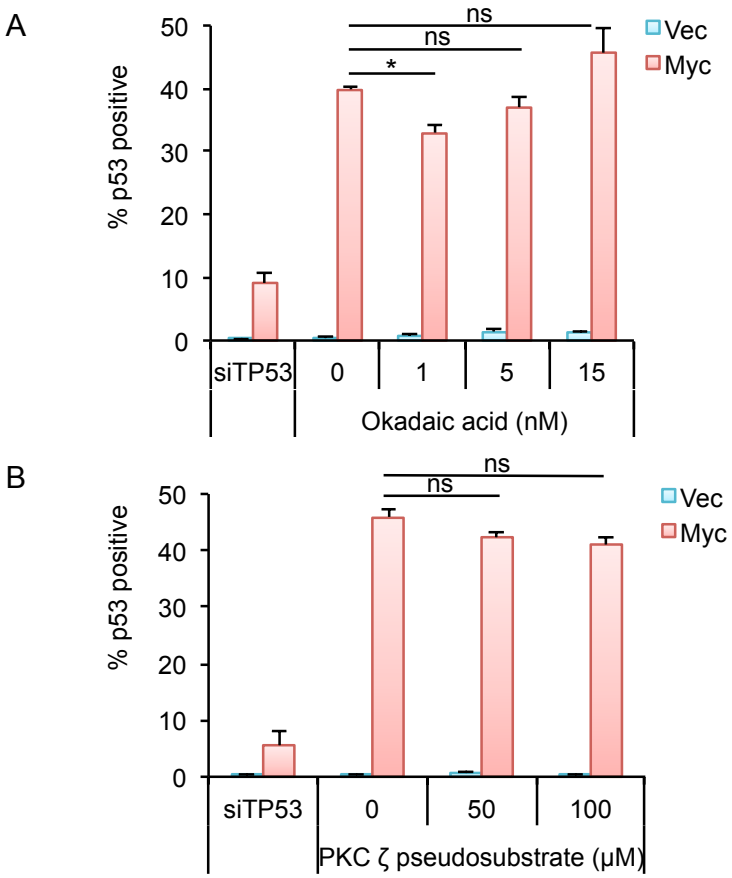

Figure 6.6. *Small molecule inhibitors of protein phosphatases and protein kinase C zeta*

Histograms shows the dose response effect of protein phosphatase inhibitor Okadaic acid (A) and protein kinase C zeta inhibitor PKCζ pseudosubstrate compared to control. Okadaic acid was previously shown to inhibit PP1 (IC_{50} = 3 - 15 nM) and PP2A (IC_{50} = 0.1-1 nM). Error bars are the standard error (n=3). * indicates a significant p-value (≤0.05; T-test). Statistics were carried out on a single representative replicate.

okadaic acid was similar to the reduction seen with siPPP2AC (see above), thereby validating the siRNA results. PKCζ pseudosubstrate did not affect MYC-driven p53 accumulation as expected from the siRNA knockdown experiments described above (figure 6.6B).

Overall these analyses suggest that PP2A regulates p53 accumulation in response to MYC-driven *de novo* ceramide synthesis; however as the reduction in p53 accumulation was not as striking as that seen with knockdown of *de novo* ceramide synthesis enzymes, PP2A is unlikely to be the sole regulator of the p53 response to increased *de novo* ceramide synthesis.

6.3 Fatty acids and PPARγ

As knockdown of enzymes involved in FA biosynthesis (particularly arachidonic acid synthesis) augmented MYC-driven p53 accumulation, it was hypothesised that addition of unsaturated FAs might reduce MYC-driven p53 accumulation. A panel of 10 unsaturated FAs with a range of chain lengths and levels of desaturation were tested, and only arachidonic acid (20:4) significantly reduced p53 accumulation in a conecentration-dependent manner (figure 6.7A and B). Linolenic acid (18:3), but not linoleic acid (18:2), also showed a trend toward decreased p53 accumulation with increasing treatment concentration. Linoleic and linolenic acid are essential FAs in mammals due to lack of the desaturase required for their synthesis.

As knockdown of *PPARG* augmented MYC-driven p53 accumulation it was hypothesised that PPARγ negatively regulates p53 (figure 6.1). PPARγ ligand Rosiglitazone was shown to significantly reduce MYC-driven p53 accumulation in a concentration-dependent manner (figure 6.8A and B). Concomitantly, PPARγ antagonist T0070907 significantly increased p53 accumulation in a concentration-dependent manner (figure 6.8A and B). These experiments demonstrate that PPARγ activity regulates p53. Furthermore, deregulation of *MYC* potently reduced levels of PPARγ compared to control cells (figure 6.9A), suggesting that *MYC* may activate p53, at least in part, through depletion of PPARγ and consequent reduction in its negative regulation of p53.

Rosiglitazone was also tested alongside knockdown of *SPTLC2*, *CERS4*, *DEGS2*, and *PPP2CA* to investigate whether these pathways were additive in terms of regulating p53 accumulation (figure 6.9B). Knockdown of *SPTLC2*, *CERS4*, and *DEGS2* had no additional effect on p53 accumulation following rosiglitazone treatment, while knockdown of *PPP2CA* slightly decreased p53 accumulation. The effect of shRNA knockdown of CERS4 on PPARγ was tested by western blot and while shCERS4 reduced p53 levels, this was not accompanied by an increase in PPARγ levels (figure 6.10). These results indicate that regulation of p53 by PPARγ signalling and sphingolipid signalling is distinct.

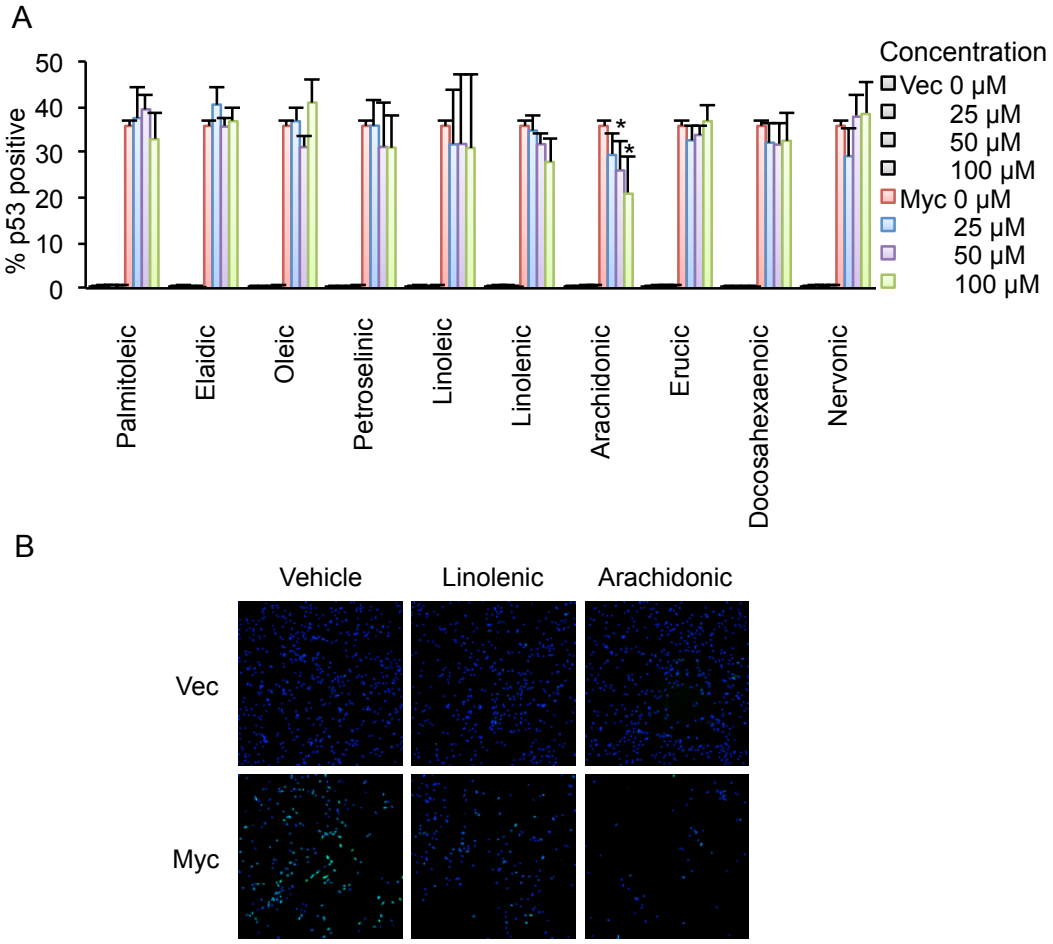

Figure 6.7. *The effect of fatty acid treatment on p53 accumulation*
(A) Histogram shows dose responsive effects of unsaturated fatty acid (FA) treatment on percent p53 positive cells. Cells were treated with vehicle control or the indicated FA concentration at the same time as *MYC* was activated with 4OHT for 48 hr. Error bars are the standard error (n=3). * indicates a significant p-value (≤0.05; T-test). Statistics were carried out on a single biological replicate. (B) Immunofluorescent images show the effect of linolenic acid or arachidonic acid treatment on p53 accumulation, as quantified in (A). Immunofluroescence shows DAPI (blue) and p53-FITC (green).

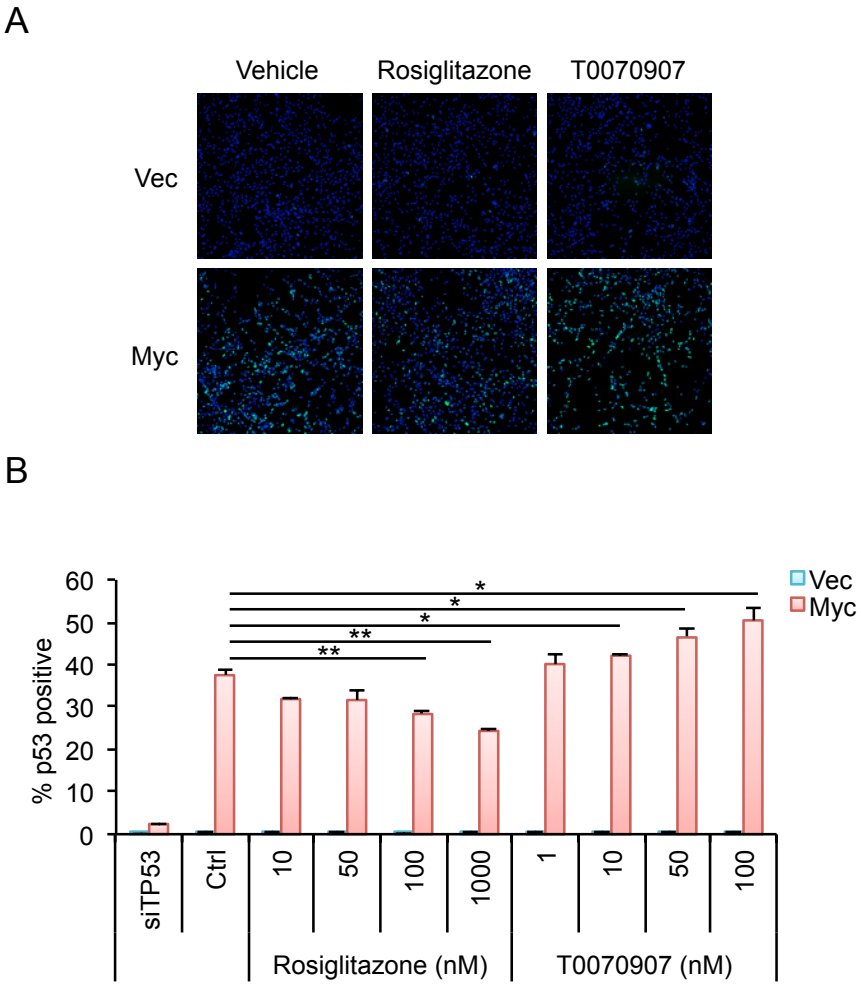

Figure 6.8. *The effect of PPARγ perturbation on p53 accumulation*
(A) Immunofluorescent images show the effect of PPARγ ligand Rosiglitazone (1000 nM) and PPARγ antagonist T0070907 (100 nM) on p53 stablilsation. Immunofluroescence shows DAPI (blue) and p53-FITC (green). (B) Histogram shows dose responsive effects on percent p53 positive cells of Rosiglitazone and T0070907. Drugs were added at the same time as 4OHT treatment for 48 hr. Error bars are the standard error (n=3). * indicates a significant p-value (≤0.05; T-test). Statistics were carried out on a single biological replicate.

A

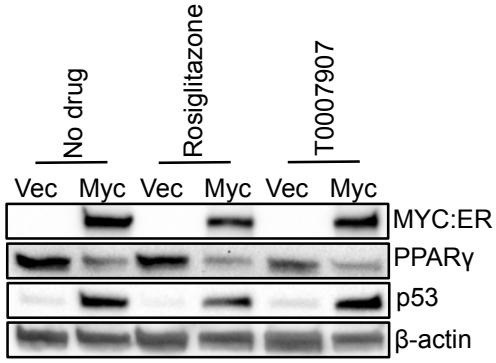

B

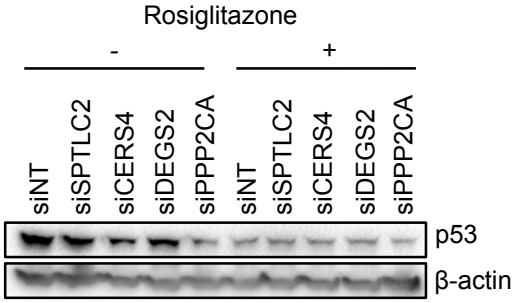

Figure 6.9. *The effect of MYC activation on PPARγ*
(A) The western blot shows the effect of *MYC* activation on PPARγ and p53 alone (no drug), as well as with 48 hr Rosiglitazone or T0007907 treatment (100 nM) (n=3). Drugs were added at the same time as 4OHT treatment for 48 hr. (B) The western blot shows the effect of *SPTLC2, CERS4, DEGS2,* or *PPP2CA* knockdown on p53 accumulation plus/minus 48 hr Rosiglitazone treatment (100 nM) (n=1). All samples were extracted from MRC5 cells following 48hr *MYC* activation with 4OHT.

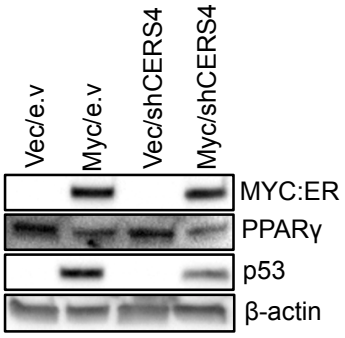

Figure 6.10. *The effect of CERS4 knockdown on PPARγ and p53*
Western blot shows the effect of CERS4 shRNA knockdown on PPARγ and p53 following 48 hr *MYC* activation with 4OHT.

6.4 Summary

In summary, data are presented in this chapter that further validate two major clusters of siRNA screen hits involved in fatty acid biosynthesis/arachidonate metabolism and *de novo* ceramide synthesis. MYC-driven *de novo* ceramide synthesis positively regulates p53, and whether this was due to a downstream target of ceramide signalling or ceramide remodelling was investigated. Analysis of known targets of ceramide signalling revealed that PP2A was required for full p53 accumulation in response to *MYC* deregulation; however knockdown or pharmacological inhibition of PP2A did not reduce p53 accumulation to the same extent as knockdown to *de novo* ceramide synthesis enzymes. This indicates that PP2A may be one of multiple proteins that regulate p53 accumulation in response to MYC-driven *de novo* ceramide synthesis.

The role of ceramides as intermediates in sphingolipid metabolism was analysed using pharamacological inhibitors. Of the compounds tested, ceranib 1, which blocks the conversion of ceramide to sphingosine, and NVP-231, which blocks the conversion of ceramide to ceramide phosphate, potently increased MYC-driven p53 accumulation. Downstream of sphingosine, sphingosine-1-phosphate receptor ligands or antagonists were tested for their effect on p53 accumulation. The compounds had no effect on p53 accumulation, indicating that increased p53 accumulation caused by ceranib 1 was due to increased ceramide levels, not inhibition of ceramide conversion into sphingosine-1-phosphate downstream. This finding agrees with *MYC* deregulated cells increasing *de novo* ceramide synthesis, but disagrees with the observation that *MYC* deregulated cells deplete total ceramide levels, indicating that p53 may respond to compartment specific increases in ceramide synthesis driven by *MYC* overexpression.

In keeping with knockdown of PPARγ/arachidonate metabolism increasing MYC-driven p53 accumulation, PPARγ activity was shown to negatively regulate p53. Deregulation of *MYC* depleted levels of AA, DPA, DHA, and PPARγ, which indicates that MYC-driven depletion of PPARγ and its ligands may be sufficient to relieve its inhibition of p53 and result in p53 accumulation. As AA, DPA, and DHA were previously documented to regulate PPARγ (Kliewer *et al.* 1997), PPARγ may be a key sensor of MYC-driven FA changes. Concomitantly, treatment with AA (but not other unsaturated FAs) reduced MYC-driven p53 accumulation. Finally, knockdown of *de novo* ceramide synthesis enzymes did not affect PPARγ levels, indicating that these two metabolic pathways independently regulate MYC-driven p53 accumulation.

7 Chapter 7- Discussion

Activation of the *MYC* oncogene drives cell proliferation and cell growth, and these attributes lead to its frequent overexpression or amplification in human cancer (Koskinen and Alitalo, 1993). In otherwise genetically intact cells, overexpression of *MYC* activates the p53 tumour suppressor pathway, which resists cell cycle progression (Finch et al., 2006; Hermeking and Eick, 1994). Despite decades of research, no transcriptional target of MYC has been found that mediates p53 pathway activation. Furthermore, the contrasting effects of MYC and p53 on cell metabolism fit with a homeostatic model, whereby p53 responds to MYC-driven metabolic changes. Whilst MYC target genes indicate MYC remodels metabolic pathways towards anabolism (reviewed in Dang, 2013), p53 has been documented to promote catabolic pathways that favour restoration of cellular energy charge and redox status (reviewed in Kruiswijk *et al.* 2015). Loss of p53 is frequently selected for in a variety of tumours (Eischen *et al.* 1999; Hill *et al.* 2015) and tumour cell lines (Farrell *et al.* 1991; Wiman *et al.* 1991), and p53-null tumours are characterised by increased proliferation with no marked effect on apoptosis (Elson *et al.* 1995; Hsu *et al.* 1995; Finch *et al.* 2006). This indicates that loss of p53 may also alleviate increased cell stress associated with relief of proliferative inhibition. In addition to p53 responding to MYC-driven metabolic changes, we further hypothesised that p53 loss conferred a metabolic advantage to *MYC* overexpressing cells.

A large loss-of-function metabolic siRNA screen was carried out to determine whether metabolic enzymes, transporters, and transcription factors regulated p53 accumulation in response to *MYC* activation. Functional annotation of 36 siRNAs revealed two key clusters of hits involved in FA synthesis/arachidonate metabolism and sphingolipid synthesis. Importantly, these were very specific areas of metabolism relative to the broad range of metabolic pathways targeted by the siRNA library. Knockdown of sphingolipid enzymes, particularly those involved in *de novo* ceramide synthesis, prevented p53 accumulation; indicating that ceramide positively regulates p53. Knockdown of enzymes involved in long-chain FA elongation and arachidonic acid metabolism augmented p53 accumulation, implicating long-chain FAs as negative regulators of p53. Knockdown of FA-responsive PPARγ (reviewed in Desvergne and Wahli, 1999), a master regulator of lipid homeostasis (reviewed in Lehrke and Lazar, 2005), was one of the strongest hits that exacerbated p53 accumulation, providing further evidence of the importance of fatty acid and lipid remodelling in regulating the p53 response to *MYC* activation.

Targetted metabolomic analysis revealed that loss of p53 increased the biosynthetic capacity of *MYC* deregulated cells. Myc/p53DN cells increased synthesis of pentose phosphate pathway intermediates, including pentose 5-phosphate, and intermediates of the serine synthesis pathway. These intermediates were used to increase synthesis of nucleotides, nucleosides, and nucleobases. Further analysis of the fate of nucleotides showed p53 loss increased RNA synthesis, DNA synthesis, and lipid precursor synthesis in *MYC* deregulated cells, supporting the hypothesis that loss of p53 confers a metabolic advantage to cells that overexpress *MYC*.

7.1 Sphingolipid synthesis

Sphingolipids are a functionally diverse class of lipids that all share a sphingosine backbone. Modification of this basic structure gives rise to multiple sphingolipid species including ceramides, ceramide phosphates, glycosylsphingolipids, sphingosine-1-phosphate, and sphingomyelins (which also contain a glycerophospholipid-derived component). Of these species, much research has focused on ceramides due to their key role as membrane components, as intermediates in the metabolism of more complex sphingolipids, and as signalling molecules (reviewed in Goñi and Alonso, 2006). Ceramides are some of the least polar and more hydrophobic lipids in membranes and have been shown to increase the molecular order, lateral phase separation, and domain formation of phospholipid bilayers (Holopainen *et al.* 1997; Hsueh *et al.* 2002). Lipid microdomains have been shown to act as platforms for membrane trafficking and intracellular signalling (reviewed in Simons and Ikonen, 1997), highlighting the importance of sphingolipids as membrane components.

In this study, knockdown of *de novo* ceramide synthesis enzymes SPTLC2, CERS4, and DEGS2 were shown to reduce p53 accumulation in response to *MYC* activation. Concomitantly, ORMDL2, which negatively regulates SPT, was identified as a hit that increases p53 accumulation. SPTLC2, CERS4, and DEGS2 were validated by individual siRNAs targeting each gene, by genetic knockdown experiments, and by genetic overexpression experiments. Stable-isotope tracer analysis by LC-MS showed that *MYC* overexpression significantly increased *de novo* ceramide synthesis, demonstrating that this is a relevant pathway for p53 to respond to. Further analysis of over 50 sphingolipid species revealed that *MYC* overexpression increased ceramides and lactosylceramides with ≥C24 FA residues, while sphingolipids with shorter-chain FA residues decreased.

The ability of ceramides to form lipid rafts is in part due to them comprising a long fatty acyl chain that can interdigitate with the cytoplasmic leaflet of the bilayer (Ohno *et al.* 2010). Ceramides and latosylceramides with longer ≥C24 FA residues were previously implicated in membrane signaling through their interaction with the Src family kinase LYN, demonstrating the role of longer-chain ceramides in membrane signalling (Sonnino *et al.* 2009). Ohno *et al.* (2010) showed that ELOVL1 was essential for the production of C24 sphingolipids, and ELOVL1 was identified as a gene whose knockdown augmented MYC-driven p53 accumulation in the siRNA screen. This suggests that inability to synthesise C24 FAs is metabolically stressful following *MYC* overexpression. Ohno *et al.* (2010) also showed that knockdown of *ELOVL1* mRNA caused a reduction in the activity of LYN, linking long-chain FA elongation to ceramide-mediated signalling. ELOVL1 deficient mice die shortly after birth due to epidermal growth barrier defects (Sassa *et al.* 2013), which may be due to decreased levels of ceramides with ≥C26 FA residues detected in the epidermis. Together these studies suggest that *MYC* overexpression drives synthesis of long-chain sphingolipids to alter membrane structure and signaling.

Whilst promotion of ceramide synthesis by MYC is novel, multiple studies have shown that ceramides respond to stress stimuli and promote an appropriate response. C16 ceramide has been shown to trigger apoptosis in response to ionising radiation through increased *de novo* ceramide synthesis driven by activation of CERS5 and CERS6 (Mesicek *et al.* 2010). A similar response was observed in *C.elegans* due to DNA double-strand breaks (Deng *et al.* 2008). ER stress was shown to trigger apoptosis by both the *de novo* synthesis of ceramide and increased acid sphingomyelinase activity, which hydrolyses ceramide from sphingomyelin (Sauane *et al.* 2010). Saune *et al.* showed that ceramide triggers apoptosis by activating PP2A to dephosphorylate anti-apoptotic protein Bcl-2. Ceramide also has a structural role in apoptosis as cytosolic cytochrome C is released from the mitochondria through ceramide channels (Colombini, 2010).

Of closer relevance to this study, ceramide has been shown to respond to moderate stress and trigger a non-apoptotic response. In *C.elegans*, a genome-wide siRNA screen revealed several hits in sphingolipid metabolism (including *de novo* synthesis), whose knockdown prevented the induction of mitochondrial repair pathways in response to mitochondrial stress (Liu *et al.* 2014b). Liu *et al.* demonstrated the importance of ceramides as mediators of cellular stress in a genome-wide context, and thus provided validation of the metabolism-focused siRNA screen described here. *MYC* deregulation was shown to induce mitochondrial chaperone gene GRP75 (the readout of the *C.elegans* screen), but not ER chaperone gene GRP78, indicating that *MYC* deregulation induces mitochondrial stress.

Several downstream targets of ceramide signalling have been described that may be important in regulating p53, including protein phosphatases PP1 and PP2A (Chalfant *et al.* 1999, 2004; Dobrowsky *et al.* 1993), and PKCζ (Müller *et al.* 1995). *MYC* overexpression was shown to increase protein levels of PP2A, but not PP1, and knockdown of the catalytic subunit of PP2A moderately reduced p53 accumulation. This was further validated using Okadaic acid, which was previously described to inhibit PP2A at low concentrations and reduced p53 levels to a similar extent as PP2A knockdown. However, PP2A knockdown or inhibition did not reduce p53 to the same extent as knockdown of *de novo* ceramide synthesis enzymes, suggesting that other proteins are involved in regulating p53 in response to increased ceramide synthesis. The role of PP2A in regulating p53 may also be context dependent as Ajay *et al.* (2010) showed that inhibition of PP2A activates p53. More studies are required to determine the involvement of PP2A in MYC-driven p53 accumulation, and an untargeted approach to identify p53 bound proteins following *MYC* overexpression may identify novel players that regulate this process.

The role of ceramides as intermediates in sphingolipid metabolism was analysed using pharmacological inhibitors. Of the compounds tested, ceranib 1, which blocks the conversion of ceramide to sphingosine, and NVP-231, which blocks the conversion of ceramide to ceramide phosphate, potently increased MYC-driven p53 accumulation. This indicated that either an inability to synthesise downstream sphingolipids, or an accumulation of ceramide, was metabolically stressful in *MYC* deregulated cells. Sphingosine-1-phosphate is synthesised from sphingosine

downstream of the ceramidase inhibited by ceranib 1, and was previously described to regulate cell growth (Zhang *et al* 1991) and block programmed cell death (Cuvillier *et al.* 1996). Sphingosine-1-phosphate receptor ligands or antagonists had no effect on p53 accumulation, indicating that increased p53 accumulation caused by ceranib 1 was due to increased ceramide levels. This is supported by CERS4 overexpression experiments that showed CERS4 overexpression increased *de novo* ceramide synthesis and p53 accumulation (albeit not to the same extent as the downstream inhibitors).

The use of pharmacological inhibitors such as ceranib 1 probably exerts cell-wide effects on multiple ceramide species, which may explain why ceranib 1 treatment has a much stronger effect on p53 accumulation compared to CERS4 overexpression, which was specific to C18-C22 ceramide species. Furthermore, while *MYC* overexpressing cells increased *de novo* ceramide synthesis, the total levels of most ceramide species decreased. This may indicate that, in the case of *MYC* overexpression, p53 responds to compartment-specific changes in ceramide synthesis, which may only be visualised using stable heavy-isotope tracer analyses as opposed to analysing the total cellular ceramide pool. It is possible that cell-wide changes in ceramide levels could induce p53 accumulation; however the mechanism of how this occurs may be distinct from how MYC-driven *de novo* ceramide synthesis promotes p53 accumulation.

Overall these data clearly demonstrate that *MYC* overexpression drives *de novo* ceramide synthesis and remodelling of sphingolipid metabolism to specifically accumulate long-chain ceramides and lactosylceramides. p53 responds to increased *de novo* ceramide synthesis driven by *MYC* overexpression, and the mechanism of how ceramide regulates p53, and whether this mechanism is cellular compartment-specific, is yet to be elucidated.

7.2 Fatty acid and glycerolipid synthesis

FAs are used in the cell for lipid biosynthesis, storage, or they can be catabolised by fatty acid oxidation (FAO) to maintain energy homeostasis. Cells can acquire FAs through the *de novo* synthesis pathway, through extracellular uptake, or through the breakdown of cellular or membrane lipids (reviewed in Eljamil *et al.* 2015). Multiple enzymes involved in FA synthesis were identified as screen hits whose knockdown augmented MYC-driven p53 accumulation. This is in keeping with previous research on MYC transcriptional targets, which include several *de novo* FA synthesis enzymes ACLY, ACACA, and FAS (Zeller *et al.* 2003; Loven *et al.* 2012).

De novo FA synthesis begins with the conversion of pyruvate into acetyl-CoA in the mitochondrial matrix, followed by condensation with oxaloacetate to produce citrate. MYC target genes ACLY and ACACA then convert citrate to cytosolic acetyl-CoA, and acetyl-CoA to malonoyl-CoA respectively. Malonyl-CoA is the 2-carbon donor used to synthesise FAs in each round of the elongation cycle. Three genes involved in the direction of carbon into acetyl-CoA synthesis were identified as hits that

increased MYC-driven p53 accumulation: aldolase B (*ALDOB*), dihydrolipoamide S-acetyltransferase (*DLAT*), and phosphopanthothenate cysteine ligase (*PPCS*). ALDOB catalyses the reversible cleavage of fructose 1,6-bisphosphate to glyceraldehyde 3-phosphate in the glycolytic pathway, and was identified as the second strongest hit in the siRNA screen. ALDOB was likely particularly important in the generation of pyruvate because all experiments in this study (unless otherwise stated) were carried out in media lacking pyruvate. DLAT encodes component E2 of the multi-enzyme pyruvate dehydrogenase complex (PDC) that converts pyruvate to acetyl-CoA. PDC therefore commits pyruvate-derived carbon to the TCA cycle (for FA synthesis) as opposed to lactate or alanine production. PPCS converts phosphopanthothenate to phosphopantothenyl cysteine in the CoA synthesis pathway (Daugherty *et al.* 2002), and total levels of phosphopantothenate were increased in cells with deregulated *MYC*.

Experiments utilising stable-isotope labelled glucose revealed that MYC significantly increased synthesis of pyruvate through glycolysis, and stable-isotope labelled pyruvate showed that MYC significantly increased incorporation of pyruvate-derived carbon into citrate. These studies confirmed that MYC drives the synthesis of metabolites that may be used for *de novo* FA synthesis.

Synthesis of FAs up to the length of palmitate (C16) occurs in the cytoplasm and is catalysed by the MYC target gene FAS (Zeller *et al.* 2003). Elongation of long-chain FAs is localised to the ER and is catalysed by elongase enzymes, of which ELOVL1 and ELOVL7 were identified as screen hits (reviewed in Eljamil *et al.* 2015). Stable-isotope labelled pyruvate was used to measure the rate of *de novo* fatty acid synthesis, and increased incorporation of label was seen in palmitate and lignocerate following *MYC* activation, supporting the necessity of elongase enzymes in *MYC* activated cells. As mentioned above, ELOVL1 was previously shown to hydrolyse C24:0-CoAs, as well as C22:0-CoAs and C26:0-CoAs; however ELOVL7 showed strong specificity for C18:3-CoAs (linolenoyl-CoA) (Ohno *et al.* 2010).

In addition to *de novo* FA synthesis, multiple siRNA screen hits were identified in arachidonate (C20:4) metabolism. Arachidonic acid (AA) may be synthesised from the hydrolysis of membrane phospholipids by phospholipase A2 (reviewed in Dennis and Norris, 2015). Two genes encoding phospholipase A2s were identified as screen hits: *PLA2G1B* and *PLA2G4B*, indicating that phospholipase A2s are required for freeing esterified arachidonic acid in the context of *MYC* overexpression. Downstream, AA can be used for eicosanoid synthesis, which is catalysed by screen hits *ALOX15B* and *ALOX12* (arachidonate lipoxygenases). The identification of multiple screen hits in arachidonate metabolism is in keeping with results presented by Hall *et al.* (2016), which showed that *MYC* overexpression remodelled arachidonate metabolism and increased phospholipase A2 activity.

As knockdown of multiple FA enzymes increased p53 accumulation, it was hypothesised that FA treatment would rescue MYC-driven p53 accumulation. From a panel of ten unsaturated FAs, only AA significantly reduced p53 accumulation in a dose-dependent manner. Linolenic acid (LA) also showed a dose-dependent

reduction of p53 accumulation, although this was not significant. The high number of screen hits in arachidonate metabolism coupled with previous data showing that arachidonate metabolites activate screen hit PPARγ (reviewed in Desvergne and Wahli, 1999), led us to investigate whether PPARγ responds to MYC-driven FA changes and subsequently regulates p53.

PPARγ was identified as the third strongest screen hit whose knockdown increased p53 accumulation. A potent, PPARγ-specific ligand Rosiglitazone significantly reduced p53 accumulation in a dose-dependent manner, while PPARγ inhibitor T0070907 potently increased p53 accumulation in a dose-dependent manner. This validated PPARγ as a negative regulator of p53. *MYC* activation depleted PPARγ levels, suggesting that MYC-driven depletion of PPARγ contributes to p53 accumulation. Analysis of over thirty FAs of varying chain length and desaturation level showed that *MYC* overexpression significantly decreased the majority of FAs, including AA and DHA, which were previously shown to activate PPARγ (reviewed in Desvergne and Wahli, 1999). This indicates that regulation of p53 by PPARγ is affected by MYC in two ways: downregulation of PPARγ itself and reduction in the FAs that activate it, leading to relief of inhibition of the pathway.

DHA treatment was previously shown to lead to increased incorporation of DHA in plasma membrane (Zerouga *et al.* 1996) and mitochondrial membrane phospholipid species (reviewed in Stanley *et al.* 2014). To investigate whether *MYC* deregulation drives remodeling of FAs into glycerophospholipid synthesis, changes in PC and PE levels following *MYC* deregulation were analysed. *MYC* activation potently increased levels of PCs with DHA residues, such that these were the only group of PCs that significantly increased from >50 PCs analysed. Several PEs with DHA and AA residues also increased; however this was not confined to polyunsaturated FA residues. These results confirmed that *MYC* deregulation remodels arachidonate metabolites into glycerophospholipid synthesis, particularly PC synthesis.

The results in this study show similarities with data presented by Hall *et al.* (2016) who found that *MYC* overexpression in KRAS-driven lung adenocarcinoma remodeled arachidonate metabolism and increased phospholipase A2 activity. The fact that arachidonate metabolism was also identified as a major screen cluster from the broad range of metabolic pathways in this study further confirms that *MYC* overexpression remodels arachidonate metabolism. However, whilst Hill *et al.* show that *MYC* overexpression increases arachidonate metabolites and AA-containing phospholipids, we found that arachidonate metabolites decrease and DHA-containing phospholipids increase. These differences are likely due to the different contexts in which *MYC* overexpression is analysed in the two studies, for example in an intact genetic background versus KRAS deregulation, and *in vitro* versus *in vivo.*

Whilst the reason for *MYC* overexpression driving increased synthesis of phospholipids with DHA residues was not addressed in this study, several studies have documented that phospholipids with DHA residues display altered membrane structure and function (see below). DHA has a high number of double bonds relative to chain-length and this attribute increases membrane fluidity, permeability,

vesicular fusion, elastic compressibility, and flip-flop rate (reviewed in Stillwell and Wassall, 2003). Furthermore, treatment with DHA was shown to improve mitochondrial tolerance to Ca^{2+}-induced mitochondrial permeability transport pore (MPTP) opening (Khairallah *et al.* 2010a, 2010b).

Aside from glycerophospholipids, FAs can also be used to synthesise triacylglycerol (TG) species, which may either be stored in lipid droplets or catabolised back to free fatty acids (reviewed in Currie *et al.* 2013). *MYC* deregulation potently increased TGs with a variety of chain lengths and desaturation levels. *MYC*-deregulated cells place a high biosynthetic demand on the cell, which may result in increased TG turnover to support lipid synthesis even in the presence of exogenous FAs.

Senkal *et al.* (2017) recently reported coregulation of triglyceride and sphingolipid metabolism. Diacylglycerol acyl transferase 2 (DGAT2), which is usually associated with the conversion of DG to TG for storage, was shown to associate with CERS and convert *de novo* ceramide into acylceramide for storage. DG and ceramide may compete to interact with DGAT2, and knockdown of GPAT2, which converts FA-CoA into LPA to synthesise DG, reduces MYC-driven p53 accumulation (table 3.2). This may indicate that in the absence of DG more ceramide is converted to acylceramide, reducing the *de novo* ceramide pool that is required to positively regulate p53. Further research to determine the effect of *MYC* overexpression on acylceramide synthesis may offer mechanistic insight into how *de novo* ceramide synthesis regulates p53.

7.3 Limitations and future research

This study indicated that *MYC* overexpression increases the synthesis of long-chain FAs and sphingolipids. However, interpretation of experimental data is limited by not combining information on total pool size with information on incorporation of heavy-isotope label into the total lipid pool. Figure 4.3 shows that the percent label incorporation from $^{13}C_3$-pyruvate to palmitate and lignocerate increases in *MYC* overexpressing cells (compared to control cells) over an 8 hr timecourse. Figure 4.3 also shows that the total levels of palmitate and lignocerate decrease, which could indicate that the increase in percent label is caused by a drop in total pool size, not by increased synthesis. Plotting the total levels of labelled and unlabelled FAs in a single figure could strengthen the conclusions that could be drawn from this data.

Data presented on MYC driving long-chain sphingolipid synthesis is more accurately interpreted as *MYC* overexpressing cells increased total levels of long-chain sphingolipids (figure 5.1) and incorporation of carbon derived from $^{13}C_2$-serine (indicating increased *de novo* ceramide synthesis; figure 5.6). This demonstrates that long-chain sphingolipids increase at a high enough rate that the increase in this *de novo* pool is not dampened by the total pool size increase. Nevertheless, it would be useful to plot this information in a single figure.

All lipids were extracted using a chloroform-based protocol due to this method being good for analysis of ceramides, phosphatidylcholines and phosphatidylethanolamines (Bligh and Dyer, 1959). Further interrogation of the lipidome using other extraction methods, such as a butanol-based protocol (Morrison *et al.* 1980), would allow detection of more polar lipids, including lysophospholipids, phosphatidic acid lipids, acylcarnitines, and sphingosine phosphates (reviewed in Tumanov and Kamphorst, 2017). It would be interesting to combine different extraction methods to further profile MYC-driven lipid remodelling.

Further research to characterise the functional relevance of MYC-driven lipid changes is required. In particular, long-chain ceramides and lactosylceramides, as well as glycerophospholipids with DHA residues, were previously implicated in remodelling membrane structure (Ohno *et al.* 2010; Stillwell and Wassall, 2003). Characterising whether *MYC* activated cells have altered plasma membrane and mitochondrial membrane composition and function may give key insight into MYC biology.

p53 was shown to respond to MYC-driven ceramide synthesis; however mechanistic insight into how ceramide activates p53 is yet to be elucidated. No known targets of ceramide signalling clearly regulated MYC-driven p53 accumulation, although PP2A seemed to be a contributor, and therefore an untargeted approach to identify p53 binding partners following *MYC* activation may be the best approach to understand underlying mechanisms. p53 also responded to MYC-driven FA remodelling via PPARγ, which negatively regulated p53. p53 binding partners may also reveal how PPARγ regulates p53.

MRC5 human fibroblasts were used in this study due to their intact genetic background meaning tumour suppressor pathways have not been selected against (as is the case in many cancer cell lines). However, following the acquisition and validation of the primary siRNA screen, this study could be strengthened by testing the relevance of MYC-driven lipid remodellng in a *Myc* overexpressing tumour model such as Eμ-*Myc* transgenic mice.

This study has given key insight into how lipid remodeling in response to oncogene activation can regulate tumour suppressor pathways. As our knowledge of the lipidome improves, it will be interesting to further characterise lipid remodeling driven by oncogene activation.

8 Chapter 8- Bibliography

Adams, J.M., Harris, A.W., Pinkert, C.A., Corcoran, L.M., Alexander, W.S., Cory, S., Palmiter, R.D. and Brinster, R.L., 1985. The c-myc oncogene driven by immunoglobulin enhancers induces lymphoid malignancy in transgenic mice. *Nature*, *318*(6046), pp.533-538.

Adhikary, S. and Eilers, M., 2005. Transcriptional regulation and transformation by Myc proteins. *Nature reviews Molecular cell biology*, *6*(8), pp.635-645.

Ajay, A.K., Upadhyay, A.K., Singh, S., Vijayakumar, M.V., Kumari, R., Pandey, V., Boppana, R. and Bhat, M.K., 2010. Cdk5 phosphorylates non-genotoxically overexpressed p53 following inhibition of PP2A to induce cell cycle arrest/apoptosis and inhibits tumor progression. *Molecular cancer*, *9*(1), p.204.

Amati, B., Brooks, M.W., Levy, N., Littlewood, T.D., Evan, G.I. and Land, H., 1993. Oncogenic activity of the c-Myc protein requires dimerization with Max. *Cell*, *72*(2), pp.233-245.

Arabi, A., Wu, S., Ridderstråle, K., Bierhoff, H., Shiue, C., Fatyol, K., Fahlén, S., Hydbring, P., Söderberg, O., Grummt, I. and Larsson, L.G., 2005. c-Myc associates with ribosomal DNA and activates RNA polymerase I transcription. *Nature cell biology*, *7*(3), p.303.

Arnold, I. and Watt, F.M., 2001. c-Myc activation in transgenic mouse epidermis results in mobilization of stem cells and differentiation of their progeny. *Current biology*, *11*(8), pp.558-568.

Assaily, W., Rubinger, D.A., Wheaton, K., Lin, Y., Ma, W., Xuan, W., Brown-Endres, L., Tsuchihara, K., Mak, T.W. and Benchimol, S., 2011. ROS-mediated p53 induction of Lpin1 regulates fatty acid oxidation in response to nutritional stress. *Molecular cell*, *44*(3), pp.491-501.

Askew, D.S., Ashmun, R.A., Simmons, B.C. and Cleveland, J.L., 1991. Constitutive c-myc expression in an IL-3-dependent myeloid cell line suppresses cell cycle arrest and accelerates apoptosis. *Oncogene*, *6*(10), pp.1915-1922.

Atilla-Gokcumen, G.E., Muro, E., Relat-Goberna, J., Sasse, S., Bedigian, A., Coughlin, M.L., Garcia-Manyes, S. and Eggert, U.S., 2014. Dividing cells regulate their lipid composition and localization. *Cell*, *156*(3), pp.428-439.

Ayer, D.E. and Eisenman, R.N., 1993. A switch from Myc: Max to Mad: Max heterocomplexes accompanies monocyte/macrophage differentiation. *Genes & development*, *7*(11), pp.2110-2119.

Ayer, D.E., Kretzner, L. and Eisenman, R.N., 1993. Mad: a heterodimeric partner for Max that antagonizes Myc transcriptional activity. *Cell*, *72*(2), pp.211-222.

Bader, G.D. and Hogue, C.W., 2003. An automated method for finding molecular complexes in large protein interaction networks. *BMC bioinformatics*, *4*(1), p.2.

Barna, M., Pusic, A., Zollo, O., Costa, M., Kondrashov, N., Rego, E., Rao, P.H. and Ruggero, D., 2008. Suppression of Myc oncogenic activity by ribosomal protein haploinsufficiency. *Nature*, *456*(7224), pp.971-975.

Barrett, J.F., Lewis, B.C., Hoang, A.T., Alvarez, R.J. and Dang, C.V., 1995. Cyclin A links c-Myc to adhesion-independent cell proliferation. *Journal of Biological Chemistry*, *270*(27), pp.15923-15925.

Bensaad, K., Tsuruta, A., Selak, M.A., Vidal, M.N.C., Nakano, K., Bartrons, R., Gottlieb, E. and Vousden, K.H., 2006. TIGAR, a p53-inducible regulator of glycolysis and apoptosis. *Cell*, *126*(1), pp.107-120.

Bligh, E.G. and Dyer, W.J., 1959. A rapid method of total lipid extraction and purification. *Canadian journal of biochemistry and physiology*, *37*(8), pp.911-917.

Bolstad, B.M., Irizarry, R.A., Åstrand, M. and Speed, T.P., 2003. A comparison of normalization methods for high density oligonucleotide array data based on variance and bias. *Bioinformatics*, *19*(2), pp.185-193.

Boon, K., Caron, H.N., van Asperen, R., Valentijn, L., Hermus, M.C., van Sluis, P., Roobeek, I., Weis, I., Voute, P.A., Schwab, M. and Versteeg, R., 2001. N‐myc enhances the expression of a large set of genes functioning in ribosome biogenesis and protein synthesis. *The EMBO journal*, *20*(6), pp.1383-1393.

Bouchard, C., Dittrich, O., Kiermaier, A., Dohmann, K., Menkel, A., Eilers, M. and Lüscher, B., 2001. Regulation of cyclin D2 gene expression by the Myc/Max/Mad network: Myc-dependent TRRAP recruitment and histone acetylation at the cyclin D2 promoter. *Genes & development*, *15*(16), pp.2042-2047.

Bouchard, C., Thieke, K., Maier, A., Saffrich, R., Hanley-Hyde, J., Ansorge, W., Reed, S., Sicinski, P., Bartek, J. and Eilers, M., 1999. Direct induction of cyclin D2 by Myc contributes to cell cycle progression and sequestration of p27. *The EMBO journal*, *18*(19), pp.5321-5333.

Bourbon, N.A., Sandirasegarane, L. and Kester, M., 2002. Ceramide-induced Inhibition of Akt Is Mediated through Protein Kinase Cζ IMPLICATIONS FOR GROWTH ARREST. *Journal of Biological Chemistry*, *277*(5), pp.3286-3292.

Brahimi-Horn, M.C., Bellot, G. and Pouysségur, J., 2011. Hypoxia and energetic tumour metabolism. *Current opinion in genetics & development*, *21*(1), pp.67-72.

Brenner, C., Deplus, R., Didelot, C., Loriot, A., Viré, E., De Smet, C., Gutierrez, A., Danovi, D., Bernard, D., Boon, T. and Pelicci, P.G., 2005. Myc represses

transcription through recruitment of DNA methyltransferase corepressor. *The EMBO journal*, *24*(2), pp.336-346.

Breslow, D.K., Collins, S.R., Bodenmiller, B., Aebersold, R., Simons, K., Shevchenko, A., Ejsing, C.S. and Weissman, J.S., 2010. Orm family proteins mediate sphingolipid homeostasis. *Nature*, *463*(7284), p.1048.

Bretones, G., Acosta, J.C., Caraballo, J.M., Ferrándiz, N., Gómez-Casares, M.T., Albajar, M., Blanco, R., Ruiz, P., Hung, W.C., Albero, M.P. and Perez-Roger, I., 2011. SKP2 oncogene is a direct MYC target gene and MYC down-regulates p27KIP1 through SKP2 in human leukemia cells. *Journal of Biological Chemistry*, *286*(11), pp.9815-9825.

Bretones, G., Delgado, M.D. and León, J., 2015. Myc and cell cycle control. *Biochimica et Biophysica Acta (BBA)-Gene Regulatory Mechanisms*, *1849*(5), pp.506-516.

Brunelle, J.K., Santore, M.T., Budinger, G.S., Tang, Y., Barrett, T.A., Zong, W.X., Kandel, E., Keith, B., Simon, M.C., Thompson, C.B. and Hay, N., 2004. c-Myc sensitization to oxygen deprivation-induced cell death is dependent on Bax/Bak, but is independent of p53 and hypoxia-inducible factor-1. *Journal of Biological Chemistry*, *279*(6), pp.4305-4312.

Burrell, R.A., McGranahan, N., Bartek, J. and Swanton, C., 2013. The causes and consequences of genetic heterogeneity in cancer evolution. *Nature*, *501*(7467), pp.338-345.

Cadenas, E. and Davies, K.J., 2000. Mitochondrial free radical generation, oxidative stress, and aging. *Free Radical Biology and Medicine*, *29*(3), pp.222-230.

Camarda, R., Zhou, A.Y., Kohnz, R.A., Balakrishnan, S., Mahieu, C., Anderton, B., Eyob, H., Kajimura, S., Tward, A., Krings, G. and Nomura, D.K., 2016. Inhibition of fatty acid oxidation as a therapy for MYC-overexpressing triple-negative breast cancer. *Nature medicine*.

Campaner, S., Doni, M., Hydbring, P., Verrecchia, A., Bianchi, L., Sardella, D., Schleker, T., Perna, D., Tronnersjö, S., Murga, M. and Fernandez-Capetillo, O., 2010. Cdk2 suppresses cellular senescence induced by the c-myc oncogene. *Nature cell biology*, *12*(1), pp.54-59.

Carroll, P.A., Diolaiti, D., McFerrin, L., Gu, H., Djukovic, D., Du, J., Cheng, P.F., Anderson, S., Ulrich, M., Hurley, J.B. and Raftery, D., 2015. Deregulated Myc requires MondoA/Mlx for metabolic reprogramming and tumorigenesis. *Cancer cell*, *27*(2), pp.271-285.

Cerami, E., Gao, J., Dogrusoz, U., Gross, B.E., Sumer, S.O., Aksoy, B.A., Jacobsen, A., Byrne, C.J., Heuer, M.L., Larsson, E. and Antipin, Y., 2012. The cBio cancer

genomics portal: an open platform for exploring multidimensional cancer genomics data.

Chalfant, C.E., Kishikawa, K., Mumby, M.C., Kamibayashi, C., Bielawska, A. and Hannun, Y.A., 1999. Long chain ceramides activate protein phosphatase-1 and protein phosphatase-2A Activation is stereospecific and regulated by phosphatidic acid. *Journal of Biological Chemistry*, *274*(29), pp.20313-20317.

Chalfant, C.E., Szulc, Z., Roddy, P., Bielawska, A. and Hannun, Y.A., 2004. The structural requirements for ceramide activation of serine-threonine protein phosphatases. *Journal of lipid research*, *45*(3), pp.496-506.

Charron, J., Malynn, B.A., Fisher, P., Stewart, V., Jeannotte, L., Goff, S.P., Robertson, E.J. and Alt, F.W., 1992. Embryonic lethality in mice homozygous for a targeted disruption of the N-myc gene. *Genes & development*, *6*(12a), pp.2248-2257.

Chen, Z., Trotman, L.C., Shaffer, D., Lin, H.K., Dotan, Z.A., Niki, M., Koutcher, J.A., Scher, H.I., Ludwig, T., Gerald, W. and Cordon-Cardo, C., 2005. Crucial role of p53-dependent cellular senescence in suppression of Pten-deficient tumorigenesis. *Nature*, *436*(7051), pp.725-730.

Cheng, Q., Lau, W.M., Chew, S.H., Ho, T.H., Tay, S.K. and Hui, K.M., 2002. Identification of molecular markers for the early detection of human squamous cell carcinoma of the uterine cervix. *British journal of cancer*, *86*(2), pp.274-281.

Chokkathukalam, A., Kim, D.H., Barrett, M.P., Breitling, R. and Creek, D.J., 2014. Stable isotope-labeling studies in metabolomics: new insights into structure and dynamics of metabolic networks. *Bioanalysis*, *6*(4), pp.511-524.

Choong, M.L., Yang, H., Lee, M.A. and Lane, D.P., 2009. Specific activation of the p53 pathway by low dose actinomycin D: a new route to p53 based cyclotherapy. *Cell cycle*, *8*(17), pp.2810-2818.

Chu, I.M., Hengst, L. and Slingerland, J.M., 2008. The Cdk inhibitor p27 in human cancer: prognostic potential and relevance to anticancer therapy. *Nature Reviews Cancer*, *8*(4), pp.253-267.

Coleman, R.A. and Lee, D.P., 2004. Enzymes of triacylglycerol synthesis and their regulation. *Progress in lipid research*, *43*(2), pp.134-176.

Colombini, M., 2010. Ceramide channels and their role in mitochondria-mediated apoptosis. *Biochimica et Biophysica Acta (BBA)-Bioenergetics*, *1797*(6), pp.1239-1244

Contractor, T. and Harris, C.R., 2012. p53 negatively regulates transcription of the pyruvate dehydrogenase kinase Pdk2. *Cancer research*, *72*(2), pp.560-567.

Cunningham, J.T., Moreno, M.V., Lodi, A., Ronen, S.M. and Ruggero, D., 2014. Protein and nucleotide biosynthesis are coupled by a single rate-limiting enzyme, PRPS2, to drive cancer. *Cell*, *157*(5), pp.1088-1103.

Currie, E., Schulze, A., Zechner, R., Walther, T.C. and Farese, R.V., 2013. Cellular fatty acid metabolism and cancer. *Cell metabolism*, *18*(2), pp.153-161.

Cuvillier, O., Pirianov, G., Kleuser, B. and Vanek, P.G., 1996. Suppression of ceramide-mediated programmed cell death by sphingosine-1-phosphate. *Nature*, *381*(6585), p.800.

Dang, C.V., 2013. MYC, metabolism, cell growth, and tumorigenesis. *Cold Spring Harbor perspectives in medicine*, *3*(8), p.a014217.

Dalla-Favera, R., Bregni, M., Erikson, J., Patterson, D., Gallo, R.C. and Croce, C.M., 1982. Human c-myc onc gene is located on the region of chromosome 8 that is translocated in Burkitt lymphoma cells. *Proceedings of the National Academy of Sciences*, *79*(24), pp.7824-7827.

Dansen, T.B., Whitfield, J., Rostker, F., Brown-Swigart, L. and Evan, G.I., 2006. Specific requirement for Bax, not Bak, in Myc-induced apoptosis and tumor suppression in vivo. *Journal of Biological Chemistry*, *281*(16), pp.10890-10895.

Das, A.K., Uhler, M.D. and Hajra, A.K., 2000. Molecular Cloning and Expression of Mammalian Peroxisomaltrans-2-Enoyl-coenzyme A Reductase cDNAs. *Journal of Biological Chemistry*, *275*(32), pp.24333-24340.

de Hoon, M.J., Imoto, S., Nolan, J. and Miyano, S., 2004. Open source clustering software. *Bioinformatics*, *20*(9), pp.1453-1454.

Dean, M., Levine, R.A., Ran, W., Kindy, M.S., Sonenshein, G.E. and Campisi, J., 1986. Regulation of c-myc transcription and mRNA abundance by serum growth factors and cell contact. *Journal of Biological Chemistry*, *261*(20), pp.9161-9166.

Deng, X., Yin, X., Allan, R., Lu, D.D., Maurer, C.W., Haimovitz-Friedman, A., Fuks, Z., Shaham, S. and Kolesnick, R., 2008. Ceramide biogenesis is required for radiation-induced apoptosis in the germ line of C. elegans. *Science*, *322*(5898), pp.110-115.

Dennis, E.A. and Norris, P.C., 2015. Eicosanoid storm in infection and inflammation. *Nature reviews. Immunology*, *15*(8), p.511.

Desvergne, B. and Wahli, W., 1999. Peroxisome proliferator-activated receptors: nuclear control of metabolism. *Endocrine reviews*, *20*(5), pp.649-688.

Dobrowsky, R.T., Kamibayashi, C., Mumby, M.C. and Hannun, Y.A., 1993. Ceramide activates heterotrimeric protein phosphatase 2A. *Journal of Biological Chemistry*, *268*(21), pp.15523-15530.

Doherty, J.R., Yang, C., Scott, K.E., Cameron, M.D., Fallahi, M., Li, W., Hall, M.A., Amelio, A.L., Mishra, J.K., Li, F. and Tortosa, M., 2014. Blocking lactate export by inhibiting the Myc target MCT1 disables glycolysis and glutathione synthesis. *Cancer research*, *74*(3), pp.908-920.

Eberlin, L.S., Gabay, M., Fan, A.C., Gouw, A.M., Tibshirani, R.J., Felsher, D.W. and Zare, R.N., 2014. Alteration of the lipid profile in lymphomas induced by MYC overexpression. *Proceedings of the National Academy of Sciences*, *111*(29), pp.10450-10455.

Edmunds, L.R., Sharma, L., Kang, A., Lu, J., Vockley, J., Basu, S., Uppala, R., Goetzman, E.S., Beck, M.E., Scott, D. and Prochownik, E.V., 2014. c-Myc programs fatty acid metabolism and dictates acetyl-CoA abundance and fate. *Journal of Biological Chemistry*, *289*(36), pp.25382-25392.

Eischen, C.M., Weber, J.D., Roussel, M.F., Sherr, C.J. and Cleveland, J.L., 1999. Disruption of the ARF–Mdm2–p53 tumor suppressor pathway in Myc-induced lymphomagenesis. *Genes & development*, *13*(20), pp.2658-2669.

Eischen, C.M., Roussel, M.F., Korsmeyer, S.J. and Cleveland, J.L., 2001. Bax loss impairs Myc-induced apoptosis and circumvents the selection of p53 mutations during Myc-mediated lymphomagenesis. *Molecular and cellular biology*, *21*(22), pp.7653-7662.

Eilers, M., Schirm, S. and Bishop, J.M., 1991. The MYC protein activates transcription of the alpha-prothymosin gene. *The EMBO journal*, *10*(1), p.133.

Eljamil, A.S, 2015. Lipid biochemistry for medical sciences. *iUniverse*, pp.1-19l

Elson, A., Deng, C., Campos-Torres, J., Donehower, L.A. and Leder, P., 1995. The MMTV/c-myc transgene and p53 null alleles collaborate to induce T-cell lymphomas, but not mammary carcinomas in transgenic mice. *Oncogene*, *11*(1), pp.181-190.

Evan, G.I., Wyllie, A.H., Gilbert, C.S., Littlewood, T.D., Land, H., Brooks, M., Waters, C.M., Penn, L.Z. and Hancock, D.C., 1992. Induction of apoptosis in fibroblasts by c-myc protein. *Cell*, *69*(1), pp.119-128.

Fanidi, A., Harrington, E.A. and Evan, G.I., 1992. Cooperative interaction between c-myc and bcl-2 proto-oncogenes. *Nature*, *359*(6395), p.554.

Farrell, P.J., Allan, G.J., Shanahan, F., Vousden, K.H. and Crook, T., 1991. p53 is frequently mutated in Burkitt's lymphoma cell lines. *The EMBO journal*, *10*(10), p.2879.

Fearon, E.R. and Vogelstein, B., 1990. A genetic model for colorectal tumorigenesis. *Cell*, *61*(5), pp.759-767.

Felsher, D.W. and Bishop, J.M., 1999. Transient excess of MYC activity can elicit genomic instability and tumorigenesis. *Proceedings of the National Academy of Sciences*, *96*(7), pp.3940-3944.

Felsher, D.W., Zetterberg, A., Zhu, J., Tlsty, T. and Bishop, J.M., 2000. Overexpression of MYC causes p53-dependent G2 arrest of normal fibroblasts. *Proceedings of the National Academy of Sciences*, *97*(19), pp.10544-10548.

Finch, A., Prescott, J., Shchors, K., Hunt, A., Soucek, L., Dansen, T.B., Swigart, L.B. and Evan, G.I., 2006. Bcl-x L gain of function and p19ARF loss of function cooperate oncogenically with Myc in vivo by distinct mechanisms. *Cancer cell*, *10*(2), pp.113-120.

Finch, A.J., Soucek, L., Junttila, M.R., Swigart, L.B. and Evan, G.I., 2009. Acute overexpression of Myc in intestinal epithelium recapitulates some but not all the changes elicited by Wnt/β-catenin pathway activation. *Molecular and cellular biology*, *29*(19), pp.5306-5315.

Fisher, R.A., 1922. On the interpretation of χ 2 from contingency tables, and the calculation of P. *Journal of the Royal Statistical Society*, *85*(1), pp.87-94.

Frank, S.R., Parisi, T., Taubert, S., Fernandez, P., Fuchs, M., Chan, H.M., Livingston, D.M. and Amati, B., 2003. MYC recruits the TIP60 histone acetyltransferase complex to chromatin. *EMBO reports*, *4*(6), pp.575-580.

Gallagher, W.M., Cairney, M., Schott, B., Roninson, I.B. and Brown, R., 1997. Identification of p53 genetic suppressor elements which confer resistance to cisplatin. *Oncogene*, *14*(2), pp.185-194.

Gandarillas, A. and Watt, F.M., 1997. c-Myc promotes differentiation of human epidermal stem cells. *Genes & development*, *11*(21), pp.2869-2882.

Gao, P., Tchernyshyov, I., Chang, T.C., Lee, Y.S., Kita, K., Ochi, T., Zeller, K.I., De Marzo, A.M., Van Eyk, J.E., Mendell, J.T. and Dang, C.V., 2009. c-Myc suppression of miR-23a/b enhances mitochondrial glutaminase expression and glutamine metabolism. *Nature*, *458*(7239), pp.762-765.

Gao, J., Aksoy, B.A., Dogrusoz, U., Dresdner, G., Gross, B., Sumer, S.O., Sun, Y., Jacobsen, A., Sinha, R., Larsson, E. and Cerami, E., 2013. Integrative analysis of

complex cancer genomics and clinical profiles using the cBioPortal. *Science signaling*, *6*(269), p.pl1.

Giono, L.E. and Manfredi, J.J., 2006. The p53 tumor suppressor participates in multiple cell cycle checkpoints. *Journal of cellular physiology*, *209*(1), pp.13-20.

Gomez-Roman, N., Grandori, C., Eisenman, R.N. and White, R.J., 2003. Direct activation of RNA polymerase III transcription by c-Myc. *Nature*, *421*(6920), pp.290-294.

Goñi, F.M. and Alonso, A., 2006. Biophysics of sphingolipids I. Membrane properties of sphingosine, ceramides and other simple sphingolipids. *Biochimica et Biophysica Acta (BBA)-Biomembranes*, *1758*(12), pp.1902-1921.

Gottlieb, E., Vander Heiden, M.G. and Thompson, C.B., 2000. Bcl-xL prevents the initial decrease in mitochondrial membrane potential and subsequent reactive oxygen species production during tumor necrosis factor alpha-induced apoptosis. *Molecular and Cellular Biology*, *20*(15), pp.5680-5689.

Gottlieb, E., Armour, S.M. and Thompson, C.B., 2002. Mitochondrial respiratory control is lost during growth factor deprivation. *Proceedings of the National Academy of Sciences*, *99*(20), pp.12801-12806.

Grandori, C. and Eisenman, R.N., 1997. Myc target genes. *Trends in biochemical sciences*, *22*(5), pp.177-181.

Grandori, C., Wu, K.J., Fernandez, P., Ngouenet, C., Grim, J., Clurman, B.E., Moser, M.J., Oshima, J., Russell, D.W., Swisshelm, K. and Frank, S., 2003. Werner syndrome protein limits MYC-induced cellular senescence. *Genes & development*, *17*(13), pp.1569-1574.

Grandori, C., Gomez-Roman, N., Felton-Edkins, Z.A., Ngouenet, C., Galloway, D.A., Eisenman, R.N. and White, R.J., 2005. c-Myc binds to human ribosomal DNA and stimulates transcription of rRNA genes by RNA polymerase I. *Nature cell biology*, *7*(3), pp.311-318.

Graves, J.A., Wang, Y., Sims-Lucas, S., Cherok, E., Rothermund, K., Branca, M.F., Elster, J., Beer-Stolz, D., Van Houten, B., Vockley, J. and Prochownik, E.V., 2012. Mitochondrial structure, function and dynamics are temporally controlled by c-Myc. *PloS one*, *7*(5), p.e37699.

Green, D.R. and Kroemer, G., 2009. Cytoplasmic functions of the tumour suppressor p53. *Nature*, *458*(7242), pp.1127-1130.

Hall, Z., Ament, Z., Wilson, C.H., Burkhart, D.L., Ashmore, T., Koulman, A., Littlewood, T., Evan, G.I. and Griffin, J.L., 2016. Myc expression drives aberrant lipid metabolism in lung cancer. *Cancer research*, *76*(16), pp.4608-4618.

Han, S., Lone, M.A., Schneiter, R. and Chang, A., 2010. Orm1 and Orm2 are conserved endoplasmic reticulum membrane proteins regulating lipid homeostasis and protein quality control. *Proceedings of the National Academy of Sciences*, *107*(13), pp.5851-5856.

Hanada, K., Hara, T. and Nishijima, M., 2000. Purification of the serine palmitoyltransferase complex responsible for sphingoid base synthesis by using affinity peptide chromatography techniques. *Journal of Biological Chemistry*, *275*(12), pp.8409-8415.

Hartwell, L.H., Culotti, J. and Reid, B., 1970. Genetic control of the cell-division cycle in yeast, I. Detection of mutants. *Proceedings of the National Academy of Sciences*, *66*(2), pp.352-359.

Hayflick, L. and Moorhead, P.S., 1961. The serial cultivation of human diploid cell strains. *Experimental cell research*, *25*(3), pp.585-621.

He, T.C., Sparks, A.B., Rago, C., Hermeking, H., Zawel, L., Da Costa, L.T., Morin, P.J., Vogelstein, B. and Kinzler, K.W., 1998. Identification of c-MYC as a target of the APC pathway. *Science*, *281*(5382), pp.1509-1512.

Heikkila, R., Schwab, G., Wickstrom, E., Loke, S.L., Pluznik, D.H., Watt, R. and Neckers, L.M., 1987. A c-myc antisense oligodeoxynucleotide inhibits entry into S phase but not progress from G0 to G1. *Nature*, *328*(6129), pp.445-449.

Henry, J.L., Coggin, D.L. and King, C.R., 1993. High-level expression of the ribosomal protein L19 in human breast tumors that overexpress erbB-2. *Cancer research*, *53*(6), pp.1403-1408.

Hermeking, H. and Eick, D., 1994. Mediation of c-Myc-induced apoptosis by p53. *SCIENCE-NEW YORK THEN WASHINGTON-*, pp.2091-2091.

Hermeking, H., Rago, C., Schuhmacher, M., Li, Q., Barrett, J.F., Obaya, A.J., O'Connell, B.C., Mateyak, M.K., Tam, W., Kohlhuber, F. and Dang, C.V., 2000. Identification of CDK4 as a target of c-MYC. *Proceedings of the National Academy of Sciences*, *97*(5), pp.2229-2234.

Hill, R.M., Kuijper, S., Lindsey, J.C., Petrie, K., Schwalbe, E.C., Barker, K., Boult, J.K., Williamson, D., Ahmad, Z., Hallsworth, A. and Ryan, S.L., 2015. Combined MYC and P53 defects emerge at medulloblastoma relapse and define rapidly progressive, therapeutically targetable disease. *Cancer Cell*, *27*(1), pp.72-84.

Hoang, A.T., Cohen, K.J., Barrett, J.F., Bergstrom, D.A. and Dang, C.V., 1994. Participation of cyclin A in Myc-induced apoptosis. *Proceedings of the National Academy of Sciences*, *91*(15), pp.6875-6879.

Hockenbery, D.M., Oltvai, Z.N., Yin, X.M., Milliman, C.L. and Korsmeyer, S.J., 1993. Bcl-2 functions in an antioxidant pathway to prevent apoptosis. *Cell*, *75*(2), pp.241-251.

Hoeferlin, L.A., Fekry, B., Ogretmen, B., Krupenko, S.A. and Krupenko, N.I., 2013. Folate stress induces apoptosis via p53-dependent de novo ceramide synthesis and up-regulation of ceramide synthase 6. *Journal of Biological Chemistry*, *288*(18), pp.12880-12890.

Hofmann, J.W., Zhao, X., De Cecco, M., Peterson, A.L., Pagliaroli, L., Manivannan, J., Hubbard, G.B., Ikeno, Y., Zhang, Y., Feng, B. and Li, X., 2015. Reduced expression of MYC increases longevity and enhances healthspan. *Cell*, *160*(3), pp.477-488.

Holopainen, J.M., Lehtonen, J.Y. and Kinnunen, P.K., 1997. Lipid microdomains in dimyristoylphosphatidylcholine–ceramide liposomes. *Chemistry and physics of lipids*, *88*(1), pp.1-13.

Hornemann, T., Richard, S., Rütti, M.F., Wei, Y. and von Eckardstein, A., 2006. Cloning and initial characterization of a new subunit for mammalian serine-palmitoyltransferase. *Journal of Biological Chemistry*, *281*(49), pp.37275-37281.

Hornemann, T., Wei, Y. and von Eckardstein, A., 2007. Is the mammalian serine palmitoyltransferase a high-molecular-mass complex?. *Biochemical Journal*, *405*(1), pp.157-164.

Hornemann, T., Penno, A., Rütti, M.F., Ernst, D., Kivrak-Pfiffner, F., Rohrer, L. and von Eckardstein, A., 2009. The SPTLC3 subunit of serine palmitoyltransferase generates short chain sphingoid bases. *Journal of Biological Chemistry*, *284*(39), pp.26322-26330.

Hsueh, Y.W., Giles, R., Kitson, N. and Thewalt, J., 2002. The effect of ceramide on phosphatidylcholine membranes: a deuterium NMR study. *Biophysical journal*, *82*(6), pp.3089-3095.

Hsu, B., Marin, M.C., El-Naggar, A.K., Stephens, L.C., Brisbay, S. and McDonnell, T.J., 1995. Evidence that c-myc mediated apoptosis does not require wild-type p53 during lymphomagenesis. *Oncogene*, *11*(1), pp.175-179.

Hu, W., Zhang, C., Wu, R., Sun, Y., Levine, A. and Feng, Z., 2010. Glutaminase 2, a novel p53 target gene regulating energy metabolism and antioxidant function. *Proceedings of the National Academy of Sciences*, *107*(16), pp.7455-7460.

Huang, D.W., Sherman, B.T. and Lempicki, R.A., 2009. Systematic and integrative analysis of large gene lists using DAVID bioinformatics resources. *Nature protocols*, *4*(1), pp.44-57.

Huang, X., Chen, Y.J., Cho, K., Nikolskiy, I., Crawford, P.A. and Patti, G.J., 2014. X13CMS: global tracking of isotopic labels in untargeted metabolomics. *Analytical chemistry*, *86*(3), pp.1632-1639.

Hydbring, P., Bahram, F., Su, Y., Tronnersjö, S., Högstrand, K., von der Lehr, N., Sharifi, H.R., Lilischkis, R., Hein, N., Wu, S. and Vervoorts, J., 2010. Phosphorylation by Cdk2 is required for Myc to repress Ras-induced senescence in cotransformation. *Proceedings of the National Academy of Sciences*, *107*(1), pp.58-63.

Inga, A., Storici, F., Darden, T.A. and Resnick, M.A., 2002. Differential transactivation by the p53 transcription factor is highly dependent on p53 level and promoter target sequence. *Molecular and cellular biology*, *22*(24), pp.8612-8625.

Iritani, B.M. and Eisenman, R.N., 1999. c-Myc enhances protein synthesis and cell size during B lymphocyte development. *Proceedings of the National Academy of Sciences*, *96*(23), pp.13180-13185.

Ivanov, X., Mladenov, Z., Nedyalkov, S., Todorov, T.G. and Yakimov, M., 1964. Experimental investigations into avian leucoses. V. Transmission, haematology and morphology of avian myelocytomatosis. *Bull. Inst. Pathol. Comp. Anim. Acad. Bulg. Sci*, *10*, pp.5-38.

Jansen-Dürr, P., Meichle, A., Steiner, P., Pagano, M., Finke, K., Botz, J., Wessbecher, J., Draetta, G. and Eilers, M., 1993. Differential modulation of cyclin gene expression by MYC. *Proceedings of the National Academy of Sciences*, *90*(8), pp.3685-3689.

Jiang, P., Du, W., Wang, X., Mancuso, A., Gao, X., Wu, M. and Yang, X., 2011. p53 regulates biosynthesis through direct inactivation of glucose-6-phosphate dehydrogenase. *Nature cell biology*, *13*(3), pp.310-316.

Jiang, P., Du, W., Mancuso, A., Wellen, K.E. and Yang, X., 2013. Reciprocal regulation of p53 and malic enzymes modulates metabolism and senescence. *Nature*, *493*(7434), pp.689-693.

Jin, L., Alesi, G.N. and Kang, S., 2015. Glutaminolysis as a target for cancer therapy. *Oncogene*.

Kalkat, M., De Melo, J., Hickman, K.A., Lourenco, C., Redel, C., Resetca, D., Tamachi, A., Tu, W.B. and Penn, L.Z., 2017. MYC Deregulation in Primary Human Cancers. *Genes*, *8*(6), p.151.

Kamijo, T., Weber, J.D., Zambetti, G., Zindy, F., Roussel, M.F. and Sherr, C.J., 1998. Functional and physical interactions of the ARF tumor suppressor with p53 and Mdm2. *Proceedings of the National Academy of Sciences*, *95*(14), pp.8292-8297.

Kawauchi, K., Araki, K., Tobiume, K. and Tanaka, N., 2008. p53 regulates glucose metabolism through an IKK-NF-κB pathway and inhibits cell transformation. *Nature cell biology*, *10*(5), pp.611-618.

Kelly, K., Cochran, B.H., Stiles, C.D. and Leder, P., 1983. Cell-specific regulation of the c-myc gene by lymphocyte mitogens and platelet-derived growth factor. *Cell*, *35*(3), pp.603-610.

Kerkhoff, E., Houben, R., Löffler, S., Troppmair, J., Lee, J.E. and Rapp, U.R., 1998. Regulation of c-myc expression by Ras/Raf signalling. *Oncogene*, *16*(2).

Khairallah, R.J., Sparagna, G.C., Khanna, N., O'Shea, K.M., Hecker, P.A., Kristian, T., Fiskum, G., Des Rosiers, C., Polster, B.M. and Stanley, W.C., 2010a. Dietary supplementation with docosahexaenoic acid, but not eicosapentaenoic acid, dramatically alters cardiac mitochondrial phospholipid fatty acid composition and prevents permeability transition. *Biochimica et Biophysica Acta (BBA)-Bioenergetics*, *1797*(8), pp.1555-1562.

Khairallah, R.J., O'Shea, K.M., Brown, B.H., Khanna, N., Des Rosiers, C. and Stanley, W.C., 2010b. Treatment with docosahexaenoic acid, but not eicosapentaenoic acid, delays Ca2+-induced mitochondria permeability transition in normal and hypertrophied myocardium. *Journal of Pharmacology and Experimental Therapeutics*, *335*(1), pp.155-162.

Kim, S., Li, Q., Dang, C.V. and Lee, L.A., 2000. Induction of ribosomal genes and hepatocyte hypertrophy by adenovirus-mediated expression of c-Myc in vivo. *Proceedings of the National Academy of Sciences*, *97*(21), pp.11198-11202.

Kim, J.H., You, K.R., Kim, I.H., Cho, B.H., Kim, C.Y. and Kim, D.G., 2004. Over-expression of the ribosomal protein L36a gene is associated with cellular proliferation in hepatocellular carcinoma. *Hepatology*, *39*(1), pp.129-138.

Kim, J., Lee, J.H. and Iyer, V.R., 2008. Global identification of Myc target genes reveals its direct role in mitochondrial biogenesis and its E-box usage in vivo. *PloS one*, *3*(3), p.e1798.

Kim, J.W., Mori, S. and Nevins, J.R., 2010. Myc-induced microRNAs integrate Myc-mediated cell proliferation and cell fate. *Cancer research*, *70*(12), pp.4820-4828.

Klefstrom, J., Västrik, I., Saksela, E., Valle, J., Eilers, M. and Alitalo, K., 1994. c-Myc induces cellular susceptibility to the cytotoxic action of TNF-alpha. *The EMBO journal*, *13*(22), p.5442.

Kliewer, S.A., Sundseth, S.S., Jones, S.A., Brown, P.J., Wisely, G.B., Koble, C.S., Devchand, P., Wahli, W., Willson, T.M., Lenhard, J.M. and Lehmann, J.M., 1997.

Fatty acids and eicosanoids regulate gene expression through direct interactions with peroxisome proliferator-activated receptors α and γ. *Proceedings of the National Academy of Sciences*, *94*(9), pp.4318-4323.

Knoepfler, P.S., Cheng, P.F. and Eisenman, R.N., 2002. N-myc is essential during neurogenesis for the rapid expansion of progenitor cell populations and the inhibition of neuronal differentiation. *Genes & development*, *16*(20), pp.2699-2712.

Koressaar T, Remm M (2007) Enhancements and modifications of primer design program Primer3. *Bioinformatics* 23(10):1289-91
Koskinen, P.J. and Alitalo, K., 1993, February. Role of myc amplification and overexpression in cell growth, differentiation and death. In *Seminars in cancer biology* (Vol. 4, No. 1, pp. 3-12).

Koskinen, P.J. and Alitalo, K., 1993, February. Role of myc amplification and overexpression in cell growth, differentiation and death. In *Seminars in cancer biology* (Vol. 4, No. 1, pp. 3-12).

Kruiswijk, F., Labuschagne, C.F. and Vousden, K.H., 2015. p53 in survival, death and metabolic health: a lifeguard with a licence to kill. *Nature reviews Molecular cell biology*, *16*(7), pp.393-405.

Kuilman, T., Michaloglou, C., Mooi, W.J. and Peeper, D.S., 2010. The essence of senescence. *Genes & development*, *24*(22), pp.2463-2479.

Laviad, E.L., Albee, L., Pankova-Kholmyansky, I., Epstein, S., Park, H., Merrill, A.H. and Futerman, A.H., 2008. Characterization of Ceramide Synthase 2 Tissue distribution, substrate specificity, and inhibition by sphingosine 1-phosphate. *Journal of Biological Chemistry*, *283*(9), pp.5677-5684.

Lavin, M.A. and Gueven, N., 2006. The complexity of p53 stabilization and activation. *Cell Death & Differentiation*, *13*(6), pp.941-950.

Lehrke, M. and Lazar, M.A., 2005. The many faces of PPARγ. *Cell*, *123*(6), pp.993-999.

Lewis, C.A., Parker, S.J., Fiske, B.P., McCloskey, D., Gui, D.Y., Green, C.R., Vokes, N.I., Feist, A.M., Vander Heiden, M.G. and Metallo, C.M., 2014. Tracing compartmentalized NADPH metabolism in the cytosol and mitochondria of mammalian cells. *Molecular cell*, *55*(2), pp.253-263.

Levine, A.J. and Puzio-Kuter, A.M., 2010. The control of the metabolic switch in cancers by oncogenes and tumor suppressor genes. *Science*, *330*(6009), pp.1340-1344.

Li, F.P., Fraumeni, J.F., Mulvihill, J.J., Blattner, W.A., Dreyfus, M.G., Tucker, M.A. and Miller, R.W., 1988. A cancer family syndrome in twenty-four kindreds. *Cancer research*, *48*(18), pp.5358-5362.

Li, J., Yen, C., Liaw, D., Podsypanina, K., Bose, S., Wang, S.I., Puc, J., Miliaresis, C., Rodgers, L., McCombie, R. and Bigner, S.H., 1997. PTEN, a putative protein tyrosine phosphatase gene mutated in human brain, breast, and prostate cancer. *science*, *275*(5308), pp.1943-1947.

Li, F., Wang, Y., Zeller, K.I., Potter, J.J., Wonsey, D.R., O'Donnell, K.A., Kim, J.W., Yustein, J.T., Lee, L.A. and Dang, C.V., 2005. Myc stimulates nuclearly encoded mitochondrial genes and mitochondrial biogenesis. *Molecular and cellular biology*, *25*(14), pp.6225-6234.

Lin, C.H., Jackson, A.L., Guo, J., Linsley, P.S. and Eisenman, R.N., 2009. Myc–regulated microRNAs attenuate embryonic stem cell differentiation. *The EMBO journal*, *28*(20), pp.3157-3170.

Lin, C.Y., Lovén, J., Rahl, P.B., Paranal, R.M., Burge, C.B., Bradner, J.E., Lee, T.I. and Young, R.A., 2012. Transcriptional amplification in tumor cells with elevated c-Myc. *Cell*, *151*(1), pp.56-67.

Lindström, M.S. and Wiman, K.G., 2003. Myc and E2F1 induce p53 through p14ARF-independent mechanisms in human fibroblasts. *Oncogene*, *22*(32), pp.4993-5005.

Little, C.D., Nau, M.M., Carney, D.N., Gazdar, A.F. and Minna, J.D., 1983. Amplification and expression of the c-myc oncogene in human lung cancer cell lines. *Nature*, *306*(5939), pp.194-196.

Liu, Y.C., Li, F., Handler, J., Huang, C.R.L., Xiang, Y., Neretti, N., Sedivy, J.M., Zeller, K.I. and Dang, C.V., 2008. Global regulation of nucleotide biosynthetic genes by c-Myc. *PloS one*, *3*(7), p.e2722.

Liu, M., Huang, C., Polu, S.R., Schneiter, R. and Chang, A., 2012. Regulation of sphingolipid synthesis through Orm1 and Orm2 in yeast. *J Cell Sci*, *125*(10), pp.2428-2435.

Liu, Y., He, Y., Jin, A., Tikunov, A.P., Zhou, L., Tollini, L.A., Leslie, P., Kim, T.H., Li, L.O., Coleman, R.A. and Gu, Z., 2014a. Ribosomal protein–Mdm2–p53 pathway coordinates nutrient stress with lipid metabolism by regulating MCD and promoting fatty acid oxidation. *Proceedings of the National Academy of Sciences*, *111*(23), pp.E2414-E2422.

Liu, Y., Samuel, B.S., Breen, P.C. and Ruvkun, G., 2014b. Caenorhabditis elegans pathways that surveil and defend mitochondria. *Nature*, *508*(7496), pp.406-410.

Locasale, J.W., 2013. Serine, glycine and one-carbon units: cancer metabolism in full circle. *Nature reviews Cancer*, *13*(8), pp.572-583.

Lovén, J., Orlando, D.A., Sigova, A.A., Lin, C.Y., Rahl, P.B., Burge, C.B., Levens, D.L., Lee, T.I. and Young, R.A., 2012. Revisiting global gene expression analysis. *Cell*, *151*(3), pp.476-482.

Lutz, W., Fulda, S., Jeremias, I., Debatin, K.M. and Schwab, M., 1998. MycN and IFNg cooperate in apoptosis of human neuroblastoma cells. *Oncogene*, *17*(3), pp.339-346.

Maddocks, O.D., Labuschagne, C.F., Adams, P.D. and Vousden, K.H., 2016. Serine metabolism supports the methionine cycle and DNA/RNA methylation through de novo ATP synthesis in cancer cells. *Molecular cell*, *61*(2), pp.210-221.

Maddocks, O.D., Athineos, D., Cheung, E.C., Lee, P., Zhang, T., van den Broek, N.J., Mackay, G.M., Labuschagne, C.F., Gay, D., Kruiswijk, F. and Blagih, J., 2017. Modulating the therapeutic response of tumours to dietary serine and glycine starvation. *Nature*, *544*(7650), pp.372-376.

Mailhes, J.B., Hilliard, C., Fuseler, J.W. and London, S.N., 2003. Okadaic acid, an inhibitor of protein phosphatase 1 and 2A, induces premature separation of sister chromatids during meiosis I and aneuploidy in mouse oocytes in vitro. *Chromosome Research*, *11*(6), pp.619-631.

Mannava, S., Grachtchouk, V., Wheeler, L.J., Im, M., Zhuang, D., Slavina, E.G., Mathews, C.K., Shewach, D.S. and Nikiforov, M.A., 2008. Direct role of nucleotide metabolism in C-MYC-dependent proliferation of melanoma cells. *Cell Cycle*, *7*(15), pp.2392-2400.

Mashanov, V.S., Zueva, O.R. and García-Arrarás, J.E., 2015. Myc regulates programmed cell death and radial glia dedifferentiation after neural injury in an echinoderm. *BMC developmental biology*, *15*(1), p.24.

Mateyak, M.K., Obaya, A.J. and Sedivy, J.M., 1999. c-Myc regulates cyclin D-Cdk4 and-Cdk6 activity but affects cell cycle progression at multiple independent points. *Molecular and cellular biology*, *19*(7), pp.4672-4683.

Matoba, S., Kang, J.G., Patino, W.D., Wragg, A., Boehm, M., Gavrilova, O., Hurley, P.J., Bunz, F. and Hwang, P.M., 2006. p53 regulates mitochondrial respiration. *Science*, *312*(5780), pp.1650-1653.

Matsuyama, S., Xu, Q., Velours, J. and Reed, J.C., 1998. The mitochondrial F 0 F 1-ATPase proton pump is required for function of the proapoptotic protein Bax in yeast and mammalian cells. *Molecular cell*, *1*(3), pp.327-336.

McGarry, J.D., Takabayashi, Y. and Foster, D.W., 1978. The role of malonyl-coa in the coordination of fatty acid synthesis and oxidation in isolated rat hepatocytes. *Journal of Biological Chemistry*, *253*(22), pp.8294-8300.

McLure, K.G. and Lee, P.W., 1998. How p53 binds DNA as a tetramer. *The EMBO journal*, *17*(12), pp.3342-3350.

McMahon, S.B., Wood, M.A. and Cole, M.D., 2000. The essential cofactor TRRAP recruits the histone acetyltransferase hGCN5 to c-Myc. *Molecular and cellular biology*, *20*(2), pp.556-562.

Mesicek, J., Lee, H., Feldman, T., Jiang, X., Skobeleva, A., Berdyshev, E.V., Haimovitz-Friedman, A., Fuks, Z. and Kolesnick, R., 2010. Ceramide synthases 2, 5, and 6 confer distinct roles in radiation-induced apoptosis in HeLa cells. *Cellular signalling*, *22*(9), pp.1300-1307.

Menssen, A. and Hermeking, H., 2002. Characterization of the c-MYC-regulated transcriptome by SAGE: identification and analysis of c-MYC target genes. *Proceedings of the National Academy of Sciences*, *99*(9), pp.6274-6279.

Meyer, N. and Penn, L.Z., 2008. Reflecting on 25 years with MYC. *Nature Reviews Cancer*, *8*(12), pp.976-990.

Mihara, M., Erster, S., Zaika, A., Petrenko, O., Chittenden, T., Pancoska, P. and Moll, U.M., 2003. p53 has a direct apoptogenic role at the mitochondria. *Molecular cell*, *11*(3), pp.577-590.

Mizutani, Y., Kihara, A. and Igarashi, Y., 2005. Mammalian Lass6 and its related family members regulate synthesis of specific ceramides. *Biochemical Journal*, *390*(1), pp.263-271.

Mizutani, Y., Kihara, A. and Igarashi, Y., 2006. LASS3 (longevity assurance homologue 3) is a mainly testis-specific (dihydro) ceramide synthase with relatively broad substrate specificity. *Biochemical Journal*, *398*(3), pp.531-538.

Mladenov, Z., Heine, U., Beard, D. and Beard, J.W., 1967. Strain MC29 avian leukosis virus. Myelocytoma, endothelioma, and renal growths: pathomorphological and ultrastructural aspects. *Journal of the National Cancer Institute*, *38*(3), pp.251-285.

Montagnoli, A., Fiore, F., Eytan, E., Carrano, A.C., Draetta, G.F., Hershko, A. and Pagano, M., 1999. Ubiquitination of p27 is regulated by Cdk-dependent phosphorylation and trimeric complex formation. *Genes & Development*, *13*(9), pp.1181-1189.

Morrish, F., Neretti, N., Sedivy, J.M. and Hockenbery, D.M., 2008. The oncogene c-Myc coordinates regulation of metabolic networks to enable rapid cell cycle entry. *Cell cycle*, *7*(8), pp.1054-1066.

Morrish, F., Isern, N., Sadilek, M., Jeffrey, M. and Hockenbery, D.M., 2009. c-Myc activates multiple metabolic networks to generate substrates for cell-cycle entry. *Oncogene*, *28*(27), pp.2485-2491.

Morrish, F. and Hockenbery, D., 2014. MYC and mitochondrial biogenesis. Cold Spring Harbor perspectives in medicine, 4(5), p.a014225.

Morrison, W.R., Tan, S.L. and Hargin, K.D., 1980. Methods for the quantitative analysis of lipids in cereal grains and similar tissues. *Journal of the Science of Food and Agriculture*, *31*(4), pp.329-340.

Müller, G., Ayoub, M., Storz, P., Rennecke, J., Fabbro, D. and Pfizenmaier, K., 1995. PKC zeta is a molecular switch in signal transduction of TNF-alpha, bifunctionally regulated by ceramide and arachidonic acid. *The EMBO journal*, *14*(9), p.1961.

Murphy, M., Stinnakre, M.G., Senamaud-Beaufort, C., Winston, N.J., Sweeney, C., Kubelka, M., Carrington, M., Bréchot, C. and Sobczak-Thépot, J., 1997. Delayed early embryonic lethality following disruption of the murine cyclin A2 gene. *Nature genetics*, *15*(1), pp.83-86.

Murphy, T.A., Dang, C.V. and Young, J.D., 2013. Isotopically nonstationary 13 C flux analysis of Myc-induced metabolic reprogramming in B-cells. *Metabolic engineering*, *15*, pp.206-217.

Nau, M.M., Brooks, B.J., Battey, J., Sausville, E., Gazdar, A.F., Kirsch, I.R., McBride, O.W., Bertness, V., Hollis, G.F. and Minna, J.D., 1985. L-myc, a new myc-related gene amplified and expressed in human small cell lung cancer. *Nature*, *318*(6041), pp.69-73.

Nau, M.M., Brooks, B.J., Carney, D.N., Gazdar, A.F., Battey, J.F., Sausville, E.A. and Minna, J.D., 1986. Human small-cell lung cancers show amplification and expression of the N-myc gene. *Proceedings of the National Academy of Sciences*, *83*(4), pp.1092-1096.

Nie, Z., Hu, G., Wei, G., Cui, K., Yamane, A., Resch, W., Wang, R., Green, D.R., Tessarollo, L., Casellas, R. and Zhao, K., 2012. c-Myc is a universal amplifier of expressed genes in lymphocytes and embryonic stem cells. *Cell*, *151*(1), pp.68-79.

Nikiforov, M.A., Chandriani, S., O'Connell, B., Petrenko, O., Kotenko, I., Beavis, A., Sedivy, J.M. and Cole, M.D., 2002. A functional screen for Myc-responsive genes reveals serine hydroxymethyltransferase, a major source of the one-carbon unit for cell metabolism. *Molecular and cellular biology*, *22*(16), pp.5793-5800.

O'Donnell, K.A., Yu, D., Zeller, K.I., Kim, J.W., Racke, F., Thomas-Tikhonenko, A. and Dang, C.V., 2006. Activation of transferrin receptor 1 by c-Myc enhances cellular proliferation and tumorigenesis. *Molecular and cellular biology*, *26*(6), pp.2373-2386.

Ohno, Y., Suto, S., Yamanaka, M., Mizutani, Y., Mitsutake, S., Igarashi, Y., Sassa, T. and Kihara, A., 2010. ELOVL1 production of C24 acyl-CoAs is linked to C24 sphingolipid synthesis. *Proceedings of the National Academy of Sciences*, *107*(43), pp.18439-18444.

Olivier, M., Goldgar, D.E., Sodha, N., Ohgaki, H., Kleihues, P., Hainaut, P. and Eeles, R.A., 2003. Li-Fraumeni and related syndromes. *Cancer research*, *63*(20), pp.6643-6650.

Olivier, M., Hollstein, M. and Hainaut, P., 2010. TP53 mutations in human cancers: origins, consequences, and clinical use. *Cold Spring Harbor perspectives in biology*, *2*(1), p.a001008.

Olovnikov, A.M., 1970. Principle of marginotomy in template synthesis of polynucleotides. *Doklady Akademii Nauk SSSR*, *201*(6), pp.1496-1499.

O'Shea, K.M., Khairallah, R.J., Sparagna, G.C., Xu, W., Hecker, P.A., Robillard-Frayne, I., Des Rosiers, C., Kristian, T., Murphy, R.C., Fiskum, G. and Stanley, W.C., 2009. Dietary ω-3 fatty acids alter cardiac mitochondrial phospholipid composition and delay Ca 2+-induced permeability transition. *Journal of molecular and cellular cardiology*, *47*(6), pp.819-827.

Osthus, R.C., Shim, H., Kim, S., Li, Q., Reddy, R., Mukherjee, M., Xu, Y., Wonsey, D., Lee, L.A. and Dang, C.V., 2000. Deregulation of glucose transporter 1 and glycolytic gene expression by c-Myc. *Journal of Biological Chemistry*, *275*(29), pp.21797-21800.

Pacilli, A., Calienni, M., Margarucci, S., D'Apolito, M., Petillo, O., Rocchi, L., Pasquinelli, G., Nicolai, R., Koverech, A., Calvani, M. and Peluso, G., 2013. Carnitine-acyltransferase system inhibition, cancer cell death, and prevention of myc-induced lymphomagenesis. *Journal of the National Cancer Institute*, p.djt030.

Pardee, A.B., 1974. A restriction point for control of normal animal cell proliferation. *Proceedings of the National Academy of Sciences*, *71*(4), pp.1286-1290.

Pelengaris, S., Khan, M. and Evan, G.I., 2002. Suppression of Myc-induced apoptosis in β cells exposes multiple oncogenic properties of Myc and triggers carcinogenic progression. *Cell*, *109*(3), pp.321-334.

Pelz, O., Gilsdorf, M. and Boutros, M., 2010. web cellHTS2: a web-application for the analysis of high-throughput screening data. *BMC bioinformatics*, *11*(1), p.185.

Pérez-Roger, I., Solomon, D.L., Sewing, A. and Land, H., 1997. Myc activation of cyclin E/Cdk2 kinase involves induction of cyclin E gene transcription and inhibition of p27 Kip1 binding to newly formed complexes. *Oncogene*, *14*(20).

Perry, R.P. and Kelley, D.E., 1970. Inhibition of RNA synthesis by actinomycin D: characteristic dose‐response of different RNA species. *Journal of cellular physiology*, *76*(2), pp.127-139.

Pierce, S.B., Yost, C., Britton, J.S., Loo, L.W., Flynn, E.M., Edgar, B.A. and Eisenman, R.N., 2004. dMyc is required for larval growth and endoreplication in Drosophila. *Development*, *131*(10), pp.2317-2327.

Pomerantz, J., Schreiber-Agus, N., Liégeois, N.J., Silverman, A., Alland, L., Chin, L., Potes, J., Chen, K., Orlow, I., Lee, H.W. and Cordon-Cardo, C., 1998. The Ink4a tumor suppressor gene product, p19 Arf, interacts with MDM2 and neutralizes MDM2's inhibition of p53. *Cell*, *92*(6), pp.713-723.

Pourdehnad, M., Truitt, M.L., Siddiqi, I.N., Ducker, G.S., Shokat, K.M. and Ruggero, D., 2013. Myc and mTOR converge on a common node in protein synthesis control that confers synthetic lethality in Myc-driven cancers. *Proceedings of the National Academy of Sciences*, *110*(29), pp.11988-11993.

Rajagopalan, H., Nowak, M.A., Vogelstein, B. and Lengauer, C., 2003. The significance of unstable chromosomes in colorectal cancer. *Nature reviews cancer*, *3*(9), pp.695-701.

R Core Team (2013). R: A language and environment for statistical computing. R Foundation for Statistical Computing, Vienna, Austria. URL http://www.R-project.org/.

Reed, J.C., Alpers, J.D., Nowell, P.C. and Hoover, R.G., 1986. Sequential expression of protooncogenes during lectin-stimulated mitogenesis of normal human lymphocytes. *Proceedings of the National Academy of Sciences*, *83*(11), pp.3982-3986.

Riebeling, C., Allegood, J.C., Wang, E., Merrill, A.H. and Futerman, A.H., 2003. Two mammalian longevity assurance gene (LAG1) family members, trh1 and trh4, regulate dihydroceramide synthesis using different fatty acyl-CoA donors. *Journal of Biological Chemistry*, *278*(44), pp.43452-43459.

Riley, T., Sontag, E., Chen, P. and Levine, A., 2008. Transcriptional control of human p53-regulated genes. *Nature reviews Molecular cell biology*, *9*(5), pp.402-412.

Rosenwald, I.B., Rhoads, D.B., Callanan, L.D., Isselbacher, K.J. and Schmidt, E.V., 1993. Increased expression of eukaryotic translation initiation factors eIF-4E and eIF-2 alpha in response to growth induction by c-myc. *Proceedings of the National Academy of Sciences*, *90*(13), pp.6175-6178.

Ruangsiriluk, W., Grosskurth, S.E., Ziemek, D., Kuhn, M., des Etages, S.G. and Francone, O.L., 2012. Silencing of enzymes involved in ceramide biosynthesis causes distinct global alterations of lipid homeostasis and gene expression. *Journal of lipid research*, *53*(8), pp.1459-1471.

Sabo, A., Kress, T.R., Pelizzola, M., De Pretis, S., Gorski, M.M., Tesi, A., Morelli, M.J., Bora, P., Doni, M., Verrecchia, A. and Tonelli, C., 2014. Selective transcriptional regulation by Myc in cellular growth control and lymphomagenesis. *Nature*, *511*(7510), p.488.

Saldanha, A.J., 2004. Java Treeview—extensible visualization of microarray data. *Bioinformatics*, *20*(17), pp.3246-3248.

Sansom, O.J., Meniel, V.S., Muncan, V., Phesse, T.J., Wilkins, J.A., Reed, K.R., Vass, J.K., Athineos, D., Clevers, H. and Clarke, A.R., 2007. Myc deletion rescues Apc deficiency in the small intestine. *Nature*, *446*(7136), pp.676-679

Sassa, T., Ohno, Y., Suzuki, S., Nomura, T., Nishioka, C., Kashiwagi, T., Hirayama, T., Akiyama, M., Taguchi, R., Shimizu, H. and Itohara, S., 2013. Impaired epidermal permeability barrier in mice lacking elovl1, the gene responsible for very-long-chain fatty acid production. *Molecular and cellular biology*, *33*(14), pp.2787-2796.

Sassa, T. and Kihara, A., 2014. Metabolism of very long-chain fatty acids: genes and pathophysiology. *Biomol Ther (Seoul)*, *22*(2), pp.83-92.

Sauane, M., Su, Z.Z., Dash, R., Liu, X., Norris, J.S., Sarkar, D., Lee, S.G., Allegood, J.C., Dent, P., Spiegel, S. and Fisher, P.B., 2010. Ceramide plays a prominent role in MDA‐7/IL‐24‐induced cancer‐specific apoptosis. *Journal of cellular physiology*, *222*(3), pp.546-555.

Schuhmacher, M., Staege, M.S., Pajic, A., Polack, A., Weidle, U.H., Bornkamm, G.W., Eick, D. and Kohlhuber, F., 1999. Control of cell growth by c-Myc in the absence of cell division. *Current Biology*, *9*(21), pp.1255-1258.

Schuhmacher, M., Kohlhuber, F., Hölzel, M., Kaiser, C., Burtscher, H., Jarsch, M., Bornkamm, G.W., Laux, G., Polack, A., Weidle, U.H. and Eick, D., 2001. The transcriptional program of a human B cell line in response to Myc. *Nucleic acids research*, *29*(2), pp.397-406.

Sears, R., Nuckolls, F., Haura, E., Taya, Y., Tamai, K. and Nevins, J.R., 2000. Multiple Ras-dependent phosphorylation pathways regulate Myc protein stability. *Genes & development*, *14*(19), pp.2501-2514.

Seitz, V., Butzhammer, P., Hirsch, B., Hecht, J., Gütgemann, I., Ehlers, A., Lenze, D., Oker, E., Sommerfeld, A., von der Wall, E. and König, C., 2011. Deep sequencing of MYC DNA-binding sites in Burkitt lymphoma. *PloS one*, *6*(11), p.e26837.

Senkal, C.E., Salama, M.F., Snider, A.J., Allopenna, J.J., Rana, N.A., Koller, A., Hannun, Y.A. and Obeid, L.M., 2017. Ceramide is metabolized to acylceramide and stored in lipid droplets. *Cell Metabolism*, *25*(3), pp.686-697.

Seo, H.R., Kim, J., Bae, S., Soh, J.W. and Lee, Y.S., 2008. Cdk5-mediated phosphorylation of c-Myc on Ser-62 is essential in transcriptional activation of cyclin B1 by cyclin G1. *Journal of Biological Chemistry*, *283*(23), pp.15601-15610.

Seoane, J., Pouponnot, C., Staller, P., Schader, M., Eilers, M. and Massagué, J., 2001. TGFβ influences Myc, Miz-1 and Smad to control the CDK inhibitor p15INK4b. *Nature cell biology*, *3*(4), pp.400-408.

Serrano, M., Lin, A.W., McCurrach, M.E., Beach, D. and Lowe, S.W., 1997. Oncogenic ras provokes premature cell senescence associated with accumulation of p53 and p16 INK4a. *Cell*, *88*(5), pp.593-602.

Shachaf, C.M., Kopelman, A.M., Arvanitis, C., Karlsson, Å., Beer, S., Mandl, S., Bachmann, M.H., Borowsky, A.D., Ruebner, B., Cardiff, R.D. and Yang, Q., 2004. MYC inactivation uncovers pluripotent differentiation and tumour dormancy in hepatocellular cancer. *Nature*, *431*(7012), pp.1112-1117.

Shannon, P., Markiel, A., Ozier, O., Baliga, N.S., Wang, J.T., Ramage, D., Amin, N., Schwikowski, B. and Ideker, T., 2003. Cytoscape: a software environment for integrated models of biomolecular interaction networks. *Genome research*, *13*(11), pp.2498-2504.

Sheiness, D.I.A.N.A., Fanshier, L.O.I.S. and Bishop, J.M., 1978. Identification of nucleotide sequences which may encode the oncogenic capacity of avian retrovirus MC29. *Journal of virology*, *28*(2), pp.600-610.

Sheth, A., Escobar-Alvarez, S., Gardner, J., Ran, L., Heaney, M.L. and Scheinberg, D.A., 2014. Inhibition of human mitochondrial peptide deformylase causes apoptosis in c-myc-overexpressing hematopoietic cancers. *Cell death & disease*, *5*(3), p.e1152.
Shi, J., Whyte, W.A., Zepeda-Mendoza, C.J., Milazzo, J.P., Shen, C., Roe, J.S., Minder, J.L., Mercan, F., Wang, E., Eckersley-Maslin, M.A. and Campbell, A.E., 2013. Role of SWI/SNF in acute leukemia maintenance and enhancer-mediated Myc regulation. *Genes & development*, *27*(24), pp.2648-2662.

Shi, L., Wu, Y.X., Yu, J.H., Chen, X., Luo, X.J. and Yin, Y.R., 2017. Research of the relationship between β-catenin and c-myc-mediated Wnt pathway and laterally spreading tumors occurrence. *Eur Rev Med Pharmacol Sci*, *21*(2), pp.252-257.

Shiraki, N., Shiraki, Y., Tsuyama, T., Obata, F., Miura, M., Nagae, G., Aburatani, H., Kume, K., Endo, F. and Kume, S., 2014. Methionine metabolism regulates maintenance and differentiation of human pluripotent stem cells. *Cell metabolism*, *19*(5), pp.780-794.

Shim, H., Dolde, C., Lewis, B.C., Wu, C.S., Dang, G., Jungmann, R.A., Dalla-Favera, R. and Dang, C.V., 1997. c-Myc transactivation of LDH-A: implications for tumor metabolism and growth. *Proceedings of the National Academy of Sciences*, *94*(13), pp.6658-6663.

Simons, K. and Ikonen, E., 1997. Functional rafts in cell membranes. *Nature*, *387*(6633), p.569.

Sonnino, S., Prinetti, A., Nakayama, H., Yangida, M., Ogawa, H. and Iwabuchi, K., 2009. Role of very long fatty acid-containing glycosphingolipids in membrane organization and cell signaling: the model of lactosylceramide in neutrophils. *Glycoconjugate journal*, *26*(6), pp.615-621.

Soucek, L. and Evan, G.I., 2010. The ups and downs of Myc biology. *Current opinion in genetics & development*, *20*(1), pp.91-95.

Staller, P., Peukert, K., Kiermaier, A., Seoane, J., Lukas, J., Karsunky, H., Möröy, T., Bartek, J., Massagué, J., Hänel, F. and Eilers, M., 2001. Repression of p15INK4b expression by Myc through association with Miz-1. *Nature cell biology*, *3*(4), pp.392-399.

Stanley, W.C., Khairallah, R.J. and Dabkowski, E.R., 2012. Update on lipids and mitochondrial function: impact of dietary n-3 polyunsaturated fatty acids. *Current opinion in clinical nutrition and metabolic care*, *15*(2), p.122.

Stillwell, W. and Wassall, S.R., 2003. Docosahexaenoic acid: membrane properties of a unique fatty acid. *Chemistry and physics of lipids*, *126*(1), pp.1-27.

Stine, Z.E., Walton, Z.E., Altman, B.J., Hsieh, A.L. and Dang, C.V., 2015. MYC, metabolism, and cancer. *Cancer discovery*, *5*(10), pp.1024-1039.

Stott, F.J., Bates, S., James, M.C., McConnell, B.B., Starborg, M., Brookes, S., Palmero, I., Ryan, K., Hara, E., Vousden, K.H. and Peters, G., 1998. The alternative product from the human CDKN2A locus, p14ARF, participates in a regulatory feedback loop with p53 and MDM2. *The EMBO journal*, *17*(17), pp.5001-5014.

Takahashi, K. and Yamanaka, S., 2006. Induction of pluripotent stem cells from mouse embryonic and adult fibroblast cultures by defined factors. *cell*, *126*(4), pp.663-676.

Tansey, W.P., 2014. Mammalian MYC proteins and cancer. *New Journal of Science*, *2014*.

Tumanov, S. and Kamphorst, J.J., 2017. Recent advances in expanding the coverage of the lipidome. *Current opinion in biotechnology*, *43*, pp.127-133.
Untergasser A, Cutcutache I, Koressaar T, Ye J, Faircloth BC, Remm M, Rozen SG (2012) Primer3 - new capabilities and interfaces. *Nucleic Acids Research* 40(15):e115

Untergasser, A., Cutcutache, I., Koressaar, T., Ye, J., Faircloth, B.C., Remm, M. and Rozen, S.G., 2012. Primer3—new capabilities and interfaces. *Nucleic acids research*, *40*(15), pp.e115-e115.

Vaarala, M.H., Porvari, K.S., Kylloenen, A.P., Mustonen, M.V., Lukkarinen, O. and Vihko, P.T., 1998. Several genes encoding ribosomal proteins are over-expressed in prostate-cancer cell lines: confirmation of L7a and L37 over-expression in prostate-cancer tissue samples. *International journal of cancer*, *78*, pp.27-32.

Van Riggelen, J., Yetil, A. and Felsher, D.W., 2010a. MYC as a regulator of ribosome biogenesis and protein synthesis. *Nature reviews Cancer*, *10*(4), pp.301-309.

Van Riggelen, J., Müller, J., Otto, T., Beuger, V., Yetil, A., Choi, P.S., Kosan, C., Möröy, T., Felsher, D.W. and Eilers, M., 2010b. The interaction between Myc and Miz1 is required to antagonize TGFβ-dependent autocrine signaling during lymphoma formation and maintenance. *Genes & development*, *24*(12), pp.1281-1294.

Vance, D.E., 2002. Phospholipid biosynthesis in eukaryotes. *New comprehensive biochemistry*, *36*, pp.205-232.

Vander Heiden, M.G., Chandel, N.S., Williamson, E.K., Schumacker, P.T. and Thompson, C.B., 1997. Bcl-x L regulates the membrane potential and volume homeostasis of mitochondria. *Cell*, *91*(5), pp.627-637.

Vander Heiden, M.G., Chandel, N.S., Schumacker, P.T. and Thompson, C.B., 1999. Bcl-x L prevents cell death following growth factor withdrawal by facilitating mitochondrial ATP/ADP exchange. *Molecular cell*, *3*(2), pp.159-167.

Vander Heiden, M.G., Li, X.X., Gottleib, E., Hill, R.B., Thompson, C.B. and Colombini, M., 2001. Bcl-x L promotes the open configuration of the voltage-dependent anion channel and metabolite passage through the outer mitochondrial membrane. *Journal of Biological Chemistry*, *276*(22), pp.19414-19419.

Varga, T., Czimmerer, Z. and Nagy, L., 2011. PPARs are a unique set of fatty acid regulated transcription factors controlling both lipid metabolism and inflammation.

Biochimica et Biophysica Acta (BBA)-Molecular Basis of Disease, *1812*(8), pp.1007-1022.

Venkataraman, K., Riebeling, C., Bodennec, J., Riezman, H., Allegood, J.C., Sullards, M.C., Merrill, A.H. and Futerman, A.H., 2002. Upstream of growth and differentiation factor 1 (uog1), a mammalian homolog of the yeast Longevity Assurance Gene 1 (LAG1), regulatesN-Stearoyl-sphinganine (C18-(Dihydro) ceramide) synthesis in a fumonisin B1-independent manner in mammalian cells. *Journal of Biological Chemistry*, *277*(38), pp.35642-35649.

Vennstrom, B., Sheiness, D., Zabielski, J. and Bishop, J.M., 1982. Isolation and characterization of c-myc, a cellular homolog of the oncogene (v-myc) of avian myelocytomatosis virus strain 29. *Journal of virology*, *42*(3), pp.773-779.

Vernon, E.G. and Gaston, K., 2000. Myc and YY1 mediate activation of the Surf-1 promoter in response to serum growth factors. *Biochimica et Biophysica Acta (BBA)-Gene Structure and Expression*, *1492*(1), pp.172-179.

Vita, M. and Henriksson, M., 2006, August. The Myc oncoprotein as a therapeutic target for human cancer. In *Seminars in cancer biology* (Vol. 16, No. 4, pp. 318-330).
Academic Press.

Vogelstein, B. and Kinzler, K.W., 1993. The multistep nature of cancer. *Trends in genetics*, *9*(4), pp.138-141.

Vousden, K.H., 2000. p53: death star. *Cell*, *103*(5), pp.691-694.

Vousden, K.H. and Lu, X., 2002. Live or let die: the cell's response to p53. *Nature Reviews Cancer*, *2*(8), pp.594-604.

Wadsworth, J.M., Clarke, D.J., McMahon, S.A., Lowther, J.P., Beattie, A.E., Langridge-Smith, P.R., Broughton, H.B., Dunn, T.M., Naismith, J.H. and Campopiano, D.J., 2013. The chemical basis of serine palmitoyltransferase inhibition by myriocin. *Journal of the American Chemical Society*, *135*(38), pp.14276-14285.

Walz, S., Lorenzin, F., Morton, J., Wiese, K.E., von Eyss, B., Herold, S., Rycak, L., Dumay-Odelot, H., Karim, S., Bartkuhn, M. and Roels, F., 2014. Activation and repression by oncogenic MYC shape tumour-specific gene expression profiles. *Nature*, *511*(7510), p.483.

Wang, J., Xie, L.Y., Allan, S., Beach, D. and Hannon, G.J., 1998. Myc activates telomerase. *Genes & development*, *12*(12), pp.1769-1774.

Wang, Q., Yang, C., Zhou, J., Wang, X., Wu, M. and Liu, Z., 2001. Cloning and characterization of full-length human ribosomal protein L15 cDNA which was overexpressed in esophageal cancer. *Gene*, *263*(1), pp.205-209.

Wang, R., Dillon, C.P., Shi, L.Z., Milasta, S., Carter, R., Finkelstein, D., McCormick, L.L., Fitzgerald, P., Chi, H., Munger, J. and Green, D.R., 2011. The transcription factor Myc controls metabolic reprogramming upon T lymphocyte activation. *Immunity*, *35*(6), pp.871-882.

Warburg, O., 1956. On the origin of cancer cells. *Science*, *123*(3191), pp.309-314.

Ward, P.S. and Thompson, C.B., 2012. Metabolic reprogramming: a cancer hallmark even warburg did not anticipate. *Cancer cell*, *21*(3), pp.297-308.

Watson, J.D., 1972. Origin of concatemeric T7DNA. *Nature*, *239*(94), pp.197-201.

Weber, J.D., Jeffers, J.R., Rehg, J.E., Randle, D.H., Lozano, G., Roussel, M.F., Sherr, C.J. and Zambetti, G.P., 2000. p53-independent functions of the p19ARF tumor suppressor. *Genes & development*, *14*(18), pp.2358-2365.

Weng, A.P., Ferrando, A.A., Lee, W., Morris, J.P., Silverman, L.B., Sanchez-Irizarry, C., Blacklow, S.C., Look, A.T. and Aster, J.C., 2004. Activating mutations of NOTCH1 in human T cell acute lymphoblastic leukemia. *Science*, *306*(5694), pp.269-271.

Wickstrom, E.L., Bacon, T.A., Gonzalez, A., Freeman, D.L., Lyman, G.H. and Wickstrom, E., 1988. Human promyelocytic leukemia HL-60 cell proliferation and c-myc protein expression are inhibited by an antisense pentadecadeoxynucleotide targeted against c-myc mRNA. *Proceedings of the National Academy of Sciences*, *85*(4), pp.1028-1032.

Wiman, K.G., Magnusson, K.P., Ramqvist, T. and Klein, G., 1991. Mutant p53 detected in a majority of Burkitt lymphoma cell lines by monoclonal antibody PAb240. *Oncogene*, *6*(9), pp.1633-1639.

Wise, D.R., DeBerardinis, R.J., Mancuso, A., Sayed, N., Zhang, X.Y., Pfeiffer, H.K., Nissim, I., Daikhin, E., Yudkoff, M., McMahon, S.B. and Thompson, C.B., 2008. Myc regulates a transcriptional program that stimulates mitochondrial glutaminolysis and leads to glutamine addiction. *Proceedings of the National Academy of Sciences*, *105*(48), pp.18782-18787.

Wonsey, D.R., Zeller, K.I. and Dang, C.V., 2002. The c-Myc target gene PRDX3 is required for mitochondrial homeostasis and neoplastic transformation. *Proceedings of the National Academy of Sciences*, *99*(10), pp.6649-6654.

Wright, J.B., Brown, S.J. and Cole, M.D., 2010. Upregulation of c-MYC in cis through a large chromatin loop linked to a cancer risk-associated single-nucleotide polymorphism in colorectal cancer cells. *Molecular and cellular biology*, *30*(6), pp.1411-1420.

Yang, W., Shen, J., Wu, M., Arsura, M., FitzGerald, M., Suldan, Z., Kim, D.W., Hofmann, C.S., Pianetti, S., Romieu-Mourez, R. and Freedman, L.P., 2001. Repression of transcription of the p27Kip1 cyclin-dependent kinase inhibitor gene by c-Myc. *Oncogene*, *20*(14), p.1688.

Yap, C.S., Peterson, A.L., Castellani, G., Sedivy, J.M. and Neretti, N., 2011. Kinetic profiling of the c-Myc transcriptome and bioinformatic analysis of repressed gene promoters. *Cell Cycle*, *10*(13), pp.2184-2196.

Yin, X.Y., Grove, L., Datta, N.S., Katula, K., Long, M.W. and Prochownik, E.V., 2001. Inverse regulation of cyclin B1 by c-Myc and p53 and induction of tetraploidy by cyclin B1 overexpression. *Cancer research*, *61*(17), pp.6487-6493.

Yuneva, M., Zamboni, N., Oefner, P., Sachidanandam, R. and Lazebnik, Y., 2007. Deficiency in glutamine but not glucose induces MYC-dependent apoptosis in human cells. *The Journal of cell biology*, *178*(1), pp.93-105.

Zeller, K.I., Jegga, A.G., Aronow, B.J., O'Donnell, K.A. and Dang, C.V., 2003. An integrated database of genes responsive to the Myc oncogenic transcription factor: identification of direct genomic targets. *Genome biology*, *4*(10), p.R69.

Zeller, K.I., Zhao, X., Lee, C.W., Chiu, K.P., Yao, F., Yustein, J.T., Ooi, H.S., Orlov, Y.L., Shahab, A., Yong, H.C. and Fu, Y., 2006. Global mapping of c-Myc binding sites and target gene networks in human B cells. *Proceedings of the National Academy of Sciences*, *103*(47), pp.17834-17839.

Zerouga, M.U.S.T.A.P.H.A., Stillwell, W.I.L.L.I.A.M., Stone, J., Powner, A. and Jenski, L.J., 1996. Phospholipid class as a determinant in docosahexaenoic acid's effect on tumor cell viability. *Anticancer research*, *16*(5), pp.2863-2868.

Zhang, H., Desai, N.N., Olivera, A., Seki, T., Brooker, G. and Spiegel, S., 1991. Sphingosine-1-phosphate, a novel lipid, involved in cellular proliferation. *J Cell Biol*, *114*(1), pp.155-167.

Zhang, Y., Xiong, Y. and Yarbrough, W.G., 1998. ARF promotes MDM2 degradation and stabilizes p53: ARF-INK4a locus deletion impairs both the Rb and p53 tumor suppression pathways. *Cell*, *92*(6), pp.725-734.

Zhang, Y. and Lu, H., 2009. Signaling to p53: ribosomal proteins find their way. *Cancer cell*, *16*(5), pp.369-377.

Zhang, C., Lin, M., Wu, R., Wang, X., Yang, B., Levine, A.J., Hu, W. and Feng, Z., 2011. Parkin, a p53 target gene, mediates the role of p53 in glucose metabolism and the Warburg effect. *Proceedings of the National Academy of Sciences*, *108*(39), pp.16259-16264.

Zhang, C., Liu, J., Liang, Y., Wu, R., Zhao, Y., Hong, X., Lin, M., Yu, H., Liu, L., Levine, A.J. and Hu, W., 2013. Tumour-associated mutant p53 drives the Warburg effect. *Nature communications*, *4*.

Zindy, F., Eischen, C.M., Randle, D.H., Kamijo, T., Cleveland, J.L., Sherr, C.J. and Roussel, M.F., 1998. Myc signaling via the ARF tumor suppressor regulates p53-dependent apoptosis and immortalization. *Genes & development*, *12*(15), pp.2424-2433.